CALCIFYING PHYTOPLANKTON IN NATURAL LABORATORIES FOR UNDERSTANDING OCEAN ACIDIFICATION

Tesis entregada a la Pontificia Universidad Católica de Chile en cumplimiento parcial de los requisitos para optar al Grado de Doctor en Ciencias con mención en Ecología

Por

FRANCISCO JAVIER DÍAZ ROSAS

Director de Tesis : Dr. Peter von Dassow

Junio 2021

A mi madre Teresa (Q.E.P.D.) y padre Francisco

AGRADECIMIENTOS

Quiero expresar mi agradecimiento a la Pontificia Universidad Católica de Chile y el Departamento de Ecología por entregarme habilidades tanto duras como blandas. A mi profesor tutor Dr. Peter von Dassow por su entrega y dedicación con este proyecto. Crucial para alcanzar esto fue el apoyo emocional de Nélida Pohl. El apoyo constante de mi padre Francisco y hermana Soledad, así como el recuerdo de mi madre me dieron fuerza durante tiempos difíciles. A Jessica Beltrán y Verónica Flores por su apoyo en los quehaceres de laboratorio. A los colegas Rodrigo Torres, Catharina Alves-de-Souza, Emilio Alarcón, Humberto González, Eduardo Menschel, Daniela Mella-Flores por su apoyo profesional. A la Universidad de Concepción y el Instituto Milenio de Oceanografía por entregarme herramientas teóricas y prácticas, y apoyo económico. Finalmente, agradecer a la Comisión Nacional de Investigación Científica y Tecnológica hoy Agencia Nacional de Investigación y Desarrollo por entregarme la Beca Chile.

TABLE OF CONTENTS

LIST OF FIGURES

LIST OF TABLES

LIST OF ACRONYSMS

AMD	Archipelago Madre de Dios
TA, A_T	Total Alkalinity
bSi	Biogenic Silica
C	Carbon
CD	Coccosphere Diameter
Chl-*a*	Chlorophyll-*a* total
DIC	Dissolved Inorganic Carbon
DSi	Dissolved Silicate
DSL	Distal Shield Length
ESP	Eastern South Pacific
FSC	Forward Scatter
IC	Inner Channel
JF	Juan Fernández Archipelago

NBP	Nathaniel B. Palmer 1305 cruise
OA	Ocean Acidification
OMI	Outlying Mean Index
OS	Otway Sound
PAR	Photosynthetically Active Radiation
PAT	Southern Patagonia
pCO_2	Partial pressure of carbon dioxide
Phyto-C	Phytoplankton Biomass
PIC	Particulate Inorganic Carbon
POC	Particulate Organic Carbon
QUI	El Quisco Bay
RDA	Redundancy Analysis
RTol	Residual Tolerance
S	Salinity
SAASW	SubAntarctic Surface Water
SEM	Scanning Electron Microscopy
SS	Skyring Sound
SSS	Sea Surface Salinity
SST	Sea Surface Temperature
T	Temperature

TC	Total Carbon
TCA	Total Central Area
TRA	Coastal to ocean transitional zone
TEPs	Transparent exopolysaccharides
Tol	Tolerance
Total-C	Total Carbon Biomass
UCA	Uncovered Central Area
UPW	Upwelling system
WSM	Western Strait of Magellan

RESUMEN

Los cocolitofóridos son organismos fitoplanctónicos unicelulares caracterizados por una cobertura de placas de calcita, los cocolitos, que son producidos dentro de la célula. Estos calcificadores, como uno de los principales grupos funcionales planctónicos, juegan un rol importante en el ciclo del carbono inorgánico y posiblemente como lastre hundiendo carbono orgánico hacia el océano profundo. La mayoría de los esfuerzos para entender las respuestas de los cocolitofóridos hacia la acidificación del océano (AO) –o el aumento del CO_2 atmosférico reduce el pH y estado de saturación (Ω) de $CaCO_3$ del océano– ha sido a través de experimentos de laboratorio, principalmente usando un pequeño set de cepas de la especie más cosmopolita y fácilmente cultivable *Emiliania huxleyi*. Esta especie resulta particularmente interesante ya que es joven (~ 291.000 años) y se ha adaptado a un amplio rango de ambientes marinos. Sin embargo, este no es el único cocolitofórido y aun dentro de esta especie hay mucha diversidad fenotípica y genética y respuestas diversas hacia la AO en el laboratorio. A pesar de los esfuerzos realizados aun no es claro como los efectos fisiológicos bajo condiciones controladas se trasladan a respuestas de campo a nivel de comunidad. Esta tesis buscó contribuir a entender este asunto estudiando la distribución, composición y nicho realizado de ensambles de

cocolitofóridos y morfotipos de *E. huxleyi* en ambientes con niveles contrastantes de pCO_2/pH/$\Omega_{calcita}$ del Pacífico Sureste, y evaluar las respuestas de diferentes morfotipos de *E. huxleyi* a niveles de pCO_2/pH ajustados en el laboratorio. Para esto, se muestrearon los cocolitofóridos en una sección costera-oceánica, aguas mesotróficas, sistemas de surgencia, y fiordos-canales de Patagonia. De un total de 40 especies, *E. huxleyi* fue la más prevalente (30-100 % abundancia relativa). Dentro de este taxón, varios morfotipos han sido descritos como estables en cultivo y diferenciados genéticamente (e.g., los morfotipos A y R). El morfotipo A moderadamente-calcificado dominó las poblaciones de *E. huxleyi* siendo sólo superado por el morfotipo R altamente-calcificado en sistemas de surgencia con alto pCO_2/bajo pH. Este cambio abrupto en composición de las poblaciones de *E. huxleyi* sugirió que estos ambientes costeros mantienen reservorios genéticos para su adaptación a la AO. Por consiguiente, se probó la hipótesis que aquellas formas están adaptados para resistir condiciones de alto pCO_2/bajo pH. Inesperadamente, los morfotipos del Pacífico Sureste no fueron más sensibles que las cepas altamente-calcificadas desde aguas contiguas con alto pCO_2/bajo pH (disminuyeron las tasas de crecimiento y razón PIC/POC). Por otro lado, análisis de nicho realizado mostraron que el morfotipo A posee un nicho más amplio y tolerante a cambios ambientales (i.e., generalista) que el nicho del morfotipo R, especializado en aguas con alto pCO_2/bajo pH. La falta de evidencia de adaptación local a condiciones de alto pCO_2/bajo pH en *E. huxleyi,* podría ser explicado por una estrecha respuesta unimodal hacia $\Omega_{calcita}$ revelado por el análisis de nicho que no fue testeado experimentalmente. Alternativamente, el morfotipo R altamente-calcificado podría ser seleccionado por una condición particular del Pacífico Sureste no identificada que se correlaciona con temperatura, salinidad y $\Omega_{calcita}$ de su nicho realizado. En suma, a pesar de poseer rápidas tasas de reemplazo y grandes tamaños poblacionales, organismos planctónicos

oceánicos no necesariamente exhiben adaptaciones a la surgencia de aguas con alto CO_2, y este ubicuo cocolitofórido podría estar cerca del límite de su capacidad para adaptar a la AO en curso.

ABSTRACT

Coccolithophores are unicellular phytoplanktonic organisms characterized by a covering of calcite plates, the coccoliths, which are produced intracellularly. These calcifiers, as one of the main planktonic functional groups, play an important role in the inorganic carbon cycle and possibly as ballast that sinks organic carbon to the deep-sea. Most efforts to understanding coccolithophore response to ocean acidification (OA) –or the raise in atmospheric CO_2 reduces ocean pH and saturation states (Ω) of $CaCO_3$– have been through lab experiments, mostly using a small set of strains of the cosmopolitan, easily cultivated species *Emiliania huxleyi*. This species is especially interesting because it is young (~ 291,000 years) and has adapted to a wide range of marine environments. However, it is not the only coccolithophore and even within that species there is a lot of phenotypic and genetic diversity and diverse responses to OA in the lab. Despite the efforts made it is unclear how the physiological effects under controlled conditions translate to community-level responses in the field. This thesis aimed to contribute to understanding this issue by studying the distribution, composition and realized niches of coccolithophore assemblages and *E. huxleyi* morphotypes in contrasting $pCO_2/pH/\Omega_{calcite}$ environments of the Eastern South Pacific, and to evaluate the responses of different *E. huxleyi*

morphotypes to targeted pCO_2/pH levels set in the lab. For this, the coccolithophores were surveyed in a coastal-oceanic section, mesotrophic waters, upwelling systems, and fjords-channels of Patagonia. From a total of 40 species, *E. huxleyi* was the most prevalent (30-100 % relative abundance). Within this taxon, several morphotypes has been described as stable in culture and genetically differentiated (e.g., the A and R morphotypes). The moderately-calcified A morphotype dominated the *E. huxleyi* populations being only surpassed by the R hyper-calcified morphotype in upwelling systems with high pCO_2/low pH. This abrupt shift in the composition of *E. huxleyi* populations suggested that these coastal environments hold genetic reservoirs for their adaptation to OA. Therefore, the hypothesis was tested that these forms are adapted to resist high pCO_2/low pH conditions. Unexpectedly, the morphotypes from the Eastern South Pacific were not more sensitive than the R hyper-calcified strains from neighboring high pCO_2/low pH waters (lowering growth rates and PIC/POC ratios). On the other hand, realized-niche analysis showed that the A morphotype has a broader niche that is more tolerant to environmental-change (i.e., generalist) than the R morphotype's niche, specialized to high pCO_2/low pH waters. The lack of evidence for local adaptation to high pCO_2/low pH conditions in *E. huxleyi*, might be explained by a narrow unimodal niche response to $\Omega_{calcite}$ revealed by niche analysis that was not tested experimentally. Alternatively, the R hyper-calcified morphotype might be selected by an unidentified condition particular to the Eastern South Pacific that correlates with temperature, salinity, and $\Omega_{calcite}$ of its realized-niche. Overall, despite their rapid turnover and large population sizes, oceanic planktonic microorganisms do not necessarily exhibit adaptations to high-pCO_2 upwelled waters, and this ubiquitous coccolithophore may be near the limit of its capacity to adapt to ongoing OA.

1 GENERAL INTRODUCTION

Coccolithophores are planktonic single-celled marine photoautotrophs mostly in the 3-20 μm range which are characterized by bearing calcite plates (coccoliths) (Monteiro *et al*., 2016). They represent one of the most abundant and widespread groups of eukaryotic marine phytoplankton (Falkowski *et al*., 2004), occurring widely throughout the world's ocean, with the exception of the high polar seas (Tyrrell and Young, 2009). In addition to being important primary producers, coccolithophores contribute to calcium carbonate ($CaCO_3$) precipitation in the epipelagic waters and its export to the deep-sea (Buitenhuis *et al*., 2019). Although $CaCO_3$ precipitation in surface waters is a source of CO_2 (the carbonate counter pump) (reviewed by Rost and Riebesell, 2004), $CaCO_3$ may enhance sinking of organic matter (the ballast effect, Klaas and Archer, 2002; Sanders *et al*., 2010), and $CaCO_3$ dissolution at depth may consume more CO_2 than is released at the surface (Smith, 2013). These functions make coccolithophores a focal group to understand the ocean carbon cycle occurring at both ecological and geological scales. Although there is increasing agreement about what ecological conditions favor coccolithophores among other groups (e.g., conditions associated with blooms, Tyrrell and Merico, 2004; Hopkins *et al*., 2015), their responses to rapid climate changes are still debated.

1.1 Drivers of climate change: the ocean acidification threat on marine biota

The climate of the Earth has undergone changes over geologic time-scales triggered by natural drivers in step with glacial/interglacial cycles. However, since the 18th century, the advent of the industrial revolution and modern agricultural practices have made humans the principal drivers of climate change (IPCC, 2018). Human greenhouse gas emissions by fossil fuel combustion is a main cause of the increase in global temperature observed since the latter half of the 20th century (IPCC, 2018). Moreover, current global atmospheric CO_2 concentrations (reaching > 414 ppm; NOAA/ESRL[1]) are the highest registered for the past 3,000,000 years (Martínez-Botí *et al*., 2015), and the present sustained rate of increase of 2.2 ppm yr^{-1} (NOAA/ESRL[2]), is the highest recorded for the last 20,000 years (Prentice *et al*., 2001). For these reasons more than 11,000 scientists around the world recently declared that "planet Earth is facing a climate emergency" (Ripple *et al*., 2019).

Apart from warming itself, human activities are also changing the ocean's chemistry, as about 30% of anthropogenic CO_2 emissions end up in the surface waters of the ocean (Sabine *et al*., 2004; Le Quéré *et al*., 2018; also Fig. 1). The net effect of dissolving CO_2 in seawater is:

$$CO_2 + H_2O \Rightarrow H_2CO_3 \Rightarrow HCO_3^- + H^+,$$

---

[1] Global trend curated by Ed Dlugokencky and Pieter Tans, NOAA/ESRL, data available at: https://www.esrl.noaa.gov/gmd/ccgg/trends/gl_trend.html last accessed 7 December 2020.

[2] Mean for 2002-2019 period reported by Ed Dlugokencky and Pieter Tans, NOAA/ESRL, data available at: https://www.esrl.noaa.gov/gmd/ccgg/trends/gl_data.html last accessed 7 December 2020.

resulting in an increase of CO_2 partial pressure (pCO_2) in surface waters and decreasing both ocean pH (0.14 units relative to preindustrial levels[3] corresponding to a 38% increase in acidity mostly during the last three decades, Fig. 1) and carbonate ions (CO_3^{2-}), a phenomenon termed ocean acidification (OA, reviews in Fabry *et al*., 2008; Hofmann *et al*., 2010). OA reduces saturation states of $CaCO_3$ minerals (calcite, aragonite, and high-Mg calcite), with $CaCO_3$ saturation state with respect to calcite, defined as:

$$\Omega_{cal} = [Ca^{2+}] \cdot [CO_3^{2-}] / Ksp_{cal},$$

where Ksp_{cal} represents the apparent solubility constant for calcite.

Although most surface waters are expected to remain super-saturated with respect to calcite ($\Omega_{cal} > 1$), which is less soluble than aragonite, the drop in Ω_{cal} might still result in decreases in calcite biomineralization (Hofmann and Schellnhuber, 2009). At the individual and population levels, OA reduces calcification rates by enhancing dissolution and producing shifts in the acid-base balance of intracellular fluids, which compromises calcification processes (reviews in Fabry *et al*., 2008; Hofmann *et al*., 2010). Growing evidence shows that marine benthic organisms, such as corals and mollusks, may mitigate the effects of OA through physiological compensating mechanisms, but this mitigation may incur an energetic cost (Findlay *et al*., 2009; Venn *et al*., 2013; Comeau *et al*., 2018). Assessing OA effects at community and ecosystem levels is a high priority (Riebesell and Gattuso, 2015), with studies

---

[3] Considering 8.2 as pH baseline and station ALOHA time-series data (adapted from Dore *et al*., 2009, available at: https://hahana.soest.hawaii.edu/hot/products/products.html last accessed 14 January 2021).

suggesting biodiversity losses resulting in reduced habitat complexity and simplification of the ecosystems (Fabricius *et al*., 2014; Agostini *et al*., 2018).

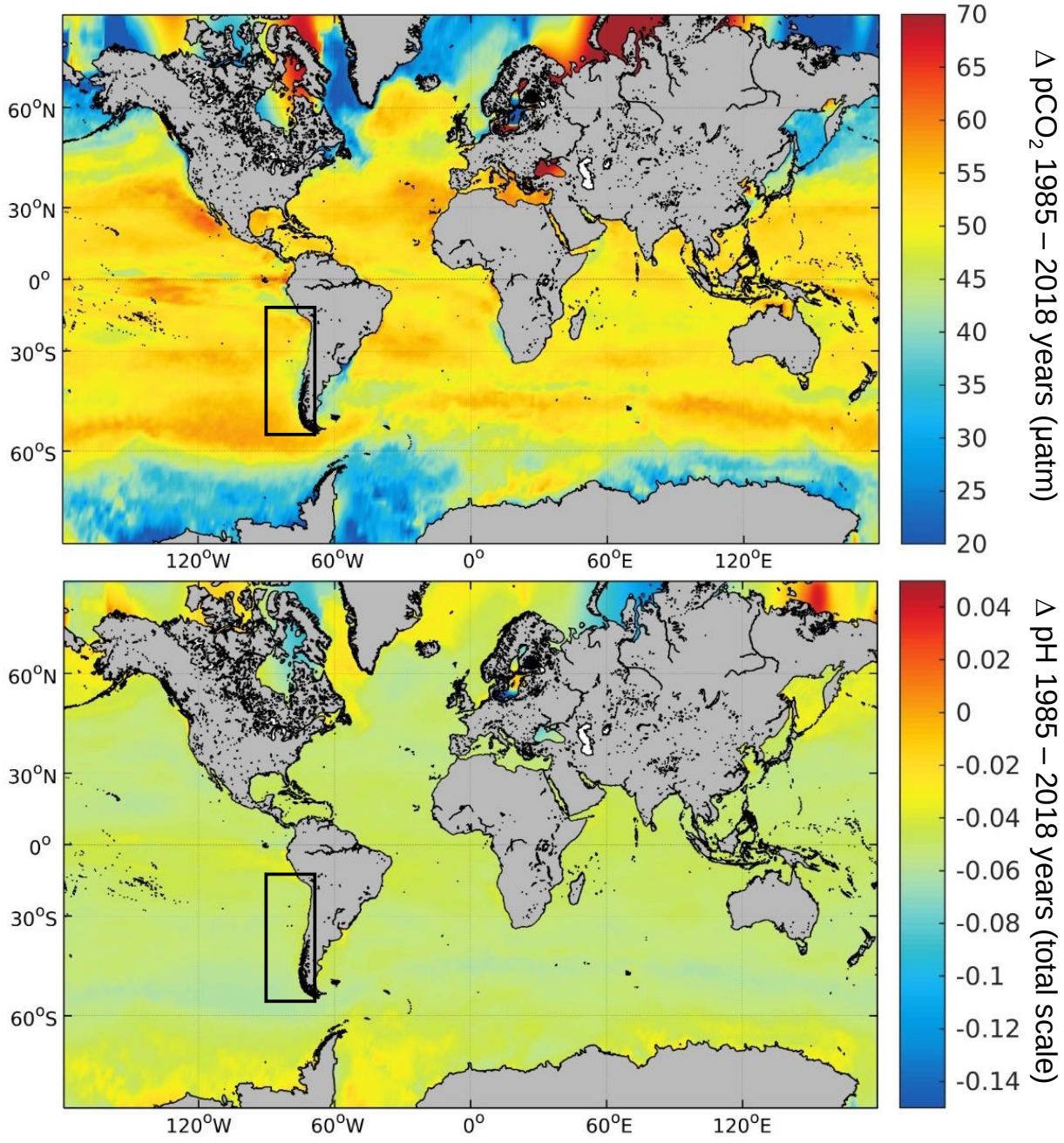

FIGURE Nº 1.1 Global change in pCO_2 and pH surface levels during 1985-2018 period. It was obtained by subtracting the 1985 and 2018 annual climatologies. The monthly 1º x 1º gridded data-set curated by Gregor and Gruber (2021) was processed and plotted using Matlab v. R2019a on Ubuntu 18.04. Surrounded by a rectangle is the oceanic region addressed by this thesis.

1.2 The role of planktonic calcifiers in the ocean's carbon cycles. Calcification in coccolithophores and the PIC:POC ratio

Coccolithophores carry out most of the $CaCO_3$ precipitation in pelagic systems and also exported to the deep-sea (Ziveri *et al*., 2007; Buitenhuis *et al*., 2019), exerting a great impact on the ocean carbon cycle and on the Earth's climate. In contrast to other calcifying organisms, calcification in coccolithophores occurs intracellularly through the production of coccoliths by use $CaCO_3$ in the form of calcite (reviewed by Taylor *et al*., 2017). Each coccolith is produced in a separate Golgi-derived vesicle, and requires the maintenance of sustained net fluxes of Ca^{2+} and inorganic carbon (primarily HCO_3^-) from the external medium.

Calcification involves the net reaction:

$$Ca^{2+} + 2HCO_3^- \Rightarrow CaCO_3 + H_2O + CO_2.$$

Thus, the effect of calcification is to lower total alkalinity and dissolved inorganic carbon pools, and increase the pCO_2 levels in pelagic systems, which represent a net CO_2 source into the atmosphere (reviewed by Rost and Riebesell, 2004). Nevertheless, when the depth variation in the stoichiometry of $CaCO_3$ production and dissolution is considered, that pelagic $CaCO_3$ is either neutral or perhaps a net CO_2 sink into the ocean (Smith, 2013). On the other hand, carbon fixation through photosynthesis reduces seawater pCO_2, balancing the ratio of calcite to organic carbon production in surface waters (the PIC:POC ratio reviewed by Paasche, 2002). Moreover, the presence of coccoliths in fecal pellets and other sinking organic aggregates increases the sinking velocity of particulate organic matter (the "ballast" hypothesis, Klaas and Archer, 2002; Sanders *et al*., 2010; Menschel and González, 2019), thereby influencing the "organic carbon pump" efficiency (reviewed by Passow and Carlson, 2012). The PIC:POC ratio fluctuates

around 1:1, due to changes at the organism (e.g., variation in gene that control calcification) and ecosystem levels (e.g., biotic and abiotic factors that influence growth and/or calcification) (Zondervan, 2007). For example, a decrease in coccolithophore $CaCO_3$ precipitation triggered by OA could increase atmospheric CO_2, via reduced efficiency of $CaCO_3$ and organic carbon pumps (e.g., Hofmann and Schellnhuber, 2009; Biermann and Engel, 2010). Although the carbon flux through the $CaCO_3$ pump is about one-tenth those from organic carbon pump (Sarmiento *et al*., 2002), the total carbon stored in limestone (primarily biogenic limestone) represent the biggest carbon reservoir in the Earth (Sigman and Boyle, 2000). For these key functional roles in global carbon cycles, a large research effort has been put into understanding the consequences of OA on coccolithophore calcification.

1.3 Classification of coccolithophores. *Emiliania huxleyi*, the most widespread and abundant coccolithophore species

Classification of coccolithophores is based predominantly on morphological characters, of which today around 280 species are recognized (Young *et al*., 2003). This monophyletic group of potentially calcifying haptophytes has been grouped into the subclass Calcihaptophycidae (Haptophyta, Prymnesiophyceae) separate from noncalcifying haptophytes *sensu stricto* (de Vargas *et al*., 2007). Within the order Isochrysidales, the family Noëlaerhabdaceae, and in particular the species *Emiliania huxleyi,* appears to numerically dominate coccolithophore assemblages in most natural samples (Paasche, 2002). For example, in the cold-waters of the subarctic North Atlantic, it can form large blooms ($> 10^6$ cells L^{-1}, Holligan *et al*., 1993; Brown and Yoder, 1994). In a wide range of other temperate, sub-tropical, and tropical waters, *E. huxleyi* is also typically found in cell abundances varying with annual productivity cycles within the range of 10^3-10^5 cells L^{-1} (Paasche, 2002). Similar ranges have been reported in both

oligotrophic (e.g., Okada and McIntyre, 1979; Baumann *et al*., 2008; Beaufort *et al*., 2008) and coastal regions (e.g., Giraudeau *et al*., 1993; Smith *et al*., 2012). This ecological versatility can be seen as a result of intraspecific genetic, genomic (Hagino *et al*., 2011; Kegel *et al*., 2013; Read *et al*., 2013; Bendif *et al*., 2014; von Dassow *et al*., 2015; Bendif *et al*., 2016) and morphological diversification (Young and Westbroek, 1991; Young *et al*., 2003). For example, Hagino *et al*. (2011), based on mitochondrial DNA, separated two major ecotypes of *E. huxleyi*, a cold-water group occurring in SubArctic North Atlantic and Pacific, and a warm-water group occurring in the subtropical Atlantic and Pacific, and in the Mediterranean Sea (also see Beaufort *et al*., 2011; Bendif *et al*., 2014). At the genome level, *E. huxleyi* exhibit extensive genome variability reflected in a diverse metabolic repertoire, which is thought to underpin its capacity to thrive in very diverse habitats under a wide variety of environmental conditions (Kegel *et al*., 2013; Read *et al*., 2013; von Dassow *et al*., 2015).

1.4 Global biogeography of coccolithophores, and a close-up to the Eastern South Pacific

Coccolithophore biogeography studies were catalyzed in the 1970's by the advent of scanning electronic microscopy that permitted directly viewing the coccoliths (reviews in Winter *et al*., 1994; Baumann *et al*., 2005; Giraudeau and Beaufort, 2007). The biogeographic zones of coccolithophores have been determined from the distinct species assemblages found in the water column and/or surface-sediments. From earlier extensive studies in the Atlantic (McIntyre and Bé, 1967) and Pacific (Okada and Honjo, 1973), the rough distribution of coccolithophores can be divided into four mayor latitudinal zones: subpolar, temperate, subtropical and tropical. In part, these latitudinal zones may reflect temperature growth optima of coccolithophore species (Buitenhuis *et al*., 2008), but even at this level, other factors can play a major role. For example, regional studies have shown that the horizontal and vertical distributions of coccolithophores

are controlled by water masses (Friedinger and Winter, 1987) and water stratification (Hagino *et al*., 2000), respectively. Moreover, floral composition varies seasonally (e.g., Okada and McIntyre, 1979), and is associated with the change in nutrient levels during upwelling events (e.g., Mitchell-Innes and Winter, 1987; Giraudeau *et al*., 1993). Finally, it has been proposed that the realized niche of *E. huxleyi* is partly defined by physical and chemical conditions unfavorable to large diatoms (Tyrrell and Merico, 2004; Smith *et al*., 2017). Nevertheless, although we have gained some clarity about the importance of these environmental controls on coccolithophore flora, it needs to be integrated with other factors, such as, mortality by grazing (e.g., Harris, 1994), viral-lysis (e.g., Vardi *et al*., 2012), iron-limitation (e.g., Nielsdóttir *et al*., 2009), and CO_2/pH gradients (e.g., Beaufort *et al*., 2011) into a comprehensive framework.

Coccolithophore biogeographic information in the Eastern South Pacific (ESP) is scarce and sporadic (McIntyre *et al*., 1970; Hagino and Okada, 2004; Beaufort *et al*., 2008; Menschel *et al*., 2016; Bendif *et al*., 2016). The study conducted by McIntyre *et al*. (1970) in the Pacific included sampling points mostly in tropical, subtropical and subpolar ESP waters (> 90º west). The cold-water variety of *E. huxleyi* (0-14 ºC temperature range) appears to dominate the floras (50-100 % of the forms present) in subpolar waters of both hemispheres (McIntyre *et al*., 1970). Three species of the genus *Gephyrocapsa*: *G. ericsonii, G. oceanica* and *G. caribbeanica* (properly, *G. muellerae*; see Young *et al*., 2003) were found living in Pacific waters. *G. oceanica* showed the most restricted range, being limited to tropical and warm subtropical waters (> 19 ºC). *G. muellerae* is the most widespread species, with a preference for cool waters ranging from 5 to 15 ºC. *G. ericsonii* reached its maximum concentration between 15-19 ºC in subtropical waters (McIntyre *et al*., 1970). Three decades later, Hagino and Okada (2004) presented a study on the horizontal distribution of coccolithophores in a longitude-latitude gradient in the

equatorial-subequatorial Pacific (between 20º N and 20º S). This study included water samples from the ESP, collected in February of 1964 off the coast of southern Peru and northern Chile. Within the main groups, the *E. huxleyi* common assemblage (ECA) was found in colder waters of the eastern equatorial and subequatorial South Pacific (Hagino and Okada, 2004). ECA was divided into two subgroups: the ECA-a and ECA-b are distributed in the SE equatorial Pacific and the neritic waters off South America, respectively. ECA-a is characterized by *E. huxleyi* and small-types of *Gephyrocapsa* and *Reticulofenestra* (reassigned to the genus *Gephyrocapsa*, see Bendif *et al*., 2016). In ECA-b, *E. huxleyi* was the only common member contributing 8-98 % of the total flora. Hagino and Okada (2004) concluded that the westward and latitudinal oligotrophication associated with the transition from the upwelling centers to the stratified waters appeared to drive coccolithophore assemblage zonation in the equatorial-subequatorial Pacific. Later, Beaufort *et al*. (2008) studied coccolithophore calcite production along temperature, salinity and productivity gradients in the ESP (~ 70-140º W). They found that east of the South Pacific Gyre (~ 110º W) Noëlaerhabdaceans (including *E. huxleyi* and several species of the genus *Gephyrocapsa*) dominated the coccolithophore community, with relative abundances ranging from 60-100 %. From 100º W to the Chilean coast, *E. huxleyi* dominated coccolithophore communities. *G. ericsonii* and *G. parvula* always formed a minor part of the coccolithophore assemblages. Beaufort *et al*. (2008) concluded that this ocean area can be considered the most extreme oligotrophic system, with the deepest chlorophyll maximum and the clearest waters ever reported (also see Morel *et al*., 2007). Coccolithophore assemblages appear to be adapted to these conditions with maximum cell density concentrated in the depth chlorophyll maximum (Beaufort *et al*., 2008).

1.5 Coccolithophore responses to ocean acidification: from short-term culture and mesocosm experiments to long-term field correlative studies

Most studies assessing the coccolithophore responses to OA have been performed in short-term culture experiments, which manipulate the carbonate system to mimic pre-industrial, present and future CO_2/pH levels. A wide range of growth, calcification (PIC) and productivity (POC) responses to changes in seawater carbonate chemistry have been reported, mostly using the cosmopolitan and most abundant species *E. huxleyi* (reviewed by Meyer and Riebesell, 2015). Field studies correlating coccolithophore community composition, abundances, calcification, and phenotypes with natural environmental gradients (in pH and other carbonate chemistry parameters) offer an important complement to culture experiments. For example, Beaufort *et al*. (2011) studied the relationship between the calcite mass production of coccolithophores and the physical-chemical environment, using modern-seawater and fossil-sedimentary samples distributed globally. They found a general pattern of decreasing calcification with increasing pCO_2 and a concomitant decrease in $[CO_3^{2-}]$. Interestingly, overall calcite mass variability was predominantly the result of genus and intra-species (morphotypes) shifts in the assemblages (also see Cubillos *et al*., 2007; D'Amario *et al*., 2018). Thus, as $[CO_3^{2-}]$ decreased, the coccolithophore assemblages shifted away from composed predominantly by large and heavily-calcified *G. oceanica* cells, through intermediate moderate-calcified (morphotype A) *E. huxleyi* to smaller lightly-calcified *E. huxleyi* cells (morphotype B/C or C; Beaufort *et al*., 2011). In two sampling sites they discovered a heavily calcified *E. huxleyi* morphotype inhabiting Pacific waters off the Chilean coast that goes against the general trend. This larger and high calcite-weight *E. huxleyi* morphotype (henceforth referred to as R hyper-calcified) has been only reported inhabiting the upwelling zones near the central coast of Chile, where relatively high

pCO_2/low pH waters emerge (Beaufort *et al*., 2011). According to Beaufort *et al*., the presence of this morphotype does not mask the main pattern of decreasing calcification at low CO_3^{2-}, but highlights the complexity of assemblage-level responses to environmental forcing factors.

In agreement with Beaufort *et al*. (2011), a reduction in *E. huxleyi* calcification state from predominantly moderate-calcified A-morphotype to lightly-calcified morphotype B/C cells was found in a north to south pH/Ω_{cal} decreasing gradients along the Argentinian Patagonian Shelf (Poulton *et al*., 2011; 2013). Conversely, Smith *et al*. (2012) found a pronounced seasonality in *E. huxleyi* morphotypes in the Bay of Biscay, with an increase in the proportion of over-calcified A-morphotype cells occurring in the winter decline of Ω_{cal} (also see Rigual-Hernández *et al*., 2020). Later, Young *et al*. (2014) found no effect of seawater carbonate chemistry on coccolithophore calcification in coccolithophore assemblages of the northwestern European continental shelf. Finally, Smith *et al*. (2012), Young *et al*. (2014), and Rigual-Hernández *et al*. (2020) concluded that carbonate chemistry is not the sole and overriding environmental factor that controls coccolithophore calcification, in contrast to the overall global trend found by Beaufort *et al*. (2011) and other field studies (Poulton *et al*., 2011; 2013; D'Amario *et al*., 2018), hence there is no overall consensus on this subject. As Beaufort *et al*. (2011) had a single cruise with few sampling points: can the presence and dominance of this heavily-calcified form be confirmed? Is it especially OA-tolerant?

1.6 The Eastern South Pacific as a natural laboratory for understand ocean acidification

The ESP off the coast of Chile and Peru presents a natural laboratory for study the responses of organisms to OA. The coastal zone is naturally acidified, with surface waters reaching very high pCO_2 (> 1,000 µatm) and low pH levels (< 7.8) during upwelling events (Friederich *et al*., 2008; Torres *et al*., 2011), values that are similar to those predicted for most of the surface ocean by

year 2100 (Orr *et al*., 2005). To the south, the Patagonia fjord-channel systems also provide especially interesting natural laboratories to investigate how coccolithophores may be affected by environmental conditions due to high variability in chemical and biotic conditions. Generally, low salinity and low alkalinity surface waters are undersaturated in dissolved CO_2 during spring-summer seasons (Torres *et al*., 2011). The Archipelago Madre de Dios (AMD) is an interesting exception, where extreme precipitation/runoff in the limestone western AMD basin produces low salinity-high alkalinity surface waters while maintaining low dissolved silicate compared with the batholith eastern basins (Torres *et al*., 2020). These features create an especially interesting contrast for exploring the influence of chemical conditions on the ecology of calcified phytoplankton, as changes in Ω_{cal} are mostly driven by freshening rather than upwelling of high pCO_2.

In this context, the ESP was utilized as natural laboratory to study how the coccolithophore species and *E. huxleyi* populations (morphotypes) vary with natural pCO_2/pH environments, as well as, evaluate their specific responses to targeted pCO_2/pH levels set in the lab, using the abundances, biomass, growth rates, and calcification-level as response variables. This thesis is comprised of two chapters that have the following content:

Over-calcified forms of the coccolithophore Emiliania huxleyi in high-CO_2 waters are not preadapted to ocean acidification focuses on experimentally test if the correlation observed between the *Emiliania huxleyi* over-calcified forms with high pCO_2/low pH levels in the ESP indicate these morphotypes are adapted to ocean acidification.

Abundances and morphotypes of the coccolithophore Emiliania huxleyi in southern Patagonia compared to neighboring oceans and northern-hemisphere fjords deals with variation

of *Emiliania huxleyi* abundances, biomass, and calcification-level with hydrology and carbonate chemistry conditions and biological features in fjords/channels systems of southern Patagonia.

2 CHAPTER ONE: Over-calcified forms of the coccolithophore *Emiliania huxleyi* in high-CO_2 waters are not preadapted to ocean acidification

Authors: Peter von Dassow[1,2,3], Francisco Díaz-Rosas[1,2], El Mahdi Bendif[4], Juan-Diego Gaitán-Espitia[5], Daniella Mella-Flores[1], Sebastian Rokitta[6], Uwe John[6,7], and Rodrigo Torres[8,9]

[1] Facultad de Ciencias Biológicas, Pontificia Universidad Católica de Chile, Santiago, Chile

[2] Instituto Milenio de Oceanografía de Chile, Concepción, Chile

[3] UMI 3614 Evolutionary Biology and Ecology of Algae, CNRS, Sorbonne Université, Pontificia Universidad Católica de Chile, Universidad Austral de Chile, Station Biologique de Roscoff, 29680 Roscoff, France

[4] Departament of Plant Sciences, University of Oxford, OX1 3RB Oxford, UK

[5] CSIRO Oceans and Atmosphere, GP.O. Box 1538, Hobart 7001, TAS, Australia

[6] Alfred Wegener Institute Helmholtz Centre for Polar and Marine Research, Bremerhaven, Germany

[7] Helmholtz Institute for Functional Marine Biodiversity (HIFMB), Ammerländer Heerstt. 231, 26129 Olderburg, Germany

[8] Centro de Investigación en Ecosistemas de la Patagonia (CIEP), Coyhaique, Chile

[9] Centro de Investigación: Dinámica de Ecosistemas marinos de Altas Latitudes (IDEAL), Punta Arenas, Chile

Correspondence to: Peter von Dassow (pvondassow@bio.puc.cl)

2.1 ABSTRACT

Marine multicellular organisms inhabiting waters with natural high fluctuations in pH appear more tolerant to acidification than conspecifics occurring in nearby stable waters, suggesting that environments of fluctuating pH hold genetic reservoirs for adaptation of key groups to ocean acidification (OA). The abundant and cosmopolitan calcifying phytoplankton *Emiliania huxleyi* exhibits a range of morphotypes with varying degrees of coccolith mineralization. We show that *E. huxleyi* populations in the naturally acidified upwelling waters of the eastern South Pacific, where pH drops below 7.8 as is predicted for the global surface ocean by the year 2100, are dominated by exceptionally over-calcified morphotypes whose distal coccolith shield can be almost solid calcite. Shifts in morphotype composition of *E. huxleyi* populations correlate with changes in carbonate system parameters. We tested if these correlations indicate that the hyper-calcified morphotype is adapted to OA. In experimental exposures to present-day vs. future pCO_2 (400 vs. 1200 µatm), the over-calcified morphotypes showed the same growth inhibition (−29.1±6.3 %) as moderately calcified morphotypes isolated from non-acidified water (−30.7±8.8 %). Under the high-CO_2–low-pH condition, production rates of particulate organic carbon (POC) increased, while production rates of particulate inorganic carbon (PIC) were

maintained or decreased slightly (but not significantly), leading to lowered PIC / POC ratios in all strains. There were no consistent correlations of response intensity with strain origin. The high-CO_2–low-pH condition affected coccolith morphology equally or more strongly in over-calcified strains compared to moderately calcified strains. High-CO_2–low-pH conditions appear not to directly select for exceptionally over-calcified morphotypes over other morphotypes, but perhaps indirectly by ecologically correlated factors. More generally, these results suggest that oceanic planktonic microorganisms, despite their rapid turnover and large population sizes, do not necessarily exhibit adaptations to naturally high-CO_2 upwellings, and this ubiquitous coccolithophore may be near the limit of its capacity to adapt to ongoing ocean acidification.

2.2 INTRODUCTION

Coccolithophores are planktonic single-celled photoautotrophs mostly in the range of 3–20 μm and characterized by bearing calcite plates (coccoliths) (Monteiro *et al*., 2016) and represent one of the most abundant and widespread groups of marine eukaryotic phytoplankton (Iglesias-Rodríguez *et al*., 2002; Litchman *et al*., 2015). In addition to being important primary producers, coccolithophores contribute most of the calcium carbonate ($CaCO_3$) precipitation in pelagic systems. Although $CaCO_3$ precipitation in the surface is a source of CO_2, i.e., the "carbonate counter pump" (Frankignoulle *et al*., 1994), $CaCO_3$ may enhance sinking of organic matter by imposing a ballast effect on sinking aggregates (Armstrong *et al*., 2002; Sanders *et al*., 2010). Thus, this plankton functional group has a complex role in ocean carbon cycles. Roughly a third of current anthropogenic CO_2 emissions are being absorbed in the ocean (Sabine *et al*., 2004), driving a decrease in pH, the conversion of CO_3^{2-} to HCO_3^-, and a drop in saturation states of the $CaCO_3$ minerals aragonite and calcite (Ω_{Ar}, Ω_{Ca}), phenomena collectively termed ocean acidification (OA; Orr *et al*., 2005). Although most surface waters are expected to remain supersaturated with respect to calcite ($\Omega_{Ca} > 1$), which is less soluble than aragonite, the drop in Ω_{Ca} might still result in decreases in calcite biomineralization (Hofmann and Schellnhuber,

2009). Understanding the response of coccolithophores to OA is thus needed for predicting how pelagic ecosystems and the relative intensity of the biological carbon pumps will change as atmospheric CO_2 continues to increase.

Many studies designed to assess coccolithophores' responses to low pH have been performed in short-term culture and mesocosm experiments on timescales of weeks to months, and carbonate systems were usually manipulated to mimic preindustrial, present, and future CO_2 levels. Mesocosm studies have shown that North Sea populations of the cosmopolitan and abundant species *Emiliania huxleyi* are negatively impacted by low-pH conditions (Engel *et al*., 2005; Riebesell *et al*., 2017). However, a wide range of growth, calcification (particulate inorganic carbon, PIC), and productivity (particulate organic carbon, POC) responses to high-CO_2–low-pH conditions have been reported in laboratory cultures of *E. huxleyi*, mostly using different regional strains (Riebesell *et al*., 2000; Iglesias-Rodriguez *et al*., 2008; Langer *et al*., 2009; Müller *et al*., 2015a, 2017; Olson *et al*., 2017; Jin *et al*., 2017). According to a recent comprehensive review and meta-analysis (Meyer and Riebesell, 2015), the mean responses of *E. huxleyi* averaged over 19 studies indicated that high-CO_2–low-pH conditions have a negative effect on PIC quotas and production rates as well as PIC / POC ratios but no consistent effects on POC quotas and production rates. The response variability among strains of *E. huxleyi* (Langer *et al*., 2009; Müller *et al*., 2015a) is also seen within the genus *Calcidiscus* (Diner *et al*., 2015) and suggests a high potential for genetic adaptation within coccolithophores.

Such adaptive capacity to high-CO_2–low-pH conditions has been suggested for *E. huxleyi* in long-term lab-based experimental evolution studies (up to 2000 generations) on clonal strains (Lohbeck *et al*., 2012; Schlüter *et al*., 2016). It is still difficult to know to which extent such experiments reflect real-world adaptation processes. First, only asexually propagating cells

have yet been explored in the lab, while sexual recombination in natural populations is expected to accelerate adaptation (McDonald *et al*., 2016). Second, calcification is costly and in nature must be maintained by providing benefits to the cell. What these benefits are remains unclear. It has been suggested that coccoliths may provide defense against grazing or parasites and modify light–UV levels reaching the cell, amongst other proposed functions (Monteiro *et al*., 2016). The benefits of calcification likely vary among species and may have changed over the course of evolution or with environmental change. For example, in paleo-oceans, it might have helped alleviate toxicity from Ca^{2+} when levels reached up to 4-fold higher than in the modern ocean during the Cretaceous (Müller *et al*., 2015b). The long-term and nonlinear declines in calcification observed in experimental adaptation to high CO_2 and low pH (Schlüter *et al*., 2016) thus might have a high potential cost if such changes occurred in nature.

Complementary to experimental approaches, observational studies that correlate coccolithophore communities and levels or rates of calcification with variability in carbonate system parameters offer important insights into possible adaptations to high CO_2 and low pH. Focusing only on *E. huxleyi* and the closely related genus *Gephyrocapsa* (both within the family Noelaerhabdaceae), a general pattern has been documented of a decreasing calcite mass of coccoliths and coccospheres with increasing pCO_2 for both modern and recent fossil coccolithophores across the world's ocean basins (Beaufort *et al*., 2011). This pattern involved shifts away from more heavily calcified *Gephyrocapsa* that dominated assemblages under the lowest pCO_2 towards a spectrum of *E. huxleyi* morphotypes that were more abundant under intermediate and high pCO_2: *E. huxleyi* "type A" morphotypes with heavier coccoliths (more calcite per coccolith) dominated *E. huxleyi* populations in waters with intermediate pCO_2 while

"type B/C" or "type C" morphotypes with successively lighter coccoliths dominated in higher-pCO_2 waters (Beaufort *et al*., 2011; Poulton *et al*., 2011).

Beyond this comparably clear pattern, the survey by Beaufort *et al*. (2011) also reported one important exception to the general trend: at two sites approaching the Chilean upwelling zone, forms of *E. huxleyi* with exceptionally over-calcified coccoliths dominated in naturally acidified upwelling waters, where pCO_2 reaches values more than 2-fold higher than the equilibrium with present-day atmospheric levels. Similarly, a year-long monthly survey of coccolithophore communities in the Bay of Biscay found that an over-calcified type A form dominated during the winter, when pCO_2 was highest, but contributed only a minor part to the *E. huxleyi* populations in summer, when pCO_2 was lowest (Smith *et al*., 2012). One explanation might be that over-calcified morphotypes are especially tolerant to such ocean acidification (OA) conditions.

The eastern South Pacific off the coast of Chile and Peru presents a natural laboratory for investigating such hypotheses regarding organisms' responses to ocean acidification. The coastal zone is naturally acidified, with surface waters frequently reaching pCO_2 levels > 1000 μatm and pH values < 7.7 during upwelling events (Friederich *et al*., 2008; Torres *et al*., 2011).

In this study, we surveyed the coccolithophore communities of the Chilean upwelling zone as well as adjacent coastal and offshore waters with varying pCO_2 levels and isolated *E. huxleyi* strains of dominant morphotypes. In lab-based experiments, three strains showing distinct over-calcification were compared with two moderately calcified type A morphotypes in terms of their response to altered CO_2 and pH (400 vs. 1200 μatm pCO_2) to investigate whether CO_2 might indeed be the environmental driver selecting for the extreme over-calcified morphotypes specific to the Chilean coast.

2.3 MATERIALS AND METHODS

2.3.1 Surveys

An oceanographic cruise (NBP 1305) was conducted on-board R/V *Nathaniel B. Palmer* (NBP) during the early austral winter (27 June–22 July 2013) along a transitional zone from coastal to open ocean waters off central-southern Peru and northern Chile (Fig. 1.1a). A total of 24 stations were sampled between 22 and 13º S and from 70 to 86º W (ranging from 47 to 1424 km from the coast). Central Chile coastal surveys were conducted onboard the R/V *Stella Maris II* (Universidad Católica de Norte) during the mid-spring of 2011 (12 October) and 2012 (28 November) and aboard a rented fishing launch (18–19 November 2012) in the high-pCO_2 upwelling zone in front of Tongoy Bay (TON), northern Chile (~ 30º S–72º W; Fig. 1.1b). These two coastal surveys consisted of seven sampling points distributed between 1 and 23 km off the coast. Another coastal sampling was conducted from a small launch (belonging to the Pontificia Universidad Católica de Chile) during the mid-spring of 2012 (10 November), in the upwelling zone in front of El Quisco Bay (QUI ~ 33º S–72º W; Fig. 1.1b). This coastal survey consisted of one sampling point located 4 km offshore. Finally, one sampling was conducted from a rented

fishing vessel during the mid-spring of 2011 (1 November), in the mesotrophic waters that surround the Juan Fernández Islands (JF; ~ 33º S–78º W; Fig. 1.1b).

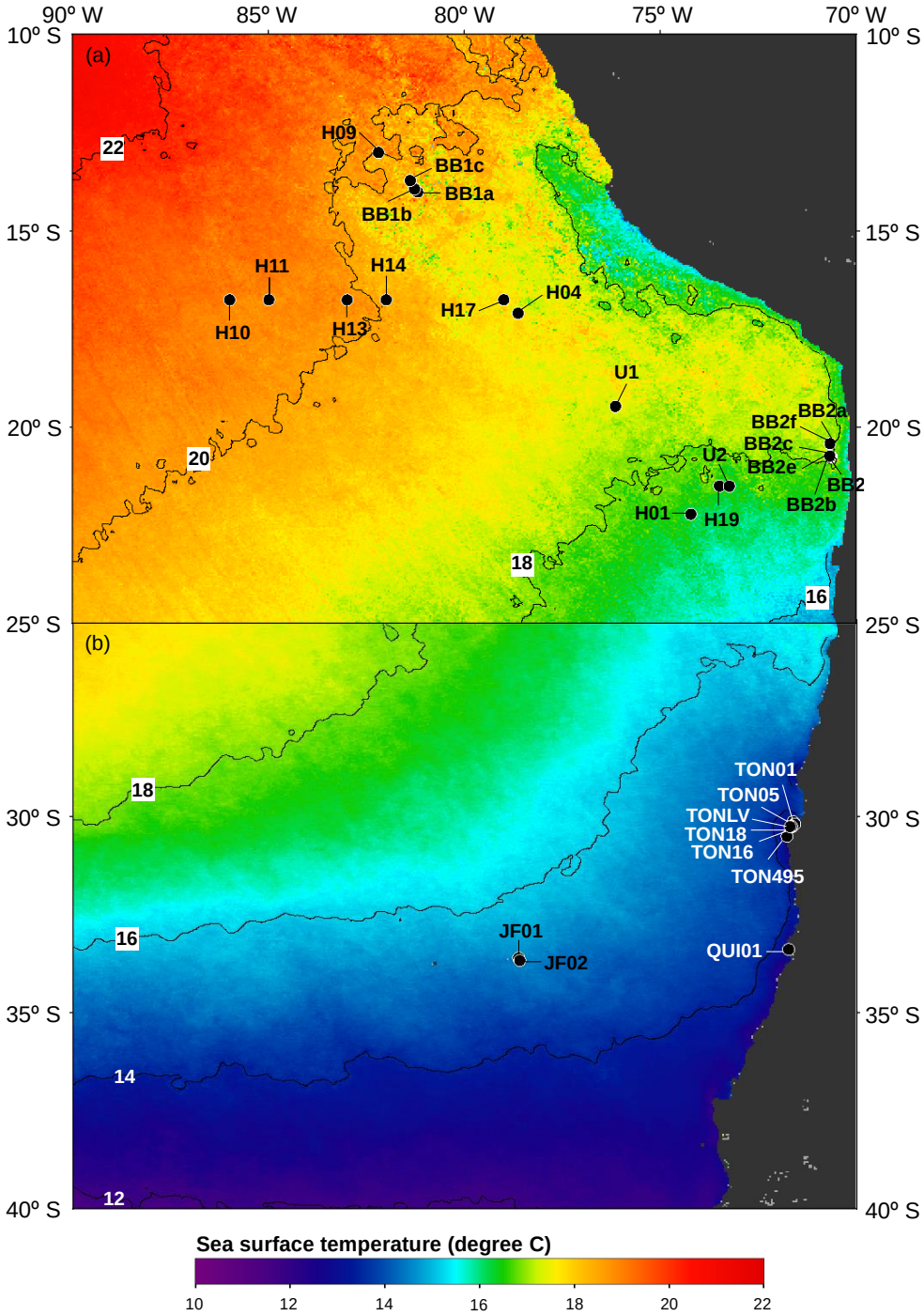

FIGURE Nº 2.1 Map of stations sampled during the NBP 1305 cruise (June–July 2013) **(a)** and in smaller field expeditions of October–November in 2011–2012 **(b)**. Sea surface temperature climatologies (2002–2014) are plotted for the months of July **(a)** and October **(b)**.

2.3.2 Physical-chemical oceanographic parameters

During the NBP cruise, temperature and salinity were measured with a SBE 25 CTD (Sea-Bird Scientific, Bellevue, WA, USA) from rosette casts or from the onboard running seawater system equipped with a SBE 45 conductivity sensor and a SBE 38 temperature sensor (both from Sea-Bird Scientific). During the 2011 cruise on the R/V *Stella Maris II*, an SBE 19 plus CTD was used (data courtesy of Beatriz Yannicelli). In other samplings, an SBE 18 plus CTD was used for water column measurements. On the 29 November 2012 cruise on the R/V *Stella Maris II*, surface samples were pumped continuously onboard in underway sampling and analyzed with a YSI Pro30 salinometer and thermometer (YSI, Yellow Springs, OH, USA).

In October 2011 and November 2012, duplicate 500 mL samples of surface seawater were collected into borosilicate bottles, fixed with 50 µL of $HgCl_2$ saturated solution, and stored until measurements of total dissolved inorganic carbon (DIC) and total alkalinity (TA). TA was determined using potentiometric titration in an open cell (Heraldsson *et al.*, 1997). Standardization was performed and the accuracy was controlled against a certified reference material (CRM Batch 115 bottled in September 2011) supplied by Andrew Dickson (Scripps Institution of Oceanography, https://www.ncei.noaa.gov/access/ocean-carbon-data-system/oceans/Dickson_CRM/batches.html, Dickson, 2010). The correction factor was approximately 1.002. Precision (variation among replicas) in TA was always less than 0.5 % (average 0.1%). DIC was determined using a fully automatic DIC analyzer (model AS-C3, Apollo SciTech, Newark, DE, USA), with variation among replicates averaging 0.1 % (max. 0.3 %). All the dissolved carbonate species from a seawater sample were extracted as CO_2 gas through acidification and nitrogen stripping. The CO_2 gas was then quantitatively detected with an infrared LI-7000 CO_2 analyzer (LI-COR Environmental, Lincoln, Nebraska USA). During

the expedition off Juan Fernández (November 2011) pH and TA were measured in fixed samples. The pH was measured on the total ion scale using spectrophotometric detection of m-cresol purple absorption in a 100 mm quartz cell thermally stabilized at 25.0º C (Dickson *et al*., 2007) with a BioSpec 1600 spectrophotometer (Shimadzu Scientific Instruments, Kyoto, Japan), with pH among replicas varying less than 0.01 units. During the NBP cruise, direct measurements of sea surface pCO_2 using nondispersive infrared detection were obtained from continuous measurements by the Research Vessel Data Acquisition System (RVDAS; Lamont-Doherty Earth Observatory, Columbia University) in addition to TA samples.

Saturation states of aragonite (Ω_{Ar}) as well as calcite (Ω_{Ca}) and other carbonate system parameters were estimated from the DIC–TA pairs (for samplings off the central Chilean coast in October 2011 and November 2012), pH–TA (for expedition off the Juan Fernández Islands in November 2011), and pCO_2–TA pairs (for the NBP 1305 cruise during June–July 2013) using CO2SYS software (Pierrot *et al*., 2006) set with Mehrbach solubility constants (Mehrbach *et al*., 1973) refitted by Dickson and Millero (Dickson and Millero, 1987). Environmental parameters are provided in supplementary Table S1.

Mean sea surface temperature and chlorophyll a (chl a) monthly climatologies (2002–2014) were obtained from the MODIS-Aqua satellite (NASA Goddard Space Flight Center, Ocean Ecology Laboratory, and Ocean Biology Processing Group, 2014) and plotted using SeaDAS (Baith *et al*., 2001) version 7.1 for Mac OS X.

2.3.3 Phytoplankton analyses

Discrete seawater samples (Niskin bottles) containing planktonic assemblages were collected at various depths within the upper 150 m, depending on depth of the maximum chl a fluorescence (as proxy of phytoplankton) and from the onboard seawater system when Niskin samples were

not available. Duplicate 100 mL samples of seawater (previously filtered through 200 μm Nitex mesh) were fixed (final concentration 1 % formaldehyde, 0.05 % glutaraldehyde, and 10 mM borate pH 8.5) and stored at 4º C until light microscopic examination.

Samples were sedimented in 100 mL Utermöhl chambers for 48 h prior to counting. The absolute abundance of microplankton (20–200 μm in size) and coccolithophores (ranging from 2.5 to 20 μm in size, but mostly comprised of species within the range of 3–10 μm including *E. huxleyi*, several species of the genera *Gephyrocapsa*, and *Calcidiscus leptoporus*) were estimated with an inverted microscope (Olympus CKX41) connected to a digital camera (Motic 5.0). For counts of large diatoms, thecate dinoflagellates, and other planktonic cells (> 50 μm in size), a 20 x objective was used. For counts of small diatoms and athecate dinoflagellates (< 50 μm in size) a 40 x objective was used. For counts of total coccolithophores, a 40 x objective was used with cross-polarized light (Edmund Optics polarizers 54 926 and 53 347).

In parallel, duplicate 250 mL samples of seawater were filtered onto polycarbonate filters (0.2 μm pore size; Millipore), which were dried and stored in petri dishes until processing for identification of coccolithophore species and *E. huxleyi* morphotypes. A small cut portion of each dried filter was sputter-coated with gold. The identification and relative abundance of coccolithophore species was performed by counting a minimum of 80 coccospheres per sample with scanning electron microscopy (SEM) using either a TM3000 (Hitachi High-Technologies, Tokyo, Japan) or a Quanta 250 (FEI, Hillsboro, Oregon, USA). Classification followed Young *et al*. (2003). To estimate the absolute abundances of each species within the Noelaerhabdaceae family, which are difficult to distinguish using light microscopy, the relative abundance of each Noelaerhabdaceae species determined with SEM counts was multiplied by the absolute abundance of total Noelaerhabdaceae cells determined from light microscopy counts. SEM

images were also used to measure the minimum and maximum coccosphere diameters and coccolith lengths of each Noelaerhabdaceae species (ImageJ software version 1.48 for Mac OS X). Also, *E. huxleyi* cells were categorized according to Young *et al*. (2003), based on the distal shield and central plate of coccoliths. For analysis, they were grouped further: lightly calcified coccoliths exhibited delicate distal shield elements that were well separated from each other extending from the central area to the outer rim. The central element was completely open, and central area elements were either lacking, lath like, or plate like (Fig. 1.2). These corresponded to the morphotypes B, B/C, C, and O (Young *et al*., 2003; Hagino *et al*., 2011), a grouping that is supported by recent genetic evidence (Krueger-Hadfield *et al*., 2014). Moderately calcified coccoliths, corresponding to morphotype A (Young *et al*., 2003; Hagino *et al*., 2011), showed thicker distal shield elements that were fused near the central area and often at the rim but were otherwise separated and a grill central area within a cleanly delimited tube. Two over-calcified morphotypes were observed. One corresponded to the morphotype A over-calcified type reported in the Bay of Biscay (Smith *et al*., 2012) with coccolith central areas completely covered or nearly completely covered by elements of the central tube, but distal shield elements not fused (here referred to as A_CC). The second, which we refer to as R/over-calcified, corresponded to the R morphotype (distal shield elements fused and slits closed), which exhibited a continuous variation from a wide and open central area (Young *et al*., 2003) to the extreme forms, so far reported only in the eastern South Pacific (Beaufort *et al*., 2011), where tube elements had completely or partially overgrown the central area.

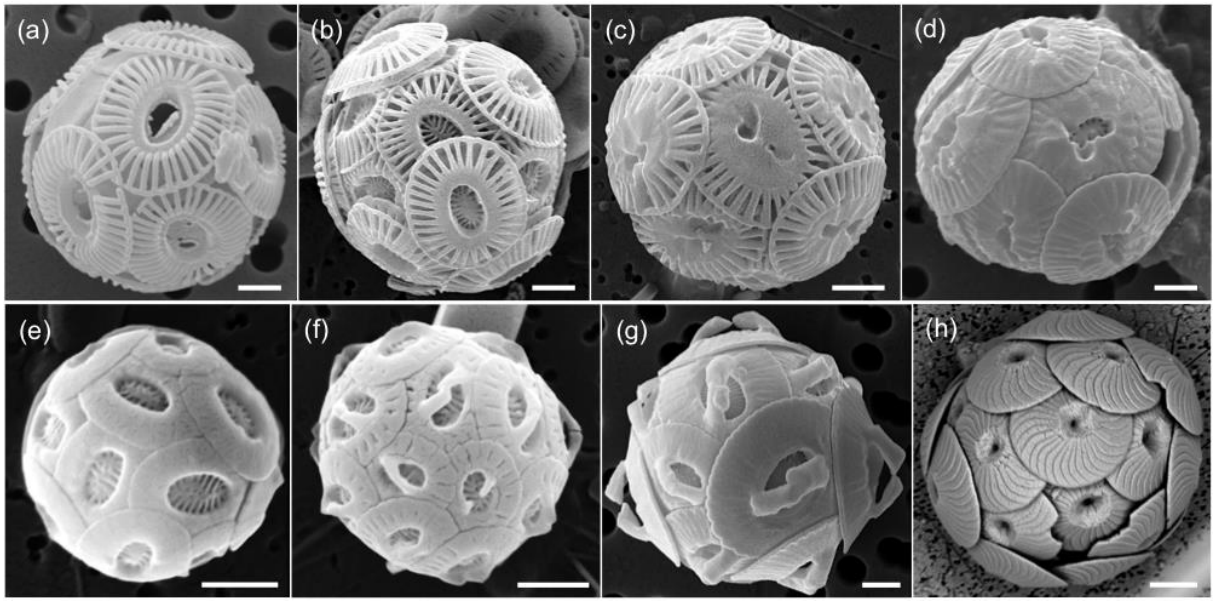

FIGURE Nº 2.2 The most abundant coccolithophores in the SE Pacific. **(a–d)** Morphotypes of *E. huxleyi*: lightly calcified **(a)**, moderately calcified A morphotype **(b)**, morphotype A_CC **(c)**, morphotype R/over-calcified **(d)**. *Gephyrocapsa parvula* **(e)**, *G. ericsonii* **(f)**, *G. muellerae* **(g)**, and *Calcidiscus leptoporus* **(h)**. Scale bars are 1 μm **(a–g)** and 3 μm **(h)**.

2.3.4 Isolation of *E. huxleyi* strains

Clonal isolates of coccolithophores were obtained from some stations through isolation of calcified cells using an Influx Mariner cell sorter as described previously (von Dassow *et al*., 2012; Bendif *et al*., 2016). During the NBP cruise, the Influx Mariner was in a portable onboard laboratory and isolation of coccolithophores occurred within 6 h of sample collection. For other samplings, live seawater samples were hand-carried to Concepción in a cooler with chilled water, and calcified cells were isolated within 24 h (without exposure to light or nutrient addition to minimize possible clonal reproduction between sampling and cell isolation). Calcified strains were identified using SEM and maintained at 15 ºC (Bendif *et al*., 2016).

2.3.5 Experimental testing of *E. huxleyi* responses to high CO_2 and low pH

The experiment was performed at the OA test facility of the Calfuco Marine Laboratory of the Universidad Austral de Chile (Torres *et al*., 2013). The aim was to investigate the effects of

short-term exposure to high-CO_2–low-pH conditions similar to those occurring in an upwelling event. The focus was on determining whether there were differences between the heavily calcified morphotypes and moderately calcified morphotypes in response to short-term exposure to CO_2, as would be expected to be experienced by phytoplankton cells from surrounding surface waters inoculating recently upwelled water, where both mooring-mounted and drifter-mounted sensors show pulses of high CO_2 over periods of about a week (Friederich *et al*., 2008). Experiments were conducted in temperature-controlled water baths at 15º C, with light intensities of 75 µmol photons m^{-2} s^{-1} in a 14 : 10 h light : dark cycle. Culture media were prepared from seawater collected in wintertime from the Quintay coast (central Chile); aged for > 1 month; enriched with 176 µM of nitrate, 7.2 µM of phosphate, and with trace metals and vitamins as described for K/2 medium (Keller *et al*., 1987); and sterilized by filtration through 0.2 µm Stericups (Merck Millipore, Billerica, MA, USA). Strains were acclimated to light and temperature conditions for at least two consecutive culture transfers, maintaining cell density below 200.000 cells mL^{-1} and ensuring exponential growth during the acclimation phase. Prior to inoculation, 4.5 L in 8 L cylindrical clear polycarbonate bottles (Nalgene) was continuously purged with humidified air with a pCO_2 of 400 and 1200 µatm for 24–48 h at the experimental temperature to allow the carbonate system to equilibrate (controlled with pH readings) as described in detail in Torres *et al*. (2013). When pH values had stabilized, four experimental bottles per strain per treatment were inoculated at an initial density of 800 cells mL^{-1} (day 0), and aeration with the air–CO_2 mixes was continued. Daily measures of pH at 25º C were made potentiometrically at 25.0º C using a Metrohm 826 pH meter (nominal accuracy ±0.003 pH units) (Metrohm, Herisau, Switzerland) with an Aquatrode Plus with Pt 1000 (Metrohm 60 253 100) electrode calibrated with tris buffer using established methodology (DOE, 1994; Torres *et*

al., 2013). Samples for TA measurement were taken on day 0 and at the end of the experiment and measured for calculation of full carbonate chemistry parameters as described above for natural seawater samples.

Daily cell counts were performed from day 2 using a Neubauer hemocytometer (as cells were too dilute for this method on day 0). Growth rate was calculated as specific growth rate μ (day^{-1}) = ln(N_f /N_0)/Δt, where N_0 and N_f are the initial and final cell concentrations and Δt is the time interval (days). The experimental cultures were harvested before cell concentrations reached 90000 cells mL^{-1} to minimize changes to the carbonate system from calcification and photosynthesis based on previous studies using R morphotype strains (Rokitta and Rost, 2012). Samples for measurement of POC and PIC were taken by filtering four 250 mL samples on 47 mm GF/F filters (pre-combusted for overnight at 500º C), which were then dried and stored in aluminium envelopes prior to measurement of C content by the Laboratorio de Biogeoquimica y Isotopos Estables Aplicados at the Pontificia Universidad Católica using a Flash EA2000 elemental analyzer (Thermo Scientific, Waltham, MA, USA), with a standard error level calculated to be within 0.008 mg C according to linear regression of calibration curves using acetanilide. For each culture, total carbon (TC) was measured on two replicate filters while POC was measured on two replicate filters after treatment by exposure for 4 h to 12 N HCl fumes (Harris *et al*., 2001; Lorrain *et al*., 2003). PIC was calculated as the difference between the TC and POC. POC and PIC concentrations were normalized to cell number, and POC and PIC production rates were obtained by multiplying cell-normalized POC and PIC quotas with specific growth rates. Samples were filtered and processed as described above for SEM analysis. For flow cytometry, 1.8 mL samples were fixed by adding 0.2 mL of a solution of 10 %

formaldehyde, 0.5 % glutaraldehyde, and 100 mM borate with a pH of 8.5 (which was stored frozen and thawed immediately before use).

SEM and flow cytometric assessments and analyses of coccoliths

Morphological analysis was performed on three replicates of each strain with a scanning electron microscope (Quanta 250) and images were analyzed with ImageJ. Attached coccoliths were measured following Rosas-Navarro *et al*. (2016). On average, a total of 606 (min. 418) coccoliths per treatment were analyzed. Coccoliths were classified into complete, incomplete, and malformed (Rosas-Navarro *et al*., 2016). In the R/over-calcified strains, fusion of radial elements and the overgrowth of inner tube elements of the distal shield complicated finer-scale assessments of coccolith formation. Therefore, we were highly conservative in categorizing coccoliths and grouped incomplete and malformed coccoliths for statistical analysis. Of all coccospheres imaged, only coccoliths that were oriented upwards (towards the beam) were selected for measurement so that coccolith length measurements were not affected by viewing angle. This meant that an average of 68 coccoliths were measured per strain per treatment. Measurements included coccolith length, the total area of the central area (defined by the inner end of distal shield radial elements), and the portion of the central area which was not covered by the inner tube.

Flow cytometry was performed using a BD Influx equipped with a 488 nm laser and small particle detector with polarization optics. The laser, optics, and stream were aligned using 3 μm Ultra Rainbow Fluorescent Particles (Spherotech, Lake Forest, IL, USA). The trigger was set on forward scatter light with the same polarization as the laser, with trigger level adjusted for each strain to ensure that all detached coccoliths could be detected. Cells were distinguished by red fluorescence (at 692 nm; due to chlorophyll). Detached coccoliths and calcified cells

were distinguished as previously described (von Dassow *et al*., 2012). Briefly, calcite-containing particles are above the diagonal formed from optically inactive particles on a plot of forward scatter with polarization orthogonal to the laser vs. forward scatter with polarization parallel to the laser. Also, calcite-containing particles are high in side scatter. Non-calcified cells fall on the diagonal formed by other particles, including cell debris, bacteria (if present), and calibration or alignment particles. Parameters analyzed included the number of detached coccoliths, percentage of calcified cells, relative change in depolarization of forward scatter light by detached coccoliths, and relative changes in red fluorescence (due to chlorophyll) of cells. All samples for a given treatment and strain were run on the same day with the same settings.

2.3.6 Statistical analysis

To test for significant correlations of environmental parameters (including carbonate chemistry) on *E. huxleyi* morphotype composition in the natural samples, redundancy analysis (RDA) was performed (see Supplement). For most analyses, we selected only data from the surface when multiple depths were available (see Sect. S1 in the Supplement for comparison of surface to deeper samples).

Data from experimental results were analyzed in Prism 6 (GraphPad software, Inc., La Jolla, CA, USA) using two-way ANOVA followed by Sidak post hoc pairwise analysis with correction for multiple comparison. Prior to testing, the PIC / POC ratio was $\log_2$-transformed while percentages (e.g., percentage of area, percentage of calcified cells) were expressed as proportions and arcsine-square-root transformed to permit the use of parametric testing. Significance was judged at the $p < 0.05$ level.

2.4 RESULTS

2.4.1 Changes in coccolithophore species and *E. huxleyi* morphotypes in natural communities vs. oceanographic conditions

Surface pH (< 10 m depth) at sampling sites ranged from 7.73 (in the El Quisco 2012 sampling) to 8.11 (in the JF sampling). In terms of carbonate chemistry, the surface waters of the ESP showed a general pattern of increasing CO_2 and decreasing pH as one moves from open ocean waters to the Chilean coastal upwelling zones; however, as expected, waters were never corrosive for calcite (Fig. 1.3a). More generally, the NBP and JF, as well as TON and QUI surveys, were conducted at a relatively low (average 411.2 ± 41.3 µatm; $N_{samples}$ = 27) and high (average 696.6 ± 110 µatm; $N_{samples}$ = 14) CO_2 levels, respectively.

Coccolithophore numerical abundances ranged from 1×10^3 cells to 76×10^3 cells L^{-1} (59 total samples) (Fig. 1.3b). A total of 40 coccolithophore species were found inhabiting the eastern South Pacific during the sampling period (Table S4). The Shannon diversity index ranged from 1.5 down to 0, while the Fisher's alpha index ranged from 4.0 down to 0, and both indices showed coccolithophore diversity was lowest in the most acidified natural waters (Fig. 1.3a and b).

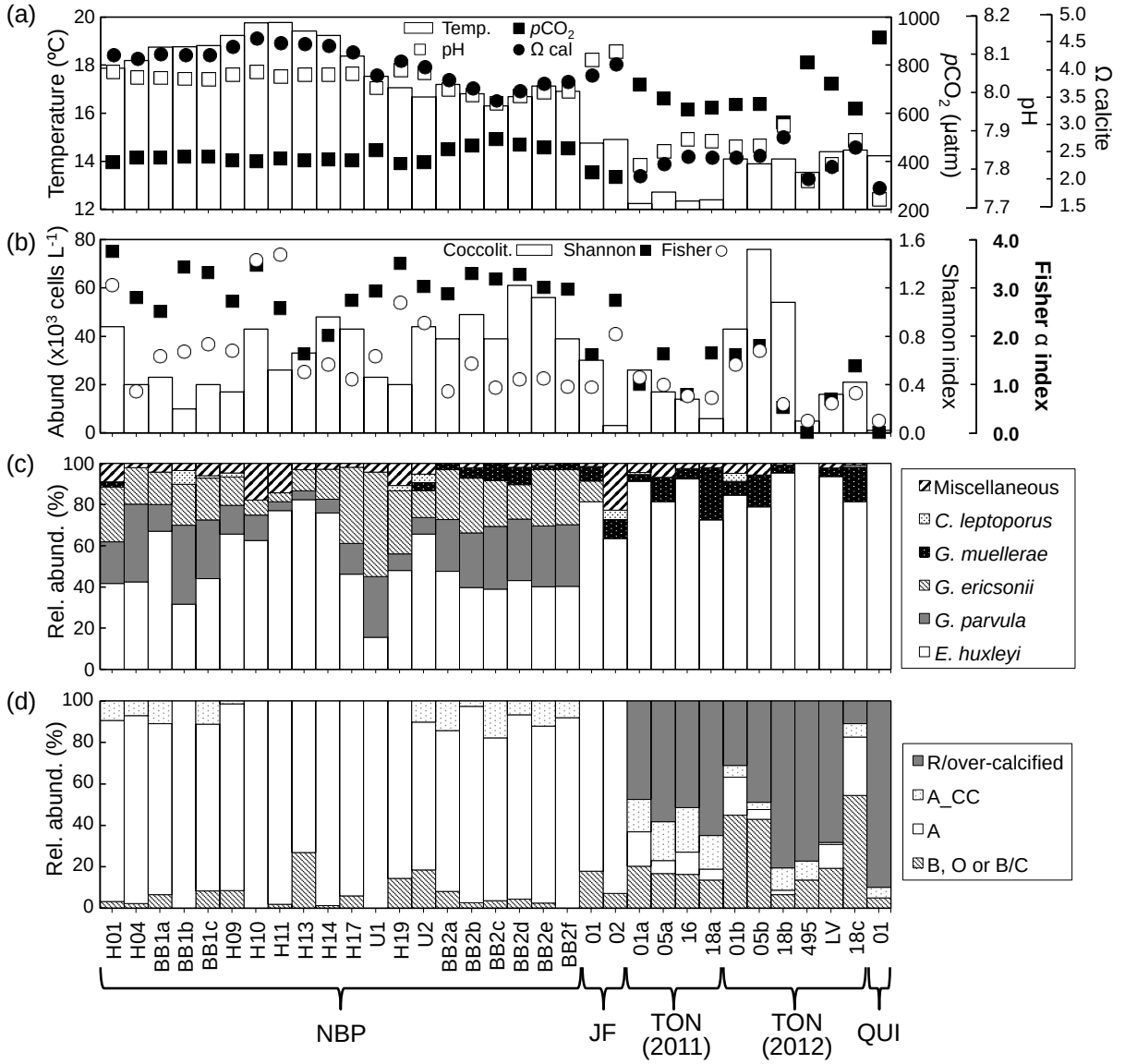

FIGURE Nº 2.3 Environmental conditions, coccolithophore community, and *E. huxleyi* morphotypes. **(a)** Temperature, pH, CO_2, and Ω calcite. **(b)** Coccolithophore abundance and Shannon and Fisher's alpha diversity indices. **(c)** Relative abundance of principal coccolithophore taxa. **(d)** Relative abundance of *E. huxleyi* morphotypes. The lightly calcified morphotypes B, O, and B/C have been grouped together.

Five species of the Noelaerhabdaceae family were observed, including *E. huxleyi*, *Gephyrocapsa ericsonii*, *G. muellerae*, *G. oceanica*, and *G. parvula*, the last of which was recently reassigned from the genus *Reticulofenestra* to the genus *Gephyrocapsa* (Bendif *et al*., 2016). The Noelaerhabdaceae family numerically dominated all coccolithophore communities

observed, representing between 72.2 and 100 % (average 94.1 ± 6.9 %) of all coccolithophores in all samples observed. The most abundant coccolithophore outside this family was *Calcidiscus leptoporus*, present at 36 % of stations and ranging in relative abundance from 0.9 % to 25.4 % (average 5.6 % ± 6.9 %). Within Noelaerhabdaceae, *E. huxleyi* was found in every sample and exhibited relative abundances ranging from 15.5 to 100 % of total coccolithophores (Fig. 1.3c). While *E. huxleyi* represented up to 100 % of the coccolithophore community in high-CO_2 waters on the central Chilean coast (stations in groups "TON (2011)", "TON (2012)", and "QUI"), it was observed in lower relative abundances of samples taken both further offshore (NBP samples H01–U2 and JF stations) and to the north (NBP samples BB2a–BB2f), where indices of coccolithophore diversity were generally higher (Fig. 1.3b and c). *Gephyrocapsa ericsonii* and *G. parvula* were essentially excluded from high-CO_2 waters.

R/over-calcified morphotypes dominated *E. huxleyi* populations in high-CO_2 waters near the central Chilean coast (samples in groups "TON (2011)", "TON (2012)", and "QUI" in Fig. 1.3; see also Fig. S3), representing on average 57.2 ± 22.9 % (range 11 to 90 %) (Fig. 1.3d). In contrast, moderately calcified A morphotype coccospheres dominated *E. huxleyi* populations in all low-CO_2 waters both further offshore (NBP samples H01-U2 and JF stations) and near the coast to the north (NBP stations BB2a–BB2f) (Figs. 3d and S3). The other over-calcified morphotype A_CC, a form characteristic of the Subtropical Front in the western Pacific (Cubillos *et al*., 2007), represented less than 20 % of total coccolithophores and did not follow a clear pattern. The lightly calcified morphotypes were usually rare except in some of the samples from near the Tongoy–Punta Lengua de Vaca upwelling (Stations in groups "TON (2011)" and "TON (2012)" in Fig. 1.3d), where they seemed to be associated with intermediate CO_2 levels.

2.4.2 Phenotypes of *E. huxleyi* clonal isolates compared to natural populations from the high-CO_2 and low-CO_2 waters

Throughout the field campaigns, a total of 260 Noelaerhabdaceae isolates were obtained and analyzed morphologically (Table 1.1; note that strains from stations nearby in time and space have been grouped). There was a bias towards isolating the dominant type within both the Noelaerhabdaceae and *E. huxleyi* species complex at each station, and only 2 % of the maintained isolates were from the *Gephyrocapsa* genus, suggesting that these closely related species are not as readily cultured as *E. huxleyi*. The lightly calcified morphotype also remained poorly represented in culture compared to the natural communities, and the A_CC type appeared moderately overrepresented. However, among the R/over-calcified and moderately calcified A morphotypes, the dominant morphotype obtained in culture always reflected the dominant morphotype in the natural community. Three representative R/over-calcified morphotype strains, showing different degrees of overlap of the central area, and two representative A morphotype strains from offshore waters were chosen for experimental analysis (Fig. 1.4).

TABLE Nº 2.1 Noëlaerhabdaceae strains isolated during this study. All sites near Tongoy were grouped in 2011 and in 2012, as were the sites at JF in 2011.

Site	Total	*E. huxleyi*				Other species		
	strains	R/over	A_CC	A	Light	*G muel.*	*G eric.*	*G parv.*
TON 2011	132	85 %	10 %	2 %	1 %	2 %	0 %	0 %
JF 2011	34	32 %	35 %	32 %	0 %	0 %	0 %	0 %
TON 2012[a]	20	90 %	10 %	0 %	0 %	0 %	0 %	0 %
Puñi. 2012[b]	10	40 %	20 %	40 %	0 %	0 %	0 %	0 %
NBP H1	15	0 %	33 %	67 %	0 %	0 %	0 %	0 %
NBP H10[c]	28	0 %	21 %	55 %	24 %	0 %	0 %	0 %
NBP BB2	21	0 %	33 %	43 %	0 %	0 %	5 %	19 %

[a] Site represented by strains CHC352 and CHC360
[b] Site represented by strain CHC342
[c] Site represented by strains CHC428 and CHC440

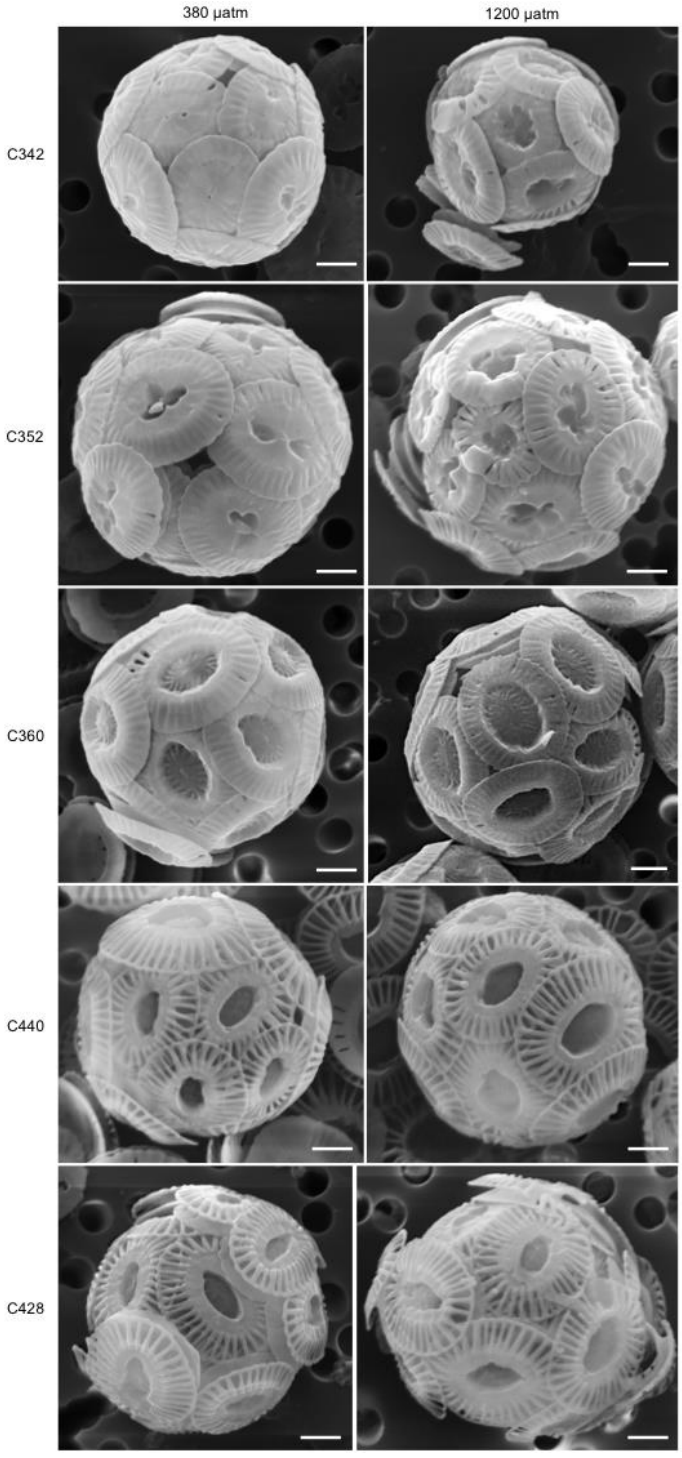

FIGURE Nº 2.4 Representative coccospheres from each strain and treatment tested in the experiment. CHC342 was isolated from the Pacific coast of Isla de Chiloé (41.9º S, 74.0º W) in November 2012. CHC352 and CHC360 were isolated from the Punta Lengua de Vaca upwelling center (30.3º S, 71.7º W) in November 2012. CHC440 and CHC428 were isolated from the station farthest west in the Pacific (station H10, at 16.7º S, 86º W) during the NBP1305 cruise in July 2013.

2.4.3 Responses of different *E. huxleyi* morphotypes to high CO_2 and low pH

Aeration with CO_2–air mixes prior to inoculation successfully equilibrated pCO_2 levels, which remained close to target levels throughout the experiment, with final pH values averaging 8.013 ± 0.029 under the control condition (400 µatm pCO_2) and 7.574 ± 0.021 under high-CO_2–low-pH conditions (1200 µatm pCO_2) (Table 1.2). Seawater remained supersaturated with respect to calcite ($\Omega_{calcite} > 1$) and $\Omega_{calcite}$ values achieved were in a similar range to those seen in the natural waters sampled (Fig. 1.3), with final values averaging $\Omega_{calcite}$ = 3.252 ± 0.260 across strains under the control condition and $\Omega_{calcite}$ = 1.423 ± 0.077 for the high-CO_2–low-pH condition (Tables 1.2 and S1). Continued aeration and keeping cell concentration below 90000 cells mL^{-1} was mostly successful in minimizing changes in carbonate system parameters. Averaging the mean values for each strain, alkalinity changed by −187 ± 132 µmol kg^{-1} (−8.24 ± 5.86 %) in the control condition and −29 ± 19 µmol kg^{-1} (−1.26 ± 0.82 %) under the high-CO_2–low-pH condition. However, for strain CHC342 the change in alkalinity under the control condition was larger (−18.64 ± 1.43 %) (discussed below). This led to a lower final dissolved CO_2 (to 12.4 ± 0.2 µmol kg^{-1}) compared to the other four strains (15.0 ± 1.3 µmol kg^{-1}).

High CO_2 and low pH significantly reduced the growth rate in all strains and there was no significant interaction between strain and high-CO_2–low-pH effects on growth rate (Fig. 1.5a; see Table 1.3 for global two-way ANOVA statistics). High CO_2 and low pH increased POC quota (POC $cell^{-1}$) in all strains. However, the interaction between strain and high CO_2 and low pH was significant (Fig. 1.5b; Table 1.3). The increase in POC quota was not significant in moderately calcified strains CHC428 and CHC440, while the hyper-calcified strain CHC342 exhibited the highest POC quota and the highest increase under OA conditions. The effect of high CO_2 and low pH on the POC production rate varied among strains: high CO_2 and low pH

TABLE Nº 2.2 Carbonate system parameters during experiment. Means ± SDs of experimental replicates at the time of inoculation (Tinoc) and harvesting (Tfinal) are given. pH at the experimental temperature is calculated from measured pH at 25º C. Treatment is specified by CO2 partial pressure (µatm) of air : CO2 mix. pCO2 units are µatm; alkalinity and [CO2] units are µmol kg−1. The average ± SDs across strains for cell-free control bottles and mean experimental bottle values are also provided. The last two rows give the average and maximum SDs between replicates among all strains.

Strain	Treat.	pCO_2		Alkalinity		pH		$\Omega_{calcite}$		Dissolved $[CO_2]$	
		T_{inoc}	T_{final}	T_{inoc}	T_{final}	T_{inoc}	T_{final}	T_{inoc}	T_{final}	T_{inoc}	T_{final}
342	400	422.0±38	332±4	2260±7	1839±25	8.020±0.033	8.029±0.033	3.531±0.225	2.891±0.097	15.8±1.4	12.4±0.2
	1200	1314±27	1257±36	2264±5	2207±19	7.574±0.008	7.582±0.008	1.402±0.026	1.400±0.022	50.8±49.4	49.4±1.0
352	400	402.5±6	370.0 *	2292±13	2168 *	8.042±0.005	8.035±0.005	3.591±0.041	3.494 *	15.6±0.2	14.2 *
	1200	1226±27.6	1341±65	2274±12	2161±20	7.601±0.007	7.561±0.018	1.440±0.015	1.339±0.057	47.6±1.1	51.4±2.5
360	400	441.4±18.7	457.4±47.7	2270±6	2126±7	8.005±0.016	7.965±0.040	3.552±0.105	3.079±0.270	16.0±0.7	16.6±1.8
	1200	1186±94.7	1409±156	2289±10	2254±4	7.623±0.032	7.545±0.043	1.648±0.107	1.370±0.128	43.0±3.4	51.5±5.8
428	400	440.3±21.5	418.5±12.9	2261±6	2157±19	8.004±0.018	8.004±0.010	3.537±0.117	3.328±0.035	15.9±0.8	15.3±0.5
	1200	1259±6.4	1247±30.6	2262±4	2250±5	7.592±0.002	7.592±0.009	1.521±0.007	1.494±0.027	45.8±0.2	45.9±1.1
440	400	457.4±26.0	381.6±5.6	2254±6	2114±17	7.988±0.021	8.033±0.005	3.259±0.127	3.469±0.104	17.3±1.0	13.8±0.3
	1200	1487±32.2	1249±55.0	2261±5	2235±7	7.522±0.009	7.591±0.019	1.243±0.022	1.512±0.050	56.2±1.2	45.1±1.8
Ave. w/o cells	400	434.0±37.1	396.7±20.7	2265±13	2273±19	8.011±0.032	8.051±0.022	3.482±0.236	3.698±0.124	16.2±1.5	14.9±0.6
	1200	1286±584.2	1290±28.1	2268±8	2239±58	7.585±0.036	7.583±0.011	1.444±0.135	1.461±0.038	49.1±4.9	47.7±0.9
Ave. with cells	400	432.7±21.0	392.0±47.8	2267±15	2081±137	8.012±0.020	8.013±0.029	3.494±0.133	3.252±0.260	16.1±0.7	14.5±1.6
	1200	1294±117.1	1301±72.1	2270±12	2241±22	7.582±0.038	7.574±0.021	1.451±0.149	1.423±0.077	48.4±5.0	48.1±3.1
Ave. SD	400	22.1	17.6	8	17	0.018	0.016	0.123	0.127	0.8	0.7
	1200	37.5	68.6	7	11	0.012	0.020	0.035	0.057	1.4	1.8
Max. SD	400	38.2	47.7	13	25	0.033	0.040	0.225	0.270	1.4	2.5
	1200	94.7	156	12	20	0.033	0.043	0.107	0.128	3.4	5.8

*Only one alkalinity sample was analysed from the 400 pCO_2 treatment for strain CHC352, as three were lost in transit between labs.

increased POC production in most strains, except for the moderately calcified strain CHC428 (Fig. 1.5c; Table 1.3). However, the change in POC production was significant in post hoc pairwise comparisons only for CHC342, in which it increased by 116 % ($p < 0.0001$). Except for strain CHC342, which exhibited the most over-calcified coccoliths (completely fused distal shield radial elements and central area nearly completely overgrown by tube elements), when all strains were considered, neither POC quota nor POC production were consistently different in R/over-calcified vs. A morphotype strains.

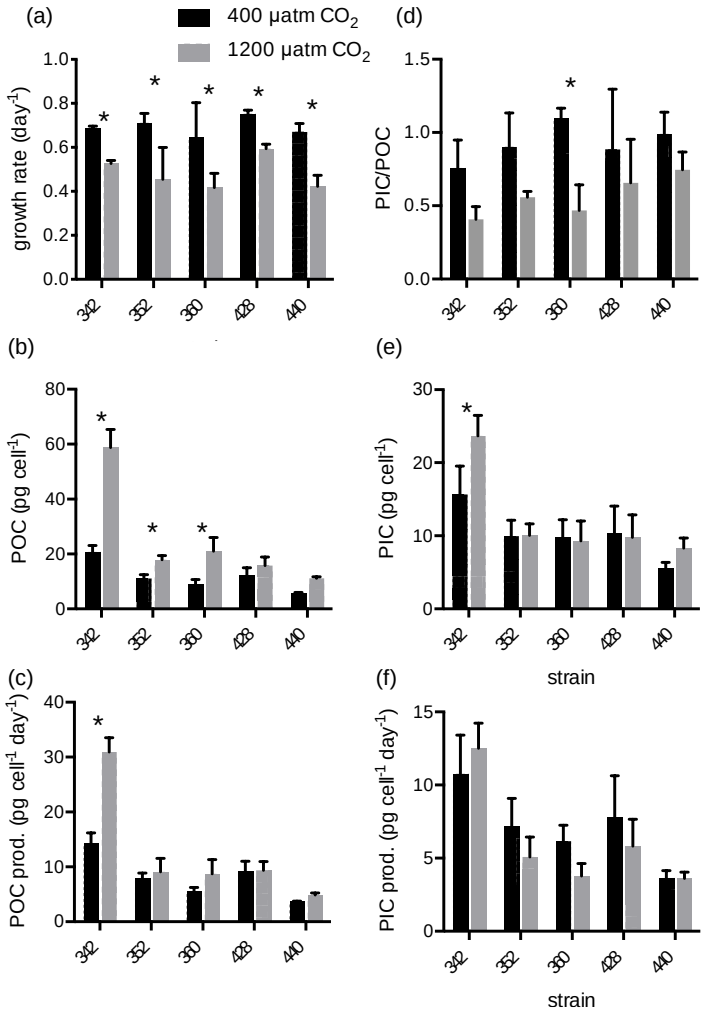

FIGURE Nº 2.5 Growth rates **(a)**, POC quotas **(b)**, POC production rates **(c)**, PIC / POC **(d)**, PIC quotas **(e)**, and PIC production rates **(f)** of *E. huxleyi* strains in response to 400 µatm (black bars) and 1200 µatm (grey bars) CO_2 treatments. See Table 1.3 for global two-way ANOVA results. The * indicates a significant difference ($p < 0.05$) in pairwise comparison between the two CO_2 treatments for a given strain, as judged by Sidak post hoc testing with correction for multiple comparison.

PIC / POC ratios dropped under high CO_2 and low pH in all strains (Fig. 1.5d). It is notable that the smallest changes in PIC / POC occurred in the two strains of moderately calcified morphotypes originating from offshore, low-pCO_2 waters, not the strains with hyper-calcified or heavily calcified morphotypes originating from coastal waters naturally exposed to high CO_2 and low pH. However, although the effect of high-CO_2–low-pH conditions was globally significant across all strains according to a two-way ANOVA (Table 1.3), in pairwise

post hoc comparisons the drop in PIC / POC ratio was only significant in CHC360 (p = 0.005). Also, the effect of strain on PIC / POC was not significant and there was no significant interaction between strain and high CO_2 and low pH (Table 1.3). PIC quotas varied among strains and the effect of high CO_2 and low pH also differed among strains (Fig. 1.5e; Table 1.3). The highest PIC quota was recorded in the hyper- calcified strain CHC342 and the lowest in the moderately calcified strain CHC440. High CO_2 and low pH increased PIC quota significantly in strain CHC342 (pairwise post hoc test, p = 0.0039), but did not change PIC quota or the change was not significant in other strains. PIC production varied among strains (Fig. 1.5f; Table 1.3) but there were no significant effects of high CO_2 and low pH or interaction between strain and high CO_2 and low pH (Table 1.3).

TABLE Nº 2.3 Global two-way ANOVA results for growth and biogeochemical parameters of strains exposed to high CO_2/low pH conditions versus control CO_2 treatment. PIC/POC values were log2-transformed prior to testing.

		Growth rate	POC	POC prod	PIC	PIC prod	PIC / POC
Source of variat.	Interact.	2.63 %	21.7 %	18.8 %	10.3 %	6.00 %	8.15 %
	Strain	13.7 %	62.8 %	77.5 %	71.3 %	69.2 %	10.9 %
	CO_2	60.9 %	23.0 %	9.67 %	3.68 %	2.13 %	37.8 %
F- values	Interact.	$F_{4,29} = 0.926$	$F_{4,25} = 36.1$	$F_{4,25} = 27.0$	$F_{4,25} = 3.08$	$F_{4,25} = 1.65$	$F_{4,25} = 1.15$
	Strain	$F_{4,29} = 4.83$	$F_{4,25} = 105$	$F_{4,25} = 111.0$	$F_{4,25} = 21.3$	$F_{4,25} = 19.0$	$F_{4,25} = 1.54$
	CO_2	$F_{1,29} = 85.7$	$F_{1,25} = 153$	$F_{1,25} = 55.6$	$F_{1,25} = 4.38$	$F_{1,25} = 2.33$	$F_{1,25} = 21.3$
p-values	Interact.	0.463	< 0.0001	< 0.0001	0.0343	0.194	0.358
	Strain	0.0041	< 0.0001	< 0.0001	< 0.0001	< 0.0001	0.222
	CO_2	< 0.0001	< 0.0001	< 0.0001	0.0466	0.139	0.0001

Decreases in alkalinity correlated with PIC (Table 1.2, Fig. S4). However, for strains CHC342 and CHC440 the drop in alkalinity was more than 2-fold greater than what would have been predicted from PIC under control conditions (but not under the high-CO_2–low-pH condition) (Supplement Sect. S3, Fig. S4). When data from strains CHC342 and CHC440 were excluded, the linear relationship between measured and predicted change in alkalinity was not significantly different than 1 : 1 (Fig. S4). When data from strains CHC342 and CHC440 were

excluded, the linear relationship between measured and predicted change in alkalinity was not significantly different than 1 : 1 (Fig. S4).

R/over-calcified coccoliths were not more resistant to high CO_2 and low pH than A morphotype coccoliths. High CO_2 and low pH significantly affected at least one morphological parameter measured in all but the A morphotype strain CHC440 (Figs. 1.4 and 1.6). The coccosphere diameters did not change significantly under high CO_2 and low pH in any of the strains (Fig. 1.6d; Table 1.4). Coccolith lengths showed inconsistent and mostly insignificant changes among strains. In the global two-way ANOVA comparison, there was an interaction between treatment and strain (Table 1.4), but the only significant change under high CO_2 and low pH detected with post hoc pairwise comparisons among treatments was a small decrease in CHC428 under high CO_2 and low pH (Fig. 1.6e; $p = 0.0334$). The percentage of the central area that was uncovered by inner tube elements increased under OA (Fig. 1.6f). The significant interaction between strain and treatment (Table 1.4) indicated that the effect of high CO_2 and low pH on this parameter varied among strains. It was most pronounced in strains CHC342 and CHC352, where the inner tube elements were heavily overgrown under low pCO_2, whereas the effect was modest in the moderately calcified strains CHC428 and CHC440 (and not significant in pairwise post hoc tests of the effect of treatment within these strains; $p > 0.05$), where the central area was mostly exposed under both conditions. The incidence of incomplete or malformed coccoliths remained very low in all strains and treatments, but high CO_2 and low pH caused a modest but significant increase (Fig. 1.6g; Table 1.4), ranging from between 0 and 1.3 % of coccoliths under low CO_2 to between 1.4 and 6.6 % under high CO_2 and low pH. This effect was greatest in R/over-calcified morphotype strains CHC342, CHC352, and CHC360, but

there was no significant interaction between strain and treatment in the two-way ANOVA when all strains were considered (Table 1.4).

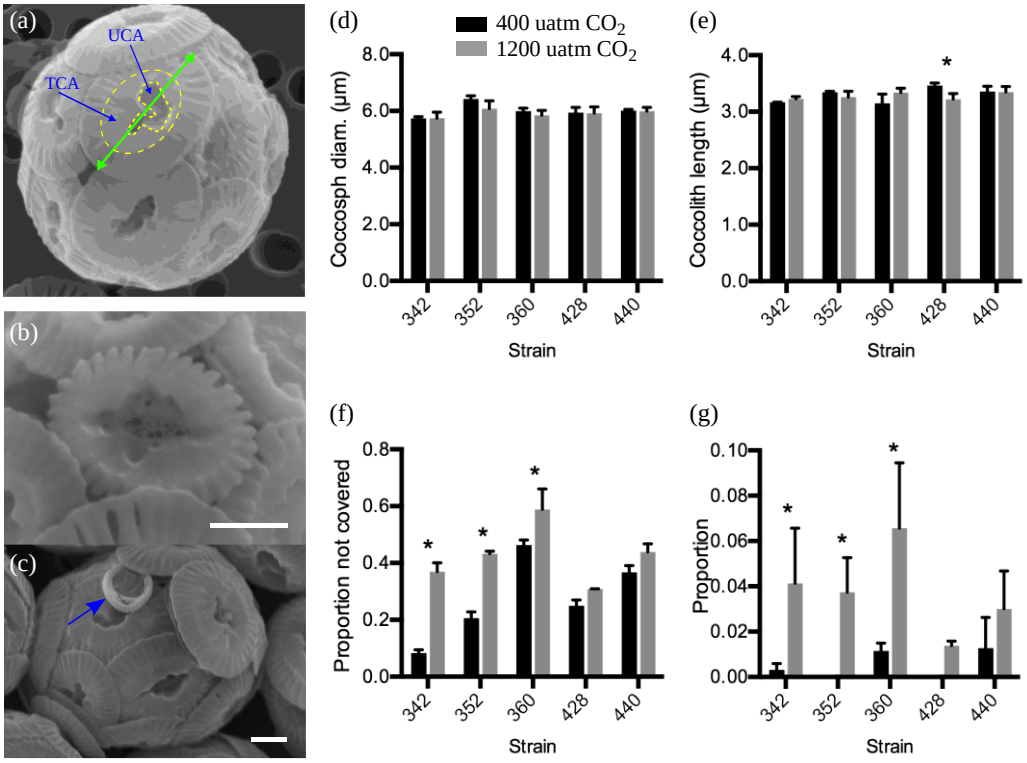

FIGURE Nº 2.6 Effects of high-CO_2–low-pH conditions on coccolithophore morphology. **(a)** Example illustrating coccolith measurements taken including coccolith length (solid line with two arrow heads), total central area including the inner tube (TCA) (defined by inner terminal of radial elements), and the part of the central area that is uncovered by tube elements (UCA). **(b)** Example of a coccolith classified as incomplete or malformed. **(c)** Example of a very incomplete coccolith (arrow). **(d)** Coccosphere diameters. **(e)** Coccolith length. **(f)** Proportion of central area not covered. **(g)** Proportion of coccoliths that were malformed or incomplete. See Table 1.4 for global two-way ANOVA results. The * indicates significant difference ($p < 0.05$) in pairwise comparison between the two CO_2 treatments for a given strain, as judged by Sidak post hoc testing with correction for multiple comparison.

Flow cytometric analysis (see example cytogram in Fig. S5) showed significant changes in several cytometric parameters in response to high CO_2 and low pH, which in some cases varied among strains (Fig. 1.7; Table 1.5). Relative chlorophyll fluorescence was increased significantly in strains CHC360, CHC440, and CHC428, but dropped significantly in CHC352

TABLE Nº 2.4 Global two-way ANOVA results for coccosphere and coccolith parameters of strains exposed to high-CO_2–low-pH conditions versus control CO_2 treatment. Proportions of central area covered and of incomplete or malformed coccoliths were arcsine-squareroot-transformed prior to testing.

		Coccosphere diameter	Coccolith length	Proportion central area covered	Proportion of coccoliths incompl. or malform.
Source of variat.	Interact.	7.58 %	34.7 %	12.3 %	4.40 %
	Strain	53.7 %	25.3 %	53.3 %	18.0 %
	CO_2	4.76 %	0.396 %	29.2 %	55.4 %
F-values	Interact.	$F_{4,19} = 1.071$	$F_{4,19} = 4.62$	$F_{4,19} = 21.9$	$F_{4,19} = 1.18$
	Strain	$F_{4,19} = 7.595$	$F_{4,19} = 3.37$	$F_{4,19} = 94.7$	$F_{4,19} = 4.83$
	CO_2	$F_{1,19} = 2.689$	$F_{1,19} = 0.211$	$F_{1,19} = 207$	$F_{1,19} = 59.6$
p-values	Interact.	0.398	0.0090	< 0.0001	0.351
	Strain	0.0008	0.0304	< 0.0001	0.0074
	CO_2	0.118	0.652	< 0.0001	< 0.0001

(Fig. 1.7a, Table 1.5). The proportion of cells which were calcified was high (> 97 %) in all strains under the 400 μatmCO_2 control treatment but dropped modestly (0.04 to 7.2 %) in all strains in the OA treatment (Fig. 1.7b). A significant interaction was detected between strain and treatment in the proportion of cells calcified (Table 1.5), and this drop in response to high CO_2 and low pH was greatest in strains CHC360 (average change of −7.2 %) and CHC440 (average change of −5.4 %), which were the only two strains for which the difference between treatments was judged significant in pairwise post hoc testing. In the control CO_2 treatment, the relative abundance of detached coccoliths, relative to the number of cells, was low (11.9 to 14.4 cell−1) in most strains but high (63 ± 34 cell−1) in strain CHC440. Despite significant variability among strains in the relative abundance of detached coccoliths, there were no significant changes under high CO_2 and low pH (Fig. 1.7c; Table 1.5). The relative forward scatter depolarization (a proxy for the amount of calcite on a cell (see von Dassow *et al*., 2012) was decreased significantly under high CO_2 and low pH (Fig. 1.7d; Table 1.5), an effect which varied among strains (Table 1.5) and was strongest in strain CHC352. The relative scatter depolarization of detached

coccoliths was also decreased under high CO_2 and low pH (Fig. 1.7e; Table 1.5), an effect that varied among strains and was largest in CHC352 and CHC428.

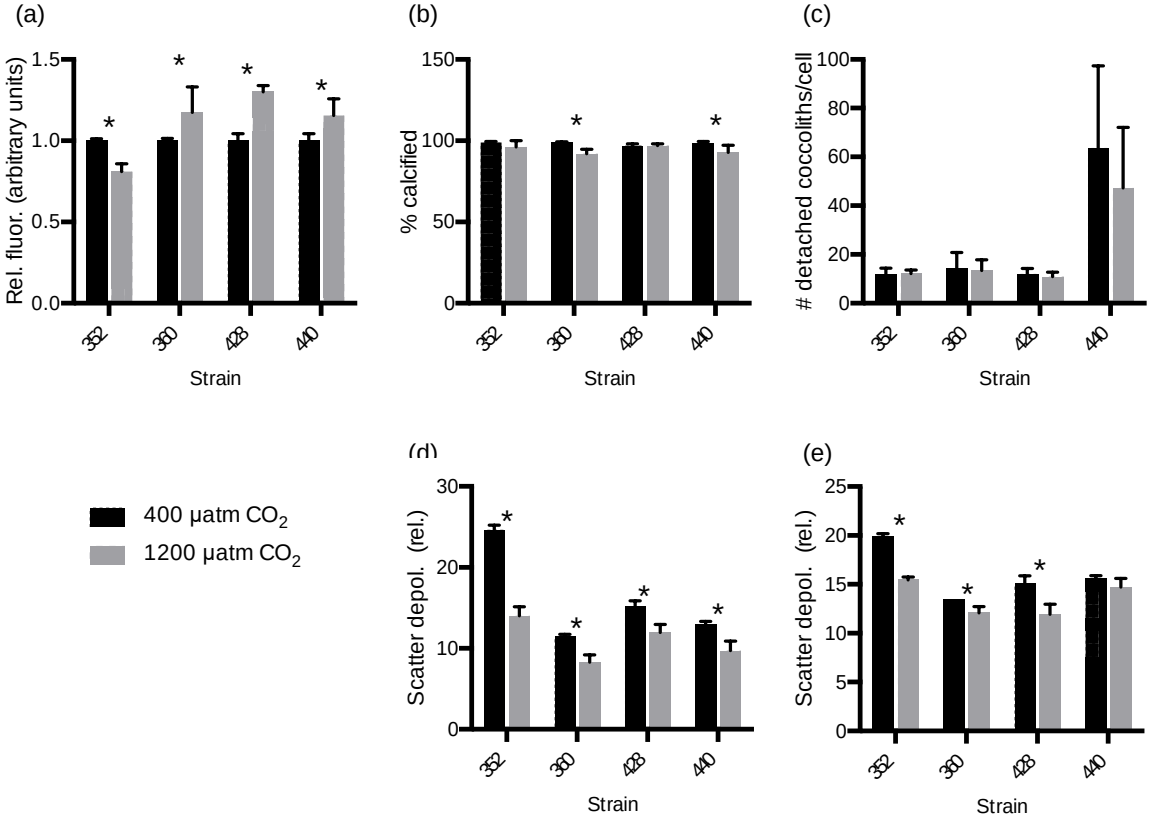

FIGURE Nº 2.7 Effects of high-CO_2 treatment on flow cytometric properties of cells and detached coccoliths for all treatments and strains. Strain CHC342 is not shown because samples were lost in transit between labs. Shown are the relative fluorescence (compared to control treatment) **(a)**, the proportion of cells that were calcified **(b)**, abundance of detached coccoliths divided by cell abundance **(c)**, relative FSC (scatter depolarization) of cells **(d)**, and detached coccoliths **(e)**. Fluorescence and FSC units are relative and the voltage for the detector for FSC perpendicularly polarized was 2-fold higher, resulting in a sensitivity approximately 2 orders of magnitude higher. Scatter depolarization was calculated for every particle as the ratio of FSC with polarizations perpendicular vs. parallel to the laser, normalized by the same ratio for non-optically active particles within the same sample. The * indicates significant difference ($p < 0.05$) in pairwise comparison between the two CO_2 treatments for a given strain, as judged by Sidak post hoc testing with correction for multiple comparison.

TABLE Nº 2.5 Global two-way ANOVA results for flow cytometric parameters. The percentages of calcified cells were expressed as a fraction and arcsine-square-root transformed prior to testing.

		Rel. red fluoresce.	% calcified	No. detached coccol.	Rel. scatter depol. cells	Rel. scatter depol. detached liths
Source of variat.	Interact.	35.0 %	18.9 %	2.27 %	11.2 %	7.85 %
	Strain	34.7 %	6.42 %	67.8 %	55.8 %	57.9 %
	CO_2	13.5 %	38.7 %	1.09 %	25.4 %	22.8 %
F-values	Interact.	$F_{3,20} = 16.0$	$F_{3,20} = 3.62$	$F_{3,20} = 0.525$	$F_{3,20} = 36.5$	$F_{3,20} = 12.3$
	Strain	$F_{3,20} = 15.9$	$F_{3,20} = 1.23$	$F_{3,20} = 15.7$	$F_{3,20} = 182$	$F_{3,20} = 90.6$
	CO_2	$F_{1,20} = 18.5$	$F_{1,20} = 22.2$	$F_{1,20} = 0.757$	$F_{1,20} = 249$	$F_{1,20} = 107$
p-values	Interact.	< 0.0001	0.0309	0.670	< 0.0001	< 0.0001
	Strain	< 0.0001	0.326	< 0.0001	< 0.0001	< 0.0001
	CO_2	0.0003	0.0001	0.395	< 0.0001	< 0.0001

2.5 DISCUSSION

While an increasing number of studies have focused on examining the potential for adaptation to OA through long-term laboratory experiments, this study has taken an alternative approach, to test for local adaptation to short-term high-CO_2 and low-pH exposure in populations of cosmopolitan phytoplankton found in waters that experience naturally acidified conditions due to upwelling of high-CO_2 water. A similar approach has recently been taken in a variety of invertebrate species (Padilla-Gamiño *et al*., 2016; Gaitán-Espitia *et al*., 2017; Vargas *et al*., 2017), finding both benthic and meroplanktonic animals, coralline algae, and holoplanktonic copepods do exhibit local adaptation in regions experiencing naturally high fluctuations in pH and CO_2.

This study confirms that R/over-calcified forms of *E. huxleyi* which appear exceptionally robust (as both the central area is extensively overgrown and the distal shield elements are fused) occur in the coastal zone of central to northern Chile. This was previously hinted from two sampling points and times (Beaufort *et al*., 2011) and has now been documented in separate years. Within the subtropical and tropical eastern South Pacific, the presence of these morphotypes coincides both with high CO_2 and low pH (low $\Omega_{calcite}$) as well as with lower

temperature (Fig. S3), and it is difficult to separate these two parameters. However, at the lowest end of the *E. huxleyi* temperature range, populations are often found to be dominated by more lightly calcified morphotypes (Cubillos *et al*., 2007); thus a relationship to temperature would have to be very nonlinear. More importantly, while a "type A over-calcified" type was reported in winter waters of the Bay of Biscay (Smith *et al*., 2012) and a heavily calcified type "A*" was reported in the Benguela coastal upwelling (Henderiks *et al*., 2012) (both exhibiting only overgrowth of the central area by tube elements but not fusion of distal shield elements), the exceptionally robust R/over-calcified forms seen near Chile have not been reported from these other upwelling systems. Therefore, we set out here to test the simplest hypothesis – focusing on a single factor – that these forms may be adapted to resist high-CO_2–low-pH conditions.

The use of targeted flow cytometry and cell sorting was successful in obtaining representatives of the different forms of *E. huxleyi* in monoculture to test whether the correlation between phenotype and environment indeed reflected local adaptation. Two of the R/over-calcified strains chosen for experimental tests (CHC352 and CHC360) originated from the high-CO_2 upwelling near Tongoy–Punta Lengua de Vaca (Table 1.1). Strain CHC342 originated from Puñihuil along the outer (western) coast of Isla de Chiloé (41.9º S). Although we lack carbonate system data from this site, the Isla de Chiloé is located approximately where the West Wind Drift arrives at the continent and turns north to form the Humboldt Current System (Thiel *et al*., 2007). Thus we considered that CHC342, exhibiting a highly over-calcified R morphotype, might represent the southern end of the *E. huxleyi* populations that drift north and experience high-CO_2–low-pH upwelling conditions. We compared these three R/over-calcified strains to two A morphotype strains isolated from low-CO_2 waters at a site 1000 km from the nearest shore (NBP cruise station H10 in Figs. 1.1 and 1.3). Organisms in such waters are expected to

experience very low fluctuations in pH (Hofmann *et al*., 2011), and so these strains were expected to exhibit low resistance to transient high-CO_2–low-pH conditions.

The high-CO_2–low-pH condition (1200 µatm CO_2) tested was chosen to represent recently upwelled water based on Torres *et al*. (1999) compared to CO_2 levels in non-upwelling surface waters (400 µatm). The high CO_2 level of 1200 µatm was also chosen considering previous laboratory studies of the response of *E. huxleyi*: results of acclimated growth rate in response to short-term changes in the carbonate system manipulated by bubbling have been reported in several studies for two R morphotype strains isolated from the Tasman Sea (where high-CO_2 upwelling is not known), of which four studies reported no significant effect on growth rate of intermediate CO_2 levels (Langer *et al*., 2009; Shi *et al*., 2009; Richier *et al*., 2011; Rokitta and Rost, 2012) compared to one which reported a decrease at 750 µatm (Iglesias-Rodriguez *et al*., 2008). For other *E. huxleyi* strains, results at intermediate CO_2 levels are not consistent among either studies or even among strains used in the same study, while all strains tested at higher levels ($\geq$ 950 µatm) have shown slight to pronounced decreases in growth rate (Langer *et al*., 2009).

The bloom-former *E. huxleyi* is often considered a fast-growing pioneer phytoplankton species (Paasche, 2002). However, calcification is costly and most evidence suggests it may confer protective or defensive functions (Monteiro *et al*., 2016). Thus we considered both growth rate and calcification–morphological responses when analyzing potential adaptation. Surprisingly, we found no evidence that the exceptionally robust form was more resistant to high CO_2 than moderately calcified forms that seemed to be excluded from the high-CO_2 upwelling waters.

The high-CO_2–low-pH treatment reduced growth rate in all strains. The decrease in growth rate was accompanied by an increase in POC quota. This might suggest that cells were getting bigger, compensating for a decreased rate of cell division (as the increase in POC production rate was not significant in four of the five strains tested). However, the decrease in growth rate was also reflected in a decrease in culture in vivo fluorescence (data not shown). Changes in coccosphere diameter were insignificant, and changes in cellular fluorescence measured by flow cytometry were small and consistent with only a small possible increase in cell biomass (and not in all strains, as CHC352 showed a decrease in this parameter). Among the few previous studies in which a period of pre-acclimation to CO_2 was not used prior to growth measurements, inconsistent and non-significant effects of growth have been seen in two R morphotype strains NZEH (PLY M219) (Shi *et al*., 2009) and RCC1216 (Richier *et al*., 2011). Another study comparing several morphotypes isolated from the Southern Ocean reported that two "A/over-calcified" strains (similar to the R morphotype strain CHC360, but with distal shield radial elements not consistently fused) were relatively resistant to high-CO_2–low-pH treatments compared to both the A morphotype and the lighter B/C morphotype in which growth and calcification were strongly inhibited (Müller *et al*., 2015a). Thus the R/over-calcified strains tested here, originating from high-CO_2 environments, were surprisingly not resistant to high CO_2. While caution is warranted in comparing the absolute resistance of the R and R/over-calcified morphotypes tested in this study to those tested in the study by Müller *et al*. (2015a) even when similar high- CO_2–low-pH treatments were tested, the robust conclusion is that the A morphotypes tested here from the eastern South Pacific were not more sensitive than the R/over-calcified strains from neighboring high-CO_2–low-pH waters.

In strain CHC342, the POC quota exceeded values previously reported in the literature for the species in response to high CO_2 and low pH by more than 3-fold. This occurred in all four replicates, sampled at the same time as the low-CO_2 replicates, so we have no evidence for this increase being a technical artefact. The increase in dissolved CO_2 in the high-CO_2–low-pH condition compared to the control condition was highest in strain CHC342 due to a higher consumption of alkalinity and/or DIC. The levels of dissolved CO_2 in the control (400 µatm pCO_2) condition for all strains fell in a range (12.4–16.6 µmol kg^{-1}) that should be saturating for photosynthesis according to one prior study (Buitenhuis *et al*., 1999), but subsaturating for POC production according to a more recent study (Bach *et al*., 2013). The experimental variability noted might have accentuated a variability among strains in the affinity of *E. huxleyi* for photosynthetic carbon uptake. Bach *et al*. (2013) also reported that growth rate was saturated at lower dissolved CO_2 levels than POC production. A similar increase in POC quota in response to high CO_2 has been reported in *Calcidiscus quadriperforatus* strain RCC 1168 to correlate with the production of transparent exopolysaccharides (TEPs) (Diner *et al*., 2015), and so we suspect that the increase in POC per cell – at least in CHC342 – might correspond partly to increased TEP production under high CO_2 and low pH.

As expected, PIC quotas varied among strains. CHC342, the strain showing the greatest degree of over-calcification, showed the highest PIC quota. Strain CHC440, the strain showing the coccoliths with the least percentage covering of the central area by the inner tube and the most delicate distal shield rim elements, showed the lowest PIC quota. However, the PIC quotas of CHC352, CHC360, and CHC428 were not different. The numbers of detached coccoliths per cell were similar among those three strains, but coccoliths produced by CHC428 were slightly

larger, partly explaining this result. The PIC / POC ratio also did not show consistent differences among morphotypes.

PIC / POC ratios decreased in all strains and all treatments, similar to what has been reported for most of the strains used in most of the previous studies (reviewed in Meyer and Riebesell, 2015). However, in future studies it will be important to understand how TEP production impacts POC and PIC / POC ratios and responds to high CO_2 and low pH, as has been shown in *Calcidiscus* (Diner *et al*., 2015). The effect of high CO_2 and low pH on calcification (PIC quota and PIC production) was variable among strains, with no clear pattern related to origin or calcification, and none of these modest effects were significant except the increase in PIC quota in CHC342, the most heavily calcified strain. While calcification rate appears to be sensitive to high CO_2 and low pH in most studies and strains of *E. huxleyi* (Meyer and Riebesell, 2015) despite periods of acclimation, or even adaptation over hundreds of generations (Lohbeck *et al*., 2012), all of the strains tested here appear to be more similar in this aspect to strains found to exhibit calcification that is relatively resistant to high CO_2 and low pH (Langer *et al*., 2009). We did not see the dramatic loss of calcification (almost all cells were calcified in all strains and treatments) that was reported, for example, in a B/C morphotype from the Southern Ocean in response to high CO_2 and low pH (Müller *et al*., 2015a).

We caution that the changes in alkalinity suggested that both strain CHC342 and strain CHC440 may have had an approximately 2-fold higher PIC quota than what was directly measured under the control CO_2 and pH condition. This could have occurred if the acidification of total particulate carbon samples did not effectively dissolve all calcium carbonate in these strains. This is surprising, as the geochemical analysis service that performed POC and PIC measurements followed a standard protocol recommended for both plankton samples and

carbonate-rich soil samples (Harris *et al*., 2001; Lorrain *et al*., 2003) that has been previously used for measuring PIC and POC quotas in *E. huxleyi* (Zondervan *et al*., 2002; Sciandra *et al*., 2003). We speculate that perhaps the coccoliths from these strains differ from other strains in organic content in some way that makes them more resistant to dissolution. For example, recent comparisons have shown that the content and composition of coccolith-associated polysaccharides varies among *E. huxleyi* strains (Lee *et al*., 2016). However, we are not aware of such an effect being reported in the literature. In any case, a possible underestimation of PIC quotas in strains CHC342 and CHC440 under the control CO_2 and pH condition would mean that the POC quota was overestimated under that condition, accentuating the increase in POC by high CO_2 and low pH. Most importantly, it implies these strains may not have experienced an increase in PIC quota in response to high CO_2 and low pH, but instead PIC quota might have actually been either maintained or decreased.

The function of coccoliths is still not certain. However, calcification is costly. It is not immediately clear if the proposed role of calcification to alleviate Ca^{2+} toxicity could cause the selection of over-calcified coccoliths in the high-CO_2–low-pH upwelling waters, as the differences in Ca^{2+} concentrations are vanishingly small compared to the levels at which calcification was observed to show this benefit in the lab (Müller *et al*., 2015b). Likewise, a possible physiological role of calcification as a carbon-concentrating mechanism to support photosynthesis in low-CO_2 waters is not supported by the current balance of evidence in published literature for *E. huxleyi* (Trimborn *et al*., 2007) as reviewed in Monteiro *et al*. (2016). In any case, such an explanation could not explain why highly calcified cells would be selected for in high-CO_2 waters. Most evidence suggests calcification may serve protective or defensive functions (Monteiro *et al*., 2016), in which case not only the rate of calcification but also the

form and quality of the coccoliths would be important. Thus we also considered responses in coccolith morphology when analyzing potential adaptation.

Both microscopic and flow cytometric measures indicated that coccolith morphology was not more resistant to high-CO_2–low-pH conditions in the R/over-calcified strains isolated from naturally high-CO_2–low-pH upwellings than in the A morphotype strains isolated from far offshore waters in equilibrium with the atmosphere that are not known to experience natural high-CO_2–low-pH episodes. The increase in the percentages of malformed or incomplete coccoliths in response to high CO_2 and low pH was most pronounced in the R/over-calcified morphotypes, although these percentages remained low in all strains and both treatments compared to other studies. In other *E. huxleyi* morphotypes, the thickness of the tube around the coccolith central area is reported to decrease modestly under acidification conditions (Bach *et al*., 2012; Young *et al*., 2014), and a similar effect was seen in the two A morphotype strains here. In our study, this effect was most pronounced, resulting in a highly eroded appearance, in the most heavily over-calcified R strains in which the tube overgrows the central area. Coccoliths are formed in intracellular compartments, and the extracellular Ω_{Ca} remained > 1 in the experiments, so this must be due to effects on the formation of coccoliths, not erosion after coccolith secretion. This also shows that the degree of covering of the central area in these types depends on condition in the R morphotype; however, the principal morphotype classification of each of the five strains did not change, as expected if morphotype is genetically determined (Young and Westbroek, 1991). The disappearance of the underlying central area (hollow coccoliths) reported in one study (Lefebvre *et al*., 2012) was not observed here. The morphological observations using SEM were supported by flow cytometric results, which also

showed changes in the relative depolarization of forward scatter light of both whole coccospheres and detached coccoliths.

The observation that the morphology and quality of coccoliths of moderately calcified A morphotype strains were comparatively little affected while R/over-calcified forms were strongly affected does not appear consistent with the hypothesis that over-calcification of distal shield elements in the *E. huxleyi* present in naturally acidified high-CO_2 water serves to compensate for high-CO_2–low-pH effects on coccoliths. Some other factor must select for the R/over-calcified morphotype in the coastal zone of Chile. An A morphotype (A*) exhibiting partial and irregular extension of inner tube elements over the central area (but not closure of spaces between distal shield radial elements) was dominant in the Benguela upwelling zone (not the more extreme R/over-calcified types) (Henderiks *et al*., 2012), while the A_CC type, although rare off the coast of Chile, was dominant in the northeastern Atlantic (Bay of Biscay) in winter (Smith *et al*., 2012). It is interesting to speculate that high-productivity conditions in eastern boundary coastal waters promote persistently higher abundances of grazers or phytopathogenic bacteria, against which the over-calcified coccoliths might provide better defense.

The lack of evidence for regional-scale local adaptation (either in terms of growth or morphology) to short-term high-CO_2–low-pH conditions in *E. huxleyi* populations that are naturally exposed to pulses of naturally high-CO_2–low-pH upwelling conditions, contrasts with the recent findings showing adaptation to OA in estuarine habitats in invertebrates and coralline algae (Padilla-Gamiño *et al*., 2016; Gaitán-Espitia *et al*., 2017; Vargas *et al*., 2017), including the neritic but holoplanktonic copepod *Acartia tonsa* (Vargas *et al*., 2017). However, among *E. huxleyi* there is variability in response to high CO_2 and low pH (Riebesell *et al*., 2000; Iglesias-

Rodriguez *et al*., 2008; Langer *et al*., 2009; Meyer and Riebesell, 2015) that appears to correlate with morphotype and origin at least in one study (Müller *et al*., 2015a). This variability may already have been subject to selection. In that case, perhaps it is appropriate to consider that the present study documented a similar resistance of offshore eastern South Pacific A morphotype strains to that of coastal strains from high-CO_2–low-pH waters. Although the offshore populations should be exposed less to high-CO_2–low-pH conditions, they might experience such conditions occasionally: intra-thermocline eddies, subsurface lenses between approximately 100 and 500 m depth, have recently been documented to transport subsurface waters low in dissolved O_2 in an offshore direction in the eastern South Pacific (Andrade *et al*., 2014; Combes *et al*., 2015). These eddies would also be expected to be high in CO_2 and low in pH, and intrusions of such water might affect organisms at the base of the euphotic zone. Such processes would still result in lower CO_2 exposure than the exposure to high CO_2 and low pH occurring at the coast. Perhaps the nearshore *E. huxleyi* populations, despite being exposed more frequently and more intensely to high-CO_2–low-pH conditions, have already reached some limit that prevents adaptation to further increases in CO_2, which limit the negative effects of these conditions on growth rate, calcification, and coccolithogenesis. Overall, the observation of consistent declines in growth rates, PIC quotas, and PIC / POC ratios, even in genotypes that naturally are exposed to high-CO_2–low-pH conditions, supports the prediction that PIC-associated POC export may decline under future OA conditions, potentially weakening the biological pump (Hofmann and Schellnhuber, 2009).

Data availability. All data are available from the corresponding author upon request. The scanning electron micrograph image datasets can be found at https://doi.org/10.5281/zenodo.1248048 (von Dassow *et al*., 2018).

Author contributions. PvD led the study, carried out sampling in field surveys, performed flow cytometric isolation of *E. huxleyi* strains, carried out statistical analysis of experimental data, supervised processing of samples with flow cytometry and electron microscopy, and wrote the paper. FDR conducted characterization of coccolithophore communities and *E. huxleyi* morphotype composition, analyzed the relationships of coccolithophore communities and *E. huxleyi* morphotypes to environmental parameters, assisted with part of the high-CO_2–low-pH experiments in the Calfuco Marine Laboratory, and helped prepare the first draft of the paper and figures. EMB participated in field studies in 2012, helped with classification of *E. huxleyi* morphotypes, and trained and supervised FDR in coccolithophore taxonomic classification. JDGE led experimental work in the Calfuco laboratory and provided key comments and editing of the paper. SR provided insights into interpretation of results and edited a draft of the paper. DMF helped plan and perform experiments in the Calfuco lab. UJ assisted with initial plans and later interpretations. RT performed chemical analysis on seawater samples and helped set up the Calfuco Marine Laboratory experiments.

Competing interests. The authors declare they have no conflicts of interest.

Acknowledgements. This work was supported by the Comisión Nacional de Investigación Científica y Tecnológica of the Chilean Ministry of Education (FONDECYT grants 1110575 and 1141106, and grant CONICYT USA 20120014 to Peter von Dassow, a doctoral fellowship CONICYT-PCHA/Doctorado Nacional/2013–21130158 to Francisco Díaz-Rosas, FONDECYT postdoc grant 312004 to Daniella Mella-Flores, and FONDEQUIP EQM130267 for the purchase of the Influx cell sorter), by the Iniciativa Cientifica Milenio of the Chilean Ministry of Economy through the Instituto Milenio de Oceanografía de Chile (grant IC 120019),

by the ASSEMBLE program (grant 227799; El Mahdi Bendif), and by International Research Network “Diversity, Evolution and Biotechnology of Marine Algae” (GDRI no. 0803) of the Centre Nacional de Recherche Scientifique (Peter von Dassow). The authors thank Jorge Navarro for access to the Calfuco Marine Laboratory, Veronica Flores for assisting with SEM analysis, and Jessica Beltrán for work as lab manager of the Santiago lab.

Edited by: Lennart de Nooijer

Reviewed by: Marius N. Müller and one anonymous referee

2.6 SUPPLEMENTARY MATERIALS

2.6.1 Variation in relative abundance of *E. huxleyi* morphotypes with depth.

We note that the dominant morphotype of *Emiliania huxleyi* was usually the same at the surface and deeper in the water column (Fig. S1-S2). One exception was a station near Punta Lengua de Vaca (Tongoy Station 18) where lightly calcified morphotypes dominated below the thermocline and R/overcalcified morphotypes dominated above (Fig. S1f). Another exception was the station 2 in the JF survey, where the lightly calcified morphotypes were dominant within and below the picnocline but the A morphotype was dominant, although at the lower total abundance (Fig. S1h). Table S3 (Supplementary section S3) gives abundances with depth at the stations shown in Fig. S1-S2.

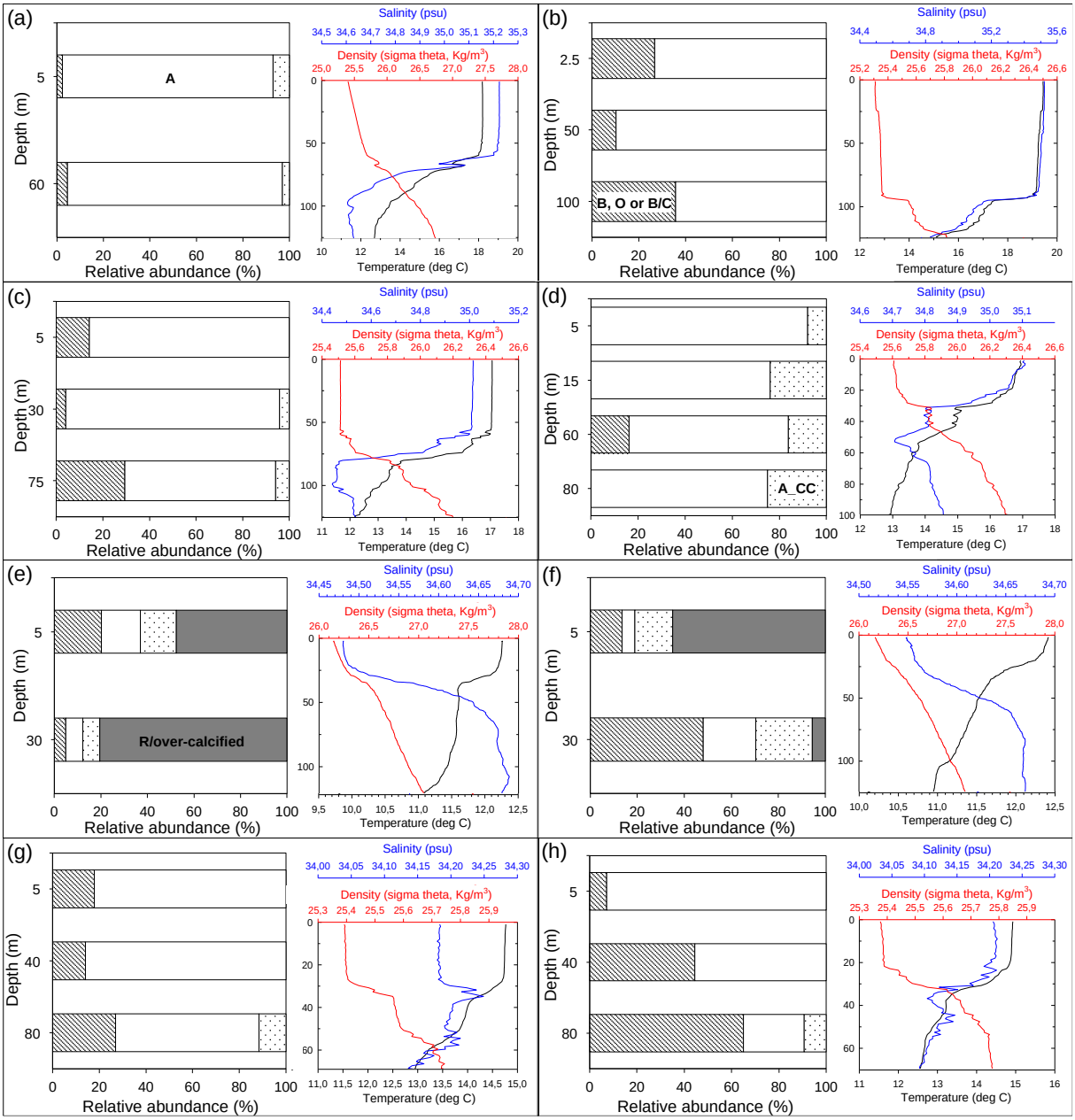

Figure S1. Relative abundances of *Emiliania huxleyi* morphotypes in the upper water column by study site. In a-d), e-f) and g-h) the relative abundances yielded by *E. huxleyi* morphotypes in NBP cruise (st. H04, H13, H19, BB2f), Tongoy Bay (st. 01 and 18) and Juan Fernandez surveys (st. 01, 02) are shown, respectively. Temperature (black), salinity (blue) and density (red) profiles for each station are shown at the right. Morphotypes are indicated on the bars.

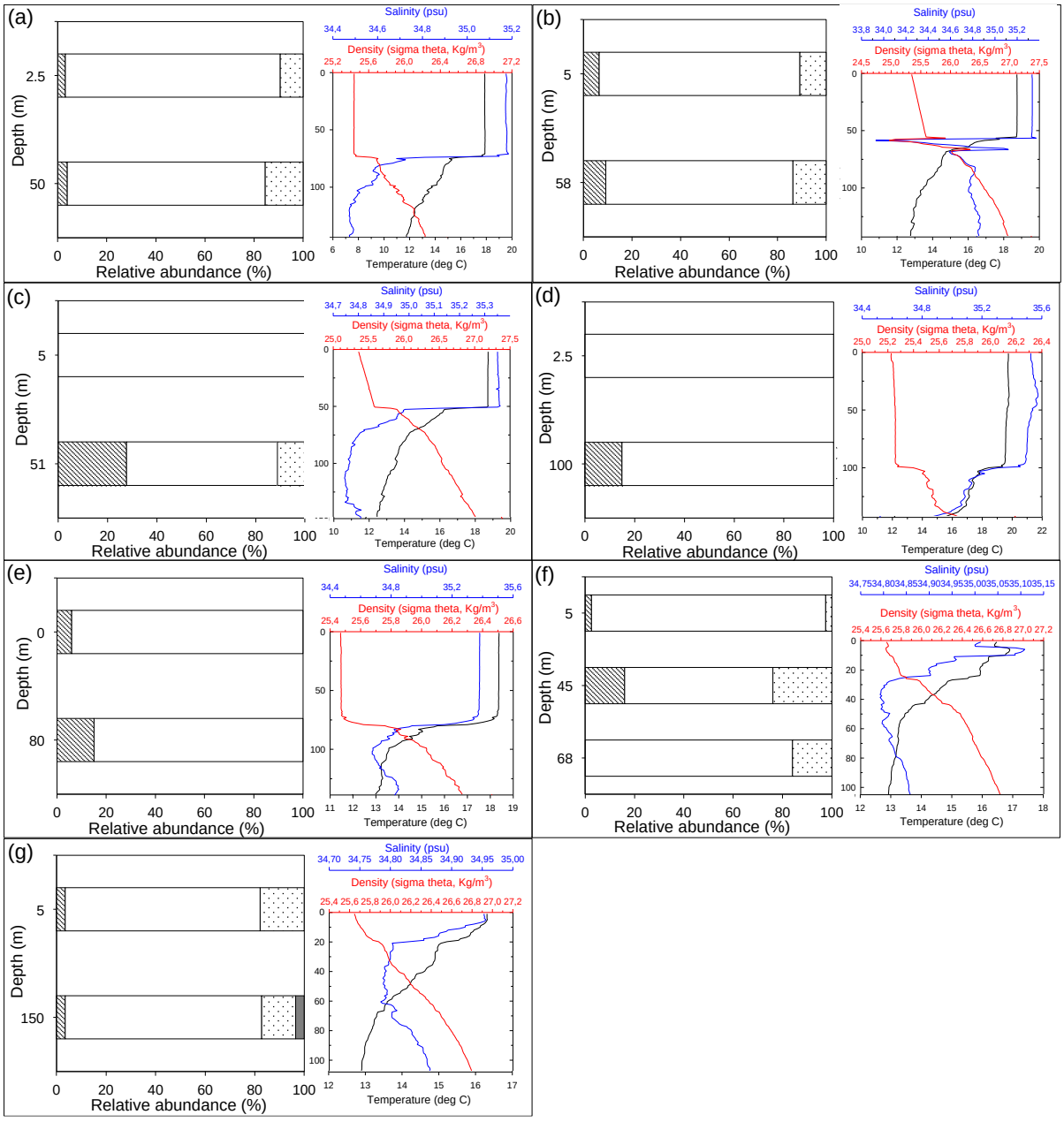

Figure S2. Relative abundances of *Emiliania huxleyi* morphotypes in the upper water column. In a-g) the relative abundances yielded by *E. huxleyi* morphotypes in NBP cruise (st. H01, BB1a, BB1b, H10, H17, BB2b, BB2c) are shown. Temperature (black), salinity (blue) and density (red) profiles for each station are shown at the right. Morphotypes are as in Fig. S1. A conductivity sensor error in BB1a caused a spike that was not filtered out successfully.

2.6.2 Redundancy analysis (RDA) methodology used and RDA results for *Emiliania huxleyi* morphotype distributions constrained by environmental variables.

To determine the abiotic variables driving the *Emiliania huxleyi* populations a redundancy analysis (RDA) was performed (rda function in vegan package Oksanen *et al*., 2007, performed in RStudio version 1.0.143 for mac OS). RDA is a direct constrained method that combine multivariate multiple linear regression with principal component analysis (Borcard *et al*., 2011). To RDA analyses we followed the methodology provide by Borcard *et al*. (2011). The variation in *E. huxleyi* morphotypes (matrix composed by relative abundances) were regressed on environmental conditions (temperature, salinity and *p*CO2), while controlling for sampling location (vector of offshore distances in km). To test for significance of RDA model and axis the pseudo-F statistic was calculated by set a minimal number of 1,000 sample permutations (Borcard *et al*., 2011). As linear dependencies between environmental variables can inflated the regression coefficient (Borcard *et al*., 2011), variance inflation factors were checked after each RDA analysis (vif.cca function in vegan package). RDA results are plotted in Fig. S3.

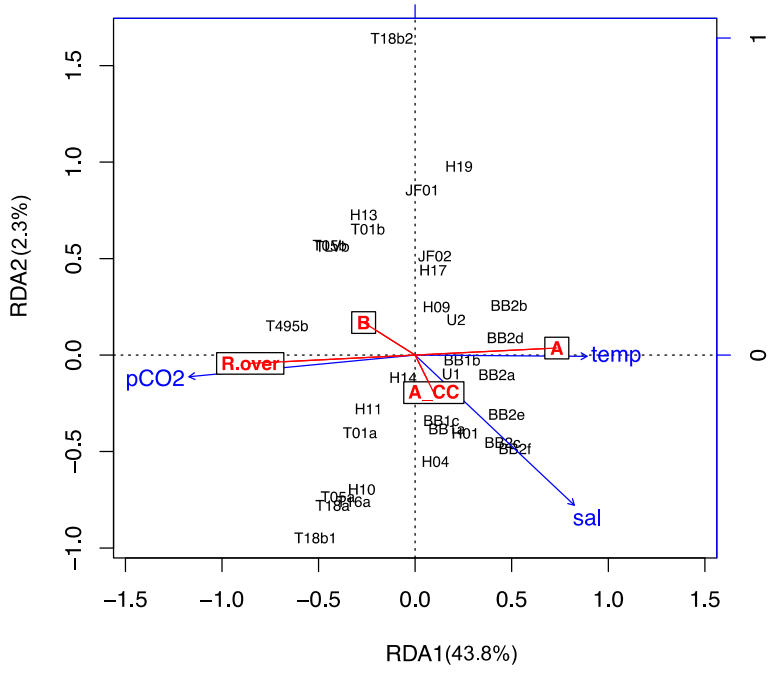

Figure S3. Redundancy analysis (RDA) results for *Emiliania huxleyi* morphotype distributions constrained by environmental variables. The relative abundances of *E. huxleyi* morphotypes (red labels) from surface stations (black labels) were constrained by three environmental variables (blue arrows). Percentage of variance explained by each RDA axis are displayed. Only the first RDA axis appeared to be significant ($p < 0.05$). RDA triplot was performed with site scores and scaling 2.

2.6.3 Measured alkalinity change versus alkalinity changes predicted from PIC and nutrient consumption.

All carbonate system parameters are provided in Supplementary Table S1. Precipitation of 1 mole of $CaCO_3$ should consume 2 moles of alkalinity. Thus there should be a linear relationship between PIC production and alkalinity decrease (Zeebe and Wolf-Gladrow, 2003). In an initial analysis we observed that alkalinity decreases in strain CHC342 at the control (400 µatm) CO_2 treatment were higher than expected (-421.4 ± 32.2 µmol kg^{-1}). Over all strains and all treatments, observed alkalinity decreases were significantly linearly related (R^2 = 0.594, p < 0.0001 for difference from a slope of 0) to the expected alkalinity decreases calculated as twice the PIC contents (in µmol kg^{-1}). However, the slope between observed and expected alkalinity change was significantly greater than 1 (slope 1.54 ± 0.22, 95% confidence interval 1.09 to 1.99). Visual inspection indicated that all replicates from strain CHC342 at the control CO_2 treatment, and three out of four replicates from strain CHC440 at the control treatment, but no other samples, were above the 95% confidence interval for the regression. We performed the regression again, eliminating all samples of CHC342 and CHC440 (both control and high CO_2/low pH treatments). In that case, there was also a significant linear relationship between observed and expected alkalinity decreases (R^2 = 0.73, p < 0.0001), but the slope was not significantly different from 1 (slope 0.89 ± 0.13, 95% confidence interval 0.62 to 1.17) (curve not shown).

Smaller alkalinity changes are also associated with the uptake of nutrients by phytoplankton (Zeebe and Wolf-Gladrow, 2003): Assuming most phosphate is in the form HPO_4^{2-} at the experimental pH, alkalinity should decrease by one mole for every mole of phosphate consumed. Alkalinity should increase by one mole for every nitrate consumed.

Table S1. Complete carbonate system parameters during the experiment. Means (Ave) ± standard deviations (SD) of experimental replicates at the time of inoculation (Initial) and harvesting (Final) are given. pH at the experimental temperature is calculated from measured pH at 25˚C. Treatment is specified by CO_2 partial pressure (µatm) of air:CO_2 mix. pCO_2 units are µatm, alkalinity, [CO_2], [HCO_3^-], and [CO_3^{2-}] units are µmol kg^{-1}. "na" indicates data not available.

Strain	Treatment		pCO_2				alkalinity				pH				[CO_2] dissolved				[HCO_3^-]				[CO_3^{2-}]				Omega-Ca			
			Initial		Final		Initial		Final		Initial		Final		Initial		Final		Initial		Final		Initial		Final		Initial		Final	
			Ave	SD	Ave	SD	Ave	SD	Ave	SD	Ave	SD	Ave	SD	Ave	SD	Ave	SD	Ave	SD	Ave	SD	Ave	SD	Ave	SD	Ave	SD	Ave	SD
342	380	cont.	399.0		386.4		2262		2268		8.041		8.053		14.92		14.43		1881		1875		153.4		158.1		3.665		3.770	
		cult.	422.0	38.2	332.4	4.3	2260	7	1839	25	8.020	0.033	8.029	0.010	15.76	1.45	12.42	0.17	1892	29	1524	16	148.1	9.6	121.1	4.1	3.531	0.225	2.891	0.097
	1200	cont.	1230		1279		2273		2268		7.604		7.586		50.79		47.78		2117		2117		62.7		60.8		1.500		1.451	
		cult.	1314	26.7	1257	36.4	2264	5	2207	19	7.574	0.008	7.582	0.010	49.36	1.03	46.92	1.32	2118	5	2060	20	58.6	1.1	58.7	0.9	1.402	0.026	1.400	0.022
352	380	cont.	418.5		373.4		2289		2294		8.027		8.071		16.18		14.30		1927		1896		145.9		160.6		3.483		3.835	
		cult.	402.5	5.9	370.0	na	2292	13	2168	na	8.042	0.005	8.035	0.021	15.56	0.23	14.17	na	1918	12	1801	na	150.4	1.7	146.4	na	3.591	0.041	3.494	na
	1200	cont.	1270		1260		2278		2138		7.589		7.595		47.88		48.27		2132		2138		58.9		60.5		1.406		1.444	
		cult.	1226	27.6	1341	64.6	2274	12	2261	20	7.601	0.007	7.561	0.018	47.58	1.06	51.37	2.48	2124	13	2122	20	60.3	0.6	56.1	2.4	1.440	0.015	1.339	0.057
360	380	cont.	423.6				2260				8.018				15.37				1884				151.6				3.623			
		cult.	441.5	18.7	457.4	47.7	2270	6	2126	7	8.005	0.016	7.965	0.040	16.00	0.67	16.64	1.78	1901	0	1799	25	148.8	8.7	129.5	11.8	3.552	0.105	3.079	0.270
	1200	cont.	na		1336		2264		2248		na		7.564		na		48.86		na		2100		na		59.4		na		1.416	
		cult.	1186	94.7	1409	156.3	2289	10	2254	4	7.623	0.033	7.545	0.043	42.98	3.39	51.46	5.80	2118	19	2111	17	69.1	4.4	57.6	5.5	1.648	0.107	1.370	0.128
428	380	cont.	432.2		419.4		2255		2250		8.009		8.019		15.65		15.38		1883		1876		149.4		150.1		3.564		3.579	
		cult.	440.3	21.5	418.5	12.9	2261	6	2157	19	8.004	0.018	8.004	0.010	15.95	0.78	15.34	0.47	1893	15	1807	20	148.3	4.9	139.6	2.3	3.537	0.117	3.328	0.035
	1200	cont.	1191		1285		2256		2268		7.614		7.585		43.13		47.09		2090		2114		66.8		62.2		1.594		1.483	
		cult.	1259	6.4	1247	30.6	2262	4	2250	5	7.592	0.002	7.592	0.009	45.76	0.23	45.87	1.13	2104	4	2094	8	63.8	0.3	62.7	1.1	1.521	0.007	1.494	0.027
440	380	cont.	496.6		407.8		2260		2281		7.958		8.060		18.78		15.33		1940		1932		129.0		144.5		3.077		3.610	
		cult.	457.4	26.0	381.6	5.6	2254	6	2114	17	7.988	0.021	8.033	0.005	17.30	0.98	13.84	0.29	1915	16	1751	7	136.6	5.3	144.8	5.5	3.259	0.127	3.469	0.104
	1200	cont.	1455		1290		2270		2274		7.533		7.586		54.77		46.61		2137		2117		53.6		63.4		1.278		1.514	
		cult.	1486	32.2	1249	55.0	2261	5	2235	7	7.522	0.009	7.591	0.019	56.18	1.21	45.05	1.82	2131	6	2077	7	52.1	0.9	63.5	1.8	1.243	0.022	1.512	0.050

Nutrient data is not available (samples were taken but lost in transit). However, when nutrients are not limiting, nitrate and phosphate are consumed (and particulate organic N and particulate organic P is formed) in approximately Redfield ratios with C, while N and P quotas are decreased under nutrient limitation (e.g., Rokitta *et al*., 2014, 2016). A corrected estimation of expected alkalinity change was calculated as:

$$\text{Expected } \Delta_{\text{alkalinity}} = -2\text{xPIC} - \text{POC}/106 + \text{POC}/6.625,$$

where PIC, POC, and alkalinity values are in μmol kg^{-1}. This estimation lacks precision. For example, if PIC is underestimated, POC is overestimated, so the correction will be overestimated. However, it aids in determining whether or not the correction could improve the match between expected and observed alkalinity. When all data is considered, the slope is 1.62 ± 0.24 (R^2 = 0.58, p < 0.0001) (Fig. S4). The slope is significantly greater than one (95% confidence interval 1.13 to 2.11), and the y-intercept is not significantly different from 0 (9.94 ± 22.5, 95% confidence interval -35.8 to 55.6). When data from strains CHC342 and CHC440 are excluded, there is also a significant relationship, with slope = 0.920 ± 0.140 (R^2 = 0.717, p < 0.0001) (Fig. S4). The slope is not significantly different from 0 (95% confidence interval 0.62 to 1.22) and the y-intercept is also not significantly different from 0 (-0.96 ± 11.93, 95% confidence interval -26.1 to 24.2). More importantly, the correction did not decrease the difference between measured and expected alkalinity changes for either strains CHC342 or CHC440 under the control CO_2/pH condition.

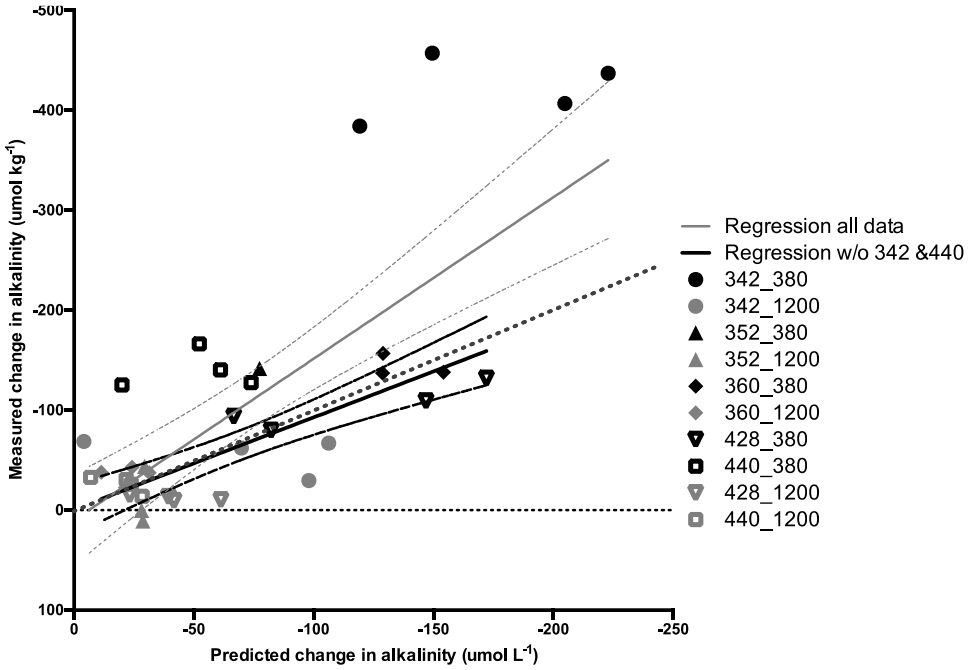

Figure S4. Measured change in alkalinity versus change in alkalinity predicted from measured PIC and POC. The grey continuous line represents the linear regression considering all data, with the grey dashed lines representing the 95% confidence interval of the regression. The black continuous and dashed lines similarly represent the linear regression and 95% confidence interval when data from strains CHC342 and CHC440 is left out. The dotted black line represents the 1:1 relationship between observed and predicted alkalinity change.

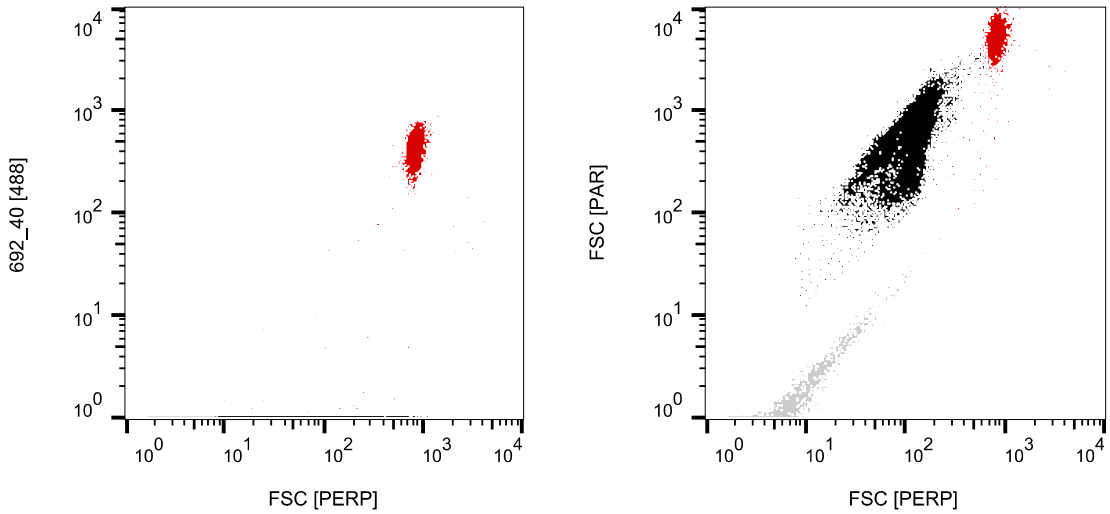

Figure S5. Example flow cytograms (of CHC352 at 400 µatm CO2) showing identification of chlorophyll-containing (red fluorescent cells) in plot of 692 nm (40 nm band pass) fluorescence (y-axis) vs forward scatter with polarization parallel to laser (FSC) (a) and cytogram of scatter depolarization (FSC with polarization perpendicular to laser vs FSC with polarization parallel to laser) (b). Chlorophyll-containing cells are represented by red dots, black dots represent detached coccoliths, and grey dots represent other particles, which are mostly not optically active and fall on a straight line in panel b.

2.6.4 Environmental parameters and associated coccolithophore counts, and taxonomic occurrences and relative abundances.

Table S2. Environmental and biological data for the Eastern South Pacific corresponding to spring 2011 (JF and TONa surveys), spring 2012 (TONb,c and QUI surveys), and winter 2013 (NBP 1305 cruise) periods.

Station ID	Latitude (South)	Longitude (West)	Z (m)	Offshore distance (km)	Temp. (ºC)	Sal. (PSU)	pCO_2 (µatm)	pH	CO_3^{2-} (µmol kg SW^{-1})	Ω calcite	Coccolith. abundances (cells L^{-1})	*E. huxleyi* morphotypes rel. abund. (%)			
												B, O, B/C	A	A_CC	R/over-cal.
JF01	-33.596	-78.630	5	650	14.76	34.18	353.9	8.09	164.1	3.93	29721	17.9	82.1	0.0	0.0
JF02	-33.660	-78.602	5	645	14.91	34.21	333.5	8.11	173.2	4.15	3336	7.1	92.9	0.0	0.0
TON01a	-30.117	-71.619	5	23	12.25	34.48	718.0	7.81	87.9	2.10	25677	20.2	16.7	15.5	47.6
TON05a	-30.181	-71.573	5	11	12.72	34.49	658.9	7.85	97.2	2.32	16579	16.7	6.3	18.8	58.3
TON16	-30.248	-71.650	5	1	12.35	34.54	614.0	7.88	103.3	2.47	13614	16.2	10.8	21.6	51.4
TON18a	-30.247	-71.694	5	6	12.40	34.55	620.8	7.87	101.9	2.43	5762	13.5	5.4	16.2	64.9
TON01b	-30.117	-71.619	5	23	14.10	33.83	635.2	7.86	101.7	2.44	42660	44.8	18.4	5.7	31.0
TON05b	-30.181	-71.573	5	11	13.90	34.18	637.7	7.86	103.4	2.47	76223	42.9	4.8	3.6	48.8
TON18b	-30.247	-71.694	5	6	14.10	34.44	559.7	7.92	117.6	2.81	54185	6.5	2.2	10.8	80.6
TON495c	-30.495	-71.774	5	8	13.54	34.50	809.4	7.77	85.6	2.05	5055	13.6	0.0	9.1	77.3
TONLVc	-30.238	-71.652	5	2	14.40	34.00	723.6	7.82	95.2	2.28	16444	19.3	11.4	1.1	68.2
TON18c	-30.247	-71.694	5	6	14.46	34.60	618.7	7.88	110.1	2.63	21330	54.3	28.3	6.5	10.9
QUI01	-33.379	-71.734	5	4	14.12	34.41	934.0	7.71	77.2	1.84	885	5.0	0.0	5.0	90.0
HYDRO01	-22.216	-74.227	2.5	414	17.88	35.18	396.0	8.06	180.7	4.31	44480	3.1	87.5	9.4	0.0
HYDRO04	-17.092	-78.635	5	701	18.19	35.22	412.2	8.04	177.8	4.24	20117	2.3	90.7	7.0	0.0
BB1a	-13.999	-81.199	5	532	18.75	35.34	413.5	8.04	181.8	4.33	22644	6.5	82.6	10.9	0.0
BB1b	-13.921	-81.277	5	527	18.76	35.35	416.6	8.04	180.9	4.31	10311	0.0	100	0.0	0.0
BB1c	-13.710	-81.389	5	560	18.82	35.39	418.1	8.04	180.9	4.31	19612	8.3	80.6	11.1	0.0
HYDRO09	-12.992	-82.198	5	622	19.24	35.42	405.2	8.05	187.4	4.46	16680	8.6	90.0	1.4	0.0
HYDRO10	-16.749	-85.998	int	1424	19.77	35.53	398.6	8.05	193.8	4.62	43267	0.0	100	0.0	0.0
HYDRO11	-16.749	-84.998	0*	1307	19.77	35.50	409.7	8.04	190.0	4.53	26082	1.9	98.1	0.0	0.0
HYDRO13	-16.750	-83.000	int	1094	19.43	35.52	403.9	8.05	189.7	4.52	33259	26.8	73.2	0.0	0.0
HYDRO14	-16.749	-82.000	0	1010	19.24	35.51	405.9	8.05	188.0	4.48	48119	1.3	98.7	0.0	0.0
HYDRO17	-16.749	-79.000	0	674	18.38	35.38	402.5	8.05	183.0	4.36	42660	6.0	94.0	0.0	0.0
U1	-19.467	-76.150	int	623	17.53	35.14	444.8	8.01	164.9	3.93	23037	0.0	100	0.0	0.0
HYDRO19	-21.499	-73.499	int	355	17.06	35.02	389.7	8.06	175.9	4.20	19829	14.3	85.7	0.0	0.0
U2	-21.502	-73.246	int	329	16.68	34.89	396.0	8.05	171.4	4.09	43547	18.4	71.4	10.2	0.0
BB2a	-20.419	-70.675	int	53	17.20	35.11	448.0	8.01	161.6	3.85	39223	8.2	77.6	14.3	0.0
BB2b	-20.769	-70.659	int	48	16.81	35.09	464.3	8.00	155.3	3.70	48524	2.6	94.9	2.6	0.0
BB2c	-20.755	-70.650	int	47	16.30	34.96	490.7	7.97	145.8	3.48	39270	3.6	78.6	17.9	0.0
BB2d	-20.742	-70.644	int	47	16.69	34.98	467.9	7.99	153.1	3.65	61059	4.4	88.9	6.7	0.0
BB2e	-20.748	-70.657	int	47	17.14	35.10	457.2	8.00	158.9	3.79	55802	2.4	85.4	12.2	0.0
BB2f	-20.732	-70.682	5	52	16.92	35.10	453.0	8.01	160.3	3.82	38881	0.0	92.0	8.0	0.0

* – bucket; int – onboard uncontaminated seawater intake (onboard running seawater system).

Table S3. Absolute abundances of coccolithophores recorded in stations that appear in Fig. S1-S2. na – no available data.

Station ID	Depth (m)	Total coccolithophore abundances (x10^3 cells L^{-1})
H04	5	20.1
	60	17.3
H13	2.5	33.3
	50	33.8
	100	5.0
H19	5	19.8
	30	44.5
	75	17.7
BB2f	5	38.9
	15	26.1
	60	na
	80	na
TON01	5	25.7
	30	7.6
TON18	5	5.8
	30	30.4
JF01	5	29.7
	40	14.7
	80	3.1
JF02	5	3.3
	40	24.5
	80	3.4
H01	2.5	44.5
	50	51.6
BB1a	5	22.6
	58	14.4
BB1b	5	10.3
	51	2.7
H10	2.5	43.3
	100	14.0
H17	0	42.7
	80	13.6
BB2b	5	48.5
	45	2.0
	68	3.1
BB2c	5	39.3
	150	na

Table S4. Taxonomic and relative abundances (%) of coccolithophore species found inhabiting the Eastern South Pacific.

Cruise/survey		Juan Fernández 2011						Tongoy Bay 2011						Tongoy Bay 2012a			Tongoy Bay 2012b			El Quisco 2012	
Station ID		01			02			01a		05a	16	18a		01b	05b	18b	495	LV	18c	01	
Depth (m)		5	40	80	5	40	80	5	30	5	5	5	30	5	5	5	5	5	5	5	15
Coccolithophore species	Family																				
Emiliania huxleyi	Noelaerhabdaceae	57	57	26	14	18	44	84	41	48	37	37	55	88	86	106	22	88	92	8	12
Gephyrocapsa parvula		0	0	0	0	0	0	0	0	0	0	0	0	0	0	0	0	0	0	0	0
Gephyrocapsa ericsonii		7	2	0	0	1	0	0	0	0	0	0	0	0	0	0	0	0	0	0	0
Gephyrocapsa muellerae		5	11	5	2	1	3	3	1	7	2	13	3	7	17	4	0	4	19	0	0
Gephyrocapsa oceanica		0	0	0	0	0	0	0	1	2	0	0	0	0	1	0	0	0	0	0	0
Rhabdosphaera clavigera	Rhabdosphaeraceae	0	0	0	0	0	0	0	0	0	0	0	0	0	0	0	0	0	0	0	0
Palusphaera vandelii		0	0	0	0	0	0	0	0	0	0	0	0	0	0	0	0	0	0	0	0
Discosphaera tubifera		0	0	0	0	1	0	0	0	0	0	0	0	0	0	0	0	0	0	0	0
Acanthoica quattrospina		0	0	0	0	0	0	0	0	0	0	0	0	0	0	0	0	0	0	0	0
Algirosphaera robusta		0	0	0	0	0	0	0	0	0	0	0	0	0	1	0	0	0	0	0	0
Syracosphaera ossa	Syracosphaeraceae	0	2	0	0	0	0	0	0	0	0	1	0	0	1	0	0	0	0	0	0
Syracosphaera prolongata		0	0	0	0	0	0	0	0	0	0	0	0	0	0	0	0	0	0	0	0
Syracosphaera squamigera		0	0	0	0	0	0	0	0	0	0	0	0	0	0	0	0	0	0	0	0
Syracosphaera molischii		0	0	0	0	0	0	3	0	2	0	0	3	3	0	0	0	2	1	0	0
Syracosphaera pulchra		1	0	0	0	0	0	0	0	0	0	0	0	0	0	0	0	0	0	0	0
Syracosphaera cf. bannockii		0	1	0	1	0	0	0	0	0	0	0	2	0	0	0	0	0	0	0	0
Syracosphaera histrica		0	0	0	0	0	0	0	0	0	0	0	0	0	0	0	0	0	0	0	0
Syracosphaera anthos		0	0	0	0	0	0	0	0	0	0	0	0	0	0	0	0	0	0	0	0
Syracosphaera lamina		0	0	0	0	0	0	0	0	0	0	0	0	0	0	0	0	0	0	0	0
Michaelsarsia elegans		0	0	0	0	0	0	0	0	0	0	0	0	0	0	0	0	0	0	0	0
Ophiaster formosus		0	0	0	0	0	0	0	0	0	0	0	0	0	0	0	0	0	0	0	0
Calciosolenia brasiliensis	Calciosoleniaceae	0	0	0	0	0	0	0	0	0	0	0	0	0	0	0	0	0	0	0	0
Calciosolenia murrayi		0	0	0	0	0	0	0	0	0	0	0	0	1	1	0	0	0	0	0	0
Oolithotus antillarum	Calciscaceae	0	0	0	0	0	0	0	0	0	0	0	1	0	0	0	0	0	0	0	0
Calcidiscus leptoporus		0	1	5	1	0	16	1	0	0	0	0	3	4	0	0	0	0	1	0	0

Hayaster perplexus		0	0	0	0	0	0	0	0	0	0	0	0	0	0	0	0	0	0	0
Umbilicosphaera sibogae		0	0	1	4	0	0	0	0	0	0	0	0	0	0	0	0	0	0	0
Alisphaera unicornis	Alisphaeraceae	0	0	0	0	0	0	0	0	0	0	0	0	0	0	0	0	0	0	0
Alisphaera pinnigera	Alisphaeraceae	0	0	0	0	0	0	0	0	0	0	0	0	0	0	0	0	0	0	0
Umbellosphaera irregularis	Umbellosphaeraceae	0	0	0	0	0	0	0	0	0	0	0	0	0	0	0	0	0	0	0
Umbellosphaera tenuis	Umbellosphaeraceae	0	0	0	0	0	0	0	0	0	0	0	0	0	0	0	0	0	0	0
Pontosphaera syracusana	Pontosphaeraceae	0	2	0	0	0	0	0	0	0	0	0	0	0	0	0	0	0	0	0
Scyphosphaera apsteinii	Pontosphaeraceae	0	0	0	0	0	0	0	0	0	0	0	0	0	0	0	0	0	0	0
Helicosphaera carteri	Helicosphaeraceae	0	1	0	0	0	0	1	0	0	0	0	0	1	2	1	0	0	0	0
Helicosphaera hyalina	Helicosphaeraceae	0	0	0	0	0	0	0	0	0	1	0	1	0	0	0	0	0	0	0
Pappomonas sp. type 2	Pappomonas sphaera	0	0	0	0	0	0	0	0	0	0	0	0	0	0	0	0	0	0	0
Florisphaera profunda	a	0	0	0	0	0	0	0	0	0	0	0	0	0	0	0	0	0	0	0
Gladiolithus flabellatus	a	0	0	0	0	0	0	0	0	0	0	0	0	0	0	0	0	0	0	0
Coronosphaera mediterranea	b	0	0	0	0	0	0	0	0	0	0	0	1	0	0	0	0	0	0	0
Tetralithoides quadrilaminata	c	0	0	0	0	0	0	0	0	0	0	0	0	0	0	0	0	0	0	0

Table S4. *continuation*

Cruise		NBP 2013																			
Station ID		H01		H04		BB1a		BB1b		BB1c	H09	H10			H11	H13			H14	H17	
Depth (m)		2.5	50	5	60	5	58	5	51	5	0-70	2.5	60	100	0	2.5	50	100	0	0	80
Coccolithophore species	Family																				
Emiliania huxleyi	Noelaerhabdaceae	33	28	43	67	47	24	19	20	37	71	35	52	69	54	56	87	42	79	50	40
Gephyrocapsa parvula	Noelaerhabdaceae	16	10	38	15	9	6	23	7	24	15	7	3	0	3	3	6	3	7	16	21
Gephyrocapsa ericsonii	Noelaerhabdaceae	21	38	18	13	11	4	12	11	17	15	4	4	5	3	7	7	7	15	40	41
Gephyrocapsa muellerae	Noelaerhabdaceae	2	0	0	0	0	0	0	0	0	0	0	0	0	0	0	0	0	0	0	0
Gephyrocapsa oceanica	Noelaerhabdaceae	0	0	0	0	0	0	0	0	0	0	0	0	0	0	0	0	0	0	0	0
Rhabdosphaera clavigera	Rhabdosphaeraceae	1	0	0	0	0	0	0	0	0	0	0	0	1	0	0	0	0	0	0	0
Palusphaera vandelii	Rhabdosphaeraceae	0	1	0	0	0	0	0	0	0	0	1	0	0	1	0	0	0	0	0	0

Discosphaera tubifera		0	0	0	0	0	0	0	0	0	0	0	0	0	0	0	0	0	0	0	0
Acanthoica quattrospina		0	0	0	0	0	0	0	0	0	0	2	0	1	1	1	0	0	0	0	0
Algirosphaera robusta		1	0	0	1	0	0	0	0	0	0	0	0	1	0	0	0	0	0	0	0
Syracosphaera ossa	Syracosphaeraceae	2	1	0	1	0	0	0	0	1	0	2	0	0	1	1	0	1	1	1	0
Syracosphaera prolongata		1	0	0	0	0	0	0	1	0	0	0	0	0	0	0	0	0	0	0	0
Syracosphaera squamigera		0	0	2	1	0	0	0	0	0	0	1	0	0	3	0	0	0	0	0	0
Syracosphaera molischii		0	0	0	0	1	0	1	0	0	2	0	0	0	1	0	1	1	0	0	0
Syracosphaera pulchra		0	0	0	0	0	0	0	0	3	0	0	0	1	0	0	0	0	0	0	0
Syracosphaera cf. bannockii		0	0	0	0	0	0	0	1	0	2	2	0	0	0	0	1	1	1	0	0
Syracosphaera histrica		0	0	0	0	0	0	0	0	0	0	1	0	0	0	0	0	0	0	0	0
Syracosphaera anthos		0	0	0	0	0	0	0	0	0	0	0	0	0	0	0	0	0	0	0	0
Syracosphaera lamina		0	0	0	0	0	0	0	0	0	0	0	0	0	0	0	0	0	0	0	0
Michaelsarsia elegans		1	0	0	0	0	0	0	0	0	0	0	1	0	0	0	0	0	0	0	0
Ophiaster formosus		0	0	0	0	0	0	0	0	0	0	0	0	0	0	0	0	1	0	0	0
Calciosolenia brasiliensis	Calciosoleniaceae	0	0	0	0	1	0	1	0	0	1	0	1	0	1	0	0	0	0	0	0
Calciosolenia murrayi		0	0	0	0	0	0	0	0	0	0	0	0	0	1	0	0	0	0	0	0
Oolithotus antillarum	Calcidiscaceae	1	2	0	0	0	0	0	1	0	0	0	0	0	0	0	1	1	0	1	1
Calcidiscus leptoporus		0	0	0	1	0	1	4	10	1	2	0	0	0	0	0	0	0	0	0	0
Hayaster perplexus		0	0	0	0	0	0	0	0	0	0	0	0	0	0	0	0	1	0	0	0
Umbilicosphaera sibogae		0	0	0	0	0	0	0	0	0	0	0	0	0	0	0	0	0	0	0	0
Alisphaera unicornis	Alisphaeraceae	0	0	0	0	1	0	0	0	0	0	0	0	0	0	0	0	0	0	0	0
Alisphaera pinnigera		0	0	0	0	0	0	0	0	0	0	0	0	0	0	0	0	1	0	0	0
Umbellosphaera irregularis	Umbellosphaeraceae	0	0	0	0	0	0	0	0	0	0	1	0	0	0	0	0	0	0	0	0
Umbellosphaera tenuis		0	0	0	0	0	0	0	0	0	0	0	0	0	1	0	0	0	0	0	0
Pontosphaera syracusana	Pontosphaeraceae	0	0	0	0	0	0	0	0	0	0	0	0	0	0	0	0	0	0	0	0
Scyphosphaera apsteinii		0	0	0	0	0	0	0	0	0	0	0	0	0	0	0	0	0	0	0	0
Helicosphaera carteri	Heli	0	0	0	0	0	0	0	0	0	0	0	1	0	0	0	0	0	0	0	0

Helicosphaera hyalina		0	0	0	0	0	0	0	0	0	0	0	0	0	0	0	0	0	0	0	0
Pappomonas sp. type 2	Pappos phaera	0	0	0	0	0	0	0	0	0	0	0	0	0	0	0	0	0	0	0	0
Florisphaera profunda	a	0	0	0	0	0	1	0	0	0	0	0	0	0	0	0	0	10	1	0	0
Gladiolithus flabellatus	a	0	0	0	0	0	0	0	0	0	0	0	0	0	0	0	0	1	0	0	0
Coronosphaera mediterranea	b	0	0	0	1	0	0	0	0	1	0	0	0	0	0	0	0	0	0	0	0
Tetralithoides quadrilaminata	c	0	0	0	0	0	0	0	0	0	0	0	0	0	0	0	0	2	0	0	0

Table S4. *continuation*

Cruise			NBP 2013 (continuation)																		
Station ID		U1	H19			U2	BB2a		BB2b			BB2c	BB2d	BB2e	BB2f						
Depth (m)		5	5	30	75	5	5	88	5	45	68	5	5	5	5	15	30	60	80	100	
Coccolithophore species	Family																				
Emiliania huxleyi	Noelaerhabdaceae	11	36	25	36	50	49	26	39	30	25	28	46	41	27	21	34	31	25	20	
Gephyrocapsa parvula	Noelaerhabdaceae	21	6	5	4	6	26	21	26	15	17	22	32	30	20	31	19	23	25	18	
Gephyrocapsa ericsonii	Noelaerhabdaceae	36	23	38	19	10	25	10	26	10	17	16	18	28	18	11	13	10	9	22	
Gephyrocapsa muellerae	Noelaerhabdaceae	0	0	1	2	3	3	4	5	2	4	6	9	2	2	3	4	4	3	0	
Gephyrocapsa oceanica	Noelaerhabdaceae	0	0	0	0	0	0	0	0	2	0	0	0	0	0	0	0	1	3	1	
Rhabdosphaera clavigera	Rhabdosphaeraceae	0	0	0	0	0	0	0	0	0	0	0	0	0	0	0	0	0	0	0	
Palusphaera vandelii	Rhabdosphaeraceae	0	0	0	0	0	0	0	0	0	0	0	0	0	0	0	0	0	0	0	
Discosphaera tubifera	Rhabdosphaeraceae	0	1	0	0	0	0	0	0	0	0	0	0	0	0	0	0	0	0	0	
Acanthoica quattrospina	Rhabdosphaeraceae	0	0	0	0	0	0	0	0	0	0	0	0	0	0	0	0	0	0	0	
Algirosphaera robusta	Rhabdosphaeraceae	0	0	1	0	0	0	0	0	0	0	0	0	0	0	0	0	0	0	0	
Syracosphaera ossa	Syracosphaeraceae	1	4	1	2	2	0	0	0	0	0	0	0	0	0	0	0	0	0	0	
Syracosphaera prolongata	Syracosphaeraceae	0	0	0	0	0	0	0	0	0	0	0	0	0	0	0	0	0	0	0	
Syracosphaera squamigera	Syracosphaeraceae	1	1	0	0	1	0	0	0	0	0	0	0	0	0	0	0	0	0	0	
Syracosphaera molischii	Syracosphaeraceae	0	0	0	0	0	0	0	1	0	0	0	0	1	0	0	0	0	0	0	
Syracosphaera pulchra	Syracosphaeraceae	0	0	1	0	0	0	0	0	0	0	0	0	0	0	0	0	0	0	0	

Syracosphaera cf. bannockii		0	0	1	0	0	0	0	1	0	0	0	2	0	0	1	0	0	0	0
Syracosphaera histrica		0	0	0	1	1	0	0	0	0	0	0	0	0	0	0	0	0	0	0
Syracosphaera anthos		0	0	1	0	0	0	0	0	0	0	0	0	0	0	0	0	0	0	0
Syracosphaera lamina		0	0	0	0	0	0	0	0	1	0	0	0	0	0	0	0	0	0	0
Michaelsarsia elegans		0	0	0	0	0	0	0	0	0	0	0	0	0	0	0	0	0	0	0
Ophiaster formosus		0	0	0	0	0	0	0	0	0	0	0	0	0	0	0	0	0	0	0
Calciosolenia brasiliensis	Calciosoleniaceae	0	0	0	0	0	0	0	0	0	0	0	0	0	0	0	0	0	0	0
Calciosolenia murrayi		0	0	0	0	0	0	0	0	0	0	0	0	0	0	0	0	0	0	0
Oolithotus antillarum	Calcidiscaceae	1	0	1	1	0	0	1	0	0	0	0	0	0	0	0	0	0	0	0
Calcidiscus leptoporus		0	2	2	2	3	0	0	0	0	0	0	0	0	0	0	0	0	0	0
Hayaster perplexus		0	0	0	0	0	0	0	0	0	0	0	0	0	0	0	0	0	0	0
Umbilicosphaera sibogae		0	0	0	3	0	0	0	0	0	0	0	0	0	0	0	0	0	0	0
Alisphaera unicornis	Alisphaeraceae	0	1	0	0	0	0	0	0	0	0	0	0	0	0	0	0	0	0	0
Alisphaera pinnigera		0	0	0	0	0	0	0	0	0	0	0	0	0	0	0	0	0	0	0
Umbellosphaera irregularis	Umbellosphaeraceae	0	0	0	0	0	0	0	0	0	0	0	0	0	0	0	0	0	0	0
Umbellosphaera tenuis		0	0	0	0	0	0	0	0	0	0	0	0	0	0	0	0	0	0	0
Pontosphaera syracusana	Pontosphaeraceae	0	0	0	0	0	0	0	0	0	0	0	0	0	0	0	0	0	0	0
Scyphosphaera apsteinii		0	1	0	0	0	0	0	0	0	0	0	0	0	0	0	0	0	0	0
Helicosphaera carteri	Helicosphaeraceae	0	0	0	0	0	0	0	0	0	0	0	0	0	0	0	0	0	0	0
Helicosphaera hyalina		0	0	0	0	0	0	0	0	0	0	0	0	0	0	0	0	0	0	0
Pappomonas sp. type 2	Papposphaera	0	0	0	0	0	0	0	0	0	0	0	0	0	0	0	0	0	0	0
Florisphaera profunda	a	0	0	0	0	0	0	0	0	0	0	0	0	0	0	0	0	0	0	0
Gladiolithus flabellatus		0	0	0	0	0	0	0	0	0	0	0	0	0	0	0	0	0	0	0
Coronosphaera mediterranea	b	0	0	0	0	0	0	0	0	0	0	0	0	0	0	0	0	0	0	0
Tetralithoides quadrilaminata	c	0	0	0	0	0	0	0	0	0	0	0	0	0	0	0	0	0	0	0

a – nannoliths *incertae sedis*, b – genus *incertae sedis*, c – narrow-rimmed placoliths.

3 CHAPTER TWO: Abundances and morphotypes of the coccolithophore *Emiliania huxleyi* in southern Patagonia compared to neighboring oceans and northern-hemisphere fjords

Authors: Francisco Díaz-Rosas[1,2], Catharina Alves-de-Souza[3], Emilio Alarcón[4,5], Eduardo Menschel[5,6], Humberto E. González[5,6], Rodrigo Torres[4,5], and Peter von Dassow[1,2,7]

[1] Facultad de Ciencias Biológicas, Departamento de Ecología, Pontificia Universidad Católica de Chile, Santiago, Chile

[2] Instituto Milenio de Oceanografía de Chile, Concepción, Chile

[3] Algal Resources Collection, Center for Marine Science, University of North Carolina Wilmington, Wilmington, USA

[4] Centro de Investigación en Ecosistemas de la Patagonia, Coyhaique, Chile

[5] Centro de Investigación Dinámica de Ecosistemas Marinos de Altas Latitudes, Punta Arenas, Chile

[6] Instituto de Ciencias Marinas y Limnológicas, Universidad Austral de Chile, Valdivia, Chile

[7] UMI 3614, Evolutionary Biology and Ecology of Algae, CNRS-UPMC Sorbonne Universités, PUCCh, UACH.

Correspondence to: Francisco Díaz-Rosas (fdiazrosas7@gmail.com), Peter von Dassow (pvondassow@bio.puc.cl)

3.1 ABSTRACT

Coccolithophores are potentially affected by ongoing ocean acidification, where rising CO_2 lowers seawater pH and calcite saturation state (Ω_{cal}). Southern Patagonian fjords and channels provide natural laboratories for studying these issues due to high variability in physical and chemical conditions. We surveyed coccolithophore assemblages in Patagonian fjords during late-spring 2015 and early-spring 2017. Surface Ω_{cal} exhibited large variations driven mostly by freshwater inputs. High Ω_{cal} conditions (max. 3.6) occurred in the Archipelago Madre de Dios. Ω_{cal} ranged from 2.0-2.6 in the western Strait of Magellan, 1.5-2.2 in the Inner Channel, and was sub-saturating (0.5) in the Skyring Sound. *Emiliania huxleyi* was the only coccolithophore widely distributed in Patagonian fjords (> 96% of total coccolithophores), only disappearing in the Skyring Sound, a semi-closed mesohaline system. Correspondence analysis associated higher *E. huxleyi* biomasses with lower diatom biomasses. The highest *E. huxleyi* abundances in Patagonia were in the lower range of those reported in Norwegian fjords. Predominant morphotypes were distinct from those previously documented in nearby oceans but similar to those of Norwegian fjords. Moderate-calcified forms of *E. huxleyi* A morphotype were uniformly distributed throughout Patagonia fjords. The exceptional R/hyper-calcified

coccoliths, associated with low Ω_{cal} values in Chilean and Peruvian coastal upwellings, were a minor component associated with high Ω_{cal} levels in Patagonia. Outlying mean index (OMI) niche analysis suggested that pH/Ω_{cal} conditions explained most variation in the realized niches of *E. huxleyi* morphotypes. The moderate-calcified A morphotype exhibited the widest niche-breadth (generalist), while the R/hyper-calcified morphotype exhibited a more restricted realized niche (specialist). Nevertheless, when considering an expanded sampling domain, including nearby Southeast Pacific coastal and offshore waters, even the R/hyper-calcified morphotype exhibited a higher niche breadth than other closely phylogenetically-related coccolithophore species. The occurrence of *E. huxleyi* in naturally low pH/Ω_{cal} environments indicates that its ecological response is plastic and capable of adaptation.

3.2 INTRODUCTION

Coccolithophores are small unicellular phytoplankton (3-30 μm) bearing intricate calcite plates called coccoliths (Monteiro *et al*., 2016). Coccolithophores carry out most calcium carbonate ($CaCO_3$) precipitation in pelagic systems (Broecker and Clark, 2009), which may enhance organic matter export by $CaCO_3$ ballasting (Klaas and Archer, 2002), while also contributing to alkalinity (Zondervan *et al*., 2001) and the carbonate counter pump (Passow and Carlson, 2012). Thus, understanding how coccolithophores and their functional roles are altered in response to environmental stressors, such as ocean acidification (OA) due to rising pCO_2, is necessary for predicting future ocean biogeochemistry.

Chemically, calcite stability in seawater can be parametrized using its saturation state, defined as $\Omega_{cal} = [Ca^{2+}]\cdot[CO_3^{2-}]/Ksp_{cal}$ (where Ksp_{cal} is the solubility constant for calcite), which is decreased by OA. When $\Omega_{cal} < 1$, calcite dissolution is thermodynamically favored, whereas calcite precipitation is favored when $\Omega_{cal} > 1$. Most of the ocean surface is predicted to remain supersaturated with respect to calcite in the future ocean (Feely *et al*., 2009), although some coastal zones may experience $\Omega_{cal} < 1$ in the euphotic zone either due to increased pCO_2 in areas of naturally high CO_2 upwelling (e.g., Franco *et al*., 2018) or due to freshening (e.g., Tynan *et*

al., 2014). Furthermore, drops in Ω_{cal} may negatively affect biological calcite production rates even before becoming undersaturated (Doney *et al*., 2009).

In contrast to other calcifying organisms, coccolith formation occurs intracellularly in Golgi-derived vesicles, involving sustained fluxes of Ca^{2+} and dissolved inorganic carbon (primarily HCO_3^-) from the external medium, and high H^+ efflux to maintain cellular pH homeostasis (reviewed by Taylor *et al*., 2017). Which extracellular carbonate chemistry parameter most influences intracellular coccolithophore calcification (e.g., whether Ω_{cal} or the HCO_3^- : H^+ ratio) is debated (Bach, 2015; Cyronak *et al*., 2016). Additionally, OA can have contrasting effects, with increased pCO_2 potentially benefiting photosynthesis. A wide range of calcification and growth responses to OA have been reported in laboratory studies of coccolithophores, mostly using the cosmopolitan and most abundant species *Emiliania huxleyi* (reviewed in Meyer and Riebesell, 2015). With some notable exceptions (e.g., Iglesias-Rodriguez *et al*., 2008), most culture studies showed reduced calcification rates of *E. huxleyi* in response to simulated OA, while there is no clear trend on growth rates. In a mesocosm experiment using a Norwegian fjord community, increased pCO_2 levels (> 500 µatm) resulted in lower growth rates of *E. huxleyi*, preventing it from blooming (Riebesell *et al*., 2017). This result contrasted with a long-term observational study showing a steady increase in coccolithophore stocks (related to diatoms and dinoflagellates) from pre-industrial to present-day high pCO_2 levels in the North Atlantic (Rivero-Calle *et al*., 2015), although both studies predict a decrease in net calcification.

Morphological variability in *E. huxleyi* has been reported with several morphotypes described so far with different degrees of calcification of the coccoliths, such as fusion of coccolith elements or calcite overgrowth (Young *et al*., 2003). However, the readily identifiable

qualitative distinctions may not easily translate into quantitative differences in the calcite produced per cell in the ecosystem, as for example, due to variability in the rate of coccoliths produced per cell (Johnsen and Bollmann, 2020). Nevertheless, cultured isolates maintain their morphotype classifications even under variable environmental conditions that can alter total calcite production and even lead to coccolith malformation (e.g., Young and Westbroek, 1991; Langer *et al*., 2011; Müller *et al*., 2015a; von Dassow *et al*., 2018; Mella-Flores *et al*., 2018). Thus, morphotypes are assumed to be genetically determined (Krueger-Hadfield *et al*., 2014) and might reflect adaptations to specific conditions.

In a global survey, Beaufort *et al*. (2011) found a general pattern of decreasing calcification with increasing pCO_2 and a concomitant decrease in CO_3^{2-}. Interestingly, calcite mass variability was predominantly the result of assemblage shifts both among closely related species and among morphotypes of the same species, from predominance of large and heavily-calcified *Gephyrocapsa oceanica* cells, through intermediate moderate-calcified *E. huxleyi* (A morphotype), to more lightly-calcified *E. huxleyi* cells (B/C or C morphotype). In the subtropical and tropical eastern South Pacific, an exceptionally hyper-calcified A morphotype of *E. huxleyi* (henceforth referred to as R/hyper-calcified; showing the complete fusion of distal shield elements and partial or complete calcite overgrowth of the coccolith central area) was dominant in coastal upwelling waters with relatively high pCO_2/low Ω_{cal} levels, causing an inversion in the trend of calcite-per-coccolith vs. Ω_{cal} seen in the rest of the ocean (Beaufort *et al*., 2011; von Dassow *et al*., 2018). Likewise, Smith *et al*. (2012) observed an increase in the proportion of *E. huxleyi*, corresponding to an "over-calcified" morphotype (with complete overgrowth of the coccolith central area but without fusion of distal shield elements, referred to hereon as A-CC for covered central area) that occurred during the winter decline of Ω_{cal}. These

results suggested that perhaps the A-CC and R/hyper-calcified morphotypes are likely resistant to low Ω_{cal}. However, while the B/C morphotype was reported to be especially sensitive to low Ω_{cal} compared to moderately calcified and over-calcified strains of morphotype A (Müller *et al*., 2015a), other experimental results did not find a higher resistance of the R/hyper-calcified subtype to high CO_2/low Ω_{cal} when compared to moderate-calcified strains of morphotype A isolated from neighboring waters (von Dassow *et al*., 2018). These results highlight that it is unclear how the physiological effects of OA on coccolithophores in culturing conditions translate to community-level responses in the field.

Fjords systems provide especially interesting natural laboratories for observing how coccolithophores may be affected by environmental conditions due to high spatial and seasonal variability in chemical and biotic conditions. In the Norwegian fjord system and the neighboring North Sea, *E. huxleyi* has been very well studied for over a century, where it forms dense spring blooms but is also prominent throughout the year (Birkenes and Braarud, 1952; Berge, 1962; Kristiansen *et al*., 1994; Fernandez *et al*., 1996; Egge *et al*., 2015). Southern Patagonia, on the Pacific side of South America, hosts the largest network of fjords and channels in the world. Aquatic ecosystems of southwest Patagonia (50-55º S) are dominated by the transition between oceanic and estuarine-brackish waters. Denser, saltier, nitrate- and phosphate-rich but silicate-poor Sub-Antarctic Surface Water (SAASW) intrudes below nitrate- and phosphate-poor but silicic acid-rich surface waters influenced by substantial freshwater inputs (copious precipitation, rivers, glacier melt; Dávila *et al*., 2002; Sievers and Silva, 2008; Torres *et al*., 2014). Generally, surface waters with low salinity and low alkalinity are undersaturated in dissolved CO_2 during spring-summer seasons (Torres *et al*., 2011). The Archipelago Madre de Dios (AMD) is an interesting exception to this pattern, where extreme precipitation/runoff in

the “limestone” basin on the western AMD produces surface waters with low salinity and high alkalinity while maintaining low dissolved silicate compared with the eastern basin (Torres *et al*., 2020). These gradients create a unique contrast for exploring the influence of chemical conditions on the ecology of calcified phytoplankton, as changes in Ω_{cal} are driven mainly by freshening rather than upwelling of high pCO_2.

In contrast to the Norwegian fjord system, *E. huxleyi* blooms have not been reported in Patagonian fjords but information on coccolithophores in these waters is scarce. A study documenting coccolithophores in the Strait of Magellan found that this group represented a minor fraction of the small-sized phytoplankton (Zingone *et al*., 2011), but other published studies have not specifically sampled for coccolithophores. The Patagonian shelf on the Atlantic side experiences large *E. huxleyi* blooms (Poulton *et al*., 2011, 2013), but satellite observations suggest coccolithophore blooms are of lower intensity in the Pacific waters to the west (Hopkins *et al*., 2019). These observations raise the question of how coccolithophore communities on the western coast and fjords-channels of Patagonia compare with nearby oceans and to fjord systems in the northern hemisphere. Here, we evaluated how physical, chemical, and biological features influence the distribution, abundance, and biomass of coccolithophores as well as the proportions of *E. huxleyi* morphotypes of varying calcification levels throughout southern Patagonia fjords. In particular, three research questions were addressed: i) What coccolithophore assemblages and *E. huxleyi* morphotypes are present in fjords/channels of southern Patagonia? ii) How do these morphotypes and the co-occurring phytoplankton (mostly diatoms) vary with physical and chemical factors? Focusing on the cosmopolitan *E. huxleyi*, iii) does the abundance and relative composition of *E. huxleyi* morphotypes reflect populations in adjacent Pacific, Atlantic, or Southern Ocean waters or instead exhibit similarities to the Norwegian fjord system?

3.3 MATERIALS AND METHODS

3.3.1 Sampling

Two cruises were conducted onboard the vessel M/N *Forrest* during the late austral spring 2015 (26 November to 03 December) and early austral spring 2017 (22 to 28 September) in southern Chilean Patagonia (~50-54º S; 71-76º W). The sampling track of 2015 was from the Archipelago Madre de Dios (AMD), crossing the Inner Channel (IC) to the western part of the Strait of Magellan (WSM), and entering eastward into the Otway and Skyring Sounds (OS, SS) to end up near Punta Arenas (Fig. 2.1a). The 2017 sampling was from the interior WSM, crossing the IC, and ending in the AMD zone (Fig. 2.1b). In both cruises, surface water (< 5 m) was pumped continuously onboard every 15-20 min for determination of salinity and temperature with a YSI-30 Termosalinometer (Yellow Springs, OH, USA) and pCO_2 with a Qubit-S157 CO_2-analyzer (Kingston, Ontario, Canada). The CO_2-analyzer was calibrated daily with 0 ppm CO_2 (air treated with soda lime) and 403 ppm air-CO_2 mixture standard (Indura, Chile). Surface samples for determination of the planktonic assemblages and chemical variables (i.e., concentration of macronutrients, opal, total chlorophyll-*a*, and the carbonate system parameters) were collected at discrete samplings stations (Fig. 2.1a-b). Twenty-one stations were sampled in 2015: five in

the AMD (st. 1-5), four in the IC (st. 6-9), nine in the WSM (st. 10-12, 16-21), two in the OS (st. 13 and 14), and one in the SS (st. 15). Eleven stations were sampled in 2017: three in the AMD (st. 30-32), five in the IC (st. 25-29), and three in the WSM (st. 22-24).

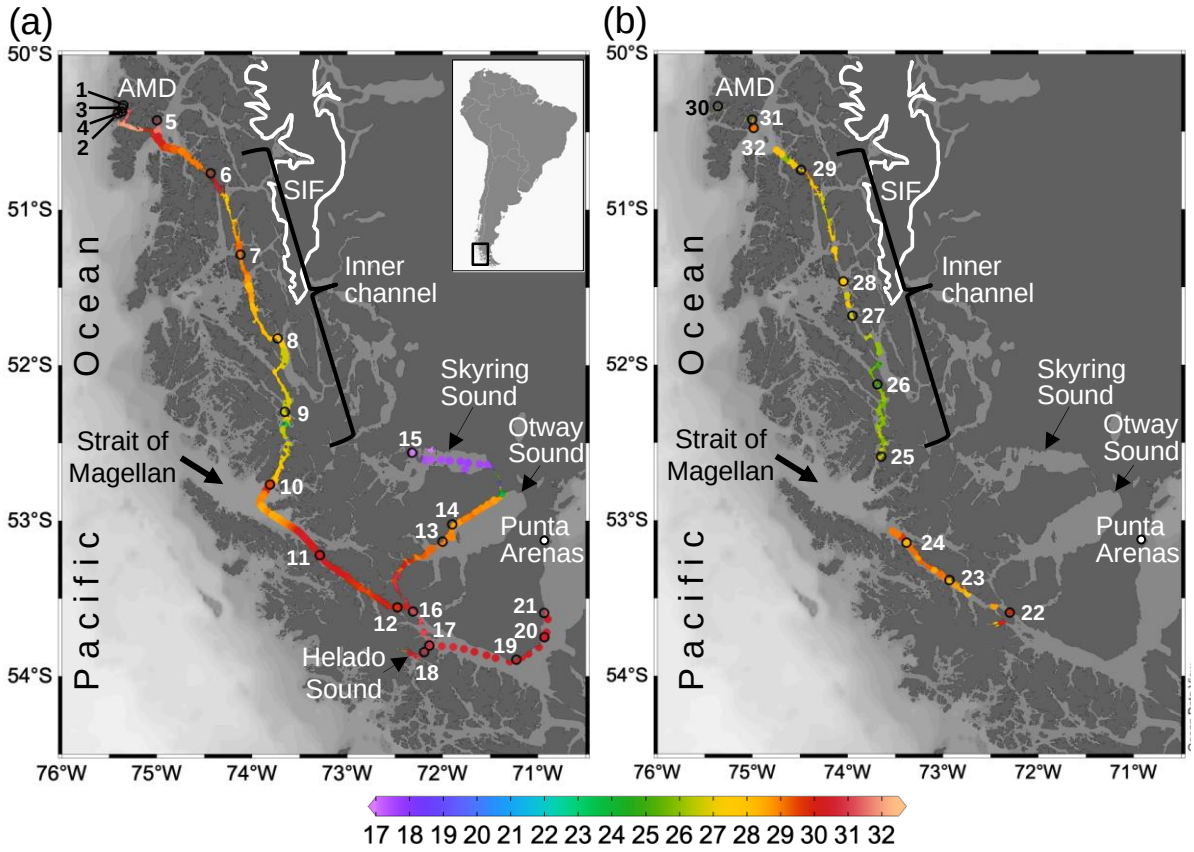

FIGURE Nº 3.1 Maps of southern Patagonia showing the study sites and stations sampled during the austral late-spring 2015 (a) and early-spring 2017 (b). Salinity recorded at the surface during the two cruises is plotted. The approximate perimeter of the Southern Ice Fields (SIF) is depicted. A zoom into the Archipelago Madre de Dios (AMD) zone with salinity and Ω calcite surface values recorded in 2015 is provided in supplementary figure S1. Maps produced by Ocean Data View (Schlitzer, 2018).

CTD vertical profiles were additionally obtained at selected localities on both cruises. In 2015, three casts were performed into the AMD zone and one cast into the SS using a CTD Seabird 19 plus (Sea-Bird Scientific, Bellevue, WA, USA) equipped with photosynthetically available radiation (PAR) and oxygen sensors. Two profiles were performed in 2017 in the AMD zone, by the deployment of a CTD Seabird 25 plus with PAR and oxygen sensors. The depth of

1% of penetration of PAR (euphotic zone) was calculated from maximum surface PAR values. CTD profile binning was 1 m. In both years, samples for the determination of plankton assemblages and chemical variables were obtained at discrete depths using 5-L Niskin bottles to which the CTDs were attached (depths pre-determined from prior studies in the region, aiming to adequately sample the surface mixed layer, pycnocline, and vertical variation in chlorophyll fluorescence). Complete environmental and biological data are provided in supplementary materials (Tables S1-S4).

3.3.2 Plankton assemblages

Samples for the determination of planktonic organisms through the Utermöhl (1958) method were collected only in 2015. For that, duplicate 100-mL water samples were pre-filtered through 200-µm Nitex mesh, fixed with a formaldehyde-glutaraldehyde solution (1% formaldehyde, 0.05% glutaraldehyde, 10 mM borate pH 8.5) and stored at 4º C. In the laboratory, water samples were brought to room temperature, gently homogenized and sedimented into 100-mL chambers for 24-48 h before counting and identification. The absolute abundances of the microplankton (20-200 µm in size) and coccolithophores (~ 6 µm in diameter) were estimated with an inverted microscope (Olympus CKX41) connected to a digital camera (Motic 5.0). For counts of diatoms, dinoflagellates, and other planktonic cells greater than about 40 µm, the whole chamber was examined at 200× magnification. When large chain-forming diatoms were in high density, between 5-60 randomly selected fields of view were examined at 200× magnification until reaching 100 chains. For counts of small diatoms, naked flagellates (including small flagellates and athecated dinoflagellates), and coccolithophores, between 1-4 transects (to reach ≥ 100 cells in total) were analyzed at 400× magnification. Counts of total coccolithophores were performed with a 40× objective with cross-polarized light (Edmund Optics polarizers 54926 and 53347).

In both cruises, samples for the identification and quantification of coccolithophores through scanning electron microscopy (SEM) analysis were obtained by filtering 200-300 mL of surface water, immediately after sampling, onto 0.8-µm polycarbonate filters that were subsequently dried at room temperature. For the identification of coccolithophores and *E. huxleyi* morphotypes, a portion of each dried filter was cut, sputter-coated with gold and examined in either a Quanta 250, Quanta FEG 250, or Quanta Inspect F50 SEM (FEI, Hillsboro, Oregon, USA). As water samples for light microscopy counts were not available for two samples from 2015 (st. 3 and st. 5 at 8 m) and all samples from 2017, total coccolithophores abundances were obtained from SEM counts for those samples. On average, 70 images per filter were captured at 1,500× magnification (276×184 µm per frame), covering 3.5 mm^2 of the filter area corresponding to 1.8-3.4 ml of water analyzed. The coccolithophores abundances were calculated using the following equation:

$$cells\ L^{-1} = \frac{effective\ filtration\ area\ (mm^2) \times total\ number\ of\ counted\ cells}{analized\ filtered\ area\ (mm^2) \times volumen\ of\ filtered\ water\ (L)}$$

To check for differences in coccolithophore counts obtained through sedimentation + inverted light-microscopy versus filtration + SEM examination (hereinafter SEM and Utermöhl counts, respectively), polycarbonate filters from three selected Utermöhl samples (showing higher, medium and lower coccolithophores abundances) were analyzed with SEM as outlined above. Coccolithophores SEM counts were consistently about twice as high compared to Utermöhl counts (average 1.84), agreeing with the correction factor suggested by Bollmann *et al*. (2002). Thus, all total coccolithophore counts obtained by the Utermöhl method were multiplied by 1.84 to be comparable to SEM counts. To estimate the absolute abundances at species- and morphotype-level, the relative abundance of each coccolithophore species or *E. huxleyi* morphotype determined from SEM counts was multiplied by the absolute abundance of

total coccolithophore cells. Saturation curves obtained for each sample confirmed that the number of analyzed coccospheres (minimum 40 coccospheres per sample) was enough to capture the specific/morphotype diversity.

SEM images taken at 20,000-25,000× magnification were used to categorize *E. huxleyi* cells in the different morphotypes according to the morphology of distal shield and the central plate of the coccoliths (following Young and Westbroek, 1991; Young *et al*., 2003; Hagino *et al*., 2011; von Dassow *et al*., 2018). Given high morphological similarities in the A morphotype coccoliths with those found by Young (1994) in Norwegian-fjords, they were here classified as lightly-, moderate-, and robust-calcified, based on the morphology of distal shields and central plates (Fig. 2.2; Table 2.1). Moreover, two extremely heavily-calcified A-morphotypes were observed: the A-CC (with closed central area but distal shield elements mostly not fused) and the R/hyper-calcified (Table 2.1; Fig. 2.2). These two morphotypes are sometimes grouped as "over-calcified" (Cubillos *et al*., 2007; Saavedra-Pellitero *et al*., 2019). However, we have observed in culture that they remain distinct under different physiological stresses (e.g., Mella-Flores *et al*., 2018; von Dassow *et al*., 2018). Due to frequent overlap in coccolith distal shield lengths and coccosphere diameters observed in moderate- and robust-calcified A-forms (Table 2.1), we consolidate them into one group (hereafter jointly referred to as "moderate-calcified A-morphotype") for statistical analyses. Moreover, we classified the malformed (teratological), incomplete, weakly-dissolved and collapsed coccoliths, following the terminology and definitions of Young and Westbroek (1991) and Young (1994). Although these malformed and collapsed coccoliths were observed in < 9 % of the morphotype-A cells, it was almost always possible to classify those abnormal coccospheres into one of the above-mentioned morphotypes

(Fig. S2). SEM images were also used to measure the orthogonal coccosphere diameters and, when available, coccolith distal shield length (ImageJ software version 1.48 for Mac OS).

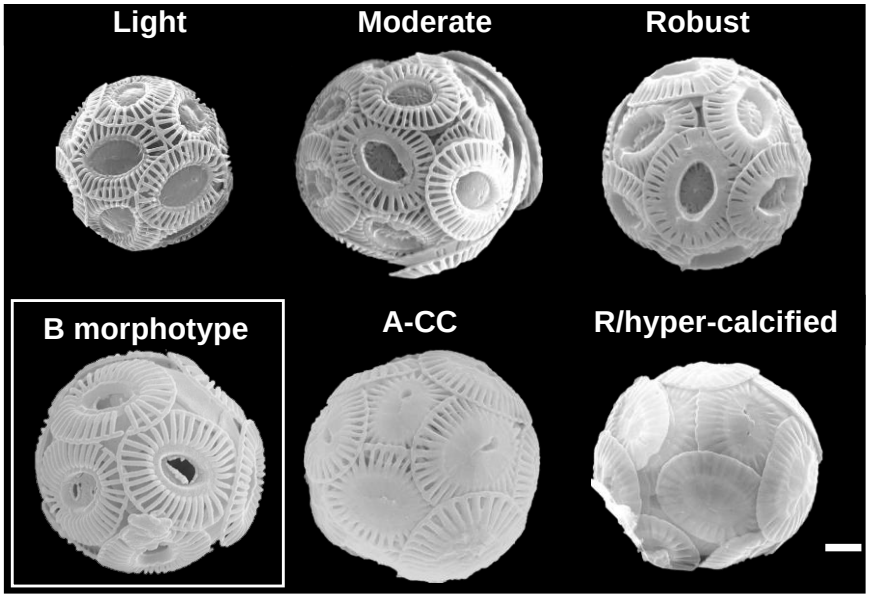

FIGURE Nº 3.2 The main five *E. huxleyi* A-morphotypes recorded in the surface waters of southern Patagonia fjords during the austral late-spring 2015 and early-spring 2017. The light-, moderate- and robust-calcified A-morphotypes (top), and the A-CC and R/hyper-calcified forms (bottom) are shown. The B-morphotype discussed in von Dassow *et al*. (2018) but nor present in this study (bottom-left) is shown for comparative purposes. For statistical analysis, the moderate- and robust-calcified A-morphotypes were merged under "moderate-calcified A-morphotype", and the few O and C specimens were categorized into the lightly-calcified subgroup. Scale bar = 1 μm.

Biovolumes (μm^3) of *E. huxleyi*, diatoms, dinoflagellates, and naked flagellates were estimated assuming recommended geometric shapes (Hillebrand *et al*., 1999; see Table S4). For *E. huxleyi*, a spherical geometric shape was assumed and the maximum diameter used for biovolume calculations. Biovolume calculations were then converted to carbon biomass by using regression equations proposed by Menden-Deuer and Lessard (2000) for diatoms (pg C $cell^{-1} = 0.288 \times volume^{0.811}$) and other protists (pg C $cell^{-1} = 0.216 \times volume^{0.939}$). We assumed a constant cytoplasm diameter to be 60 % of the mean *E. huxleyi* coccosphere diameter (O'Brien *et al*., 2013), whereas cytoplasm volumes of 50 % and 78 % were used for diatoms and dinofla-

TABLE Nº 3.1 Classification of *E. huxleyi* coccospheres based on the calcification level of coccoliths. Mean ± standard deviations of distal shield length and coccosphere diameter are given. The number of coccoliths and coccospheres measured is indicated in the parenthesis.

Morph	Calcification	Distal shield and central area distinguish features	Distal shield length (μm)	Coccosphere size (μm)	Comparable morphotype	Reference
A	Light	Delicate and well separated distal shield elements (> 50 % of distal shield elements is slits), which end up into a wide central area consisted of plate or lath-like elements	3.3 ± 0.3 (15)	5.7 ± 0.5 (15)	Under-calcified	Young, 1994
A	Moderate	Straight low-profile distal shield formed by thicker elements (< 50-25 % of distal shield area is open between elements) fused to tube elements delimiting a grilled cleanly to semi-open central area	3.5 ± 0.3 (430)	6.3 ± 0.9 (430)	Typical A-morphotype	Young and Westbroek, 1991 Young *et al*., 2003 Hagino *et al*., 2011
A	Robust	Robust calcification of elements (< 25 % of distal shield area is open between elements) from partially to nearly completely fused extending from the outer rim to a wide to narrow central area delimited by robust tubes	3.3 ± 0.3 (259)	5.9 ± 0.7 (259)	A over-calcified Type A A calcified	Young, 1994 Henderiks *et al*., 2012 Saavedra-Pellitero *et al*., 2019[b]
A	CC	Thicker to robust but not fused elements and central area completely or nearly completely covered	3.0 ± 0.2 (26)	5.7 ± 0.6 (26)	Over-calcified	Young *et al*., 2003 Cubillos *et al*., 2007 Smith *et al*., 2012 Saavedra-Pellitero *et al*., 2019[b]
A	R/hyper	Heavily calcified distal shield elements completely fused and central area grilled but partly or completely covered	3.7 ± 0.4 (13)	7.2 ± 1.0 (13)	Over-calcified R-type R over-calcified	Cubillos *et al*., 2007 Beaufort *et al*., 2011 von Dassow *et al*., 2018 Saavedra-Pellitero *et al*., 2019[b]
B[a]	Light	Distal shield elements in low-profile and larger distal shield length compared with light A-morphotype	not observed	not observed		Young and Westbroek, 1991 Young *et al*., 2003 Hagino *et al*., 2011

[a] No unambiguous B morphotype (or B/C or C) coccoliths were observed in Patagonian samples but it is included for comparative purposes. The lightly calcified *E. huxleyi* in the dataset of von Dassow *et al*. 2018 included a continuum of characteristics from A to B and B/C or C. [b] The Plate Ib-c of Saavedra-Pellitero *et al*. (2019) are grouped together as "over-calcified" in that reference but are distinguished in the present study as R/hyper-calcified and A-CC morphotypes. Plate Ie of Saavedra-Pellitero *et al*. (2019) corresponds to over-calcified A morphotype in Young (1994) and the present study. Similarly, the "Type A overcalcified" in Fig. 3c of Cubillos *et al*. (2007) corresponds to the A-CC morphotype here (as distal shield elements are not fused or only partly fused in most coccoliths) while Fig. 3d of the same reference, identified also as "Type A overcalcified" appears to show both nearly complete fusion of distal shield element as well as nearly complete over-calcification covering the central area, so corresponds to the R/hyper-calcified morphotype in the present study.

gelates respectively (i.e., total cellular volume minus frustule or theca and vacuole volumes; Sicko-Goad *et al*., 1984). Absolute abundance data were standardized to cells L^{-1} and multiplied by specific carbon contents per cell (pg $cell^{-1}$) to derive total carbon biomass (Total C; µg C L^{-1}). We used the biogenic silica concentration (µmol opal L^{-1}) as a proxy of diatom biomass along the 2017 track, as samples for microscopy counts were not available. For this, the bSi concentration was converted into carbon units using the average net silicate to carbon ratio of 0.52 (mol/mol) found by Brzezinski *et al*. (2003) in the Southern Ocean. There was a significant linear relationship between diatom carbon biomass estimated with microscopy/allometry and those calculated from bSi concentration in 2015 samples ($R^2 = 0.60$, $p < 0.05$, slope = 0.8; N = 11), with an offset (16 µg C L^{-1}) likely from other contributors to bSi (e.g., silicoflagellates, radiolarians) as well as the contribution of *Minidiscus* spp. (data not shown) not included in microscopy/allometric carbon estimation. The presence/absence of diatoms was confirmed qualitatively in 2017 by SEM images at 1,500× magnification, and a semi-quantitative evaluation was made as follows: low (few cells), intermediate (at least one species with several cells or chains) and high (many species with several cells or chains). It should be kept in mind that there can be substantial variation in diatom carbon-biomass estimated by microscopy vs. bSi, due to variability in diatom C:Si ratios (Leblanc *et al*., 2018).

3.3.3 Chemical analyses

Macronutrients, opal, total chlorophyll-*a* (chlo-*a*), pH and total alkalinity (A_T) were determined as described in Torres *et al*. (2020). Full carbonate system parameters (including Ω_{cal}) were estimated from pH, A_T, salinity, temperature (25 °C as input and *in situ* temperature as output conditions), pressure (0 dbar as input and depth as output conditions) using CO2Sys Excel macro spreadsheet version 2.1 (Pierrot *et al*., 2006) with Mehrbach set of solubility constants

(Mehrbach *et al*., 1973) refitted by Dickson and Millero (Dickson and Millero, 1987). To extrapolate full carbonate parameters from pCO_2 (onboard sensor) and salinity measurements where alkalinity samples were not directly available (due to mismatch in chemical and biological sampling along the IC-WSM 2015 track), the regression curve for the salinity-A_T relationship (μmol kg^{-1}) = 63.4 × salinity + 101 (R^2 = 0.99, N = 186; Torres *et al*., 2020) was used to derive A_T estimated from salinity. It is important to note that this relationship has been stable for over a decade in Patagonia (Torres *et al*., 2011; Torres *et al*., 2020). pCO_2 values delivered by the onboard sensor (underway sampling) correlated with pCO_2 calculated from A_T-pH pairs (discrete sampling) in the same 2015 samples (R^2 = 0.56, $p < 0.001$; N = 17), with an overestimation of 6 μatm (2%). The differences between measured and calculated pCO_2 values are small compared to the high ranges in the variability of pCO_2, salinity, A_T, and pH, and should not affect the objectives of the present study. Exceptionally, the calculated pCO_2 values for SS were overestimated by up to 36% concerning pCO_2 measurements (comparing 15 readings from the sensor with three calculated values). This disagreement could be due to various local factors that increase the sensitivity of calculated pCO_2 to A_T (Abril *et al*., 2015) or pH uncertainties due to differences in salinity between buffers and samples. Therefore, it should be kept in mind that in the case of SS, the uncertainties in the carbonate system could be more substantial. Finally, in order to calculate the bicarbonate [HCO_3^-] to proton [H^+] ratio (in mol/μmol), the [HCO_3^-] was divided by the $antilog_{10}$ of –pH (total H^+ scale).

3.3.4 Statistical data analysis

All statistical analyses were performed in R software using packages freely available on the CRAN repository (R Core Team, 2019). As measurements for nitrate, phosphate, DSi, bSi, and

chlo-*a* in 2015 were scattered and uncoupled from plankton sampling, these variables were used only descriptively and not included in the statistical analyses.

3.3.4.1 Environmental gradients

Physical-chemical data obtained from the surface at the discrete sample stations both in 2015 and 2017 were combined in a unique matrix and standardized by subtracting the mean and dividing by the standard deviation (Legendre and Legendre, 2012). We used the *varclus* function in the 'Hmisc' package based on Spearman's correlation to detect redundant environmental variables (N = 32). Temperature, salinity, in situ pH, and Ω_{cal} were selected as they are non-redundant based on Spearman's correlation < 0.75 (Fig. S3) and they are easiest to interpret from a biological or cell physiological point of view. To these four, we also included CO_2. It was moderately correlated with pH (Spearman correlation = 0.8), but represents the substrate for photosynthesis and is typically incorporated as a driving variable in ocean acidification studies. The selected standardized variables were then used in two separate cluster analyses to recognize groups of sampling stations with similar characteristics in 2015 (N = 21) and 2017 (N = 11). For that, Euclidean distance matrixes were first calculated based on selected standardized variables (*vegdist* function in the 'vegan' package) and then included in hierarchical cluster analyses based on the Ward method using the *hclust* function in the basic 'stats' package.

3.3.4.2 Testing for a relationship of *Emiliania huxleyi* vs. diatoms

To characterize the diatom species associated with the different *E. huxleyi* morphotypes and other coccolithophore species, we performed a non-metric multidimensional scaling (nMDS) using the *metaMDS* function in the 'vegan' package, based on the log-transformed [ln (x+1)] coccolithophore and diatom abundances in Patagonia (only 2015) and the other coastal and oceanic locations (von Dassow *et al*., 2018) (N = 52). The function heatmap of the basic 'stats'

package was then used to plot the abundance of the coccolithophore and diatom species related to the clusters based on the nMDS scores of species/morphotypes and samples. As both the OMI and nMDS analyses suggested a clear separation between Patagonia fjords and the other coastal/oceanic areas, we used the IndVal analysis (Dufrene and Legendre, 1997) to identify indicator species for both areas, based on log-transformed abundances (*indval* function in 'labdsv' package).

We aimed to assess how *E. huxleyi* and diatom biomasses were related to each other and with the environmental conditions throughout Patagonia fjords. However, the different methods used to estimate diatom biomass in both years precluded the use of *E. huxleyi*:diatom ratios. Moreover, the use of regression-based analyses was not recommended due to the absence of a linear relationship between *E. huxleyi* and the different physical-chemical variables. To overcome these limitations, we created three categorical variables for both *E. huxleyi* and diatom biomasses (low, intermediate, and high) based on their < 25, 25-75 and > 75 percentiles, respectively. We then performed a correspondence analysis (CA) using the function *cca* in the 'vegan' package, based on the presence or absence of these new categoric variables in each sample (N = 32), followed by fitting the standardize physical-chemical variables to the CA plot using the *envfit* function (10,000 permutations).

3.3.4.3 Niche analysis

We used the outlying mean index (OMI) analysis (Dolédec *et al*., 2000) to assess the main environmental conditions associated with the realized niche of the different *E. huxleyi* morphotypes. The OMI index represents the marginality (i.e., niche position) and measures the distance between the average habitat conditions used by a given population and the average environmental conditions across the study area (represented by the point where the two

multivariate axes intersect at zero). The tolerance (Tol) accounts for the dispersion of samples containing organisms of the population from the average environmental condition (i.e., niche breadth), whereas the residual tolerance (RTol) accounts for the proportion of the variability unexplained by the variables included in the analysis (Dolédec *et al*., 2000). Thereby, a species having a low OMI (species score close to zero, located in the center of the multivariate space) and high Tol is one that utilizes a wider array of resources and maintains populations within a wider variety of conditions (i.e., generalist), when compared with the specialized and less resilient species with more restricted realized-niche associated to high OMI and low Tol (Dolédec *et al*., 2000).

The OMI analysis was performed using the *niche* function in the 'ade4' package (Dray and Dufour, 2007), considering simultaneously the data obtained for 2015 and 2017 (N = 32). To compare the patterns observed in Patagonia to other localities in the south eastern Pacific, a complementary OMI analysis was performed, including records of coccolithophore assemblages and *E. huxleyi* morphotypes from nearby coastal and oceanic waters (published by von Dassow *et al*., 2018) in addition to the data used in the first analysis (N = 64). A 1.84× correction factor was applied to these data, as coccolithophore counts from von Dassow *et al*. (2018) were obtained by the Utermöhl method. In both cases, data were arranged in two matrices, one containing the coccolithophore abundances and a second matrix with the standardized physical-chemical variables. Coccolithophore abundances were previously Hellinger-transformed (Legendre and Legendre, 2012). Since Hellinger transformation is obtained by the squared root of relative abundances, the potential biases from comparing data from both SEM and Utermöhl counts was minimized. The statistical significance of the morphotypes/species marginality was tested using the Monte Carlo method included in the

'ade4' package (10,000 permutations). The *envfit* function in the 'vegan' package (Oksanen *et al*., 2007) was then used to fit the five environmental variables to the OMI scores (10,000 permutations).

3.4 RESULTS

3.4.1 The late-spring southern Patagonia 2015

The hierarchical clustering based on the surface values of the selected physical-chemical variables in the austral late-spring 2015 (i.e., salinity, temperature, Ω_{cal}, pH and pCO_2) showed a clear separation between the sampling station at the Skyring Sound (SS; st. 15) and the other localities (Fig. 2.3a). The other stations were grouped in two main clusters: one cluster composed of stations in the Archipelago Madre de Dios (AMD) and the Inner Channel (IC) and a second one composed mainly of stations in the western part of the Strait of Magellan (WSM). Samples from the Otway Sound (OS; sts. 13-14) were distributed between the two clusters. The cluster separation seemed to be mainly related to temperature and salinity dissimilarities, while stations 4 and 15 differed from others by their relatively low pCO_2/high Ω_{cal} and high pCO_2/low Ω_{cal} conditions, respectively (Fig. 2.3b). Surface salinity ranged from > 29 in the AMD and southernmost WSM stations to as low as 17 in the SS (st. 15), with intermediate values throughout the IC and in the OS (range: 26-29; Fig. 2.3a-b). A north-south gradient of decreasing surface temperature was recorded from 9.0-10.0 °C around the AMD zone to 7.1 °C near Helado Sound (sts. 17-18; Fig. 2.3a-b, S4a). Surface waters were mostly undersaturated relative to

atmospheric pCO_2 (< 400 µatm) with minimum values at st. 4 in the AMD (241 µatm). CO_2 oversaturation was only observed at the SS (542 µatm). Similar to salinity, Ω_{cal} varied widely, ranging from highly over-saturated conditions in the AMD zone (Ω_{cal} range: 2.5-3.6, pH in situ range: 8.03-8.21), intermediate levels in the interior WSM (Ω_{cal} range: 2.4-2.6; pH range: 8.04-8.07), lower levels in the southern IC zone (Ω_{cal} 2.0-2.2, pH ~ 8.0) and a sub-saturated extreme

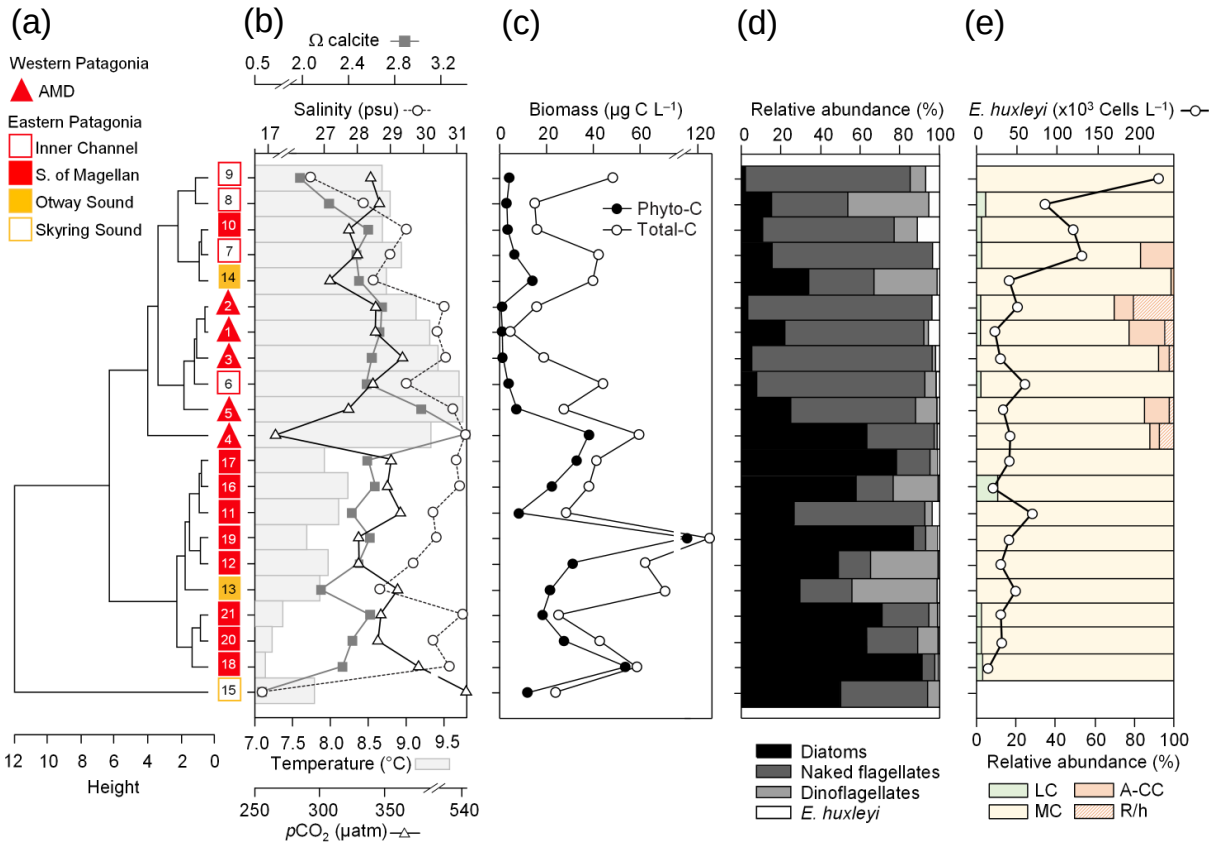

FIGURE Nº 3.3 Physical and chemical conditions, carbon biomass by microplankton and phytoplankton assemblages, and abundance and calcification-level of *E. huxleyi* recorded in surface waters of southern Patagonia during the austral late-spring 2015. (a) hierarchical clustering on salinity, temperature, pH, pCO_2 and Ω calcite surface values on 21 water samples collected for plankton analysis, (b) salinity, temperature, Ω calcite, and pCO_2 levels, (c) total carbon biomass by the nano- and micro-plankton assemblages (Total-C, all items between 5-200 µm in length) and phytoplankton assemblages (Phyto-C, diatoms + coccolithophores), (d) relative carbon biomass by diatoms, naked flagellates, dinoflagellates, and *E. huxleyi*, and (e) total abundances of *E. huxleyi* and relative abundances of four *E. huxleyi* morphotypes. All samples were taken < 5 m in depth. Stations 5-7, 11-13, 18-21 were conducted at night. LC = *E. huxleyi* lightly-calcified A-morphotype, MC = *E. huxleyi* moderate-calcified A-morphotype, A-CC = *E. huxleyi* A-CC morphotype, R/h = *E. huxleyi* R/hyper-calcified morphotype.

reached in the SS sampled site (Ω_{cal} 0.5, pH 7.73, Fig. 2.3a-b, S5a). Moderate to low DSi (< 6 µM) and nitrate (NO_3^- < 6 µM) were recorded in southern Patagonia, dropping to a minimum in the southern IC zone (Table 2.2, Fig. S6).

The AMD and IC zones showed relatively low phytoplankton biomasses (< 20 µg C L^{-1}) dominated by naked flagellates (Fig. 2.3c-d), whereas diatoms were associated with higher phytoplankton biomasses (> 40 µg C L^{-1}) in Eleuterio Channel (st. 4; mostly chains of *Chaetoceros* spp.) and the WSM (sts. 12, 16-21; mostly chains of *Leptocylindrus* spp., *Chaetoceros* spp., and *Thalassiosira* spp.). The contribution of dinoflagellates to biomass was highest in IC st. 8, OS sts. 13-14 and WSM sts. 12 and 16. Coccolithophores only accounted for 0.2-12.8 % of total-C biomass (0.1-4.0 µg C L^{-1}), reaching > 6 % only in the southern IC (sts. 8-10) where diatom biomasses were among the lowest observed. *E. huxleyi* dominated the coccolithophore assemblages in all samples (> 98 %), with a few *Syracosphaera* spp. coccospheres (mostly collapsed) found at the AMD (Table S2). *E. huxleyi* abundances (Fig. 2.3e) ranged from 0 to 2.76×10^5 cells L^{-1}, being most abundant in southern IC (> 1.03×10^5 cells L^{-1} in sts. 7-10) and only absent from SS (st. 15), which was the only station where conditions were corrosive to calcite (Ω_{cal} < 1). *E. huxleyi* populations were mostly composed of the moderate A morphotype (which also included cells of the robust-calcified A-morphotype; see Methods) (Fig. 2.3e, Table 2.3). No B (or B/C or C) morphotypes were detected, and few lightly-calcified A cells were observed. The heavily A-CC and R/hyper-calcified morphotypes were restricted to the AMD zone.

Three vertical profiles were performed in the AMD estuarine zone (Fig. 2.4): one at the "limestone" western AMD basin (st. 3), one between the western and eastern AMD basins (st. 4), and one at the easternmost basin (st. 5, Fig. 2.4, S1). All samples were taken within the eupho-

TABLE Nº 3.2 Physical and chemical conditions, and photosynthetic and silicified biomass proxies in the surface waters (< 5 m) of southern Patagonia fjords. Mean, standard deviation (SD) and range of each variable and number of samples for the late-spring 2015 and early-spring 2017 are shown. Only values matching planktonic samples discussed in the text are included, except for chlorophyll-*a* (chlo-*a*), opal, nitrate and silicate 2015 for which values are between 3-28 km decoupled from biological sampling. The mean and SD do not include the Skyring Sound 2015 station as it shows extreme values for all variables (see Table S1). However, the values from that sample are shown in parenthesis for comparison. n.a = no available data.

Survey	Late-spring 2015			Early-spring 2017		
	Mean ± SD	Range	*n*	Mean ± SD	Range	*n*
Temperature (ºC)	8.6 ± 0.9	(7.8) 7.1 – 10.0	22	7.1 ± 0.6	6.3 – 8.1	12
Salinity	30.0 ± 1.2	(16.9) 26.6 – 31.3	22	27.9 ± 1.3	25.1 – 29.8	12
pCO_2 (µatm)	337 ± 33	241 – 386 (542)	22	368 ± 28	320 – 412	12
Ω calcite	2.6 ± 0.4	(0.5) 2.0 – 3.6	22	2.0 ± 0.3	1.5 – 2.4	12
CO_3^{2-} (µmol kg^{-1})	106 ± 15	(21) 79 – 150	22	83 ± 11	59 – 96	12
HCO_3^- (µmol kg^{-1})	1,739 ± 61	(1,144) 1,572 – 1,811	22	1,701 ± 60	1,606 – 1,811	12
pH (total scale)	8.07 ± 0.04	(7.73) 8.03 – 8.21	22	8.02 ± 0.03	7.95 – 8.08	12
A_T (µmol kg^{-1})	2,006 ± 80	(1,197) 1,773 – 2,097	22	1,911 ± 79	1,757 – 2,037	12
DIC (µmol kg^{-1})	1,861 ± 67	(1,193) 1,667 – 1,935	22	1,802 ± 66	1,687 – 1,920	12
HCO_3^-/H^+ (mol/µmol)	0.205 ± 0.023	(0.061) 0.168 – 0.274	22	0.179 ± 0.016	0.144 – 0.203	12
Chlo-*a* total (µg L^{-1})	2.0 ± 1.1	(0.49) 0.3 – 5.4	24	1.9 ± 1.3	0.2 – 3.9	12
Opal (µmol L^{-1})[a]	0.8 ± 0.4	0.5 – 1.8 (2.1)	13	1.7 ± 0.7	0.6 – 2.8	12
Nitrate (µmol L^{-1})	3.3 ± 1.3	(0.32) 0.5 – 6.1	24	9.0 ± 2.0	6.0 – 12.8	12
Silicate (µmol L^{-1}) [a]	2.3 ± 1.8	(1.5) 0.2 – 6.1	13	5.3 ± 3.1	2.2 – 12.4	12
Phosphate (µmol L^{-1})	n.a.	n.a.	--	0.7 ± 0.2	0.3 – 1.0	12

[a] 2015 range is from the Archipelago Madre de Dios to the inner channel zone along 50.4-52.6º S.

TABLE Nº 3.3 Relative percentages of *E. huxleyi* A-morphotypes recorded throughout southern Patagonia fjords. Mean, standard deviation (SD), and maximum and minimum percentages of five *E. huxleyi* morphotypes recorded in inner surface waters of southern Patagonia (PAT; n = 883 cells counted in 23 samples) and down to 50 m in the Archipelago Madre de Dios western zone (AMD; n = 1,012 cells counted in 27 samples) during the austral late-spring 2015 and early-spring 2017.

Morphotype/ Sample set	Lightly-calcified			Moderate-calcified			Robust-calcified			A-CC			R/hyper-calcified		
	Mean ± SD	Max	Min	Mean ± SD	Max	Min	Mean ± SD	Max	Min	Mean ± SD	Max	Min	Mean ± SD	Max	Min
PAT 2015 + 2017	2.6 ± 3.1	10.8	0	62.7 ± 18.7	97.5	26.3	34.5 ± 18.9	71.1	2.5	0.1 ± 0.5	2.5	0	0	---	---
AMD 2015 + 2017	3.4 ± 7.1	33.3	0	40.4 ± 14.6	65.8	8.3	39.0 ± 14.8	72.5	15.0	12.4 ± 9.5	41.7	2.5	4.8 ± 5.4	20.5	0

tic zone (1 % PAR), which extended down to 36 and 30 m in sts. 3 and 4, respectively (st. 5 was conducted at night, Fig. S7a-c). All three sites were sharply stratified in the upper 10 m, with

pycnoclines around 5 m. Temperature decreased while salinity increased with depth (Fig. 2.4a-c). In station 3, Ω_{cal} varied little with depth, remaining in the range 2.5-2.7 (Fig. S7g) even across the shallow pycnocline. In station 4, Ω_{cal} showed the highest values and highest range; A_T, pCO_2, and HCO_3^- increased sharply with depth in the upper 10 m, while Ω_{cal} decreased from over 3.6 to less than 2.9 at 9 m, and 2.7 at 29 m (Fig. S7h). Finally, at station 5, Ω_{cal} decreased steadily from 3 at the surface to 2.4 at 25 m (Fig. S7i). Based on total chlo-*a* levels and fluorescence signals, most photosynthetic biomass occurred in the upper 15 m of the water column in sts. 3-4, peaking at the surface in st. 4 (5.4 μg L^{-1}). However, in station 5, total chlo-*a* levels and fluorescence signals were more constant with depth, dropping proportionally less by 25 m from maximal values, when compared to the other stations. The "silicate" estuarine zone (st. 4-5) showed higher photosynthetic biomass and bSi than the "limestone" site (Fig. 2.4a-c, S7d-f). *E. huxleyi* mostly occurred in the well-illuminated upper layer, most notably in the "limestone" western AMD waters, where diatom abundance and biomass were low compared to the communities recorded in "silicate" sites (Fig. 2.4d-f). Although the moderate A morphotype was predominant at all depths in the three stations (Fig. 2.4g-i), a higher proportion of the A-CC morphotype (up to 31 % relative abundance) was observed in the upper 15 m of the "limestone" western AMD when compared to the other two stations. The lightly-calcified and R/hyper-calcified morphotypes were present in a lower proportion (< 10 %).

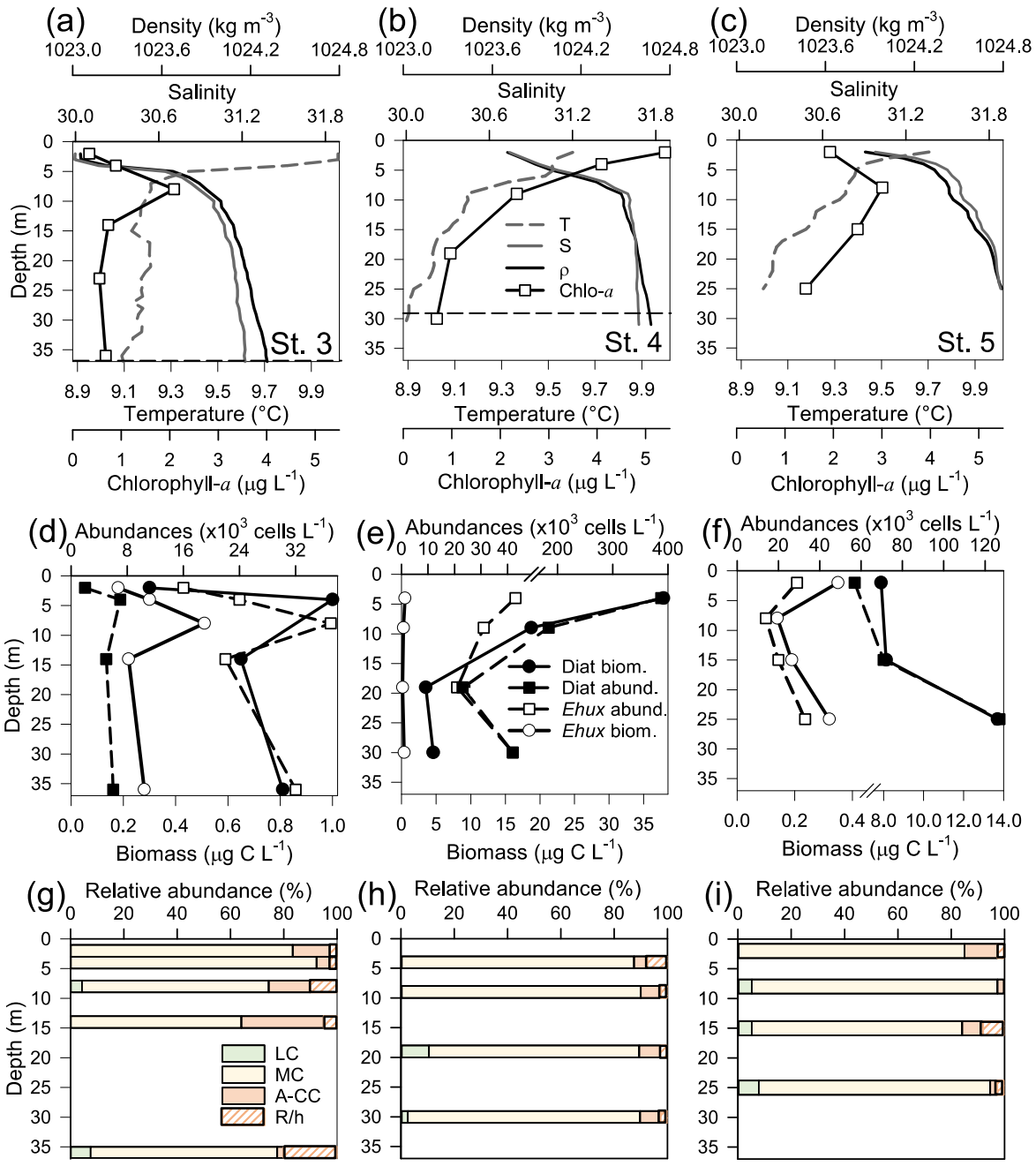

FIGURE Nº 3.4 Physical, chemical, and biological vertical profiles recorded in the Archipelago Madre de Dios during austral late-spring 2015. Temperature, salinity, density and total chlorophyll-*a* (a-c), abundance and total carbon biomass of *E. huxleyi* (*Ehux*) and diatoms (Diat; d-f), and relative abundance of four *E. huxleyi* morphotypes (g-i) in the W-AMD (st. 3 left), between (st. 4 middle), and E-AMD zones (st. 5 right). Dotted lines in panels a-b indicate depths of 1 % PAR penetration (st. 5 was conducted at night). Morphotype abbreviations as in Fig. 2.3. See figure S7 for additional variables.

3.4.2 The early-spring southern Patagonia 2017

The hierarchical clustering based on the physical-chemical conditions in austral early-spring 2017 indicated a separation between the WSM and the IC, whereas the three stations in the AMD were distributed between the two clusters (Fig. 2.5a). Surface salinity ranged from 25 to 30 along the south-north track, with saltier waters (> 28) around the AMD (sts. 30-32) and southward in the WSM zone (sts. 22-24), and fresher waters in the southern IC (< 27 at sts. 25-27) (Fig. 2.5b). Surface temperatures ranged from a minimum of 6.3 °C in the southern IC to > 7.7 °C in the AMD and northern IC (max. 8.1 °C in st. 29, Fig. 2.5a-b, S4b). Surface waters were undersaturated with respect to pCO_2 in all stations (range: 320-396 µatm) except for station 26 (412 µatm). Lower Ω_{cal} levels prevailed in the southern IC (range: 1.5-1.9) with higher Ω_{cal} in the AMD zone (range: 2.1-2.4; Fig. 2.5b, S5b). Nitrate, silicate and phosphate concentrations (Fig. 2.5c) were mostly in the range 6.0-8.3, 2.2-5.4, and 0.3-0.7 µM, respectively, with the highest levels of nitrate (9.5-12.8 µM) and phosphate (0.8-1.0 µM) in sts. 22-23, 26 and 30, whereas stations 30 and 26 registered the highest DSi (12 and 7 µM, Fig. 2.5c, Table 2.2). Higher photosynthetic biomass (chlo-*a* > 2.7 µg L^{-1}) was recorded around the eastern AMD (st. 29, 31-32) and WSM station 23, while the western AMD (st. 30), southern IC (st. 25-26), and WSM (st. 22) yielded the lowest measured biomass (chlo-*a* < 1.3 µg L^{-1}; Fig. 2.5d). Variation in chlo-*a* reflected variation in diatom biomass (Fig. 2.5d).

The dominant coccolithophore during early-spring 2017 was again *E. huxleyi* (> 96 %). Abundances ranged from 1.69×10^4 to 9.06×10^4 cells L^{-1} (Fig. 2.5e). The *E. huxleyi* carbon biomass averaged 0.5 ± 0.3 µg C L^{-1} (in 11 samples), reaching both maximal and minimal values (0.2 and 1 µg C L^{-1}, respectively) in the southern IC (sts. 25-27). In contrast, the opal-derived diatom carbon biomass averaged 40±17 µg C L^{-1}, with lower values (< 18 µg C L^{-1}) in the AMD

st. 30 and IC st. 25 (Fig. 2.5d). While fixed samples for standard microplankton analysis were not available, large chains of *Skeletonema* spp., *Thalassiosira* spp., and *Chaetoceros* spp. were noted as frequent in samples observed by SEM (Fig. S8), and were likely significant contributors to opal. Similar to the 2015 survey, the moderate A morphotype dominated the *E. huxleyi* assemblages along the 2017 track (Fig. 2.5e). Cells of the lightly-calcified A morphotype were sporadically observed, whereas the highly-calcified A-CC and R/hyper-calcified morphotypes were again restricted to the AMD zone (Fig. 2.6e-f, Table S1; note the low abundances of the R/hyper-calcified morphotype were only detected at other depths, so do not appear in Fig. 2.5e).

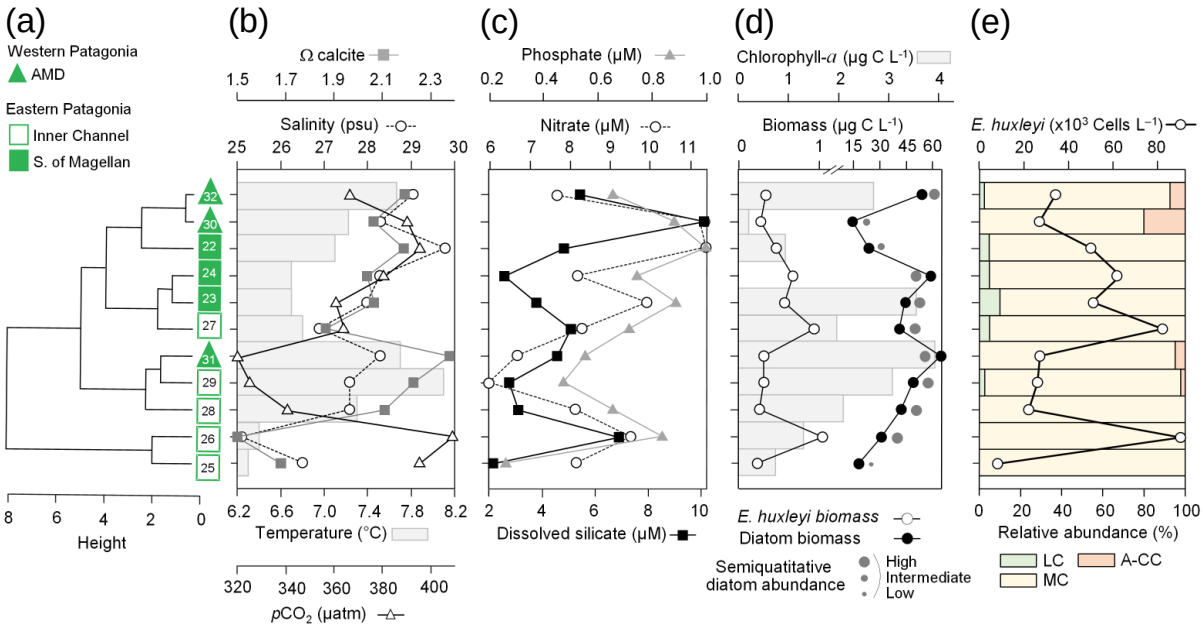

FIGURE Nº 3.5 Physical, chemical and nutrient conditions, chlorophyll-*a* levels, carbon biomass by *E. huxleyi* and diatoms, and abundances and calcification-level of *E. huxleyi* recorded in surface waters of southern Patagonia during the austral early-spring 2017. (a) hierarchical clustering on temperature, salinity, pH, pCO_2 and Ω calcite surface values on 11 water samples collected for plankton analysis, (b) salinity, temperature, Ω calcite and pCO_2 levels, (c) nitrate, dissolved silicate, and phosphate levels, (d) total chlorophyll-*a* and total carbon biomass by *E. huxleyi* and diatoms, and semi-quantitative estimation of diatom abundances (SEM), and (e) total abundances of *E. huxleyi* and relative abundances of three *E. huxleyi* morphotypes. All samples were taken < 5 m in depth. Stations 25-26 and 30 were conducted at night. Morphotype abbreviations as in Fig. 2.3.

Two CTD profiles were performed in the AMD zone: one in the "limestone" western AMD basin (st. 30) and another profile southwest of Escribano Island at the "silicate" eastern AMD basin (st. 32) (Fig. 2.6). The profiles covered the euphotic zone (down to 27 m in st. 32; st. 30 was conducted at night) as well as sub-surface layers (25-75 m depth). In both stations, temperature and salinity increased with depth, with maximum density stratification between 5-10 m. In the western AMD profile, Ω_{cal} was low at the surface (2.1) due to the lowest salinity, but rose to a maximum at 5 m due to a minimum in pCO_2 and increasing salinity, whereas below 20 m, pCO_2 rose and Ω_{cal} dropped (Fig. S9e). At the eastern AMD site, in contrast, Ω_{cal} increased with depth despite increasing pCO_2 (Fig. S9f). At both stations, photosynthetic biomass was mainly confined to the upper 25 m of the water column, with chlo-*a* peaks at 5 and 10 m (0.7 and 3.1 $\mu g\ L^{-1}$, respectively), and dropping close to zero below 40 m in the western AMD, while remaining near 1 $\mu g\ L^{-1}$ even at depths $\geq$ 50 m in the eastern AMD (Fig. 2.6a-b, S9a-b). The eastern AMD zone exhibited higher chlo-*a* and [bSi] when compared to the western AMD, despite no depletion of phosphate, nitrate and DSi were observed at either site (Fig. 2.6a-b, S9a-d). At both sites, *E. huxleyi* dominated the coccolithophore assemblages across all depths, with another six coccolithophore species observed in sub-surface AMD waters (Table S3). *E. huxleyi* and diatom abundances were highest in the surface at both sites (Fig. 2.6c-d). However, reflecting the chlo-*a* profile, estimated diatom biomass remained relatively high at depth compared to surface values (dropping by only about 40 %), and *E. huxleyi* abundance and biomass also dropped less with depth in the eastern AMD compared to the western AMD (Fig. 2.6c-d). In both stations, the composition of *E. huxleyi* morphotypes was similar at all depths, characterized by the predominance of the moderately-calcified morphotype followed by highly-calcified A-CC

(Fig. 2.6e-f). The lightly-calcified and R/hyper-calcified morphotypes were either undetected or represented a minor fraction of coccolithophore assemblages.

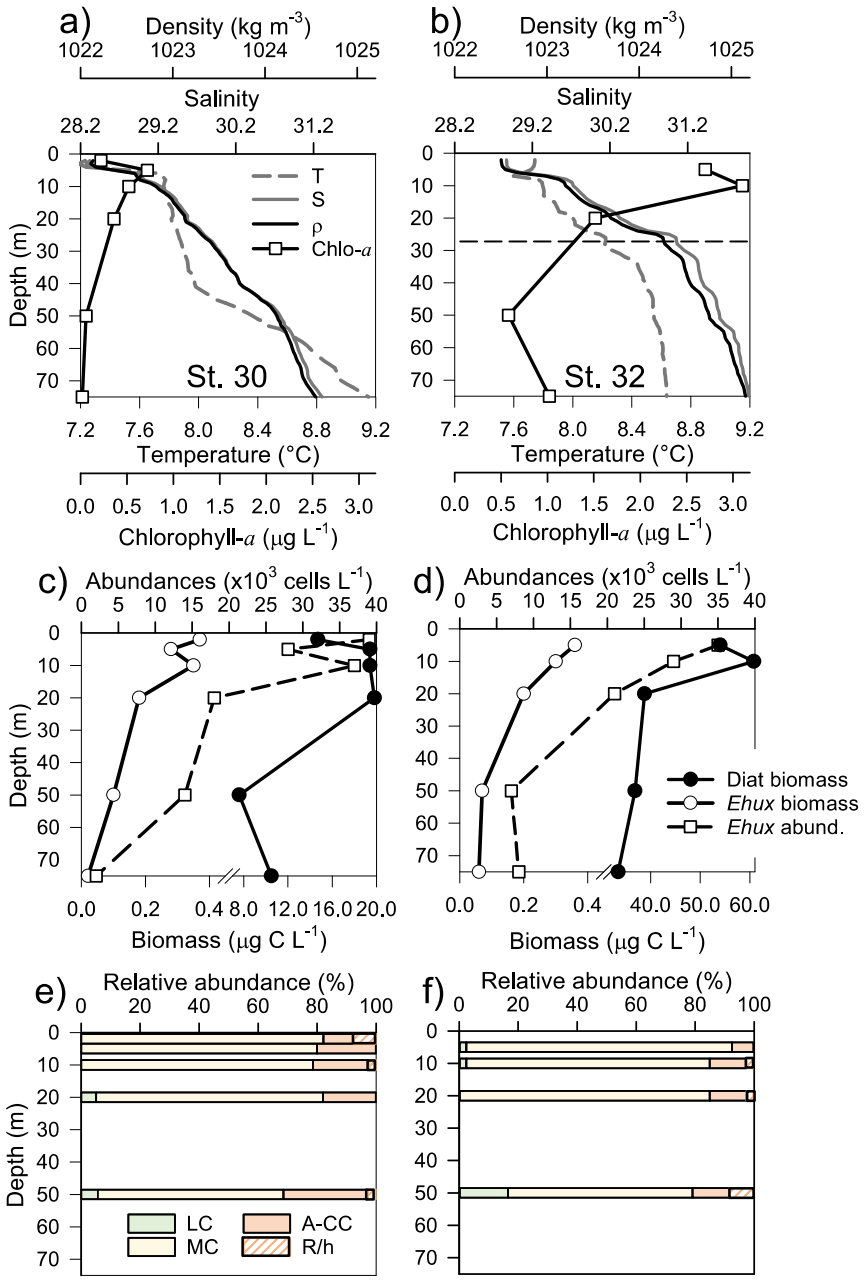

FIGURE Nº 3.6 Physical, chemical, and biological vertical profiles recorded in the Archipelago Madre de Dios during the austral early-spring 2017. Temperature, salinity, density, and total chlorophyll-*a* (a-b), abundance of *E. huxleyi* and total carbon biomass of *E. huxleyi* (Ehux) and diatoms (Diat; c-d), and relative abundances of four *E. huxleyi* morphotypes (e-f) in the W-AMD (st. 30 left) and the E-AMD (st. 32 right). Dotted line in panel b indicates depth of 1 % PAR penetration (st. 30 was conducted at night). Morphotype abbreviations as in figure 2.3. See figure S9 for additional variables.

3.4.3 *Emiliania huxleyi* abundance vs. diatoms

The nMDS depicted a clear separation between the Patagonia fjords and the oceanic/coastal areas regarding the composition of coccolithophorid and diatom assemblages (Fig. S10). The IndVal analysis (Table S5) identified only the *E. huxleyi* moderate-calcified morphotype as an indicator of the fjord locations, along with the diatoms *Thalassiosira* spp., *Stephanopyxis turris, Leptocylindrus* spp. and *Chaetoceros* spp. The coastal/oceanic locations were more characterized by the lighty-calcified and A-CC morphotypes and the other coccolithopore species (i.e., *G. ericsonii*, *G. muellerae*, *G. parvula*), as well as the diatoms cf. *Lioloma* spp., Pennate diatoms (< 50 μm length), *Nitzschia* spp., cf. *Pseudo-nitzschia cuspidata*, and cf. *Asteromphalus sarcophagus*.

The two first axes of the CA accounted for 60 % of the total explained variability and indicated that the highest *E. huxleyi* and low diatom biomasses were associated with increasing temperatures (Fig. S11). Intermediate *E. huxleyi* biomasses were associated with high diatom biomasses and increasing gradients of salinity, pH and Ω_{cal}, whereas low *E. huxleyi* biomasses were associated with intermediate diatom biomasses and increasing pCO_2. However, none of the considered environmental variables had a significant fit in the *envfit* test.

3.4.4 Niche analysis of *Emiliania huxleyi* morphotype responses to environmental conditions

The OMI analysis depicted differences in the realized niches of the *E. huxleyi* morphotypes throughout Patagonia fjords in 2015 and 2017 (Fig. 2.7a, Table S6). The OMI plot showed station 15 from 2015 as an outlier, characterized by extremely low salinity and high pCO_2. The OMI axis 1 (91.02 % of explained variability) was negatively related to Ω_{cal}, whereas the OMI axis 2 (8.42 % of explained variability) was positively related to salinity and pH and negatively

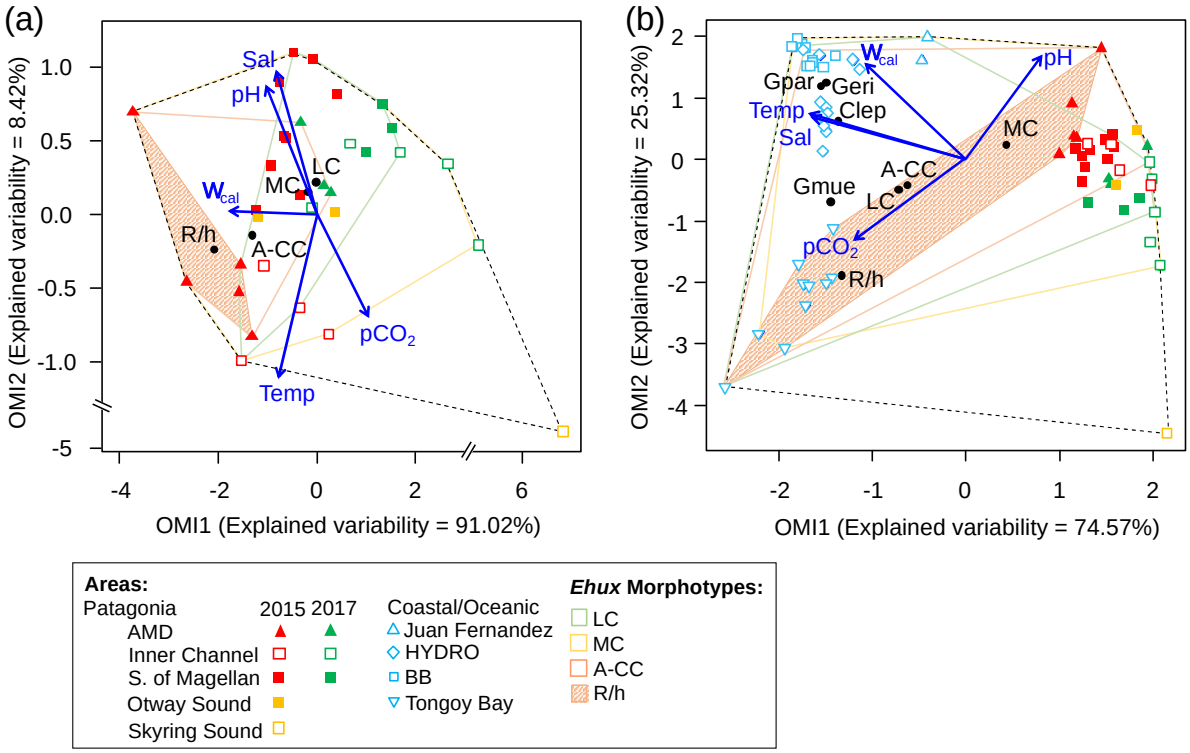

FIGURE Nº 3.7 Outlying Mean Index (OMI) niche analysis by *E. huxleyi* (*Ehux*) morphotypes populating the surface waters of southern Patagonia, and complemented with coccolithophores and *Ehux* morphotypes from nearby coastal and oceanic waters constrained by environmental conditions. (a) Biplot representing the realized-niche of four *E. huxleyi* morphotypes during the austral late-spring 2015 and early-spring 2017 in Patagonia, where black circles indicate the mean habitat condition used by each morphotype (niche-position) and polygons delimit their respective niche-breadth (i.e., tolerance). Blue vectors represent the gradients of environmental variables. (b) Realized-niches of *Ehux* morphotypes and other coccolithophore species in Patagonia fjords (this study) and nearby coastal/oceanic waters (data from von Dassow *et al*., 2018). Polygons of other coccolithophore species in (b) are not shown for simplicity. Temp = temperature, Sal = salinity, LC = *E. huxleyi* lightly-calcified A-morphotype, MC = *E. huxleyi* moderate-calcified A-morphotype, A-CC = *E. huxleyi* A-CC morphotype, R/h = *E. huxleyi* R/hyper-calcified morphotype, Gpar = *Gephyrocapsa parvula*, Geri = *Gephyrocapsa ericsonii*, Gmue = *Gephyrocapsa muellerae*, Clep = *Calcidiscus leptoporus*.

related to temperature and pCO_2. The *envfit* test indicated that all variables had a significant fit ($R^2 > 0.88$, $p < 0.01$; Table S7). Only the moderate A and R/hyper-calcified morphotypes showed significant OMIs ($p < 0.05$, Table S6). The moderate A morphotype was the most generalist (OMI = 0.07, Tol = 1.23), observed in all samples (except st. 15 in 2015). The R/hyper-calcified morphotype, observed exclusively in the AMD zone, was the most specialized morphotype

(OMI = 4.77, Tol = 0.75). The A-CC morphotype (OMI = 1.43, Tol = 1.68), observed in the AMD and northern IC, showed intermediate habitat preferences (Fig. 2.7a), but the OMI for this morphotype did not meet the threshold for significance ($p = 0.060$). The RTol for the R/hyper-calcified morphotype was 12 % (Table S6), indicating that most variability in its realized niche was accounted for by the environmental variables included in the analysis.

The complementary OMI analysis (Fig. 2.7b, Table S8) indicated a clear separation between the Patagonian fjords and coastal and oceanic waters off central and northern Chile and Peru. The OMI axis 1 (74.57 % of explained variability) was negatively related to temperature, salinity and Ω_{cal}, whereas the OMI axis 2 (25.32 % of explained variability) was positively related to pH and negatively related to pCO_2. The *envfit* test indicated that all variables had a significant fit ($R^2 > 0.88$, $p < 0.01$; Table S9). All coccolithophore species and *E. huxleyi* morphotypes showed significant OMIs ($p < 0.05$, Table S8). The lightly-calcified, moderate-calcified and A-CC morphotypes, characterized as the most generalists, showed similar realized niches (OMI = 0.25-0.75, Tol = 2.85-2.96), whereas the R/hyper-calcified form was again the most specific of the *E. huxleyi* morphotypes (OMI = 5.25, Tol = 1.97) and restricted to the coastal upwelling and AMD zones (Fig. 2.7b, Table S8). Regarding the other coccolithophore species, *G. muellerae* was common to both coastal and oceanic areas but still showed a higher degree of specialization (Tol = 1.03) than the *E. huxleyi* morphotypes, whereas *C. leptoporus*, *G. ericsonii* and *G. parvula* showed preference for oceanic conditions with low Tol values (0.15-0.38; Table S8). The R/hyper-calcified morphotype, *G. ericsonii* and *G. parvula* showed very low RTol (< 4.6 %), indicating that most of their realized-niche variation was accounted for by environmental variables in the analysis (Table S8).

3.5 DISCUSSION

3.5.1 Patagonian coccolithophore communities dominated by *E. huxleyi*

Emiliania huxleyi was the only coccolithophore widely distributed along the fjords and inner channels of southern Patagonia and always represented > 96 % of total coccolithophore abundance and biomass, during both early/late spring. The low diversity of coccolithophores assemblages, dominated by *E. huxleyi*, is common to both the Patagonian and Norwegian fjord systems. In the case of southern Patagonia, the neighboring Pacific has higher diversity (Beaufort *et al*., 2008; Menschel *et al*., 2016; von Dassow *et al*., 2018), but the Southern Ocean assemblages also show low diversity dominated by *E. huxleyi* (Cubillos *et al*., 2007; Saavedra-Pellitero *et al*., 2014; Charalampopoulou *et al*., 2016; Saavedra-Pellitero *et al*., 2019). The low diversity in southern Patagonian waters thus may partly reflect this latitudinal trend.

3.5.2 Abundance of *E. huxleyi* in Patagonia compared to nearby oceans

During the early/late spring, standing stocks of *E. huxleyi* in the Patagonian fjords and inner seas were moderate compared with those documented in nearby coastal and oceanic regions and within the range of background stocks reported in the Norwegian fjords and North Sea (Table 2.4 and references therein). The high *E. huxleyi* abundances typical of spring blooms in the

Norwegian fjords were not observed in either early or late spring in the present study despite the similar temperature, salinity, and Ω_{cal} conditions in both fjord systems. No *E. huxleyi* blooms

TABLE N° 3.4 Comparison of *E. huxleyi* standing stocks and morphotypes recorded in northern and Patagonia fjords systems and nearby coastal/ocean locations. Temperature and salinity ranges are shown. Only data < 10 m in depth were included. ESP = Eastern South Pacific, SO = Southern Ocean, APS = Atlantic Patagonian Shelf, SU = summer, SP = spring, WI = winter, AU = autumn, n.a. = no available data.

Location	Concentration cells $\times 10^3$ L^{-1}	*E. huxleyi*/ Coccolith.[a]	Main Morph	Year/ Season	Temp. range	Salinity range	References
- *Northern Hemisphere fjords:*							
Oslo fjord	24 – 36,000[b]	n.a.	n.a.	1939/SU	8.2 – 19.6	8.2 – 28.4	Birkenes and Braarud, 1952
Western coast and fjords	250 – 115,000[b]	n.a.	n.a.	1955/SU	11 – 15	28 – 33	Berge, 1962
Oslo fjord	385 – 14,500[b]	n.a.	n.a.	1981/SU	16 – 20	20 – 21	Paasche and Kristiansen, 1982
Bokna fjord	3,000 – 4,000[b]	n.a.	n.a.	1981/SU	11 – 13	28 – 30	Erga, 1989
Samnanger fjord	< 10 – 7,000[c]	n.a.	A	1992/SU	8 – 10	10 – 30	Kristiansen *et al.*, 1994; Young, 1994
Fauskangerpollen, Nordåsvannet	1 – 28,000[b]	n.a.	n.a.	1993/SP	7 – 16	15 – 30	Fernández *et al.*, 1996
- *Nearby coastal and oceanic zones*:							
Norwegian Sea	200 – 3,000[d]	dominate	n.a.	1987 – 1992	6 – 10	> 35	Samtleben *et al.*, 1995
Norwegian Sea	< 10 – 3,000[d]	dominate	n.a.	1987 – 1995	6 – 10	> 35	Baumann *et al.*, 2000
Outer Oslo fjord, Skagerrak	All year round[e]	n.a.	n.a.	2009 – 2011	2 – 16	22 – 33	Egge *et al.*, 2015
Outer Oslo fjord, Skagerrak	171 – 254[d]	n.a.	A	2013/SU	18.5	23.7	Gran-Stadniczeñko *et al.*, 2017
Northeast Atlantic and North Sea	100 – 1,500[f]	dominate	A, B	1990/SU	n.a.	n.a.	van Bleijswijk *et al.*, 1991
North and Norwegian Seas	< 3 – 900[d]	40 – 100	A[i]	2008/SU	11 – 18	30 – 35	Charalampopoulou *et al.*, 2011
- *Patagonia fjords*:							
W. Magellan Straits ~ 52-54° S	~ 100[b]	dominate	n.a.	1991/SU	n.a.	n.a.	Zingone *et al.*, 2011
Fjords and channels ~ 50-54° S	12 – 276[b]	> 98	A	2015/SP	7.1 – 10.0	26.6 –31.3	This study
Fjords and channels ~ 50-54° S	17 – 91[d]	> 96	A	2017/SP	6.3 – 8.1	25.1 – 29.8	This study
- *Nearby coastal and oceanic zones*:							
ESP along ~16-20° S; 73-80° W	1 – 34[g]	8 – 99	A	1964/SU	21.9 – 24.9	n.a.	Hagino and Okada, 2006
ESP along ~30-33° S; 72-98° W	up to 350[h]	60 – 90	A, R[j]	2004/SP	14.8 – 19.8	34.1 – 35.1	Beaufort *et al.*, 2008, 2011
ESP along ~35-38° S; 73-78° W	12 – 134[b]	> 50	A, R[j]	2004/SP	10.7 – 15.3	33.4 – 34.6	Menschel *et al.*, 2016
ESP along ~12° S; 77-78° W	1 – 531[b]	> 76	A, R[j]	2014-15/AU,SP	14 – 21	35 – 35.2	Alvites, 2016
ESP along ~13-33° S; 70-86° W	1 – 76[b]	30 – 100	A, R[j]	2011-13/SP,WI	12.3 – 19.8	33.8 – 35.5	von Dassow *et al.*, 2018
SO Pacific ~ 45-55° S; 80-100° W	n.a.	50 – 100	C	1967-1970	1 – 14	n.a.	McIntyre *et al.*, 1970
SO Pacific ~ 54-58° S; 80-97° W	31 – 61[d]	dominate	C, B/C	2009/SU	4.3 – 5.7	~ 34.1	Saavedra-Pellitero *et al.*, 2014
SO Drake Passage ~ 57-62° S	1 – 580[d]	> 80	B/C	2009/SU	2 – 10	33.7 – 34.0	Charalampopoulou *et al.*, 2016
SO Drake Passage ~ 56-62° S	1 – 214[d]	dominate	B/C	2016/SU	2 – 10	33.3 – 34.0	Saavedra-Pellitero *et al.*, 2019
APS along ~ 38-54° S; 51-63° W	180 – 3,060[d]	dominate	B/C	2008/SP	7 – 18	33.4 – 35.6	Poulton *et al.*, 2011, 2013

[a] *E. huxleyi* as a component of larger coccolithophore assemblages. When information about other coccolithophores was provided, the percentage abundance of *E. huxleyi* is given or if it was noted that *E. huxleyi* was dominant. "n.a" means no information about other coccolithophores was provided. [b] estimated through sedimentation chamber and inverted microscopy, [c] estimated by Palmer-Maloney chamber and inverted microscopy, [d] estimated through filtration and scanning electron microscopy analysis, [e] estimated by high-throughput sequencing and operational taxonomic units (OTUs) analysis they found *E. huxleyi* throughout the year but concentrated between summer-autumn, [f] cultured strains were identified at morphotype-level by use immunofluorescence assay, and abundances estimated through scanning electron microscopy analysis, [g] estimated through filtration and cross-polarized microscope, [h] estimated using an automated coccosphere recognition software, [i] the "characteristic" *E. huxleyi* morphotype showed in Fig. 4, [j] the R/hyper-calcified morphotype dominating the *E. huxleyi* assemblages in neritic zones.

have been reported in Patagonia fjords, although this might be due to limited observations and methodological issues. For example, many phytoplankton studies in the area (e.g., Alves-de-Souza *et al*., 2008; González *et al*., 2013) as well as standard phytoplankton monitoring in the zone (Vivanco and Seguel, 2009) often rely on samples fixed with acid-Lugol's, which would not preserve coccoliths, or have only focused on larger phytoplankton size classes (e.g., Paredes *et al*., 2014).

3.5.3 Variation in *E. huxleyi* with environmental factors

It has been previously proposed that the realized niche of *E. huxleyi* is partly defined by physical and chemical conditions unfavorable to large diatoms (Tyrrell and Merico, 2004; Smith *et al*., 2017). During late-spring Patagonia fjords, *E. huxleyi* reached higher abundances in the southern IC when the temperature was above 8 °C and macronutrients, and larger diatoms were the lowest, consistent with the pattern previously reported more generally for nano-phytoplankton based on size-fractionated chlo-*a* for this geographic area (e.g., Cuevas *et al*., 2019). However, the CA analysis showed that the lowest levels of *E. huxleyi* were associated with intermediate levels of larger diatoms, and intermediate levels of *E. huxleyi* were associated with highest levels of larger diatoms, suggesting a unimodal relationship between these two planktonic groups, possibly affected by environmental and biotic factors not assessed in this study.

The Ω_{cal} – a parameter assumed to constraint calcification in coccolithophores – was subject to large spatial variations in surface waters, from relatively high Ω_{cal} levels in the AMD zone (range: 2.1-3.6), moderate Ω_{cal} in the interior WSM, low Ω_{cal} in the southern IC (range: 1.5-2.2) and sub-saturating in the SS (0.5). The range of surface Ω_{cal} recorded along southern Patagonia was comparable to those reported for the Norwegian seas (Jones *et al*., 2019).

Whereas the highest Ω_{cal} values observed at the AMD were not as high as those observed in the global ocean (Takahashi *et al*., 2014), the lower values at the southern IC were comparable to values reported previously (range: 1.8-2.8) from high CO_2 upwelling conditions in central and northern Chile (Beaufort *et al*., 2008, 2011; von Dassow *et al*., 2018). While low surface Ω_{cal} at coastal waters of northern and central Chile are related to the upwelling of high pCO_2-DIC enriched subsurface waters, the freshening (and the associated drop in DIC, salinity, and $[Ca^{2+}]$ caused by dilution) and latitudinal/seasonal cooling (enhancing CO_2 solubility) have major roles in lowering $[CO_3^{2-}]$ and Ω_{cal} in southern Patagonia. These contrasting systems offered the possibility to observe if the ecological trends related to low Ω_{cal} depend on context.

3.5.4 Comparison of *E. huxleyi* morphotypes in Patagonia to nearby oceans vs. Norwegian fjords

There was some variability in the vertical distribution of the *E. huxleyi* morphotypes in the water column. The lightly-calcified coccoliths appeared associated with subsurface waters in both seasons sampled at the locations, so they might be associated with intrusion of these waters. However, the samples within the euphotic zone were generally similar to each other within a given sample station. Thus, for the purposes of the questions in this study, the use of surface samples to describe morphotype distributions is expected to be reasonable, but we caution that more subtle patterns could have been revealed if more vertical profiles have been obtained.

The *E. huxleyi* populations in the Patagonian fjords were completely distinct from surrounding coastal or open ocean populations in the eastern South Pacific, the Southern Ocean, and the Atlantic. The Atlantic Patagonian Shelf *E. huxleyi* populations are reported to be dominated by B/C morphotypes (Poulton *et al*., 2011, 2013). Southern open ocean populations of *E. huxleyi* are dominated by B morphotypes (including the B, B/C, C, and O types; Saavedra-

Pellitero *et al*., 2014; Saavedra-Pellitero *et al*., 2019), and A morphotypes were reported to represent only a small fraction. However, none of the B, B/C, or C morphotypes were detected in Patagonian inland waters. Although the moderate-calcified and robust-calcified A morphotypes have also been shown to be present in eastern South Pacific coastal and open ocean waters (von Dassow *et al*., 2018), the dominance of these A morphotypes was particular to Patagonian interior waters, as revealed by the IndVal analysis (these A moderate-calcified and robust-calcified A morphotypes were consolidated for final statistical analyses as they are not easily distinguished by objective morphological characters and were present in all samples, and preliminary analysis revealed completely overlapping realized niches). The moderate-calcified and robust-calcified A morphotypes are also observed as dominant in the Norwegian fjords (Table 2.4) (Young, 1994). The lightly-calcified A morphotype was rare, and did not show any clear pattern in its distribution. The A-CC morphotype has been associated with coastal upwelling zones in the Atlantic (Giraudeau *et al*., 1993; Smith *et al*., 2012; Henderiks *et al*., 2012) but not reported from the Norwegian fjords or the Southern Ocean. In both early/late spring, the R/hyper-calcified and A-CC *E. huxleyi* appeared only at the Pacific border of southern Patagonia (AMD zone). Thus, *E. huxleyi* populations of both Patagonian fjords and Norwegian fjords share a similar morphotype composition.

3.5.5 Niche analysis *E. huxleyi* morphotypes related to carbonate chemistry conditions

The broader niche-breadth by the moderate-calcified A morphotype contrasted with the marginal niche of the R/hyper-calcified forms in Patagonia (Fig. 2.7a). In order to extend the realized-niches derived in Patagonia, we complemented the OMI analysis with a sample set of nearby oceanic and coastal sites (data from von Dassow *et al*., 2018), in some of which the moderate-calcified A morphotype, unlike in Patagonia, was less abundant than other *E. huxleyi*

morphotypes and coccolithophore species. According to OMI analysis, the niche-differentiation along Patagonia is mostly driven by the pH/Ω_{cal} conditions, but temperature and salinity conditions also become important. In this extended domain, both the moderate-calcified A morphotype and the A-CC morphotype appeared to be generalists, with high Tol values (Fig. 2.7b). The lightly-calcified morphotype also appeared to be a generalist. However, we caution that while the lightly calcified *E. huxleyi* were exclusively lightly-calcified A morphotype in Patagonia, there was a continuum of lightly-calcified A, B, and B/C morphotypes (and some lightly calcified cells were difficult to classify among these types) in the coastal and oceanic sites. In contrast, the very distinct R/hyper-calcified morphotype exhibited restricted preferences in terms of Ω_{cal}, temperature, and salinity, but a broad niche in terms of CO_2 and pH (Fig. 2.7b).

The R/hyper-calcified morphotype, in which there is both fusion of distal shield elements and closure or partial closure by over-calcification of the central area, has so far only been reported as prevalent in high CO_2/low pH upwelling zone of the eastern South Pacific (Beaufort *et al*., 2011; Alvites, 2016; von Dassow *et al*., 2018), although it has seen (and reported as rare) in both Australian waters (Cubillos *et al*., 2007) and the Drake Passage (Saavedra-Pellitero *et al*., 2019). Experimental findings that the R/hyper-calcified morphotype did not perform better than the moderate-calcified A morphotype under high CO_2/low pH/low Ω_{cal} (von Dassow *et al*., 2018) might be explained by the OMI analysis suggesting a possible narrow unimodal response to Ω_{cal}, that would not have been detected in the experiments of von Dassow *et al*. (2018), where Ω_{cal} values of 1.4 vs. 3.3 were tested in the lab. Alternatively, the R/hyper-calcified morphotype might be selected by an unidentified condition particular to the Southeastern Pacific that correlates with the Ω_{cal}, temperature, and salinity of its realized niche.

A striking result from the OMI analysis was that all the *E. huxleyi* morphotypes, even the more specialized R/hyper-calcified type, exhibited much greater niche breadth (higher Tol values) than the other coccolithophore species. The three *Gephyrocapsa* species are very close relatives of *E. huxleyi* and phylogenetically should be considered as congenerics (Bendif *et al*., 2016; Bendif *et al*., 2019), but all showed lower niche breadth than the *E. huxleyi* morphotypes. The small *G. parvula* and *G. ericsonii* showed Tol values that were more than 10-fold lower than the most specialist *E. huxleyi* morphotype. Despite the evidence for a genetic underpinning of *E. huxleyi* morphotype (Krueger-Hadfield *et al*., 2014), as well as evidence of a high level of genomic content variability in *E. huxleyi* (von Dassow *et al*., 2015), phylogenetic and phylogenomic evidences do not clearly support for it to be split into different species (Bendif *et al*., 2016; Filatov, 2019). If the ubiquitous taxon is less susceptible to environmental change compared to marginal taxa (i.e., marginality or richness vs. tolerance are inversely correlated; Dolédec *et al*., 2000; Hernández *et al*., 2015), the exceptional generalist behavior exhibited by *E. huxleyi* compared to other coccolithophores suggests it may be more plastic and more adaptable in the face of environmental change.

3.6 CONCLUSIONS

Our study of how *E. huxleyi* populations and morphotypes respond to the highly dynamic physical and chemical environments of southern Patagonia yielded seven principal findings:

1. The only coccolithophore that was a regular and ubiquitous component of the phytoplanktonic assemblages throughout the surface waters of the southern Patagonian fjords/channels was *E. huxleyi*. It occurred under a wide range of carbonate chemistry conditions and was only absent in the SS zone where $\Omega_{cal} < 1$.
2. Although *E. huxleyi* never reached more than a small fraction of total phytoplankton biomass, it reached moderate abundances comparable to adjacent coastal and oceanic areas, and within the lower range of stocks reported from Norwegian fjords.
3. *E. huxleyi* abundance was highest when assemblages of large diatoms were lowest, in waters with lower macronutrients, consistent with it being most important in the absence of large diatoms.

4. In terms of morphotypes, the *E. huxleyi* populations in the southern Patagonian fjords/channels were similar to Norwegian fjords and very distinct from populations previously documented in the eastern South Pacific, Southern Ocean/Drake Passage, and the Patagonian Shelf of the Atlantic.
5. Niche analysis shows that the moderate A morphotype and A-CC morphotypes are generalists, whereas the R/hyper-calcified morphotype has a more marginal (specialized) realized niche.
6. The association of the R/hyper-calcified morphotype to high Ω_{cal} in southern Patagonia, where Ω_{cal} is driven principally by freshwater input, contrasts with its dominance of the upwelling system of central Chile to Peru, where low Ω_{cal} is due to high CO_2. This morphotype occupies a narrow range of Ω_{cal} values compared to the ACC and moderate A-morphotypes.
7. The moderate A, A-CC, and R/hyper-calcified *E. huxleyi* morphotypes all display higher niche breadth (more generalist behavior) than closely related coccolithophores, suggesting that *E. huxleyi* may be ecologically more plastic and have more capacity for adaptation in the face of environmental change than other coccolithophores.

Data availability. All data resulting from this study are available from the corresponding author upon request. The scanning electron micrograph image datasets can be found at https://zenodo.org/record/4292020

Sample availability. Material for SEM characterization (filter sections) are in Dr. von Dassow's laboratory and can be requested.

Author contributions. FDR (Conceptualizaton; Investigation; Data curation; Formal Analysis; Writing – original draft preparation; Writing – review & editing) lead the study, carried out sampling in 2015 survey, carried out light and SEM microscopic analysis, conducted characterization of microplankton and *E. huxleyi* assemblages and morphotype composition, performed biovolume/allometric analysis, analyzed the relationships between *E. huxleyi* and environmental and biological variables, and wrote the first drafts of paper. PvD (Conceptualizaton; Funding acquisition; Supervision; Validation; Visualization; Writing – original draft preparation; Writing – review & editing) trained and supervised FDR in *E. huxleyi* assemblages quantification and characterization, guided analysis strategies performed extensive re-writes of the text and figures, and provided continuous insights into interpretation of results and how to structure the manuscript. CAdS (Formal Analysis; Supervision; Validation; Visualization; Writing – review & editing) trained and supervised FDR in microplankton light-microscopy qualitative and quantitative analysis, performed nMDS, CA, and OMI niche analysis, guided interpretations of these results, and helped with extensive re-writes of the text and figures. EA (Investigation; Formal Analysis; Writing – review & editing) and RT (Funding acquisition; Investigation; Formal Analysis; Writing – review & editing) performed the analysis of carbonate system parameters, nutrients, opal and chl-*a* and helped characterize the physical environments. EM (Investigation; Formal Analysis; Writing – review & editing) carried out sampling and CTD deployment during the 2017 survey, and together with HG (Funding acquisition; Writing – review & editing) provided insights into the interpretation of oceanographic results. All co-authors provided key comments and editing of the final draft of the paper.

Competing interests. The authors declare no competing interests

Acknowledgments. This study was supported by the Comisión Nacional de Investigación Científica y Tecnológica (now Agencia Nacional de Investigación y Desarrollo) (FONDECYT grants 1140385 and 1181614, a doctoral fellowship CONICYT-PCHA/DoctoradoNacional/2013–21130158 to FDR), by the Iniciativa Científica Milenio of the Agencia Nacional de Investigación y Desarrollo through the Instituto Milenio de Oceanografía de Chile (Proyecto IC120019) and the Centro de Investigación: Dinámica de Ecosistemas Marinos de Altas Latitudes de Chile (grant FONDAP 15150003). The authors thank the captain and crew of the M/N Forrest, Paulina Möller and Sebastián Cornejo for assisting with onboard parameters recording and CTD deployment during the 2015 survey, Dr. Jeremy Young for help in classification of *E. huxleyi* morphotypes. SEM analysis was performed in the Centro de Investigación en Nanotecnología y Materiales Avanzados of the Facultad de Física of the Pontificia Universidad Católica de Chile (Proyecto FONDEQUIP EQM150101).

3.7 SUPPLEMENTARY MATERIALS

3.7.1 Tables

- Environmental parameters and *E. huxleyi* morphotypes abundances and biovolume (Table S1);
- Plankton abundances (Tables S2, S3);
- Biovolume calculations for main micro-plankton species (Table S4);
- Indicator value (IndVal) analysis based on coccolithophore and diatoms species for Patagonian Fjords and nearby Coastal/Oceanic areas (Table S5);
- Niche parameters yielded by *E. huxleyi* morphotypes in Patagonia Fjords (Table S6) more nearby Coastal/Oceanic areas (Table S8);
- Envfit results of five environmental variables fitted on the OMI spaces (Tables S7, S9).

TABLE S1. Physical and chemical parameters and associated relative abundance and biovolume of *E. huxleyi* morphotypes recorded in southern Patagonia during the austral late-spring 2015 and early-spring 2017. Asterisks indicate samples included in the statistical analysis (chosen to be representative of the upper 5 m). When more than one sample was available in the upper 5 m, the sample closest to 5 m was chosen. na = no available data. LC = *E. huxleyi* lightly-calcified A-morphotype, MC = *E. huxleyi* moderate-calcified A-morphotype, A-CC = *E. huxleyi* A-CC morphotype, R/h = *E. huxleyi* R/hypercalcified morphotype.

Station	Date/hour dd.mm.yy/hh:mm	Depth (m)	Latitude S deg.	Longitude W deg.	Temp. (ºC)	Sal. (psu)	pCO_2 (µatm)	Ωcal	pH	NO_3^- (µM)	DSi (µM)	PO_4^{3-} (µM)	Opal (µM)	*E. huxleyi* (%)				Volume ($µm^3$)
														LC	MC	A-CC	R/h	
1*	26.11.15/10:15	1	50.3280	75.3516	9.31	30.42	343	2.67	8.066	na	na	na	na	2.50	75.0	17.50	5.00	106.7
2*	26.11.15/12:09	1	50.3794	75.4093	9.13	30.63	343	2.69	8.067	na	na	na	na	2.56	66.7	10.26	20.51	121.5
3	26.11.15/16:00	1	50.3467	75.3633	9.97	29.98	386	2.53	8.027	6.12	6.13	na	0.51	0.00	83.3	13.89	2.78	115.9
3*	26.11.15/16:00	4	50.3467	75.3633	9.42	30.68	364	2.60	8.045	4.16	na	na	0.51	0.00	92.3	5.13	2.56	123.4
3	26.11.15/16:00	8	50.3467	75.3633	9.20	30.96	359	2.70	8.056	na	na	na	0.50	4.29	70.0	15.71	10.00	138.2
3	26.11.15/16:00	14	50.3467	75.3633	9.32	31.09	354	2.70	8.058	na	na	na	0.78	0.00	64.1	30.77	5.13	98.1
3	26.11.15/16:00	36	50.3467	75.3633	9.03	31.20	365	2.66	8.050	4.36	4.20	na	0.53	7.50	70.0	2.50	20.00	85.5
4	27.11.15/11:02	1	50.3688	75.3656	9.54	30.95	241	3.64	8.205	1.06	na	na	1.75	na	na	na	na	na
4*	27.11.15/11:02	4	50.3688	75.3656	9.33	31.28	266	3.42	8.170	2.94	na	na	1.80	0.00	87.5	5.00	7.50	113.0
4	27.11.15/11:02	9	50.3688	75.3656	9.09	31.56	347	2.86	8.073	4.75	na	na	1.08	0.00	90.0	7.50	2.50	89.1
4	27.11.15/11:02	19	50.3688	75.3656	9.12	31.67	347	2.84	8.072	7.92	na	na	1.04	10.53	78.9	7.89	2.63	75.1
4	27.11.15/11:02	30	50.3688	75.3656	8.91	31.68	375	2.68	8.044	5.02	na	na	0.55	2.56	87.2	7.69	2.56	85.3
5*	28.11.15/21:30	1	50.4252	74.9988	9.75	30.89	322	3.03	8.101	2.43	1.30	na	0.75	0.00	85.0	12.50	2.50	120.9
5	28.11.15/21:30	8	50.4252	74.9988	9.26	31.66	350	2.81	8.066	3.27	2.65	na	1.07	5.26	92.1	2.63	0.00	99.3
5	28.11.15/21:30	15	50.4252	74.9988	9.18	31.75	386	2.61	8.029	4.20	2.56	na	1.38	5.26	78.9	7.89	7.89	94.9
5	28.11.15/21:30	25	50.4252	74.9988	8.99	31.88	425	2.44	7.994	5.53	4.49	na	1.80	7.89	86.8	2.63	2.63	94.6
6*	29.11.15/02:10	2	50.7649	74.4343	9.70	29.5	341	2.56	8.060	na	na	na	na	2.56	97.4	0.00	0.00	101.4
7*	29.11.15/06:00	2	51.2884	74.1223	8.94	29.0	329	2.47	8.068	na	na	na	na	2.78	97.2	0.00	0.00	102.4
8*	29.11.15/10:10	2	51.8275	73.7327	8.79	28.2	346	2.23	8.041	na	na	na	na	4.65	95.3	0.00	0.00	91.5
9*	29.11.15/14:00	2	52.3000	73.6567	8.68	26.6	339	1.98	8.030	2.94	0.34	na	na	0.00	100.0	0.00	0.00	148.2
10*	29.11.15/18:10	2	52.7672	73.8111	8.69	29.5	323	2.57	8.080	na	na	na	na	2.56	97.4	0.00	0.00	146.8
11*	29.11.15/22:20	2	53.2203	73.2871	8.11	30.3	362	2.43	8.042	na	na	na	na	0.00	100.0	0.00	0.00	159.6
12*	30.11.15/02:05	2	53.5578	72.4752	7.97	29.7	330	2.49	8.073	na	na	na	na	0.00	100.0	0.00	0.00	131.2
13*	30.11.15/06:30	2	53.1332	72.0012	7.86	28.7	360	2.16	8.029	na	na	na	na	0.00	100.0	0.00	0.00	107.9
14*	30.11.15/10:10	2	53.0217	71.8995	8.74	28.5	308	2.49	8.089	na	na	na	na	0.00	100.0	0.00	0.00	93.3
15*	01.12.15/10:06	2	52.5610	72.3209	7.79	16.92	542	0.54	7.725	0.32	1.53	na	2.07	absent	absent	absent	absent	absent

16*	02.12.15/14:10	2	53.5844	72.3092	8.23	31.1	352	2.63	8.061	na	na	na	na	10.81	89.2	0.00	0.00	116.2
17*	02.12.15/15:52	2	53.8024	72.1398	7.92	31.0	355	2.56	8.056	na	na	na	na	0.00	100.0	0.00	0.00	122.7
18*	02.12.15/22:10	2	53.8447	72.1946	7.12	30.8	376	2.35	8.031	na	na	na	na	3.13	96.9	0.00	0.00	124.2
19*	03.12.15/02:34	2	53.8929	71.2269	7.69	30.4	330	2.58	8.079	na	na	na	na	0.00	100.0	0.00	0.00	111.1
20*	03.12.15/04:10	2	53.7483	70.9321	7.20	30.3	345	2.43	8.060	na	na	na	na	2.63	97.4	0.00	0.00	87.5
21*	03.12.15/05:44	2	53.5924	70.9326	7.35	31.2	347	2.59	8.066	na	na	na	na	2.63	97.4	0.00	0.00	80.0
22*	22.09.17/10:20	2	53.5925	72.3000	7.1	29.8	396	2.19	8.011	11.39	4.83	1.00	1.04	5.13	94.9	0.00	0.00	90.5
23*	22.09.17/14:05	2	53.3833	72.9328	6.7	28.0	364	2.02	8.025	9.93	3.80	0.89	1.92	10.26	89.7	0.00	0.00	110.7
24*	22.09.17/17:00	2	53.1424	73.3807	6.7	28.3	383	2.01	8.011	8.21	2.59	0.75	2.57	5.00	95.0	0.00	0.00	108.5
25*	23.09.17/00:02	2	52.5913	73.6485	6.3	26.5	396	1.67	7.978	8.17	2.16	0.26	0.78	0.00	100.0	0.00	0.00	123.6
26*	23.09.17/04:05	2	52.1247	73.6899	6.4	25.1	412	1.48	7.952	9.52	6.90	0.84	1.34	0.00	100.0	0.00	0.00	114.1
27*	23.09.17/08:22	2	51.6840	73.9500	6.8	26.9	365	1.85	8.012	8.31	5.09	0.72	1.79	5.13	94.9	0.00	0.00	112.8
28*	23.09.17/10:08	2	51.4631	74.0435	7.3	27.6	342	2.09	8.044	8.14	3.11	0.66	1.83	0.00	100.0	0.00	0.00	111.0
29*	23.09.17/16:45	2	50.7479	74.4892	8.1	27.6	327	2.21	8.060	5.97	2.76	0.47	2.13	2.50	95.0	2.50	0.00	117.4
30	24.09.17/23:00	2	50.3368	75.3630	7.23	28.32	384	2.09	8.014	11.38	10.17	0.89	0.64	0.00	82.1	10.26	7.69	93.9
30*	24.09.17/23:00	5	50.3368	75.3630	7.74	28.95	365	2.27	8.037	12.83	12.41	0.91	0.84	0.00	80.0	20.00	0.00	100.6
30	24.09.17/23:00	10	50.3368	75.3630	7.77	29.27	381	2.23	8.021	12.09	10.94	0.90	0.84	0.00	78.6	19.05	2.38	90.7
30	24.09.17/23:00	20	50.3368	75.3630	7.82	29.59	377	2.27	8.025	13.25	13.35	0.92	0.86	5.13	76.9	17.95	0.00	97.5
30	24.09.17/23:00	50	50.3368	75.3630	8.40	30.79	449	2.16	7.965	14.76	15.16	1.18	0.33	5.71	62.9	28.57	2.86	67.5
30	24.09.17/23:00	75	50.3368	75.3630	9.18	31.34	712	1.62	7.794	16.22	18.52	1.62	0.46	scarce	scarce	scarce	scarce	scarce
31*	26.09.17/14:45	2	50.4243	75.0016	7.70	28.30	320	2.38	8.080	6.69	4.57	0.55	2.81	0.00	94.9	5.13	0.00	110.9
32*	26.09.17/14:50	5	50.4777	74.9857	7.67	29.06	363	2.21	8.032	7.71	5.43	0.66	2.34	2.50	90.0	7.50	0.00	103.2
32	26.09.17/14:50	10	50.4777	74.9857	7.80	29.77	369	2.29	8.031	10.45	8.96	0.92	2.63	2.50	82.5	12.50	2.50	104.7
32	26.09.17/14:5	20	50.4777	74.9857	8.02	30.41	380	2.34	8.024	12.73	9.13	1.02	1.68	0.00	85.0	12.50	2.50	92.2
32	26.09.17/14:5	50	50.4777	74.9857	8.55	31.61	402	2.43	8.010	12.72	9.13	1.09	1.60	16.67	62.5	12.50	8.33	94.9
32	26.09.17/14:5	75	50.4777	74.9857	8.64	32.06	399	2.53	8.017	12.97	9.82	1.16	1.45	scarce	scarce	scarce	scarce	scarce

TABLE S2. Abundances in cells per liter of planktonic items found in southern Patagonia during the austral late-spring 2015.

	St.1 (1 m)	St.2 (1 m)	St.3 (1 m)	St.3 (4 m)	St.3 (14 m)	St.3 (36 m)	St.4 (4 m)	St.4 (9 m)	St.4 (19 m)	St.4 (30 m)	St.5 (1 m)	St.5 (15 m)	St.5 (25 m)
- Diatoms													
Centric small (5-40 µm diameter)	1,130	550	0	770	490	970	740	440	660	1,520	1,360	960	780
Centric medium (40-100 µm diam.)	0	0	0	0	0	10	0	0	0	0	0	0	0
Chaetoceros spp.	1,700	480	1,010	2,860	1,990	2,370	321,809	141,381	14,780	29,960	33,300	56,020	119,110
Leptocylindrus spp.	170	100	0	440	230	280	30,460	6,960	2,220	3,740	3,360	2,020	720
Rhizosolenia spp.	440	240	80	280	150	100	1,420	800	440	440	420	460	100
Eucampia spp.	0	0	0	0	0	0	120	40	0	0	40	80	0
Asterionellopsis spp.	0	0	40	40	40	0	680	0	0	160	0	0	0
Corethron spp.	20	20	30	50	30	50	20	20	0	40	120	200	140
Cerataulina spp./*Guinardia* spp.	0	0	0	130	40	0	980	160	30	60	3,580	40	780
Pennate large (> 100 µm length)	20	10	40	10	20	0	20	80	20	20	10	80	20
Pennate medium (50-100 µm length)	60	0	0	0	0	0	0	0	0	20	0	20	20
Pennate small (< 50 µm length)	10	130	50	10	0	10	0	60	60	120	120	40	0
Thalassionema spp.	0	0	0	0	0	0	0	0	0	0	0	0	80
Licmophora spp.	0	60	10	10	30	0	0	0	0	20	0	20	20
Pseudo-nitzschia spp.	1,020	730	810	1,790	1,310	1,820	22,360	30,076	2,540	4,200	7,380	4,460	3,340
Nitzschia spp.	150	40	0	110	0	40	260	60	40	40	200	40	180
Stephanopyxis turris	0	0	0	0	0	0	100	280	80	20	220	140	400
Thalassiosira spp.	0	20	90	100	100	50	7,160	3,040	1,960	720	1,840	2,020	210
Skeletonema spp.	0	80	0	0	70	60	1,840	80	260	1,180	2,500	720	1,260
Striatella spp.	560	0	0	160	0	0	0	0	0	0	0	0	0
Ditylum spp.	0	0	0	0	0	0	20	0	20	0	0	0	0
Plagiogrammopsis spp.	100	0	0	0	0	0	0	0	0	0	0	160	0
Detonula spp.	0	0	90	0	0	0	0	120	0	0	2,820	3,060	0
- Dinoflagellates													
Ceratium pentagonium	0	0	0	10	0	0	0	0	0	0	0	0	0
Ceratium lineatum	0	0	0	0	0	0	0	0	0	0	10	0	0
Protoperidinium spp.	0	0	0	30	40	20	120	40	20	0	380	0	20
Dinophysis spp.	0	0	0	0	20	0	10	140	0	0	0	0	0
Gymnodinium spp. > 60 µm length	20	0	10	20	0	0	140	20	0	0	280	60	0
Scrippsiella spp.	0	0	610	0	50	0	0	0	0	0	1,300	20	0

Pyrophacus spp.	0	0	0	0	10	0	40	80	20	0	80	60	0
Naked flagellates	12,232	54,994	21,229	64,698	12,940	20,218	75,616	20,016	8,593	23,049	65,103	52,163	22,240
- Coccolithophores													
Emiliania huxleyi	20,089	51,868	15,811	24,056	21,949	32,240	43,154	31,454	21,018	42,410	28,768	19,717	33,234
Syracosphaera spp.	0	1,330	0	0	0	0	0	786	0	0	0	0	0
- Dictyochophyceae													
Pseudochattonella verruculosa	50	1,180	1,270	640	0	10	0	0	20	0	3,280	460	80
- Silicoflagellates													
Unidentified Silicoflagellates	20	40	0	10	80	30	60	30	0	20	40	80	20
- Foraminifera													
Unidentified Foraminifera	0	0	0	0	20	0	0	40	20	20	100	0	0
- Ciliates													
Tintinnids	0	0	0	0	20	50	20	0	20	60	340	140	120
Oligotrichida + Cyclotrichiida	220	250	1,330	7,620	280	150	860	2,260	520	180	3,760	3,600	160

TABLE S2. *continuation*

	St.6 (2 m)	St.7 (2 m)	St.8 (2 m)	St.9 (2 m)	St.10 (2 m)	St.11 (2 m)	St.12 (2 m)	St.13 (2 m)	St.14 (2 m)	St.15 (2 m)	St.16 (2 m)	St.17 (2 m)	St.18 (2 m)
- Diatoms													
Centric small (5-40 µm diameter)	820	340	0	680	780	1,540	380	260	320	800	520	820	140
Centric medium (40-100 µm diam.)	20	0	60	20	40	40	0	0	60	0	20	20	10
Chaetoceros spp.	920	120	140	2,880	4,020	10,500	1,120	0	101,194	14,680	67,014	920	63,200
Leptocylindrus spp.	44,052	1,060	0	9,760	59,352	358,127	1,180	50	0	58,160	2,880	44,052	4,520
Rhizosolenia spp.	20	120	20	20	60	40	0	0	0	20	60	20	0
Eucampia spp.	0	0	0	0	120	0	0	0	0	0	0	0	0
Asterionellopsis spp.	0	0	0	0	300	0	0	0	0	4,160	6,200	0	7,840
Corethron spp.	0	0	0	0	0	0	0	10	0	0	0	0	0
Cerataulina spp./*Guinardia* spp.	0	1,480	860	560	500	200	40	0	600	620	540	0	0
Pennate large (> 100 µm length)	20	20	0	0	20	0	80	0	20	40	50	20	20
Pennate medium (50-100 µm length)	0	20	0	0	0	60	40	30	0	0	0	0	0
Pennate small (< 50 µm length)	60	0	0	0	140	0	0	10	0	20	1,140	60	240
Thalassionema spp.	0	80	0	0	0	0	0	0	7,220	260	820	0	180
Licmophora spp.	0	0	20	0	0	0	0	0	10	0	10	0	10
Pseudo-nitzschia spp.	8,180	0	0	60	60	180	160	0	0	340	540	8,180	180
Nitzschia spp.	4,120	20	0	0	40	20	0	0	780	40	1,880	4,120	560

Stephanopyxis turris	160	100	0	0	200	240	4,220	2,780	0	2,020	1,120	160	960
Thalassiosira spp.	0	1,880	700	840	2,860	4,740	120	20	5,720	13,420	48,772	0	102,964
Skeletonema spp.	620	0	0	0	0	0	0	0	920	0	680	620	0
Striatella spp.	0	0	0	0	0	0	0	0	280	0	0	0	0
Ditylum spp.	0	0	0	0	0	0	0	0	0	40	20	0	0
Plagiogrammopsis spp.	0	0	0	0	0	0	0	0	0	320	0	0	0
Detonula spp.	0	3,540	1,840	0	0	0	0	0	600	4,800	0	0	540
- Dinoflagellates													
Ceratium pentagonium	0	380	100	40	10	1,320	1,960	700	10	460	0	0	20
Ceratium lineatum	0	0	0	0	0	0	320	60	0	0	10	0	0
Protoperidinium spp.	0	0	760	240	180	780	120	70	400	440	20	0	140
Dinophysis spp.	0	0	60	0	120	160	240	450	80	200	20	0	0
Gymnodinium spp. > 60 µm length	0	200	160	20	0	60	640	390	40	0	60	0	60
Scrippsiella spp.	20	340	80	560	0	80	80	0	0	100	200	20	60
Pyrophacus spp.	0	120	60	140	80	540	280	160	40	340	200	0	100
Naked flagellates	134,249	21,633	151,637	40,032	71,168	36,797	68,338	49,332	40,436	26,890	26,082	134,249	13,614
- Coccolithophores													
Emiliania huxleyi	161,454	102,676	276,035	146,574	69,567	25,296	48,734	42,410	0	17,298	42,410	161,454	11,719
Syracosphaera spp.	0	0	0	0	0	0	0	0	0	0	0	0	0
- Dictyochophyceae													
Pseudochattonella verruculosa	300	700	3,720	240	0	40	100	10	0	0	240	300	20
- Silicoflagellates													
Unidentified Silicoflagellates	200	100	40	0	60	0	0	0	0	20	10	200	0
- Foraminifera													
Unidentified Foraminifera	0	0	0	0	0	0	40	0	0	20	0	0	0
- Ciliates													
Tintinnids	120	20	0	0	280	200	80	80	140	20	160	140	30
Oligotrichida + Cyclotrichiida	780	700	980	2,580	9,100	840	720	1,900	1,490	340	860	460	360

TABLE S2. *continuation*

	St.19 (2 m)	St.20 (2 m)	St.21 (2 m)
- Diatoms			
Centric small (5-40 µm diameter)	280	1,000	1,080
Centric medium (40-100 µm diam.)	0	120	0

Chaetoceros spp.	331,825	254,800	154,560
Leptocylindrus spp.	29,540	0	0
Rhizosolenia spp.	20	0	0
Eucampia spp.	0	0	0
Asterionellopsis spp.	26,820	800	1,280
Corethron spp.	0	0	0
Cerataulina spp./*Guinardia* spp.	840	640	0
Pennate large (> 100 µm length)	140	80	20
Pennate medium (50-100 µm length)	40	0	60
Pennate small (< 50 µm length)	560	0	20
Thalassionema spp.	260	0	40
Licmophora spp.	20	0	0
Pseudo-nitzschia spp.	1,260	960	980
Nitzschia spp.	2,400	40	0
Stephanopyxis turris	2,060	0	220
Thalassiosira spp.	166,348	3,320	3,320
Skeletonema spp.	200	0	0
Striatella spp.	0	0	0
Ditylum spp.	0	0	0
Plagiogrammopsis spp.	680	0	0
Detonula spp.	0	24,200	15,560
- Dinoflagellates			
Ceratium pentagonium	100	40	20
Ceratium lineatum	160	0	0
Protoperidinium spp.	980	880	320
Dinophysis spp.	80	0	0
Gymnodinium spp. > 60 µm length	220	0	0
Scrippsiella spp.	600	280	200
Pyrophacus spp.	500	440	40
Naked flagellates	33,764	40,841	22,240
- Coccolithophores			
Emiliania huxleyi	41,293	31,994	25,296
Syracosphaera spp.	0	0	0
- Dictyochophyceae			

Pseudochattonella verruculosa	100	80	240
- Silicoflagellates			
Unidentified Silicoflagellates	20	0	0
- Foraminifera			
Unidentified Foraminifera	0	0	0
- Ciliates			
Tintinnids	50	0	60
Oligotrichida + Cyclotrichiida	600	3,280	740

TABLE S3. Abundances in cells per liter of coccolithophores found in southern Patagonia during the austral early-spring 2017.

	St.22 (2 m)	St.23 (2 m)	St.24 (2 m)	St.25 (2 m)	St.26 (2 m)	St.27 (2 m)	St.28 (2 m)	St.29 (2 m)	St.30 (2 m)	St.30 (5 m)	St.30 (10 m)	St.30 (20 m)	St.30 (50 m)
Emiliania huxleyi	51,257	51,552	62,099	16,948	90,551	82,742	23,407	26,512	38,558	27,924	37,466	17,862	13,747
Acanthoica quattrospina	0	0	0	0	0	0	0	0	0	0	436	0	0
Coronosphaera mediterranea	0	0	0	0	0	0	0	0	0	0	0	0	0
Gephyrocapsa muellerae	0	0	0	0	0	0	0	0	0	0	0	0	0
Helicosphaera carteri	0	0	0	0	0	0	0	0	0	0	0	0	430
Calciosolenia murrayi	0	0	0	0	0	0	0	0	0	0	0	0	0
Alisphaera unicornis	0	0	0	0	0	0	0	0	0	0	0	0	0

TABLE S3. *continuation*

	St.30 (75 m)	St.31 (2 m)	St.32 (5 m)	St.32 (10 m)	St.32 (20 m)	St.32 (50 m)	St.32 (75 m)
Emiliania huxleyi	2,062	27,965	34,797	28,812	21,186	7,406	7,733
Acanthoica quattrospina	0	0	1,289	847	1,695	0	0
Coronosphaera mediterranea	0	0	0	0	847	436	2,148
Gephyrocapsa muellerae	1,031	0	0	0	0	0	859
Helicosphaera carteri	0	0	0	0	0	0	0
Calciosolenia murrayi	0	0	0	0	0	436	0
Alisphaera unicornis	0	0	0	0	0	0	430

TABLE S4. Biovolume and equivalent spherical diameter (ESD) of main planktonic species found in southern Patagonia during the austral late-spring 2015. * Assuming frustule or theca and vacuole volumes representing 50 % and 22 % of the total volume of diatoms and dinoflagellates respectively. [a]group composed of small flagellates and athecated dinoflagellates cells including *Torodinium* spp., *Gimnodinium* spp., *Gyrodinium* spp.

	Geometric shape	Volume formula	Trophy	N	Volume (μm^3)*	ESD (µm)
- Diatoms						
Chaetoceros spp.	Elliptic prism	π/4•a•b•h	AU	26	2371.8	16.5
Centric small 5-40 µm diameter	Cylinder	π/4•d^2•h	AU	26	11115.5	27.7
Centric medium 40-100 µm diameter	Cylinder	π/4•d^2•h	AU	13	148346.5	65.7
Leptocylindrus spp.	Cylinder	π/4•d^2•h	AU	28	1848.6	15.2
Rhizosolenia spp.	Cylinder	π/4•d^2•h	AU	31	36804.9	41.3
Asterionellopsis spp.	Prism on triangle-base	1/2•a•b•h	AU	8	319.4	8.5
Corethron spp.	Cylinder + 2 half spheres	π•d^2• (h/4+d/6)	AU	20	11438.9	28.0
Cerataulina spp./*Guinardia* spp.	Cylinder	π/4•d^2•h	AU	18	11304.1	27.8
Pennate large > 100 µm length	Prism on parallelogram	1/2•a•b•h	AU	23	25217.9	36.4
Pennate medium 50-100 µm length	Prism on parallelogram	1/2•a•b•h	AU	2	3513.9	18.9
Pennate small < 50 µm length	Prism on parallelogram	1/2•a•b•h	AU	7	1334.0	13.7
Thallassiosena spp.	Rectangular box	a•b•h	AU	15	508.0	9.9
Licmophora spp.	Truncated square pyramid	1/3•(a^2+a•b+b^2)•h	AU	7	18826.1	33.0
Pseudo-nitzschia spp.	Prism on parallelogram	1/2•a•b•h	AU	11	1638.5	14.6
Nitzschia spp. < 40 µm length	Prism on parallelogram	1/2•a•b•h	AU	15	206.7	7.3
Amphiprora spp.	Elliptic prism	π/4•a•b•h	AU	2	50391.5	45.8
Stephanopyxis turris	Cylinder + 2 half spheres	π•d^2•(h/4+d/6)	AU	25	331885.0	85.9
Thalassiosira spp.	Cylinder	π/4•d^2•h	AU	36	15652.8	31.0
Skeletonema spp.	Cylinder + 2 half spheres	π•d^2• (h/4+d/6)	AU	2	685.4	10.9
Striatella spp.	Elliptic prism	π/4•a•b•h	AU	2	1632.1	14.6
Ditylum spp.	Prism on triangle-base	1/2•a•b•h	AU	2	70323.2	51.2
Plagiogrammopsis spp.	Elliptic prism	π/4•a•b•h	AU	3	1120.9	12.9
Detonula spp.	Cylinder	π/4•d^2•h	AU	21	2530.1	16.9
- Dinoflagellates						
Neoceratium fusus	2 cones	(π/12•a^2•b1) + (π/12•a^2•b2)	M	2	45529.2	44.3
Neoceratium pentagonium	Ellipsoid + cylinder + 2 cones	(π/6•a1•b1•h) + (π/4•b2^2•a2) + (π/12•b3^2•a3) + (π/12•b4^2•a4)	M	15	154344.3	66.6

Neoceratium lineatum	Ellipsoid + cylinder + 2 cones	(π/6•a1•b1•h) + (π/4•b2^2•a2) + (π/12•b3^2•a3) + (π/12•b4^2•a4)	M	7	24032.2	35.8
Protoperidinium spp.	2 cones	(π/12•a^2•b1) + (π/12•a^2•b2)	H	40	17705.2	32.3
Dinophysis spp.	Ellipsoid	(π/6•a•b•h)	H	19	17511.3	32.2
Gymnodinium spp. > 60 µm in length	Ellipsoid	(π/6•a•b•h)	H, M	29	55523.5	47.3
Pyrophacus spp.	Ellipsoid	(π/6•a•b•h)	M	20	59512.2	48.4
Scrippsiella-like spp.	2 cones	(π/12•a^2•b1) + (π/12•a^2•b2)	A, H	27	2950.3	17.8
Naked flagellates 10-60 µm in length[a]	Ellipsoid	(π/6•a•b•h)	H, M	17	2527.1	16.9

TABLE S5. Indicator value analysis (IndVal) of coccolithophores and diatom species representative of Patagonian Fjords and nearby Coastal/Oceanic locations. Only species with IndVal higher than 0.5 are shown.

	Code	**IndVal**	***p*-value**
Patagonia Fjords			
Thalassiosira spp.	Thala	0.8292	0.001
Stephanopyxis turris	Ste.tu	0.7778	0.001
Leptocylindrus spp.	Lepto	0.6706	0.001
*Chaetocero*s spp.	Chae	0.5895	0.008
Emiliania huxleyi moderate-calcified A-morphotype	MC	0.538	0.004
Coastal/Oceanic areas			
cf. *Lioloma* spp.	Liol	0.7374	0.001
Pennate < 50 µm length	Pen.sm	0.6789	0.001
Gephyrocapsa ericsonii	Geri	0.6061	0.001
Nitzschia spp. 50-100 µm length	Nit.me	0.6061	0.001
cf. *Pseudo-nitzschia cuspidata*	Pcus	0.6061	0.001
Emiliania huxleyi lighty-calcified A-morphotype	LC	0.5953	0.003
Gephyrocapsa parvula	Gpar	0.5758	0.002
*Emiliania huxley*i A-CC morphotype	A-CC	0.5648	0.003
Gephyrocapsa muellerae	Gmue	0.5455	0.001
Nitzschia spp. > 100 µm length	Nit.la	0.5152	0.001
cf. *Asteromphalus sarcophagus*	Asar	0.5152	0.001

TABLE S6. Niche parameters yielded by the Outlying Mean Index (OMI) analysis for four *Emiliania huxleyi* morphotypes found in Patagonia fjords during the austral late-spring 2015 and early-spring 2017 (see Fig. 2.7a). Niche parameters are given in absolute and percentage of variability of each morphotype. Inertia = total variability, OMI = Outlying Mean Index (i.e., marginality), Tol = Tolerance, RTol = Residual Tolerance (i.e., proportion of total variability unexplained by the environmental variables included in the analysis), OMI% = percentage of variability given by OMI, Tol% = percentage of variability given by Tol, RTol% = percentage of variability given by RTol. *p*-values are given by the number of random permutations out of 10,000 that yielded a higher value than the observed marginality. Morphotypes in bold were the ones significant ($p < 0.05$).

	Code	Inertia	Absolute values			Percentage of variability			*p*-value
			OMI	Tol	RTol	OMI%	Tol%	RTol%	
Lightly-calcified A-morphotype	LC	1.96	0.07	0.32	1.57	3.5	16.4	80.1	0.7190
Moderate-calcified A-morphotype	**MC**	**2.77**	**0.07**	**1.23**	**1.47**	**2.5**	**44.3**	**53.2**	**0.0271**
A-CC A-morphotype	A-CC	3.59	1.43	1.68	0.49	39.8	46.7	13.5	0.0598
R/hyper-calcified A-morphotype	**R/h**	**6.24**	**4.77**	**0.75**	**0.72**	**76.4**	**12.1**	**11.5**	**0.0403**

TABLE S7. Results of five environmental variables fitted on the OMI space showed in Fig. 2.7a (using the envfit function of the vegan package, R software).

	Code	OMI1	OMI2	R^2	*p*-value
Temperature	Temp	-0.57	0.82	1.00	< 0.001
Salinity	Sal	-0.65	-0.76	0.89	< 0.001
pCO_2	pCO_2	0.84	0.54	0.88	< 0.001
Ω calcite	Ωcal	-0.98	-0.21	0.97	< 0.001
pH	pH	-0.76	-0.65	0.98	< 0.001

TABLE S8. Niche parameters yielded by the Outlying Mean Index (OMI) analysis for four *E. huxleyi* morphotypes and other four coccolithophore species in Patagonia Fjords, and nearby Coastal/Oceanic areas (see Fig. 2.7b). Niche parameters are given in absolute and percentage of variability of each morphotype/species. Inertia = total variability, OMI = Outlying Mean Index (i.e., marginality), Tol = Tolerance, RTol = Residual Tolerance (i.e., proportion of total variability unexplained by the environmental variables included in the analysis), OMI% = percentage of total variability given by OMI, Tol% = percentage of total variability given by Tol, RTol% = percentage of variability given by RTol. *p*-values are given by the number of random permutations out of 10,000 that yielded a higher value than the observed marginality (OMI). All coccolithophores and *E. huxleyi* morphotypes tested were significant ($p < 0.05$).

	Code	Inertia	Absolute values			Percentage of variability			*p*-value
			OMI	Tol	RTol	OMI%	Tol%	RTol%	
Lightly-calcified A-morphotype	LC	5.76	0.75	2.85	2.15	13.0	49.7	37.3	< 0.001
Moderate-calcified A-morphotype	MC	3.86	0.25	2.96	2.28	6.4	34.5	59.0	0.003
A-CC A-morphotype	A-CC	5.24	0.58	2.91	1.70	11.1	56.5	32.4	< 0.001
R/hyper-calcified A-morphotype	R/h	8.42	5.25	1.97	0.19	62.3	35.4	2.2	< 0.001
Gephyrocapsa parvula	Gpar	4.24	3.92	0.15	0.17	92.3	3.6	4.1	< 0.001
Gephyrocapsa ericsonii	Geri	4.24	3.89	0.16	0.19	91.7	3.7	4.6	< 0.001
Gephyrocapsa muellerae	Gmue	5.52	2.58	1.03	1.91	46.8	18.6	34.6	0.011
Calcidiscus leptoporus	Clep	5.65	2.33	0.38	2.94	41.2	6.7	52.1	< 0.001

TABLE S9. Results of five environmental variables fitted on the OMI space showed in Fig. 2.7b (using rhe envfit function of the vegan package, R software).

	Code	OMI1	OMI2	R^2	*p*-value
Temperature	Temp	-0.91	0.41	0.94	< 0.001
Salinity	Sal	-0.93	0.38	0.88	< 0.001
pCO_2	pCO_2	-0.66	-0.75	1.00	< 0.001
Ω calcite	Ωcal	-0.57	0.82	0.99	< 0.001
pH	pH	0.44	0.90	0.97	< 0.001

3.7.2 Figures

- Salinity and Ω calcite surface levels into the Archipelago Madre de Dios during late-spring 2015 (Fig. S1);
- *E. huxleyi* calcification anomalies observed in Patagonia Fjords (Fig. S2);
- Analysis of redundancy of environmental variables (Fig. S3);
- Surface temperature (Fig. S4) and Ω calcite (Fig. S5) recorded throughout Patagonia Fjords during the late-spring 2015 and early-spring 2017;
- Nutrients and planktonic proxies recorded throughout Patagonia fjords (Fig. S6);
- Physical, chemical and biological vertical conditions in the Archipelago Madre de Dios during late-spring 2015 (Fig. S7) and early-spring 2017 (Fig. S9);
- SEM image showing the phytoplankton assemblages inhabit Southern Patagonian waters during early-spring 2017 (Fig. S8);
- Non-metric multidimensional scaling (nMDS) based on coccolithophore and diatom abundances in Patagonia Fjords and nearby Coastal/Oceanic areas (Fig. S10a) and heatmap based on nMDs scores (Fig. S10b);
- Correspondence analysis (CA) between *E. huxleyi* and diatom biomasses in relation with environmental conditions recorded in Patagonia Fjords during late-spring 2015 and early-spring 2017 (Fig. S11).

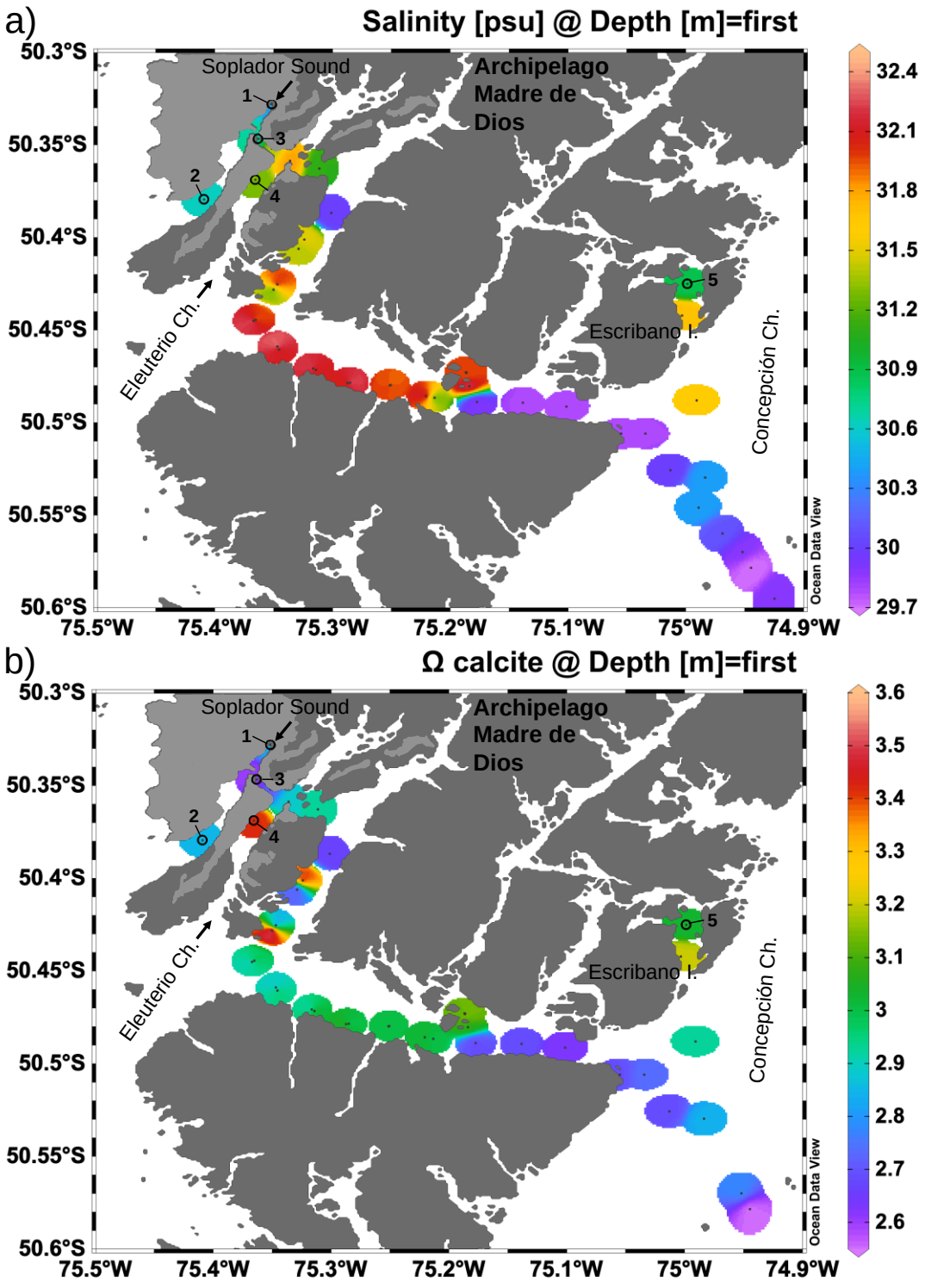

FIGURE S1. Salinity and Ω calcite levels recorded in the surface waters of the Archipelago Madre de Dios during the austral spring 2015. Sampling stations for plankton analysis are labelled in black (open circles). Light- and dark-gray continental masses depict the "limestone" western and "silicate" eastern basins, respectively. Maps produced by Ocean Data View (Schlitzer, 2018).

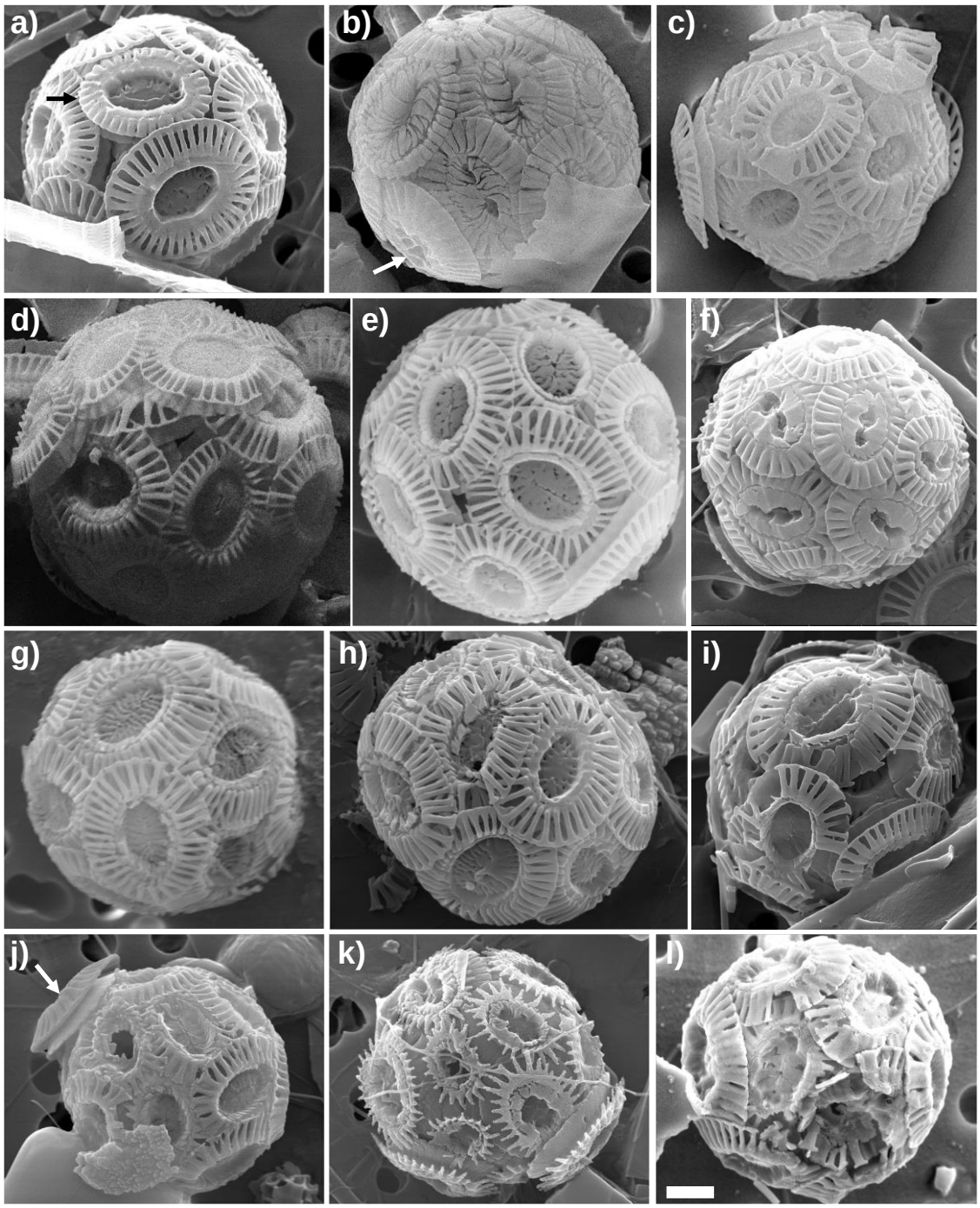

FIGURE S2. Primary and secondary calcification anomalies in *E. huxleyi* specimens collected in southern Patagonia during the austral late-spring 2015 and early-spring 2017. (a-c) incomplete formation (left, black arrow) and teratological malformations of coccoliths (center and right), (d-f) weak dissolution of the light A, moderate A, and A-CC coccoliths, (g-i) coccoliths exhibiting thinning or missing of tube elements and weakening or loss of T-shaped elements resulting in the distal shield elements rest in part or wholly on the proximal shield, (j-l) severe secondary dissolution. White arrow in images b and j indicate recently extruded "normal" calcified coccoliths. Scale bar = 1 µm.

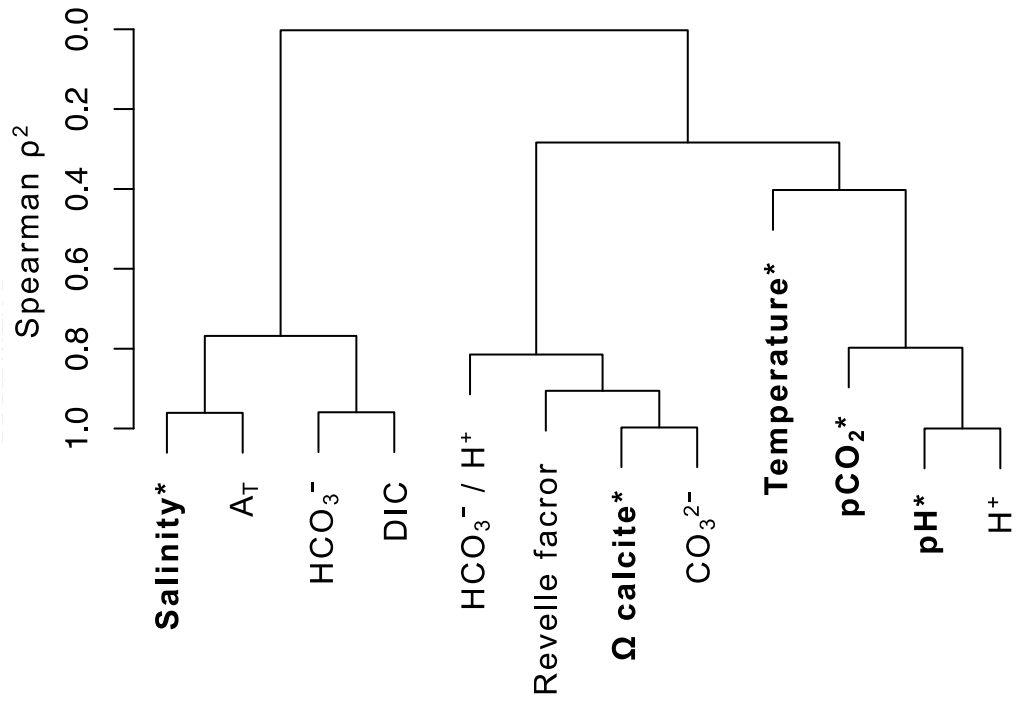

FIGURE S3. Analysis of redundancy of environmental variables. Spearman correlation was computed on 12 physical and chemical variables on 32 surface samples (< 5 m depth) collected for plankton analysis in late-spring 2015 (N = 21) and early-spring 2017 (N = 11). Variables selected for further statistical analsis are indicated in bold and with asterisk.

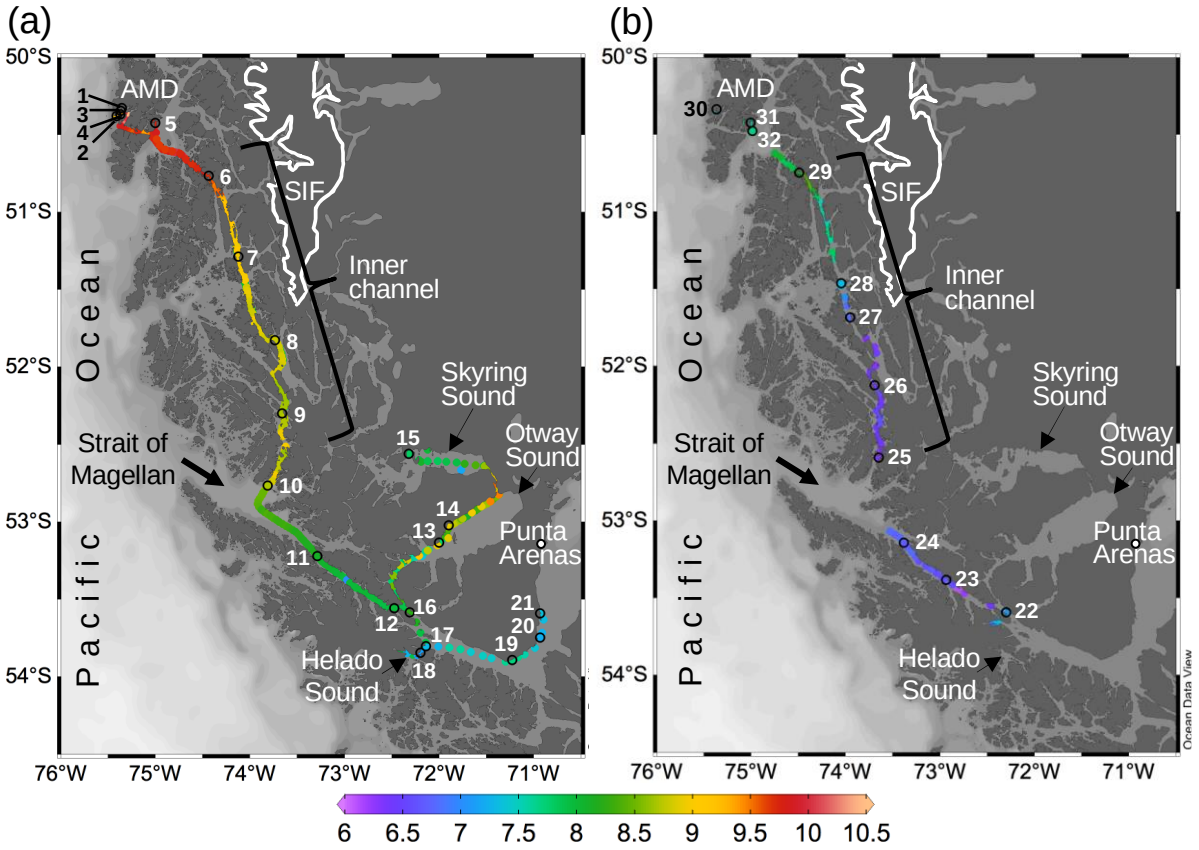

FIGURE S4. Maps of southern Patagonia showing the study sites and stations sampled during the austral late-spring 2015 (a) and early-spring 2017 (b). Temperature recorded at the surface during the two cruises is plotted. The approximate perimeter of the Southern Ice Fields (SIF) is depicted. Maps produced by Ocean Data View (Schlitzer, 2018).

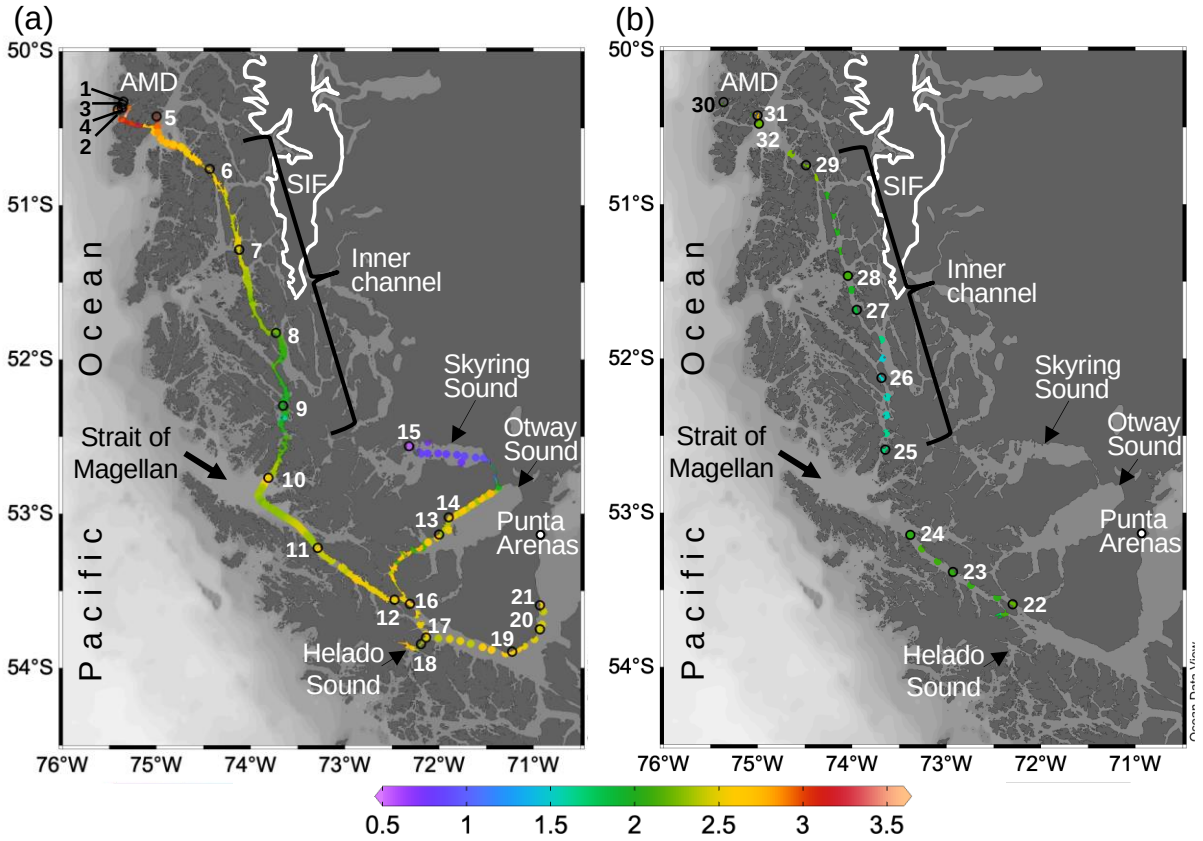

FIGURE S5. Maps of southern Patagonia showing the study sites and stations sampled during the austral late-spring 2015 (a) and early-spring 2017 (b). Ω calcite recorded at the surface during the two cruises is plotted. The approximate perimeter of the Southern Ice Fields (SIF) is depicted. A zoom into the Archipelago Madre de Dios (AMD) zone with Ω calcite and salinity surface values recorded in 2015 is provided in supplementary figure S1. Maps produced by Ocean Data View (Schlitzer, 2018).

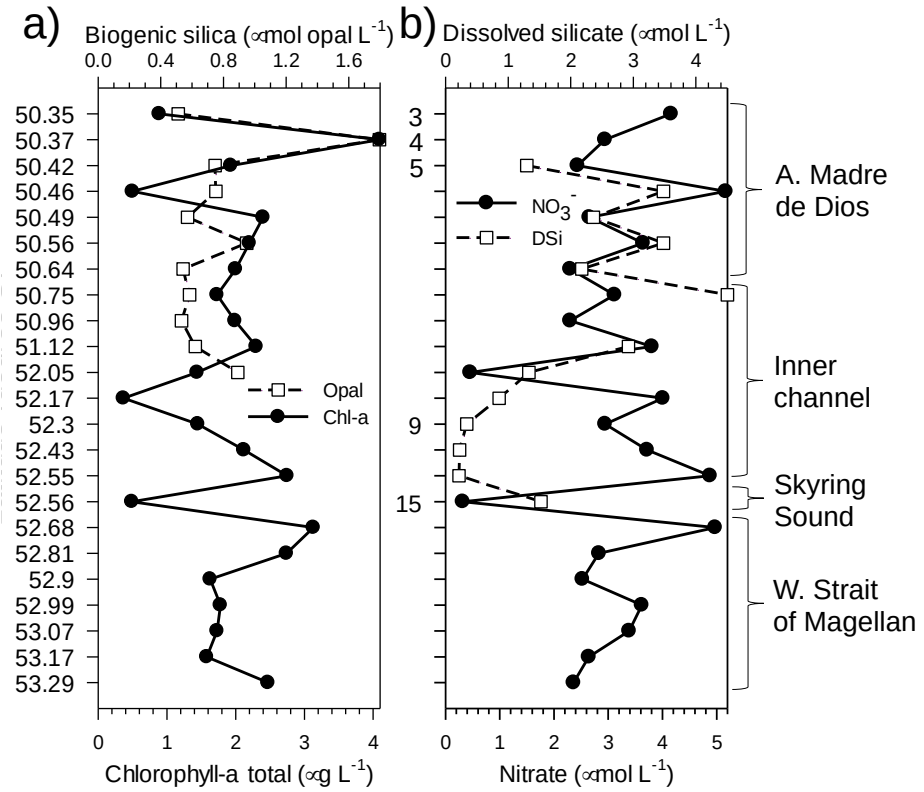

FIGURE S6. Concentration of nutrients and planktonic proxies recorded in surface waters of southern Patagonia during late-spring 2015. Chlorophyll-*a* and biogenic silica (a), and nitrate and dissolved silicate (b) are shown. Study sites and station ID discussed in the text are given in plot b).

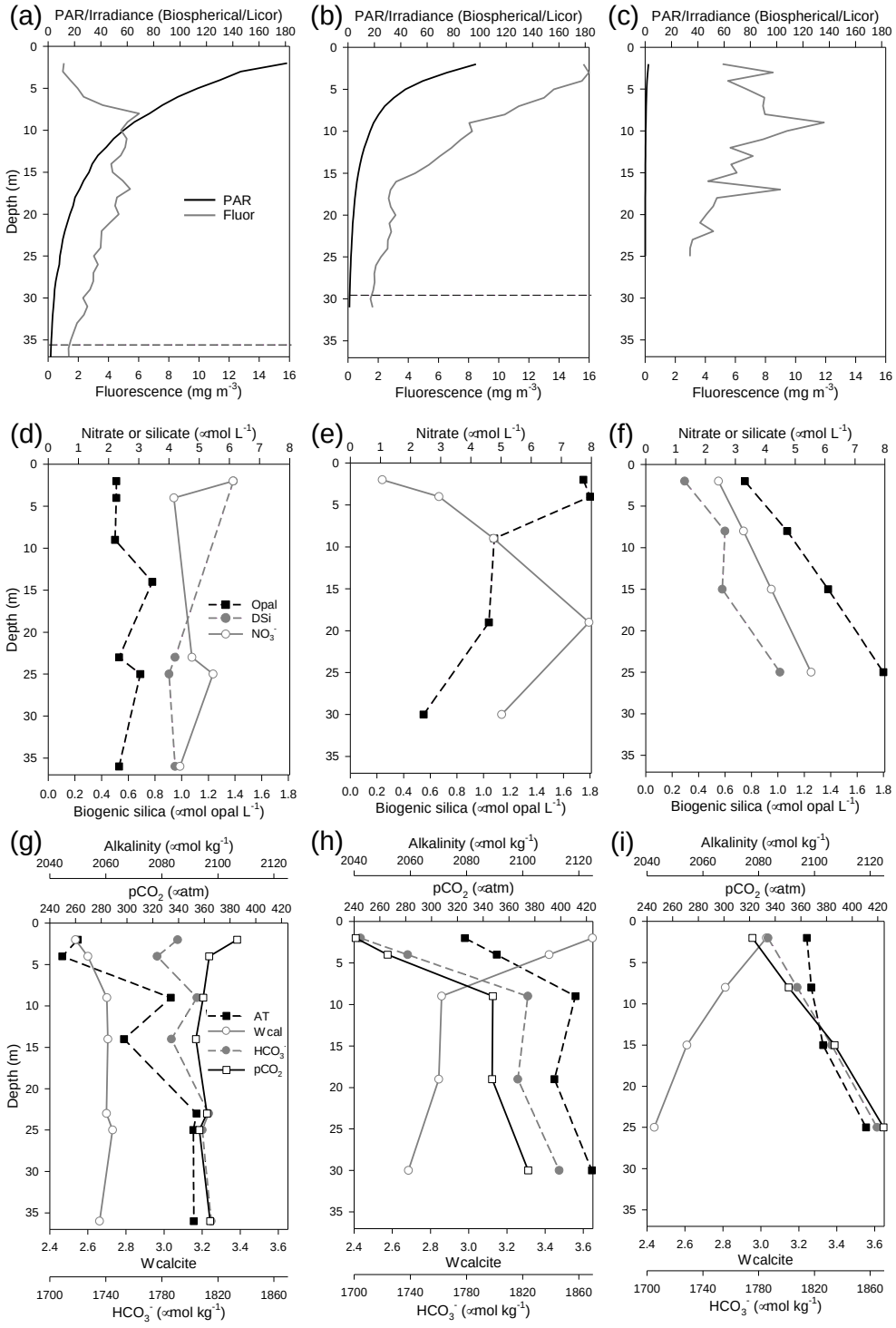

FIGURE S7. Physical, chemical, and biological vertical profiles recorded in the Archipelago Madre de Dios during austral late-spring 2015. Photosynthetically Available Radiation (PAR) and fluorescence signals (a-c), biogenic silica, nitrate and dissolved silicate (d-f), and pCO_2, alkalinity total, Ω calcite, and HCO_3^- (g-i) in the W-AMD (st. 3 left), between (st. 4 middle), and E-AMD zones (st. 5 right). Dotted lines in panels a-b indicate depths of 1% PAR penetration (st. 5 was conducted at night).

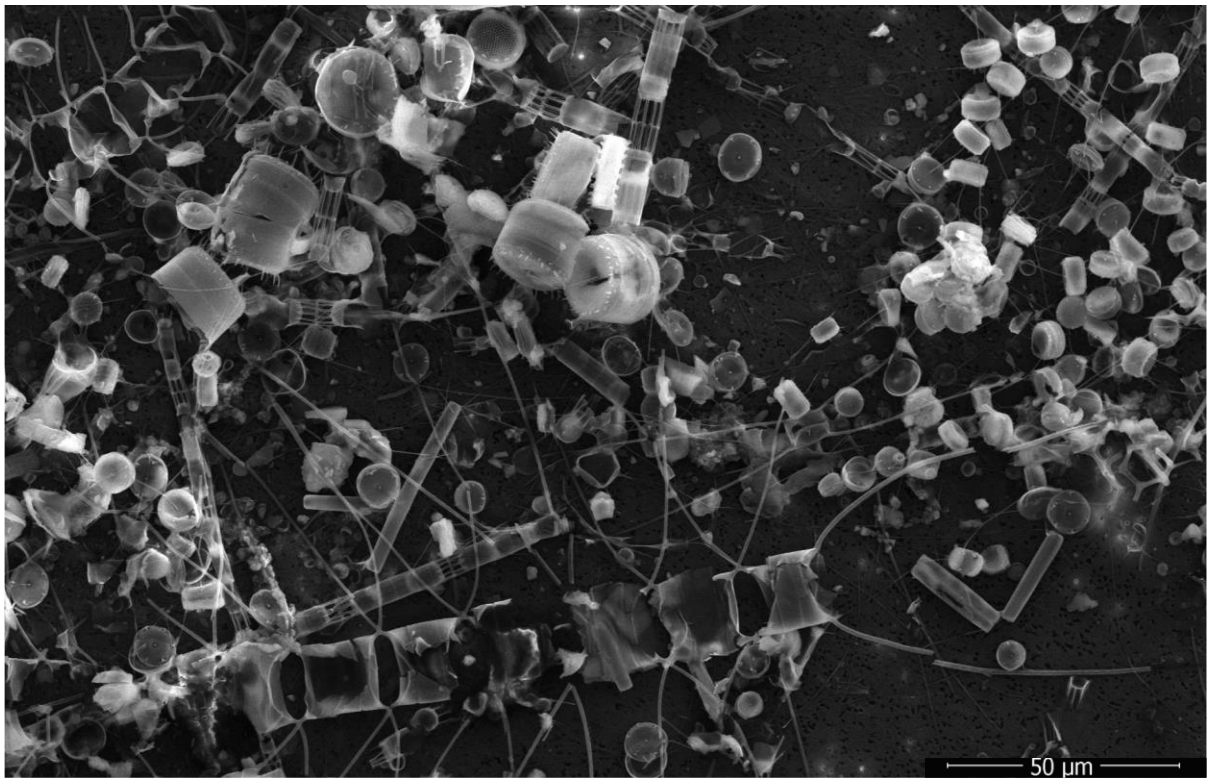

FIGURE S8. SEM image taken at 1,500x (st. 23) showing the phytoplankton assemblages during the austral early-spring 2017 comprised mostly by diatoms.

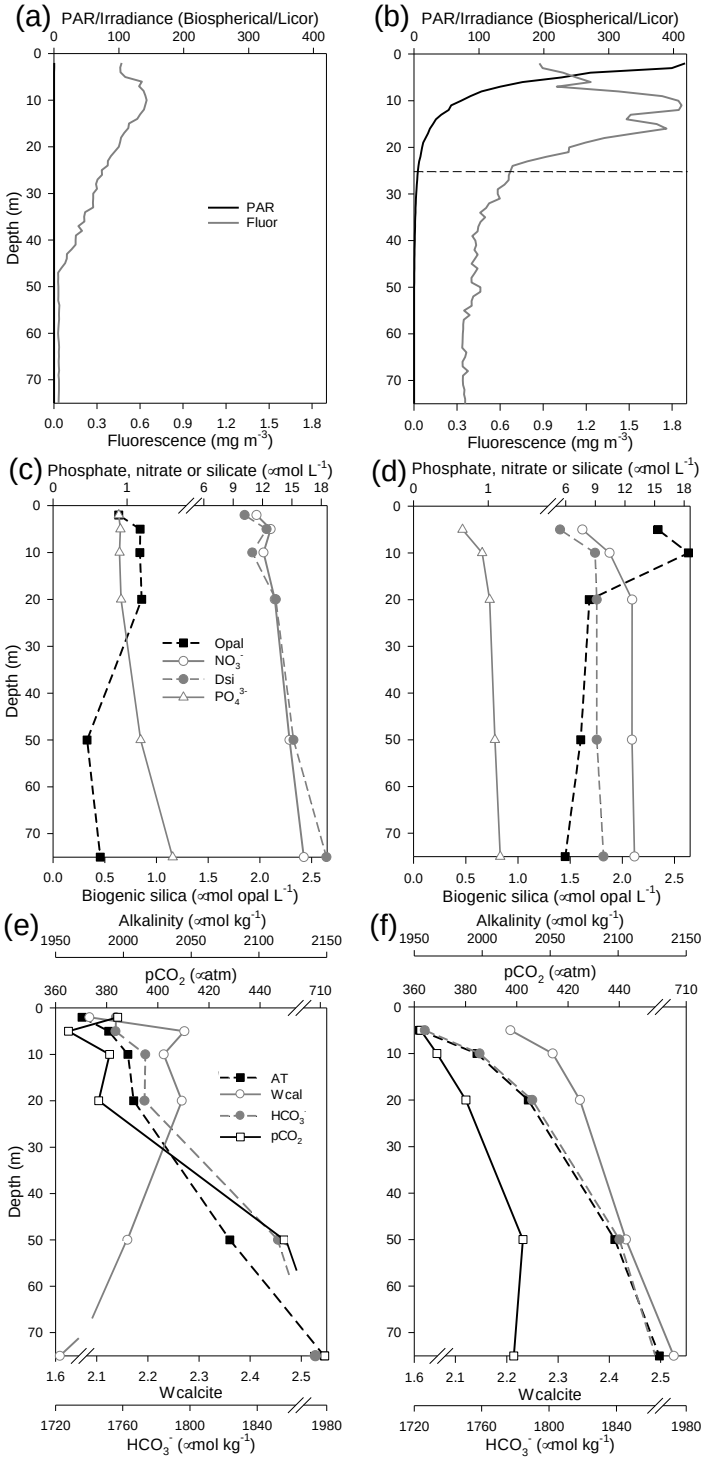

FIGURE S9. Physical, chemical, and biological vertical profiles recorded in the Archipelago Madre de Dios during austral early-spring 2017. Photosynthetically Available Radiation (PAR) and fluorescence signals (a-b), biogenic silica, nitrate, dissolved silicate and phosphate (c-d), and pCO_2, alkalinity total, Ω calcite, and HCO_3^- (e-f) in the W-AMD (st. 30 left) and E-AMD zones (st. 32 right). Dotted lines in panels a-b indicate depths of 1% PAR penetration (st. 30 was conducted at night).

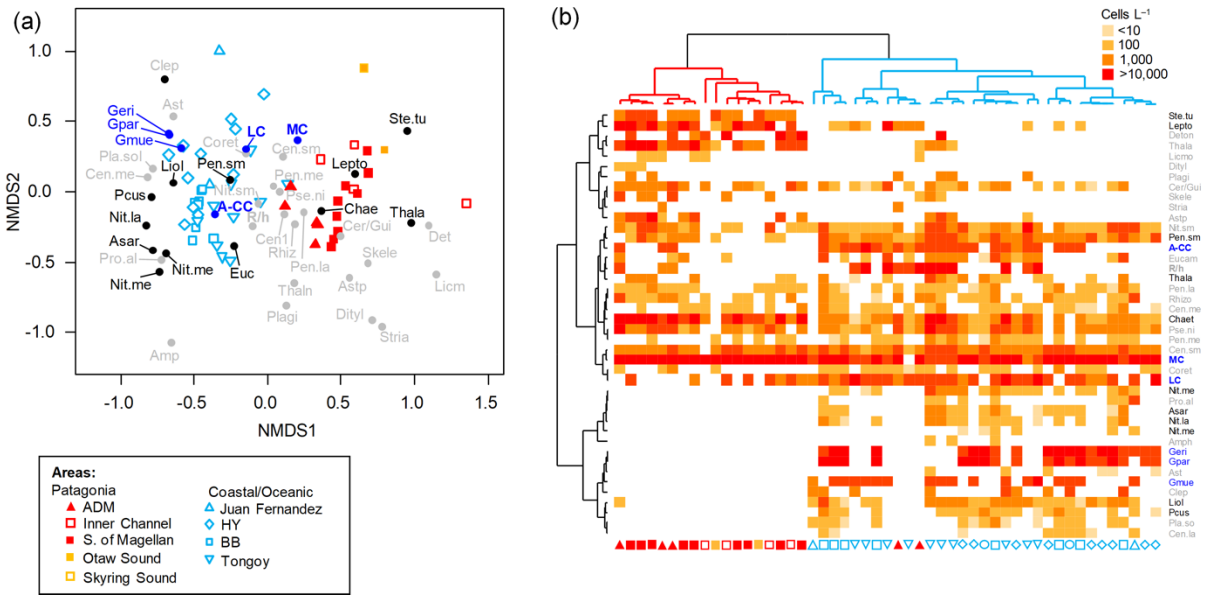

FIGURE S10. (a) Non-metric multidimensional scaling (nMDS) based on coccolithophore and diatom abundances attained in southern Patagonia fjords during late-spring 2015 (this study) and other coastal/oceanic areas (data from von Dassow *et al*., 2018). (b) Heatmap showing abundances of coccolithophore and diatom species used in the nMDS. The horizontal dendrogram (based on the nMDS samples scores) shows a clear separation between Patagonia fjords (red cluster) and coastal/oceanic (blue cluster) areas, whereas the vertical dendrogram (based on the nMDS species scores) indicates the separation of species in two main clusters. Black and blue species labels depict species with significant values in the IndVal analysis. A-CC = *Emiliania huxleyi* A-CC morphotype; Amphi = *Amphiprora* spp.; Asar = cf. *Asteromphalus sarcophagus*; Aster = *Asteromphalus* spp.; Astp = *Asterionellopsis* spp.; Cen.la = Centric diatoms > 100 µm diameter; Cen.me = Centric diatoms 40-100 µm diameter; Cen.sm = Centric diatoms < 40 µm diameter; Chae = *Chaetoceros* spp.; Clep = *Calcidiscus leptoporus*; Coret = *Corethron* spp.; Cer/Gui = *Cerataulina* spp. + *Guinardia* spp.; Deton = *Detonula* spp.; Dityl = *Ditylum* spp.; Eucam = *Eucampia* spp.; Geri = *Gephyrocapsa ericsonii*; Gmue = *Gephyrocapsa muellerae*; Gpar = *Gephyrocapsa parvula*; LC = *Emiliania huxleyi* lightly-calcified A-morphotype; Lepto = *Leptocylindrus* spp.; Licmo = *Licmophora* spp.; Liol = cf. *Lioloma* spp.; MC = *Emiliania huxleyi* moderate-calcifield A-morphotype; Nit.la = *Nitzschia* spp. large > 100 um length; Nit.me = *Nitzschia* spp. medium 100-50 um length; Nit.re = *Nitzschia reversa*; Nit.sm = *Nitzschia* spp. < 50 µm length; Pcus = cf. *Pseudo-nitzschia cuspidata*; Pen.la = Pennate diatoms > 100 µm length; Pen.me = Pennate diatoms 50-100 µm length; Pen.sm = Pennate diatoms < 50 µm length; Pla.so = *Planktoniella sol*; Plagi = *Plagiogrammopsis* spp.; Pro.al = *Proboscia alata*; Pse.ni = *Pseudo-nitzschia* spp.; R/h = *Emiliania huxleyi* R/hyper-calcified morphotype; Rhizo = *Rhizosolenia* spp.; Skele = *Skeletonema* spp.; Ste.tu = *Stephanopyxis turris*; Stria = *Striatella* spp.; Thala = *Thalassiosira* spp.; Thala = *Thalassionema* spp.

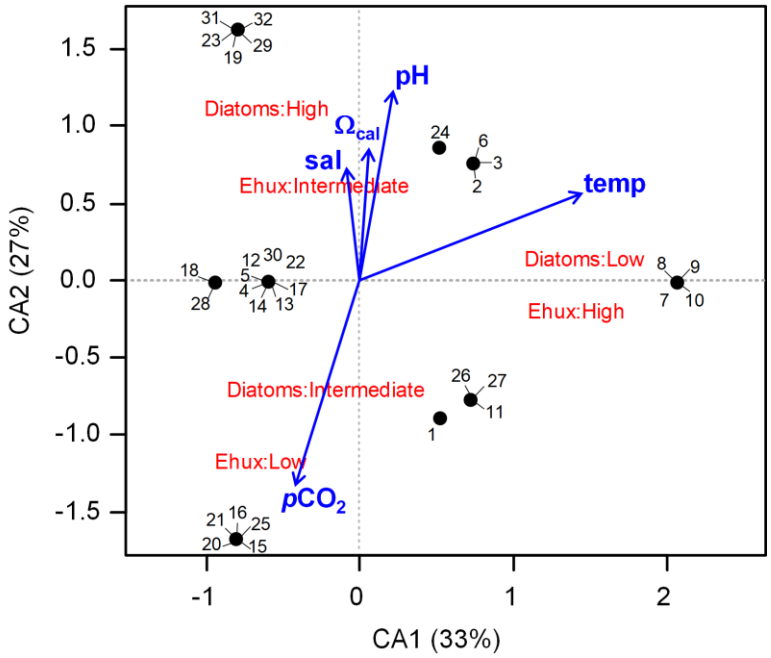

FIGURE S11. Correspondence analysis (CA) assessing the relationship between *E. huxleyi* and diatom biomasses converted to categoric values (i.e., low, intermediate, and high biomasses) in Patagonia fjords during late-spring 2015 and early-spring 2017. The *envit* function of the 'vegan' package (R software) was used to fit the environmental variables to the CA plot (no variable was significant; $p > 0.05$).

4 GENERAL DISCUSSION

Over the last 20 years, a large research effort has been put to understand the effects of OA phenomena on marine organisms and derived biogeochemical and ecological processes (e.g., plankton, molluscs, corals, crustaceans, vertebrates)[4]. Playing pivotal roles in marine ecosystems and biogeochemical cycles due to their roles as calcified phytoplankton (reviewed by Passow and Carlson, 2012; Balch, 2018), coccolithophores, especially the cosmopolitan species *E. huxleyi*, have attracted broad attention[5]. While short-term culture and mesocosm experiments (weeks to months) have suggested that OA can result in a decline in *E. huxleyi*

---

[4] A search in Google scholar yielded 56,700 related articles for the "ocean acidification" keyword.

[5] A search in Google scholar yielded 11,100 related articles for the "ocean acidification" and "coccolithophores" or "*Emiliania huxleyi*" keywords.

calcification and population growth (Meyer and Riebesell, 2015; Riebesell *et al*., 2017), long-term culture experiments (> 1 year) have revealed a potential for adaptation to OA, including a restoration of calcification (Lohbeck *et al*., 2012; Schlüter *et al*., 2016). Moreover, while some observational studies report a strong correlation between *E. huxleyi* calcification and carbonate chemistry conditions (Beaufort *et al*., 2011; Poulton *et al*., 2011; D'Amario *et al*., 2018), other studies did not find such a relationship (Smith *et al*., 2012; Young *et al*., 2014; Rigual-Hernández *et al*., 2020). These results highlight that it is unclear how the physiological effects of OA on *E. huxleyi* under controlled laboratory conditions translate to community-level responses in the field. This thesis aimed to contribute by studying the distribution and composition of coccolithophore assemblages and *E. huxleyi* morphotypes in contrasting pCO_2/pH environments of the ESP (chs. 1-2), and evaluate the responses of *E. huxleyi* morphotypes to targeted pCO_2/pH levels set in the lab (ch. 1). Here, the key results are compiled, and these findings discussed in the light of previous OA research.

4.1 Contrasting carbonate chemistry conditions constrained the distribution of coccolithophore species and *E. huxleyi* morphotypes in the Eastern South Pacific

The ESP is now known to offer an exceptional set of natural laboratories for studying how plankton respond to different carbonate chemistry conditions, as it contains a set of environments that exhibit wide contrasts in these parameters (Torres *et al*., 2011; Beaufort *et al*., 2011; Vargas *et al*., 2017). The ESP is one of the most poorly sampled oceanic regions of the planet in terms of plankton biomass and diversity, particularly concerning coccolithophores (O'Brien *et al*., 2013; de Vries *et al*., 2021). In order to help fill this gap, coccolithophore assemblages were surveyed in a coastal to ocean transitional section (TRA – NBP1305 cruise), mesotrophic waters (JF – around the Juan Fernández Islands), and coastal upwelling (UPW – in

front of Tongoy and El Quisco Bays) and fjords-channels systems (PAT – along southern Patagonia), along with in-situ physical and chemical conditions (Fig. 4.1). These four subsets of

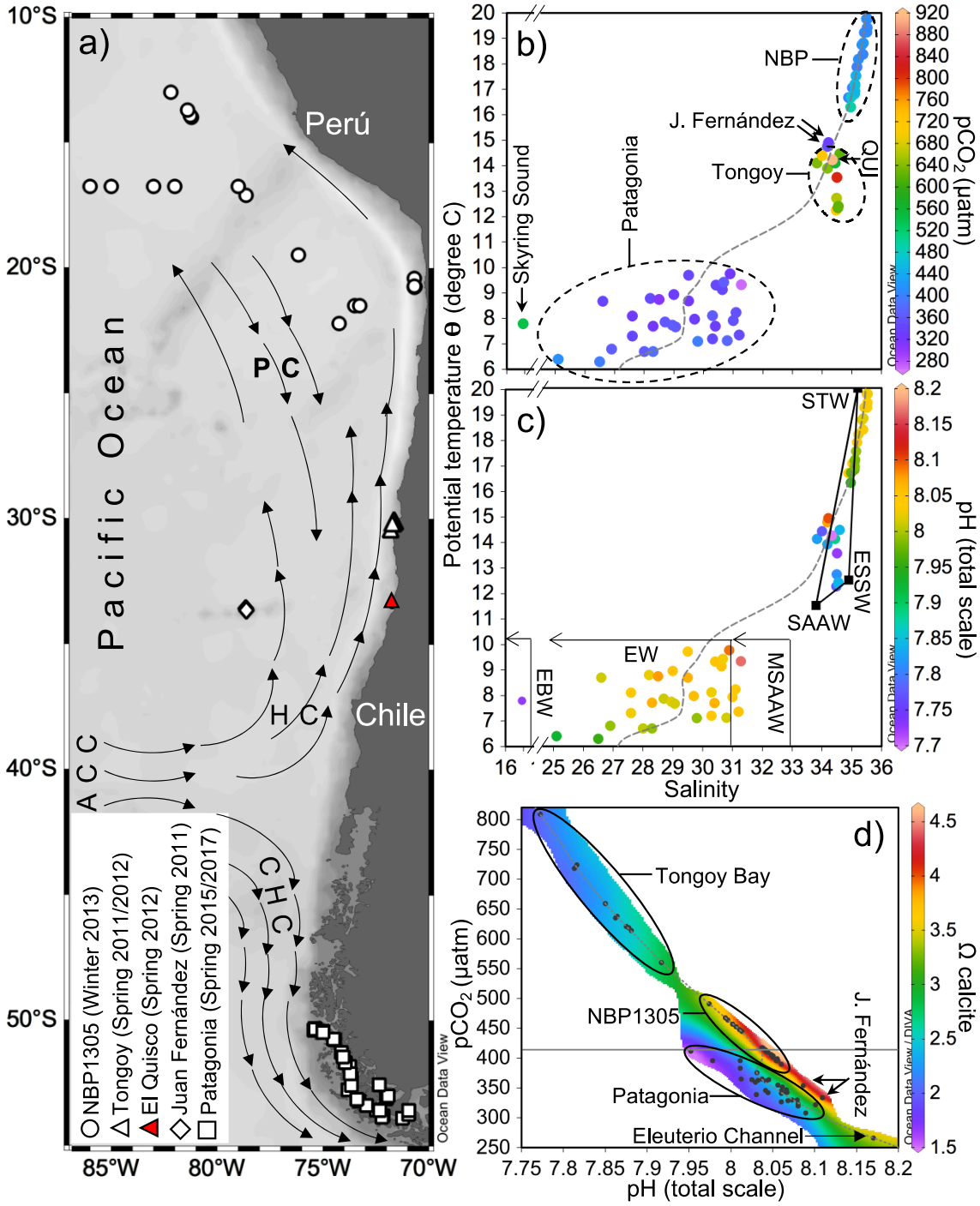

FIGURE Nº 4.1 Map of the Eastern South Pacific showing the study sites and sampled stations (a). Surface temperature, salinity, pCO_2, pH and Ω_{cal} in-situ conditions (b-d). Surface currents (a, arrows), a piece-wise linear least-squares fit of data (b-d, dash lines), T-S pairs and salinity ranges (c), and current global atmospheric pCO_2 level (d, solid line) are shown. ACC–Antarctic

Circumpolar Current, HC–Humboldt Current, CHC– Cape Horn Current, PC–Peru-Chile undercurrent, STW–Subtropical Water, ESSW–Equatorial Subsurface Water, SAAW–Subantarctic Water, MSAAW–Modified Subantarctic Water, EW–Estuarine Water, EBW–Estuarine Brackish Water. Map and plots produced by Ocean Data View (Schlitzer, 2018).

samples, having different T-S pairs or distance from the coast (Fig. 4.1 a-c), are further analyzed separately, and given the greater T-S variation recorded in PAT this subset was divided into the inner channel (IC), western Strait of Magellan (WSM), and Archipelago Madre de Dios (AMD) major basins. Moreover, for simplicity, the sampling efforts made during the mid-spring 2011/2012 in front of Tongoy, as well as during the late-spring 2015/early-spring 2017 in southern Patagonia will be discussed together.

The sampling covered a wide range of SST and SSS conditions: from warmer saline TRA waters, through temperate and less saline UPW and JF zones, and colder and freshened PAT waters (Fig. 4.1 a-c, Table 4.1). The T-S triangle indicates the hydrological influence of Subtropical Equatorial Subsurface/Subantarctic water masses on the TRA and UPW/JF sampled sites, respectively, whereas the lower T-S pairs from PAT resulted mostly from latitudinal-cooling and freshening. As expected from chemical equilibrium, an inverse-relationship between pCO_2 and pH was obtained along the study sites, which encompassed a wide range of carbonate chemistry conditions: from TRA waters with pCO_2–pH–Ω_{cal} levels around current global averages, towards UPW acidified or high pCO_2/low pH local conditions, and up to mostly CO_2-undersaturated PAT waters with local low, mid, and high pH–Ω_{cal} levels at the IC, WSM, and AMD, respectively (Table 4.1). While relatively low Ω_{cal} levels characterized both UPW and PAT systems, there was an important difference: The upwelling of high pCO_2-DIC enriched subsurface waters governed Ω_{cal} at UPW. In contrast, at PAT (i.e., centered at the IC zone; Fig. 4.1 d) freshwater diluted salinity and $[Ca^{2+}]$ and, importantly, partially decoupled Ω_{cal} from pH-pCO_2. The distribution and composition of coccolithophore assemblages and *E. huxleyi*

morphotypes were linked to these carbonate chemistry conditions aimed to detect potential eco-physiological adaptations to cope with OA. In addition, an effort was put to evaluate the role of co-occurring microplankton (especially diatoms) in the coccolithophore-environment interactions.

TABLE Nº 4.1 Surface physical and chemical in-situ conditions of study sites discussed here (64 stations in total). The average, standard deviation, and range (in parenthesis) are given.

	Transitional	J. Fernández	Upwelling	Southern Patagonia		
	n = 20	*n* = 2	*n* = 11	AMD *n* = 8	IC *n* = 5	WSM *n* = 12
Temperature (degree C)	18.0 ± 1.1 (16.3-19.8)	14.8	13.5 ± 0.9 (12.3-14.5)	8.8 ± 0.9 (7.7-9.8)	7.4 ± 1.2 (6.3-8.8)	7.6 ± 0.6 (6.7-8.7)
Salinity	35.2 ± 0.2 (34.9-35.5)	34.2	34.4 ± 0.3 (33.8-34.6)	30.0 ± 1.1 (28.3-31.3)	26.7 ± 1.1 (25.1-28.2)	30.0 ± 1.0 (28.0-31.2)
pCO_2 (µatm)	425 ± 29 (390-491)	344	683 ± 102 (560-913)	336 ± 33 (241-365)	372 ± 31 (339-412)	355 ± 22 (323-396)
pH (total scale)	8.03 ± 0.03 (7.97-8.06)	8.10	7.84 ± 0.06 (7.72-7.92)	8.07 ± 0.04 (8.03-8.17)	8.00 ± 0.04 (7.95-8.04)	8.05 ± 0.02 (8.01-8.08)
CO_3^{2-} (µmol kg^{-1})	174 ± 14 (146-194)	169	98 ± 11 (77-118)	109 ± 17 (90-141)	74 ± 12 (59-90)	98 ± 9 (81-108)
Ω calcite	4.1 ± 0.3 (3.5-4.6)	4.0	2.3 ± 0.3 (1.8-2.8)	2.7 ± 0.4 (2.2-3.4)	1.8 ± 0.3 (1.5-2.2)	2.4 ± 0.2 (2.0-2.6)

The results confirmed coccolithophore composition and distributions expected from both earlier and more recent studies in the ESP (McIntyre *et al*., 1970; Hagino and Okada, 2004; Beaufort *et al*., 2008; Menschel *et al*., 2016; Bendif *et al*., 2016). The coccolithophores were widely distributed in the ESP, and *E. huxleyi* was the most prominent species, being present in all samples (30-100 % rel. abundance) except for Skyring Sound in PAT (Fig. 4.2). The four species of *Gephyrocapsa* were more restricted: the smaller *G. ericsonii* and *G. parvula* cells both inhabited TRA waters, *G. muellerae* mainly inhabited coastal waters, while *G. oceanica* was

very scarce (and therefore was not included in further statistical analysis). Another large coccolithophore, *Calcidiscus leptoporus*, did not show any clear pattern in its distribution.

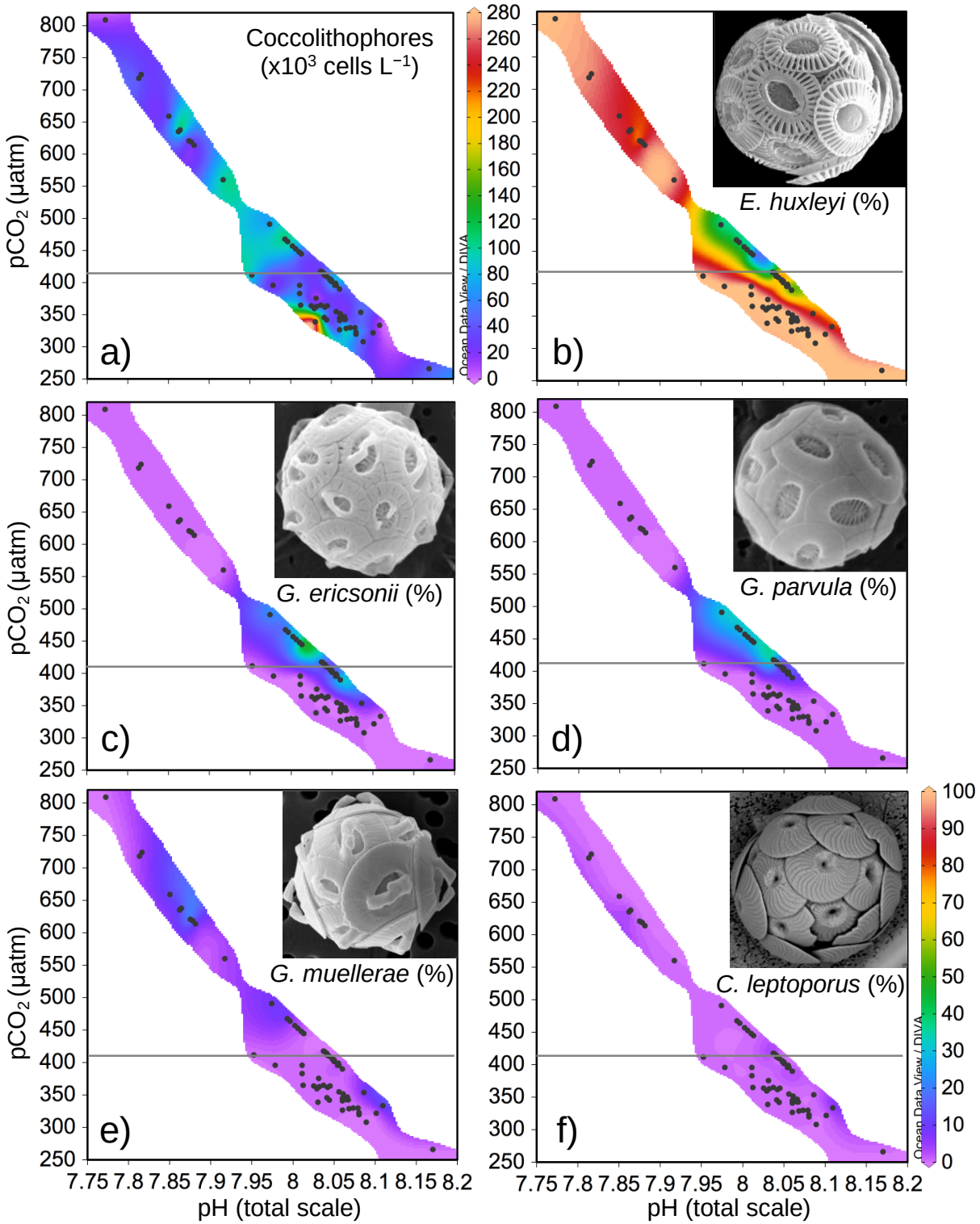

FIGURE Nº 4.2 Total and relative abundances by coccolithophore assemblages (a) and five coccolithophore species (b-f) yielded along pCO_2-pH levels recorded in the Eastern South Pacific. Corresponding study sites and Ω_{cal} levels are shown in Fig 4.1 d). Horizontal line indicates current global atmospheric pCO_2 level.

The longitudinal transition from nearby stable offshore waters towards more fluctuating coastal zones seemed to modulate the coccolithophore-environment interactions. In particular, the predominance during two springs of *E. huxleyi* (i.e., lower evenness) in both UPW and PAT coastal systems under similar low pH-Ω_{cal}, but contrasting T-S conditions, suggested that this taxon is the most adaptable and resilient to environmental change. This was examined by comparing the niche breadth and tolerance to SST, SSS, pCO_2, pH and Ω_{cal} by the main coccolithophore species and *E. huxleyi* morphotypes co-occurring in the ESP (see below).

The moderate-calcified A morphotype dominated the *E. huxleyi* populations in almost all sampled sites (67-100 % rel. abundance), with the only exception of the R hyper-calcified cells that surpassed it in the UPW zones (Fig. 4.3). The lightly-calcified and A-CC morphotypes did not show any clear pattern in its distribution, and with the former actually may include a hidden diversity (e.g., B, B/C, C, O and even lightly calcified A forms), whereas the A-CC seems to be a single relatively well defined morphotype. In the case of southern Patagonia, the *E. huxleyi* populations were distinct from surrounding coastal or open ocean populations in the ESP (i.e., mostly the typical moderate-calcified A morphotype and the hyper-calcified R morphotype; see Hagino and Honjo, 2006; Beaufort *et al*., 2008; 2011; Menschel *et al*., 2016; Alvites, 2016), the Southern Ocean (mostly B/C and C forms, see Saavedra-Pellitero *et al*., 2014; 2019; Charalampopoulou *et al*., 2016), and the Atlantic (mostly B/C forms, see Poulton *et al*., 2011; 2013), but sharing similar intra-morphotype A composition with the Norwegian fjords (see Young, 1994), suggesting they are shaped by local factors. The abrupt shifts in composition of *E. huxleyi* populations from predominantly moderate-calcified cells in the ESP towards hyper-calcified forms in the UPW zones led us to test the causes behind this pattern (see below).

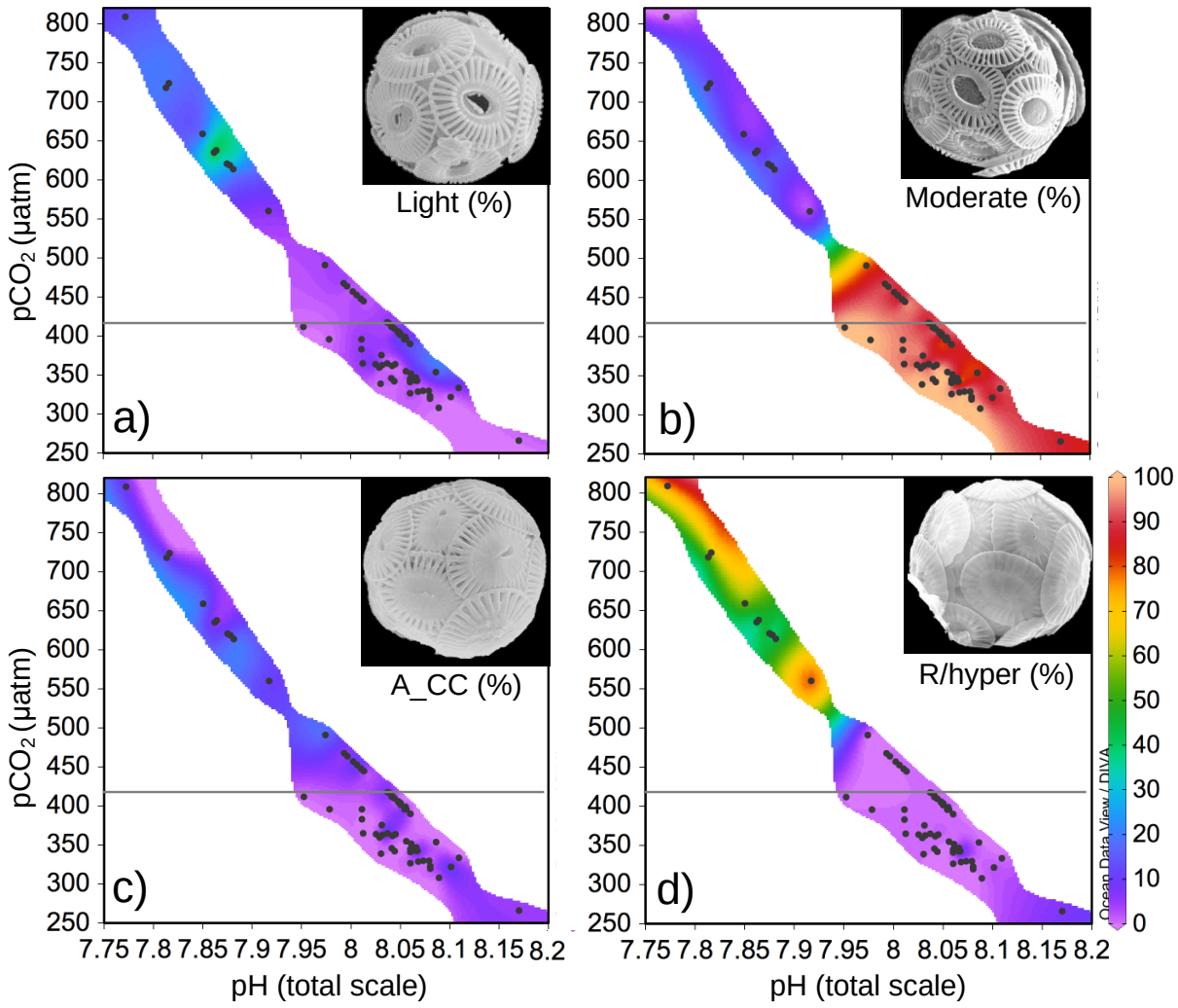

FIGURE Nº 4.3 Relative abundances by main *Emiliania huxleyi* morphotypes (a-d) yielded along pCO_2 and pH levels recorded in the Eastern South Pacific. Corresponding study sites and Ω_{cal} levels are shown in Fig. 4.1 d). Horizontal line indicates current global atmospheric pCO_2 level.

4.2 Niche analysis of coccolithophore species and *E. huxleyi* morphotypes related to physical and chemical conditions

In order to assess the main environmental conditions associated with the realized niche of the different coccolithophore species and *E. huxleyi* morphotypes, Outlying Mean Index (OMI) niche analyses were performed. The OMI analysis separates the realized-niches according to their average position on the marginality axis (i.e., niche position) and respective tolerance to it

(i.e., niche breadth). Marginality (OMI) measures the distance between the average habitat conditions used by the species and the average conditions across the study area, whereas tolerance (Tol) accounted for the dispersion of samples containing the species under study from the origin (i.e., the most general habitat conditions) (Dolédec *et al*., 2000). Thereby, a species having a lower OMI and higher Tol is the species that utilizes a greater array of resources and maintains populations within a wider variety of conditions (generalist species), as compared with opportunist or specialized and less resilient species with a more restricted niches (or high OMI and low Tol). In addition, a subspace orthogonal to the marginality axis yielded a residual tolerance (RTol) that accounts for the variation in species unexplained by the selected variables (Dolédec *et al*., 2000). Unlike the more commonly used multivariate analysis, such as, CCA or RDA, the OMI co-inertia analysis gives equal weights to species-rich and species-poor sites in defining the sampling domain, and makes no assumption about the shape of species' response curves (Dolédec *et al*., 2000).

The moderate-calcified A morphotype showed the broader niche-breadth and tolerance within the sampling domain (i.e., generalist) compared with more restricted niche the R hyper-calcified morphotype in terms of Ω_{cal}, SST, and SSS, although the latter morphotype showed a broad niche in terms of pCO_2 and pH. Interestingly, the other four coccolithophore species showed narrower realized-niches than even the more specialized *E. huxleyi* morphotypes. If the ubiquitous taxon is less susceptible to environmental change that marginal ones (i.e., marginality or richness vs. tolerance are inversely correlated; Dolédec *et al*., 2000; Hernández *et al*., 2015), the exceptional generalist behavior exhibited by *E. huxleyi* compared to other coccolithophores suggests it may be more plastic and more adaptable in the face of environmental change.

4.3 The relationship between *E. huxleyi* and diatoms

It has been previously proposed that the realized niche of *E. huxleyi* is partly defined by physical and chemical conditions unfavorable to large diatoms (i.e., the expectation of a *E.* huxleyi-diatoms inverse relationship; see Tyrrell and Merico, 2004; Smith *et al*., 2017). To test for such a relationship, a correspondence analysis was performed based on the presence or absence of low, intermediate or high *E. huxleyi* and diatom carbon biomass in 32 samples taken along southern Patagonia with SST, SSS, pCO_2, pH and Ω_{cal} as environmental variables.

An initial unimodal *E. huxleyi* - diatom biomass relationship shifted to a correspondence between the lowest diatom - highest *E. huxleyi* stocks (Fig. 4.4), possibly being affected by environmental (e.g., turbulence and nutrients supply; see Margalef, 1978; Brzezinski *et al*., 2011) and biotic factors (e.g., top-down control; see Nejstgaard *et al*., 1997) not assessed in this study. Another group of nano-sized centric diatoms (*Minidiscus* ~ 3 µm diameter) not included in the correspondence analysis (it was overlooked by light microscope analysis but seen and quantified with SEM) also co-occurred with *E. huxleyi* in fjords-channels of Patagonia (results not shown). Overall, whereas *E. huxleyi* and diatoms tend to co-occur in Patagonian waters, the former is at its best in environments that support low productivity (e.g., the low salinity/nutrients southern IC zone), but when diatoms are very abundant, they crowd out *E. huxleyi*.

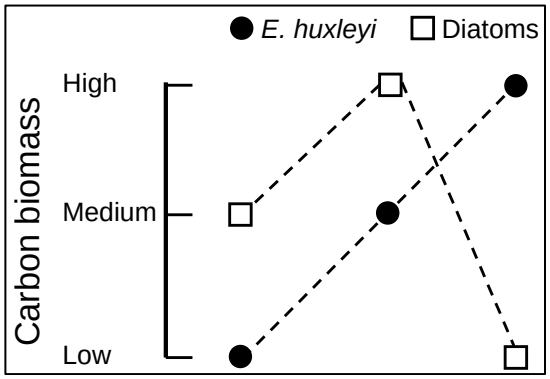

FIGURE Nº 4.4 Correspondence between the low, medium, and high carbon biomass yielded by *E. huxleyi* and diatoms in Patagonia during the late-spring 2015 and early-spring 2017.

4.4 Are field correlations between high pCO_2/low pH waters and hyper-calcification indicative of local adaptation to cope with OA?

This study confirmed in two separate years the occurrence of R hyper-calcified forms of *E. huxleyi* in coastal waters of central to northern Chile under relatively high pCO_2/low pH conditions. This exceptionally robust R-morphotype has been reported stable under different lab physiological stresses (e.g., Mella-Flores *et al*., 2018; von Dassow *et al*., 2018). Such a hyper-calcified morphotype has caught the attention because it does not follow the overall pattern exhibited by *E. huxleyi* showing reduced calcification in environments with increased pCO_2/decrease pH levels, but according to Beaufort *et al*. (2011) it highlights the complexity of assemblage-level responses to environmental forcing factors.

To the best of our knowledge, the R hyper-calcified morphotype has only been seen thriving in waters off the coast of Chile and Peru, where pCO_2 reaches values about 2-fold higher than the equilibrium with present-day atmospheric levels (see Fig. 4.1 d above). Recent findings indicated that marine multicellular organisms (e.g., invertebrates, coralline algae, copepods) inhabiting waters with natural high fluctuations in pH are more tolerant to OA than conspecifics occurring in nearby stable waters (e.g., Gaitán-Espitia *et al*., 2017; Vargas *et al*., 2017), suggesting the ESP upwelling systems might hold genetic reservoirs for adaptation of *E. huxleyi* to OA. Therefore, through culture experiments we tested the simplest hypothesis – focusing on a single factor – that these forms are adapted to resist high pCO_2/low pH conditions.

The high pCO_2/low pH treatment reduced growth rate of five *E. huxleyi* tested strains, whereas PIC/POC ratios also decreased in all strains and all treatments, similar to what has been reported for most of the strains used in most of the previous OA studies (reviewed in Meyer and Riebesell, 2015). We concluded that the A morphotypes from the eastern South Pacific were

not more sensitive than the R/over-calcified strains from neighboring high pCO_2/low pH waters. It is noteworthy that the B, B/C, C and O morphotypes were not tested and the results of Müller *et al*. (2015) suggest they might be much more sensitive. Such lack of evidence for regional-scale local adaptation to short-term high pCO_2/low pH conditions in *E. huxleyi* populations (but see Müller *et al*., 2015a), might be explained by the OMI analysis suggesting a narrow unimodal response to Ω_{cal}, that would not have been detected by our experiments, where Ω_{cal} values of 1.4 vs. 3.3 were tested (i.e., the R hyper-calcified morphotype might have been observed to better resist intermediate Ω_{cal} values compared to the A type). Alternatively, the R/hyper-calcified morphotype might be selected by an unidentified condition particular to the ESP that correlates with the Ω_{cal}, SST, and SSS of its realized niche. Overall, despite their rapid turnover and large population sizes, oceanic planktonic microorganisms do not necessarily exhibit adaptations to naturally high-pCO_2 upwellings, and this ubiquitous coccolithophore may be near the limit of its capacity to adapt to ongoing OA.

The function of coccoliths is still not certain. Considering different selective forces that may be acting on coccolithophores, numerous calcification-hypothesis have been put forward (reviewed by Monteiro *et al*., 2016). Recently, Müller (2019) separated these hypotheses by distinguishing "process" benefits during the development and genesis of coccoliths (e.g., intracellular Ca^{2+} control and detoxification) or "end-product" benefits depending on the prevailing ecological settings (e.g., ballasting for nutrient acquisition, grazing and virus and/or bacterial-infection protection, light bundling under dimmed conditions, UV photoprotection). A meta-analysis coupling cost-benefit analysis and modelling estimated that up to 37% of the photosynthesis energy budget is required to support *E. huxleyi* calcification, and concluded that grazing and/or viral- and bacterial-infection protections are likely to be advantageous functions

for most coccolithophores, while recognizing the lack of empirical results outside of *E. huxleyi* (Monteiro *et al*., 2016). By contrast, a meta-analysis of mesocosm experiments found that *E. huxleyi* calcification failed to deter micro-zooplankton grazers (i.e., naked and calcified cells were consumed indiscriminately; see Mayers *et al*., 2020), and a virus-*E. huxleyi* culture-based study concluded that the coccosphere provides limited protection against virus infection (Haunost *et al*., 2020). However, other results show that virus infection can at the same time influence host calcification and, in absence of lysis, remove virus (i.e., different coccoliths morphologies structure virus infection which in turn can trigger PIC flux; see Johns *et al*., 2019). Relevant to this debate are the striking results that disruption of calcification halted the entire lifecycle of *Coccolithus braarudii*, whereas *E. huxleyi* continued to grow (i.e., calcification is facultative in *E. huxleyi* but obligatory in some coccolithophores; see Walker *et al*., 2018). Overall, these results pointed out that the benefits of calcification, if any, are niche-, species-, morphotype-, and lifecycle-specific, and that excessive reductionism or generalization must be avoided (Müller, 2019).

4.5 Projected impacts of OA on the distribution of coccolithophore species and *E. huxleyi* morphotypes in the Eastern South Pacific

While early field and experimental studies highlighted the detrimental effects of OA on *E. huxleyi* growth rate, calcification, and coccolithogenesis (e.g., Riebesell *et al*., 2000; Beaufort *et al*., 2011), more recent studies suggest a capacity to adapt to a high pCO_2/low pH global ocean. For example, a multidecadal increase in coccolithophore occurrences compared to diatoms and dinoflagellates matched the increase in pCO_2 and SST occurred in the North Atlantic (Rivero-Calle *et al*., 2015), and other seasonal monitoring studies reports the rise of over-calcified forms coinciding with winter high pCO_2/low pH levels in waters off the Biscay

Bay (Smith *et al*., 2012), eastern Scottish coast (León *et al*., 2018), and southwest Pacific (Rigual-Hernández *et al*., 2020). Regarding the ESP, as a consequence of unabated anthropogenic CO_2 emissions (see General Introduction) the high pCO_2/low pH levels observed in coastal zones are expected to further expand offshore by 2050 (Egger, 2011). In that scenario, and based on the realized-niche breadth and tolerance yielded by four coccolithophore species and five *E. huxleyi* morphotypes along SST, SSS, pCO_2, pH, and Ω_{cal} levels (see above), one could predict a niche expansion by the *E. huxleyi* moderate-calcified populations in the near future, up to a certain limit, however, where the growth and calcification may be seriously impaired, as indicated by our experimental work (see above). Such a prevalence of the *E. huxleyi* moderately-calcified forms having lower cellular PIC quotas and PIC/POC ratios than the R hyper-calcified morphotype (Beaufort *et al*., 2011) and other coccolithophore species (Gafar *et al*., 2019), supports the prediction that PIC-associated POC export may decline under future OA conditions, potentially weakening the biological pump (Hofmann and Schellnhuber, 2009).

REFERENCES

Abril, G., Bouillon, S., Darchambeau, F., Teodoru, C., Marwick, T., Tamooh, F., Ochieng, F., Geeraert, N., Deirmendjian, L., Polsenaere, P. y Borges, A. (2015). Technical note: large overestimation of pCO_2 calculated from pH and alkalinity in acidic, organic-rich freshwaters. Biogeosciences. 12, 67–78.

Agostini, S., Harvey, B., Wada, S., Kon, K., Milazzo, M., Inaba, K. y Hall-Spencer, J. (2018). Ocean acidification drives community shifts towards simplified non-calcified habitats in a subtropical–temperate transition zone. Scientific Reports. 8, 11354.

Alves-de-Souza C., González, M. y Iriarte, J. (2008). Functional groups in marine phytoplankton assemblages dominated by diatoms in fjords of southern Chile. J. Plankton Res. 30, 1233–1243.

Alvites, D. (2016). Variabilidad espacial y calcificación de las comunidades de cocolitofóridos en el sistema de afloramiento costero frente al Callao-Perú. Tesis de Maestro, Universidad Peruana Cayetano Heredia, pp. 128.

Andrade, I., Hormazábal, S. y Combes, V. (2014). Intrathermocline eddies at the Juan Fernández Archipelago, southeastern Pacific Ocean. Lat. Am. J. Aquat. Res. 42, 888–906.

Armstrong, R. A., Lee, C., Hedges, J. I., Honjo, S. y Wakeham, S. G. (2002). A new, mechanistic model for organic carbon fluxes in the ocean based on the quantitative association of POC with ballast minerals. Deep-Sea Res. Pt. II. 49, 219–236.

Bach, L. T., Bauke, C., Meier, K. J. S., Riebesell, U. y Schulz, K. G. (2012). Influence of changing carbonate chemistry on morphology and weight of coccoliths formed by *Emiliania huxleyi*. Biogeosciences. 9, 3449–3463.

Bach, L. T., Mackinder, L. C. M., Schulz, K. G., Wheeler, G., Schroeder, D. C., Brownlee, C. y Riebesell, U. (2013). Dissecting the impact of CO_2 and pH on the mechanisms of photosynthesis and calcification in the coccolithophore *Emiliania huxleyi*. New Phytol. 199, 121–134.

Bach, L. (2015). Reconsidering the role of carbonate ion concentration in calcification by marine organisms. Biogeosciences. 12, 4939–4951.

Baith, K., Lindsay, R., Fu, G. y McClain, C. R. (2001). SeaDAS, a data analysis system for ocean-color satellite sensors. Eos T. Am. Geophys. Un. 82, 202–203.

Balch, W. (2018). The ecology, biogeochemistry, and optical properties of coccolithophores. Annu. Rev. Mar. Sci. 10, 71–98.

Barton, A., Dutkiewicz, S., Flierl, G., Bragg, J. y Follows, M. (2010). Patterns of diversity in marine phytoplankton. Science. 327, 1509–1511.

Baumann, K.-H., Andruleit, H. y Samtleben, C. (2000). Coccolithophores in the Nordic Seas: comparison of living communities with surface sediment assemblages. Deep-Sea Research II. 47, 1743–1772.

Baumann, K.-H., Andruleit, H., Böckel, B., Geisen, M. y Kinkel, H. (2005). The significance of extant coccolithophores as indicators of ocean water masses, surface water temperature, and paleoproductivity: a review. Paläontologische Zeitschrift. 79, 93–112.

Baumann, K.-H., Boeckel, B. y Čepek, M. (2008). Spatial distribution of living coccolithophore along an east-west transect in the subtropical South Atlantic. J. Nannoplankton Res. 30, 9–21.

Beaufort, L., Couapel, M., Buchet, N., Claustre, H. y Goyet, C. (2008). Calcite production by coccolithophores in the south east Pacific Ocean. Biogeosciences. 5, 1101–1117.

Beaufort, L., Probert, I., de Garidel-Thoron, T., Bendif, E., Ruiz- Pino, D., Metzl, N., Goyet, C., Buchet, N., Coupel, P., Grelaud, M., Rost, B., Rickaby, R. y de Vargas, C. (2011). Sensitivity of coccolithophores to carbonate chemistry and ocean acidification. Nature. 476, 80–83.

Bendif, E., Probert, I., Carmichael, M., Romac, S., Hagino, K. y de Vargas, C. (2014). Genetic delineation between and within the widespread coccolithophore morpho-species *Emiliania huxleyi* and *Gephyrocapsa oceanica* (Haptophyta). J. Phycol. 50, 140–148.

Bendif, E., Probert, I., Díaz-Rosas, F., Thomas, D., van den Engh, G., Young, J. y von Dassow, P. (2016). Recent reticulate evolution in the ecologically dominant lineage of coccolithophores. Front. Microbiol. 7, 784.

Bendif, E., Nevado, B., Wong, E., Hagino, K., Probert, I., Young, J., Rickaby, R. y Filatov, D. (2019). Repeated species radiations in the recent evolution of the key marine phytoplankton lineage *Gephyrocapsa*. Nature communications. 10:4234.

Berge, G. (1962). Discoloration of the sea due to *Coccolithus huxley* I "bloom". Sarsia. 6, 27–40.

Biermann, A. y Engel, A. (2010). Effect of CO_2 on the properties and sinking velocity of aggregates of the coccolithophore *Emiliania huxleyi*. Biogeosciences. 7, 1017–1029.

Birkenes, E. y Braarud, T. (1952). Phytoplankton in the Oslo fjord during a "*Coccolithus huxleyi*-summer", Avhandl. Norske Videnskaps - Akd. Oslo. I. Mat. Naturv. Klasse. 2, 1–23.

Bollmann, J., Cortés, M., Haidar, A., Brabec, B., Close, A., Hofmann, R., Palma, S., Tupas, L. y Thierstein, H. (2002). Techniques for quantitative analyses of calcareous marine phytoplankton. Marine Micropaleontology. 44, 163–185.

Borcard, D., Gillet, F. y Legendre, P. (2011). Numerical ecology with R. Springer Science+Business Media, pp. 306.

Broecker, W. y Clark, E. (2009). Ratio of coccolith $CaCO_3$ to foraminifera $CaCO_3$ in late Holocene deep sea sediments. Paleoceanography. 24, 1–11.

Brown, Ch. y Yoder, J. (1994). Coccolithophorid blooms in the global ocean. Journal of Geophysical Research. 99, 7467–7482.

Brzezinski, M., Dickson, M., Nelson, D. y Sambrotto, R. (2003). Ratios of Si, C and N uptake by microplankton in the Southern Ocean. Deep Sea Research Part II: Topical Studies in Oceanography. 50, 619–633.

Brzezinski, M., Baines, S., Balch, W., Beucher, Ch., Chai, F., Dugdale, R., Krause, J., Landry, M., Marchi, A., Measures, Ch., Nelson, D., Parker, A., Poulton, A., Selph, K., Strutton, P., Taylor, A. y Twining, B. (2011). Co-limitation of diatoms by iron and silicic acid in the equatorial Pacific. Deep-Sea Research II. 58, 493-511.

Buitenhuis, E. T., De Baar, H. J. W. y Veldhuis, M. J. W. (1999). Photosynthesis and calcification by *Emiliania huxleyi* (Prymnesiophyceae) as a function of inorganic carbon species. J. Phycol. 35, 949–959.

Buitenhuis, E., Pangerc, T., Franklin, D., Le Quéré, C. y Malin, G. (2008). Growth rates of six coccolithophorid strains as a function of temperature. Limnol. Oceanogr. 53, 1181–1185.

Charalampopoulou, A., Poulton, A., Tyrrell, T. y Lucas, M. (2011). Irradiance and pH affect coccolithophore community composition on a transect between the North Sea and the Arctic Ocean. Mar. Ecol. Prog. Ser. 431, 25–43.

Charalampopoulou, A., Poulton, A., Bakker, D., Lucas, M., Stinchcombe, M. y Tyrrell, T. (2016). Environmental drivers of coccolithophore abundance and calcification across Drake Passage (Southern Ocean). Biogeosciences. 13, 5917–5935.

Combes, V., Hormazabal, S. y Di Lorenzo, E. (2015). Interannual variability of the subsurface eddy field in the Southeast pacific. J. Geophys. Res.-Oceans. 120, 4907–4924.

Comeau, S., Cornwall, Ch., DeCarlo, T., Krieger, E. y McCulloch, M. (2018). Similar controls on calcification under ocean acidification across unrelated coral reef taxa. Global Change Biology. 24, 4857–4868.

Cook, S., Whittock, L., Wright, S. y Hallegraeff, G. (2011). Photosynthetic pigment and genetic differences between two Southern Ocean morphotypes of *Emiliania huxleyi* (Haptophyta). J. Phycol. 47, 615–626.

Cubillos, J. C., Wright, S. W., Nash, G., De Salas, M. F., Grif- fiths, B., Tilbrook, B., Poisson, A. y Hallegraeff, G. M. (2007). Calcification morphotypes of the coccolithophorid *Emiliania huxleyi* in the Southern Ocean: changes in 2001 to 2006 compared to historical data. Mar. Ecol.-Prog. Ser. 348, 47–54.

Cuevas, A., Tapia, F., Iriarte, J., González, H., Silva, N. y Vargas, C. (2019). Interplay between freshwater discharge and oceanic waters modulates phytoplankton size-structure in fjords and channel systems of the Chilean Patagonia. Progress in Oceanography. 173, 103–113.

Cyronak, T., Schulz, K. y Jokiel, P. (2016). The Omega myth: what really drives lower calcification rates in an acidifying ocean. ICES J. Mar. Sci. 73, 558–562.

D'Amario, B., Ziveri, P., Grelaud, M. y Oviedo, A. (2018). *Emiliania huxleyi* coccolith mass modulation by morphological changes and ecology in the Mediterranean Sea. PLoS ONE. 13, e0201161

Dávila, P., Figueroa, D. y Müller, E. (2002). Freshwater input into the coastal ocean and its relation with the salinity distribution off austral Chile (35–55°S). Continental Shelf Research. 22, 521–534.

de Vargas, C., Aubry, M.-P., Probert, I. y Young, J. (2007). Origin and evolution of coccolithophores: from coastal hunters to oceanic farmers, en "Evolution of primary producers in the sea", editado por P. Falkowski and A. Knoll, Academic Press.

de Vries, J., Monteiro, F., Wheeler, G., Poulton, A., Godrijan, J., Cerino, F., Malinverno, E., Langer, G. y Brownlee, C. (2021). Haplo-diplontic life cycle expands coccolithophore niche. Biogeosciences. 18, 1161–1184.

Dickson, A. G. y Millero, F. J. (1987). A comparison of the equilibrium constants for the dissociation of carbonic acid in seawater media. Deep Sea Research Part A. Oceanographic Research Papers. 34, 1733–1743.

Dickson, A. G., Sabine, C. L. y Christian, J. R. (2007). Guide to Best Practices for Ocean CO_2 Measurements. PICES Special Publication 3, pp. 191.

Dickson, A. G. (2010). Standards for ocean measurements. Oceanography. 23, 34–47.

Diner, R. E., Benner, I., Passow, U., Komada, T., Carpenter, E. J. y Stillman, J. H. (2015). Negative effects of ocean acidification on calcification vary within the coccolithophore genus *Calcidiscus*. Marine Biology. 162, 1287–1305.

Dlugokencky, E. y Tans, P. Trends in atmospheric carbon dioxide. National Oceanic and Atmospheric Administration, Earth System Research Laboratory (NOAA/ESRL), http://www.esrl.noaa.gov/gmd/ccgg/trends/global.html, last accessed 7 December 2020.

DOE. (1994). Handbook of methods for the analysis of the various parameters of the carbon dioxide system in sea water, editado por A. Dickson y C. Goyet, ORNL/CDIAC-74, available at: https://www.ncei.noaa.gov/access/ocean-carbon-data-system/oceans/handbook.html (last access: 29 August 2013).

Dolédec, S., Chessel, D. y Gimaret-Carpentier, C. (2000). Niche separation in community analysis: A new method. Ecology. 81, 2914–2927.

Doney, S., Fabry, V., Feely, R. y Kleypas, J. (2009). Ocean acidification: the other CO_2 problem, Annu. Rev. Mar. Sci. 1: 169–192.

Dore, J., Lukas, R., Sadler, D., Church, M. y Karl, D. (2009). Physical and biogeochemical modulation of ocean acidification in the central North Pacific. Proc. Natl. Acad. Sci. 106, 12235–12240.

Dray, S. y Dufour, A. (2007). The ade4 package: implementing the duality diagram for ecologists. J. Stat. Softw. 22, 1–20.

Dufrene, M. y Legendre, P. (1997). Species assemblages and indicator species: the need for a flexible asymmetrical approach. Ecol. Monogr. 67, 345–366.

Egge, E., Johannessen, T., Andersen, T., Eikrem, W., Bittner, L., Larsen, A., Sandaa, R. y Edvardsen, B. (2015). Seasonal diversity and dynamics of haptophytes in the Skagerrak, Norway, explored by high-throughput sequencing, Mol. Ecol., 24, 3026–3042.

Egger, M. (2011). Ocean acidification in the Humboldt current system. Master Thesis. Department of Environmental Sciences ETH Zurich.

Engel, A., Zondervan, I., Aerts, K., Beaufort, L., Benthien, A., Chou, L., Delille, B., Gattuso, J.-P., Harlay, J., Heemann, C., Hoffmann, L., Jacquet, S., Nejstgaard, J., Pizay, M.-D., Rochelle-newall, E., Schneider, U., Terbrueggen, A. y Riebesell, U. (2005). Testing the direct effect of CO_2 concentration on a bloom of the coccolithophorid *Emiliania huxleyi* in mesocosm experiments. Limnol. Oceanogr. 50, 493–507.

Erga, S. (1989). Ecological studies on the phytoplankton of Boknafjorden, western Norway. 1. The effect of water exchange processes and environmental factors on temporal and vertical variability of biomass. Sarsia. 74, 161–176.

Fabricius, K., De'ath, G., Noonan, S. y Uthicke, S. (2014). Ecological effects of ocean acidification and habitat complexity on reef-associated macroinvertebrate communities. Proc. R. Soc. B. 281, 20132479.

Fabry, V. J., Seibel, B. A., Feely, R. A. y Orr, J. C. (2008). Impacts of ocean acidification on marine fauna and ecosystem processes. ICES Journal of Marine Science. 65, 414–432.

Falkowski, P., Katz, M., Knoll, A., Quigg, A., Raven, J., Schofield, O. y Taylor, F. (2004). The evolution of modern eukaryotic phytoplankton. Science. 305, 354–360.

Feely, R., Doney, S. y Cooley, S. (2009). Ocean acidification: Present conditions and future changes in a high-CO_2 world. Oceanography. 22, 36–47.

Fernández, E., Marañón, E., Harbour, D., Kristiansen, S. y Heimdal, B. (1996). Patterns of carbon and nitrogen uptake during blooms of *Emiliania huxleyi* in two Norwegian fjords. J. Plankton Res. 18, 2349–2366.

Filatov, D. (2019). Extreme Lewontin's paradox in ubiquitous marine phytoplankton species. Mol. Biol. Evol. 36, 4–14.

Findlay, H., Wood, H., Kendall, M., Spicer, J., Twitchett, R. y Widdicombe, S. (2009). Calcification, a physiological process to be considered in the context of the whole organism. Biogeosciences Discussions. 6, 2267–2284.

Franco, A., Gruber, N., Frölicher, T. y Artman, L. (2018). Contrasting impact of future CO_2 emission scenarios on the extent of $CaCO_3$ mineral undersaturation in the Humboldt Current System. J. Geophys. Res. Oceans. 123, 2018–2036.

Frankignoulle, M., Canon, C. y Gattuso, J-P. (1994). Marine calcification as a source of carbon dioxide: Positive feedback of increasing atmospheric CO_2. Limnol. Oceanogr. 39, 458–462.

Friederich, G. E., Ledesma, J., Ulloa, O. y Chavez, F. P. (2008). Air–sea carbon dioxide fluxes in the coastal southeastern tropical Pacific. Prog. Oceanogr. 79, 156–166.

Friedinger, P. y Winter, A. (1987). Distribution of modern coccolithophore assemblages in the southwest Indian Ocean off southern Africa. Journal of Micropalaeontology. 6, 49–56.

Gafar, N., Eyre, B. y Schulz, K. (2019). Particulate inorganic to organic carbon production as a predictor for coccolithophorid sensitivity to ongoing ocean acidification. Limnology and Oceanography Letters. 4, 62–70.

Gaitán-Espitia, J. D., Villanueva, P. A., Lopez, J., Torres, R., Navarro, J. M. y Bacigalupe, L. D. (2017). Spatio-temporal environmental variation mediates geographical differences in phenotypic responses to ocean acidification. Biol. Letters. 13, 20160865.

Giraudeau, J., Monteiro, P. y Nikodemus, K. (1993). Distribution and malformation of living coccolithophores in the northern Benguela upwelling system off Namibia. Marine Micropaleontology. 22, 93–110.

Giraudeau, J. y Beaufort, L. (2007). Coccolithophores: from extant populations to fossil assemblages, en “Developments in Marine Geology”, editado por C. Hillaire-Marcel y A. De Vernal, Elsevier Science.

González, H., Castro, L., Daneri, G., Iriarte, J., Silva, N., Tapia, F., Teca, E. y Vargas, C. (2013). Land-ocean gradient in haline stratification and its effects on plankton dynamics and trophic carbon fluxes in Chilean Patagonian fjords (47–50ºS). Progress in Oceanography. 119, 32–47.

Gran-Stadniczeñko, S., Šupraha, L., Egge, E. y Edvardsen, B. (2017). Haptophyte diversity and vertical distribution explored by 18S and 28S ribosomal RNA gene metabarcoding and scanning electron microscopy. J. Eukaryot. Microbiol. 64, 514–532.

Hagino, K., Okada, H. y Matsuoka, H. (2000). Spatial dynamics of coccolithophore assemblages in the Equatorial Western-Central Pacific Ocean. Marine Micropaleontology. 39, 53–72.

Hagino, K. y Okada, H. (2004). Floral response of coccolithophores to progressive oligotrophication in the south equatorial current, Pacific Ocean, en "Global Environmental Change in the Ocean and on Land", editado por M. Shiyomi, M. *et al*., TERRAPUB.

Hagino, K. y Okada, H. (2006). Intra- and infra-specific morphological variation in selected coccolithophore species in the equatorial and subequatorial Pacific Ocean. Marine Micropaleontology. 58, 184–206.

Hagino, K., Bendif, E. M., Young, J. R., Kogame, K., Probert, I., Takano, Y., Horiguchi, T., de Vargas, C. y Okada, H. (2011). New evidence for morphological and genetic variation in the cosmopolitan coccolithophore *Emiliania huxleyi* (Prymnesiophyceae) from the cox1b-atp4 genes. J. Phycol. 47, 1164–1176.

Harris, R. (1994). Zooplankton grazing on the coccolithophore *Emiliania huxleyi* and its role in inorganic carbon flux. Marine Biology. 119, 431–439.

Harris, D., Horwáth, W. R. y van Kessel, C. (2001). Acid fumigation of soils to remove carbonates prior to total organic carbon or carbon-13 isotopic analysis. Soil Sci. Soc. Am. J. 65, 1853– 1856.

Haunost, M., Riebesell, U. y Bach, L. (2020). The calcium carbonate shell of *Emiliania huxleyi* provides limited protection against viral infection. Frontiers in Marine Science. 7, 530757.

Henderiks, J., Winter, A., Elbrächter, M., Feistel, R., Van Der Plas, A., Nausch, G. y Barlow, R. (2012). Environmental controls on *Emiliania huxleyi* morphotypes in the Benguela coastal upwelling system (SE Atlantic). Mar. Ecol. Prog. Ser. 448, 51–66.

Heraldsson, C., Anderson, L. G., Hassellöv, M., Hulth, S. y Olsson, K. (1997). Rapid, high-precision potentiometric titration of alkalinity in ocean and sediment pore waters. Deep-Sea Res. Pt. I. 44, 2031–2044.

Hernández, T., Bacher, C., Soudant, D., Belin, C. y Barillé, L. (2015). Assessing phytoplankton realized niches using a French national phytoplankton monitoring network. Estuarine, Coastal and Shelf Science. 159, 15–27.

Hillebrand, H., Dürselen, C., Kirschtel, D., Pollingher, U. y Zohary, T. (1999). Biovolume calculation for pelagic and benthic microalgae. J. Phycol., 35(2), 403–424.

Hofmann, M. y Schellnhuber, H.-J. (2009). Oceanic acidification affects marine carbon pump and triggers extended marine oxygen holes, P. Natl. Acad. Sci. USA. 106, 3017–3022.

Hofmann, G. E., Barry, J. P., Edmunds, P. J., Gates, R. D., Hutchins, D. A., Klinger, T. y Sewell, M. A. (2010). The Effect of Ocean Acidification on Calcifying Organisms in Marine Ecosystems: An Organism-to-Ecosystem Perspective. Annu. Rev. Ecol. Evol. Syst. 41, 127–147.

Hofmann, G. E., Smith, J. E., Johnson, K. S., Send, U., Levin, L. A., Micheli, F., Paytan, A., Price, N. N., Peterson, B., Takeshita, Y., Matson, P. G., de Crook, E., Kroeker, K. J., Gambi, M. C., Rivest, E. B., Frieder, C. A., Yu, P. C. y Martz, T. R. (2011). High-frequency dynamics of ocean pH: A multi-ecosystem comparison. PLoS One. 6, e28983.

Holligan, P., Fernández, E., Aiken, J., Balch, W., Boyd, P., Burkill, P., Finch, M., Groom, S., Malin, G., Muller, K., Purdie, D., Robinson, C., Trees, Ch., Turner, S. y van der Wal, P. (1993). A biogeochemical study of the coccolithophore, *Emiliania huxleyi*, in the North Atlantic. Global Biogeochem. Cycles. 7, 879–900.

Hopkins, J., Henson, S., Painter, S., Tyrrell, T. y Poulton, A. (2015). Phenological characteristics of global coccolithophore blooms. Global Biogeochem. Cycles. 29, 239–253.

Hopkins, J., Henson, S., Poulton, A. y Balch, W. (2019). Regional characteristics of the temporal variability in the global particulate inorganic carbon inventory. Global Biogeochem. Cycles. 33, 1328–1338.

Iglesias-Rodríguez, M. D., Brown, C. W., Doney, S. C., Kleypas, J., Kolber, D., Kolber, Z., Hayes, P. K. y Falkowski, P. G. (2002). Representing key phytoplankton functional groups in ocean carbon cycle models: Coccolithophorids. Global Biogeochem. Cycles. 16, 1–20.

Iglesias-Rodriguez, M. D., Halloran, P. R., Rickaby, R. E. M., Hall, I. R., Colmenero-Hidalgo, E., Gittins, J. R., Green, D. R. H., Tyrrell, T., Gibbs, S. J., von Dassow, P., Rehm, E., Armbrust, E. V. y Boessenkool, K. P. (2008). Phytoplankton calcification in a high-CO_2 world. Science. 320, 336–340.

IPCC. (2018). Global Warming of 1.5°C. An IPCC Special Report on the impacts of global warming of 1.5°C above pre-industrial levels and related global greenhouse gas emission pathways, in the context of strengthening the global response to the threat of climate change, sustainable development, and efforts to eradicate poverty, editado por V. Masson-Delmotte, P. Zhai, H.-O. Pörtner, D. Roberts, J. Skea, P.R. Shukla, A. Pirani, W. Moufouma-Okia, C. Péan, R. Pidcock, S. Connors, J.B.R. Matthews, Y. Chen, X. Zhou, M.I. Gomis, E. Lonnoy, T. Maycock, M. Tignor, y T. Waterfield, IPCC, pp. 630.

Jin, P., Ding, J., Xing, T., Riebesell, U. y Gao, K. (2017). High levels of solar radiation offset impacts of ocean acidification on calcifying and non-calcifying strains of *Emiliania huxleyi*. Mar. Ecol. Prog. Ser. 568, 47–58.

Johns, Ch., Grubb, A., Nissimov, J., Natale, F., Knapp, V., Mui, A., Fredricks, H., Van Mooy, B. y Bidle, K. (2019). The mutual interplay between calcification and coccolithovirus infection. Environmental microbiology. 21(6), 1896–1915.

Johnsen, S. y Bollmann, J. (2020). Coccolith mass and morphology of different *Emiliania huxleyi* morphotypes: A critical examination using Canary Islands material. PLoS ONE. 15, e0230569.

Jones, E., Chierici, M., Skjelvan, I., Norli, M., Børsheim, K., Lødemel, H., Sørensen, K., King, A., Lauvset, S., Jackson, K., de Lange, T., Johannsessen, T. y Mourgues, C. (2019). Monitoring ocean acidification in Norwegian seas in 2018, Rapport, Miljødirektoratet, M-1417|2019.

Kegel, J., John, U., Valentin, K. y Frickenhaus, S. (2013). Genome variations associated with viral susceptibility and calcification in *Emiliania huxleyi*. PLoS ONE. 8, e80684.

Keller, M. D., Selvin, R. C., Claus, W. y Guillard, R. R. (1987). Media for the culture of oceanic ultraphytoplankton. J. Phycol. 23, 633–638.

Klaas, C. y Archer, D. (2002). Association of sinking organic matter with various types of mineral ballast in the deep sea: Implications for the rain ratio. Global Biogeochem. Cycles. 16, 1116.

Kristiansen, S., Thingstad, F., van der Wal, P., Farbrot, T. y Skjoldal, E. (1994). An *Emiliania huxleyi* dominated subsurface bloom in Samnangerfjorden, western Norway. Importance of hydrography and nutrients. Sarsia. 79, 357–368.

Krueger-Hadfield, S. A., Balestreri, C., Schroeder, J., Highfield, A., Helaouët, P., Allum, J., Moate, R., Lohbeck, K. T., Miller, P. I., Riebesell, U., Reusch, T. B. H., Rickaby, R. E. M., Young, J., Hallegraeff, G., Brownlee, C. y Schroeder, D. C. (2014). Genotyping an *Emiliania huxleyi* (prymnesiophyceae) bloom event in the North Sea reveals evidence of asexual reproduction. Biogeosciences. 11, 5215–5234.

Langer, G., Nehrke, G., Probert, I., Ly, J. y Ziveri, P. (2009). Strain-specific responses of *Emiliania huxleyi* to changing seawater carbonate chemistry. Biogeosciences. 6, 2637–2646.

Langer, G., Probert, I., Nehrke, G. y Ziveri, P. (2011). The morphological response of *Emiliania huxleyi* to seawater carbonate chemistry changes: an inter-strain comparison. J. Nannoplankton Res. 32, 29–34.

Leblanc, K., Quéguiner, B., Diaz, F., Cornet, V., Michel-Rodriguez, M., Durrieu de Madron, X., Bowler, C., Malviya, S., Thyssen, M., Grégori, G., Rembauville, M., Grosso, O., Poulain, J., de Vargas, C., Pujo-Pay, M. y Conan, P. (2018). Nanoplanktonic diatoms are globally overlooked but play a role in spring blooms and carbon export. Nature communications. 9, 953.

Lee, R. B. Y., Mavridou, D. A. I., Papadakos, G., McClelland, H. L. O. y Rickaby, R. E. M. (2016). The uronic acid content of coccolith-associated polysaccharides provides insight into coccolithogenesis and past climate. Nat. Commun. 7, 13144.

Lefebvre, S. C., Benner, I., Stillman, J. H., Parker, A. E., Drake, M. K., Rossignol, P. E., Okimura, K. M., Komada, T. y Carpenter, E. J. (2012). Nitrogen source and pCO_2 synergistically affect carbon allocation, growth and morphology of the coccolithophore *Emiliania huxleyi*: Potential implications of ocean acidification for the carbon cycle. Glob. Change Biol. 18, 493– 503.

Legendre, P. y Legendre, L. (2012). Numerical Ecology. 3rd English edition. Elsevier Science, pp. 1006.

Le Quéré, C., Andrew, R. M., Friedlingstein, P., Sitch, S., Hauck, J., Pongratz, J., Pickers, P. A., Korsbakken, J. I., Peters, G. P., Canadell, J. G., Arneth, A., Arora, V. K., Barbero, L., Bastos, A., Bopp, L., Chevallier, F., Chini, L. P., Ciais, P., Doney, S. C., Gkritzalis, T., Goll, D. S., Harris, I., Haverd, V., Hoffman, F. M., Hoppema, M., Houghton, R. A., Hurtt, G., Ilyina, T., Jain, A. K., Johannessen, T., Jones, C. D., Kato, E., Keeling, R. F., Goldewijk, K. K., Landschützer, P., Lefèvre, N., Lienert, S., Liu, Z., Lombardozzi, D., Metzl, N., Munro, D. R., Nabel, J. E. M. S., Nakaoka, S., Neill, C., Olsen, A., Ono, T., Patra, P., Peregon, A., Peters, W., Peylin, P., Pfeil, B., Pierrot, D., Poulter, B., Rehder, G., Resplandy, L., Robertson, E., Rocher, M., Rödenbeck, C., Schuster, U., Schwinger, J., Séférian, R., Skjelvan, I., Steinhoff, T., Sutton, A., Tans, P. P., Tian, H., Tilbrook, B., Tubiello, F. N., van der Laan-Luijkx, I. T., van der Werf, G. R., Viovy, N., Walker, A. P., Wiltshire, A. J., Wright, R., Zaehle, S. y Zheng, B. (2018). Global Carbon Budget 2018. Earth System Science Data. 10, 2141–2194.

León, P., Walsham, P., Bresnan, E., Hartman, S., Hughes, S., Mackenzie, K. y Webster, L. (2018). Seasonal variability of the carbonate system and coccolithophore *Emiliania huxleyi* at a Scottish Coastal Observatory monitoring site. Estuarine, Coastal and Shelf Science. 202, 302–314.

Litchman, E., de Tezanos Pinto, P., Edwards, K. F., Klausmeier, C. A., Kremer, C. T. y Thomas, M. K. (2015). Global biogeochemical impacts of phytoplankton: A trait-based perspective. J. Ecol. 103, 1384–1396.

Lohbeck, K. T., Riebesell, U. y Reusch, T. B. H. (2012). Adaptive evolution of a key phytoplankton species to ocean acidification. Nat. Geosci. 5, 917–917.

Lorrain, A., Savoye, N., Chauvaud, L., Paulet, Y.-M. y Naulet, N. (2003). Decarbonation and preservation method for the analysis of organic C and N contents and stable isotope ratios of low-carbonate suspended particulate material. Anal. Chim. Acta. 491, 125–133.

Malviya, S., Scalco, E., Audic, S., Vincent, F., Veluchamy, A., Poulain, J., Wincker, P., Iudicone, D., de Vargas, C., Bittner, L., Zingone, A. y Bowler, C. (2016). Insights into global diatom distribution and diversity in the world's ocean. P. Natl. Acad. Sci. USA. 111, 1516–1525.

Margalef, R. (1978). Life-forms of phytoplankton as survival alternatives in an unstable environment. Oceanologica Acta. 1, 493–509.

Martínez-Botí, M., Foster, G., Chalk, T., Rohling, E., Sexton, P., Lunt, D., Pancost, R., Badger, M. y Schmidt, D. (2015). Plio-Pleistocene climate sensitivity evaluated using high-resolution CO_2 records. Nature. 518, 49–54.

Mayers, K., Poulton, A., Bidle, K., Thamatrakoln, K., Schieler, B., Giering, S., Wells, S., Tarran, G., Mayor, D., Johnson, M., Riebesell, U., Larsen, A., Vardi, A. y Harvey, E. (2020). The possession of coccoliths fails to deter microzooplankton grazers. Frontiers in Marine Science. 7, 569896.

McDonald, M. J., Rice, D. P. y Desai, M. M. (2016). Sex speeds adaptation by altering the dynamics of molecular evolution. Nature. 531, 233–236.

McIntyre, A., Bé, A. y Roche, M. (1970). Modern Pacific coccolithophorida: a paleontological thermometer. Trans. N. Y. Acad. Sci. 32, 720–731.

Mehrbach, C., Culberson, C., Hawley, J. y Pytkowicx, R. (1973). Measurement of the apparent dissociation constants of carbonic acid in seawater at atmospheric pressure. Limnol. Oceanogr. 18, 897–907.

Mella-Flores, D., Machon, J., Contreras-Porcia, L., Mesa-Campbell, S. y von Dassow, P. (2018). Differential responses of *Emiliania huxleyi* (Haptophyta) strains to copper excess. Cryptogamie, Algologie. 39, 481–509.

Menden-Deuer, S. y Lessard, E. (2000). Carbon to volume relationships for dinoflagellates, diatoms, and other protist plankton. Limnol. Oceanogr. 45, 569–579.

Menschel, E., González, H. y Giesecke, R. (2016). Coastal-oceanic distribution gradient of coccolithophores and their role in the carbonate flux of the upwelling system off Concepción, Chile (36°S). J. Plankton Res. 38, 798–817.

Meyer, J. y Riebesell, U. (2015). Reviews and Syntheses: Responses of coccolithophores to ocean acidification: a meta-analysis. Biogeosciences. 12, 1671–1682.

Mitchell-Innes, B. y Winter. A. (1987). Coccolithophores: a major phytoplankton component in mature upwelled waters off the Cape Peninsula, South Africa in March, 1983. Marine Biology. 95, 25–30.

Monteiro, F. M., Bach, L. T., Brownlee, C., Bown, P., Rickaby, R. E. M., Poulton, A. J., Tyrrell, T., Beaufort, L., Dutkiewicz, S., Gibbs, S., Gutowska, M. A., Lee, R., Riebesell, U., Young, J. y Ridgwell, A. (2016). Why marine phytoplankton calcify. Sci. Adv. 2, e1501822.

Morel, A., Gentili, B., Claustre, H., Babin, M., Bricaud, A., Ras, J. y Tièche, F. (2007). Optical properties of the “clearest” natural waters. Limnology and Oceanography. 52, 217–229.

Müller, M. N., Trull, T. W. y Hallegraeff, G. M. (2015a). Differing responses of three Southern Ocean *Emiliania huxleyi* ecotypes to changing seawater carbonate chemistry, Mar. Ecol. Prog. Ser. 531, 81–90.

Müller, M. N., Barcelos e Ramos, J., Schulz, K. G., Riebesell, U., Kaz´mierczak, J., Gallo, F., Mackinder, L., Li, Y., Nesterenko, P. N., Trull, T. W. y Hallegraeff, G. M. (2015b). Phytoplankton calcification as an effective mechanism to alleviate cellular calcium poisoning. Biogeosciences. 12, 6493–6501.

Müller, M. N., Trull, T. W. y Hallegraeff, G. M. (2017). Independence of nutrient limitation and carbon dioxide impacts on the Southern Ocean coccolithophore *Emiliania huxleyi*. ISME J. 11, 1777– 1787.

Müller, M. N. (2019). On the genesis and function of coccolithophore calcification. Frontiers in Marine Science. 6, 49

NASA Goddard Space Flight Center, Ocean Ecology Laboratory, Ocean Biology Processing Group. Moderate-resolution Imaging Spectroradiometer (MODIS) Aqua mapped SST monthly climatology Data; NASA OB.DAAC, Greenbelt, MD, USA. https://oceandata.sci.gsfc.nasa.gov/MODIS-Aqua/ (last access: 14 December 2020).

Nejstgaard, J., Gismervik, I. y Solberg, P. (1997). Feeding and reproduction by *Calanus finmarchicus*, and microzooplankton grazing during mesocosm blooms of diatoms and the coccolithophore *Emiliania huxleyi*. Mar. Ecol. Prog. Ser. 147, 197–217.

Nielsdóttir, M., Moore, Ch., Sanders, R., Hinz, D. y Achterberg, E. (2009). Iron limitation of the postbloom phytoplankton communities in the Iceland Basin. Global Biogeochem. Cycles. 23, GB3001.

O’Brien, C., Peloquin, J., Vogt, M., Heinle, M., Gruber, N., Ajani, P., Andruleit, H., Arístegui, J., Beaufort, L., Estrada, M., Karentz, D., Kopczynska, E., Lee, R., Poulton, A., Pritchard, T. y Widdicombe, C. (2013). Global marine plankton functional type biomass distributions: coccolithophores. Earth Syst. Sci. Data. 5, 259–276.

Okada, H. y Honjo, S. (1973). The distribution of oceanic coccolithophorids in the Pacific. Deep-Sea Research. 20, 355–374.

Okada, H. y McIntyre, A. (1979). Seasonal distribution of modern coccolithophores in the western North Atlantic Ocean. Marine Biology. 54, 319–328.

Oksanen, J., Blanchet, F., Kindt, R., Legendre, P., Minchin, P., O'Hara, R., Simpson, G., Solymos, P., Stevens, M. y Wagner, H. (2007). Vegan: Community Ecology Package. R package version 2.3-1. Available at: https://cran.r-project.org/web/packages/vegan/index.html (last accessed 14 December 2020).

Olson, M. B., Wuori, T. A., Love, B. A. y Strom, S. L. (2017). Ocean acidification effects on haploid and diploid *Emiliania huxleyi* strains: Why changes in cell size matter. J. Exp. Mar. Biol. Ecol. 488, 72–82.

Orr, J. C., Fabry, V. J., Aumont, O., Bopp, L., Doney, S. C., Feely, R. A., Gnanadesikan, A., Gruber, N., Ishida, A., Joos, F., Key, R. M., Lindsay, K., Maier-Reimer, E., Matear, R., Monfray, P., Mouchet, A., Najjar, R. G., Plattner, G.-K., Rodgers, K. B., Sabine, C. L., Sarmiento, J. L., Schlitzer, R., Slater, R. D., Totterdell, I. J., Weirig, M.-F., Yamanaka, Y. y Yool, A. (2005). Anthropogenic ocean acidification over the twenty- first century and its impact on calcifying organisms. Nature. 437, 681–686.

Paasche, E. y Kristiansen, S. (1982). Ammonium regeneration by microzooplankton in the Oslofjord. Mar. Biol. 69, 55–63.

Paasche, E. (2002). A review of the coccolithophorid *Emiliania huxleyi* (Prymnesiophyceae) with particular reference to growth, coccolith formation, and calcification-photosynthesis interactions. Phycologia. 40, 503–529.

Padilla-Gamiño, J. L., Gaitán-Espitia, J. D., Kelly, M. W. y Hofmann, G. E. (2016). Physiological plasticity and local adaptation to elevated pCO_2 in calcareous algae?: an ontogenetic and geographic approach. Evol. Appl. 9, 1043–1053.

Paredes, M., Montecino, V., Anic, V., Egaña, M. y Guzmán, L. (2014). Diatoms and dinoflagellates macroscopic regularities shaped by intrinsic physical forcing variability in Patagonian and Fuegian fjords and channels (48º–56ºS). Progress in Oceanography. 129, 85–97.

Passow, U. y Carlson, C. (2012). The biological pump in a high CO_2 world. Mar. Ecol. Prog. Ser. 470, 249–271.

Pierrot, D., Lewis, E. y Wallace, D. (2006). MS Excel Program Developed for CO2 System Calculations. ORNL/CDIAC-105a. Carbon Dioxide Information Analysis Center, Oak Ridge National Laboratory, U.S. Department of Energy, Oak Ridge, Tennessee.

Poulton, A. J., Young, J. R., Bates, N. R. y Balch, W. M. (2011). Biometry of detached *Emiliania huxleyi* coccoliths along the Patagonian Shelf. Mar. Ecol. Prog. Ser. 443, 1–17.

Poulton, A. J., Painter, S., Young, J., Bates, N., Bowler, B., Drapeau, D., Lyczsckowski, E. y Balch, W. (2013). The 2008 *Emiliania huxleyi* bloom along the Patagonian Shelf: Ecology, biogeochemistry, and cellular calcification. Global Biogeochem. Cycles. 27, 1023–1033.

Prentice, C., Farquhar, G., Fasham, M., Goulden, J., Heimann, M., Jaramillo, V., Kheshigi, H., Le Quere, C., Scholes, R. y Wallace, D. (2001). The carbon cycle and atmospheric carbon dioxide, en "Climate Change 2001: The Scientific Basis (Contribution of Working Group I to the Third Assessment Report of the Intergovernmental Panel on Climate Change)", editado por J. Houghton, Y. Ding, D.J. Griggs, M. Noguer, P.J. van der Linden, X. Dai, K. Maskell, y C.A. Johnson, Cambridge University Press. Cambridge.

R Core Team. (2019). R: A language and environment for statistical computing. R Foundation for Statistical Computing, Vienna, Austria. URL http://www.R-project.org/.

Read, B., Kegel, J., Klute, M., Kuo, A., Lefebvre, S., Maumus, F., Mayer, Ch., Miller, J., Monier, A., Salamov, A., Young, J., Aguilar, M., Claverie, J.-M-, Frickenhaus, S., Gonzalez, K., Herman, E., Lin, Y.-Ch., Napier, J., Ogata, H., Sarno, A., Shmutz, J., Schroeder, D., de Vargas, C., Verret, F., von Dassow, P., Valentin, K., Van de Peer, Y., Wheeler, G., *Emiliania huxleyi* Annotation Consortium, Dacks, J., Delwiche, Ch., Dyhrman, S., Glöckner, G., John, U., Richards, T., Worden, A., Zhang, X. y Grigoriev, I. (2013) Pan genome of the phytoplankton *Emiliania huxleyi* underpins its global distribution. Nature. 499, 209–213.

Richier, S., Fiorini, S., Kerros, M. E., von Dassow, P. y Gattuso, J-P. (2011). Response of the calcifying coccolithophore *Emiliania huxleyi* to low pH/high pCO_2: From physiology to molecular level. Mar. Biol. 158, 551–560.

Riebesell, U., Zondervan, I., Rost, B., Tortell, P. D., Zeebe, R. E. y Morel, F. M. (2000). Reduced calcification of marine plankton in response to increased atmospheric CO_2. Nature. 407, 364–367.

Riebesell, U. y Gattuso, J-P. (2015). Lessons learned from ocean acidification research. Nature Climate Change. 5, 12–14.

Riebesell, U., Bach, L. T., Bellerby, R. G. J., Monsalve, J. R. B., Boxhammer, T., Czerny, J., Larsen, A., Ludwig, A. y Schulz, K. G. (2017). Competitive fitness of a predominant pelagic calcifier impaired by ocean acidification. Nature Geosciences. 10, 19–23.

Rigual-Hernández, A., Trull, T., Flores, J., Nodder, S., Eriksen, R., Davies, D., Hallegraeff, G., Sierro, F., Patil, S., Cortina, A., Ballegeer, A., Northcote, L., Abrantes, f. y Rufino, M. (2020). Full annual monitoring of Subantarctic *Emiliania huxleyi* populations reveals highly calcified morphotypes in high-CO_2 winter conditions. Scientific Reports. 10: 2594.

Ripple, W., Wolf, C., Newsome, T., Barnard, P., Moomaw, W. (2020). World Scientists' Warning of a Climate Emergency. BioScience. 70, 8–12.

Rivero-Calle, S., Gnanadesikan, A., Del Castillo, C., Balch, W. y Guikema, S. (2015). Multidecadal increase in North Atlantic coccolithophores and the potential role of rising CO_2. Science. 350, 1533–1537.

Rokitta, S. y Rost, B. (2012). Effects of CO_2 and their modulation by light in the life-cycle stages of the coccolithophore *Emiliania huxleyi*. Limnol. Oceanogr. 57, 607–618.

Rokitta, S., von Dassow, P., Rost, B. y John, U. (2014). *Emiliania huxleyi* endures N-limitation with an efficient metabolic budgeting and effective ATP synthesis. BMC Genomics. 15, 1051.

Rokitta, S., von Dassow, P., Rost, B. y John, U. (2016). P- and N-depletion trigger similar cellular responses to promote senescence in eukaryotic phytoplankton. Frontiers in Marine Science. 3, 109.

Rosas-Navarro, A., Langer, G. y Ziveri, P. (2016). Temperature affects the morphology and calcification of *Emiliania huxleyi* strains. Biogeosciences. 13, 2913–2926.

Rost, B. y Riebesell, U. (2004). Coccolithophores and the biological pump: responses to environmental changes, en "Coccolithophores", editado por H. Thierstein y J. Young, Springer.

Saavedra-Pellitero, M., Baumann, K., Flores, J. y Gersonde, R. (2014). Biogeographic distribution of living coccolithophores in the Pacific sector of the Southern Ocean. Marine Micropaleontology. 109, 1–20.

Saavedra-Pellitero, M., Baumann, K., Fuertes, M., Schulz, H., Marcon, Y., Vollmar, N., Flores, J. y Lamy, F. (2019). Calcification and latitudinal distribution of extant coccolithophores across the Drake Passage during late austral summer 2016. Biogeosciences. 16, 3679–3702.

Sabine, C. L., Feely, R. A., Gruber, N., Key, R. M., Lee, K., Bullister, J. L., Wanninkhof, R., Wong., C. S., Wallace, D. W. R., Tilbrook, B., Millero, F. J., Peng, T.-H., Kozyr, A., Ono, T. y Rios, A. F. (2004). The Oceanic Sink for anthropogenic CO_2. Science. 305, 367–371.

Samtleben, C., Schäfer, P., Andruleit, H., Baumann, A., Baumann, K., Kohly, A., Matthiessen, J., Schröder-Ritzrau, A. y 'Synpal' Working Group. (1995). Plankton in the Norwegian-Greenland Sea: from living communities to sediment assemblages - an actualistic approach. Geol. Rundsch. 84, 108–136.

Sanders, R., Morris, P. J., Poulton, A. J., Stinchcombe, M. C., Charalampopoulou, A., Lucas, M. I. y Thomalla, S. J. (2010). Does a ballast effect occur in the surface ocean? Geophys. Res. Lett. 37, 1–5.

Sarmiento, J., Dunne, J., Gnanadesikan, A., Key, R., Matsumoto, K. y Slater, R. (2002). A new estimate of the $CaCO_3$ to organic carbon export ratio. Global Biogeochem. Cycles. 16, 1107.

Schlitzer, R. (2018). Ocean Data View, https://odv.awi.de/.

Schlüter, L., Lohbeck, K. T., Gröger, J. P., Riebesell, U. y Reusch, T. B. H. (2016). Long-term dynamics of adaptive evolution in a globally important phytoplankton species to ocean acidification. Sci. Adv. 2, e1501660.

Sciandra, A., Harlay, J., Lefèvre, D., Lemée, R., Rimmelin, P., Denis, M. y Gattuso, J-P. (2003). Response of coccolithophorid *Emiliania huxleyi* to elevated partial pressure of CO_2 under nitrogen limitation. Mar. Ecol. Prog. Ser. 261, 111–122.

Shi, D., Xu, Y. y Morel, F. M. M. (2009). Effects of the pH/pCO_2 control method on medium chemistry and phytoplankton growth. Biogeosciences. 6, 1199–1207.

Sicko-Goad, L., Schelske, C. y Stoermer, E. (1984). Estimation of intracellular carbon and silica content of diatoms from natural assemblages using morphometric techniques. Limnol. Oceanogr. 29, 1170–1178.

Sievers, H. y Silva, N. (2008). Water masses and circulation in austral Chilean channels and fjords, en "Progress in the oceanographic knowledge of Chilean interior waters, from Puerto Montt to Cape Horn", editado por N. Silva y S. Palma, Comité Oceanográfico Nacional.

Sigman, D. y Boyle, E. (2000). Glacial/interglacial variations in atmospheric carbon dioxide. Nature. 407, 859–869.

Silva, N., Rojas, N. y Fedele, A. (2009). Water masses in the Humboldt Current System: Properties, distribution, and the nitrate deficit as a chemical water mass tracer for Equatorial Subsurface Water off Chile. Deep-Sea Research II. 56, 1004–1020.

Smith, H. E. K., Tyrrell, T., Charalampopoulou, A., Dumousseaud, C., Legge, O. J., Birchenough, S., Pettit, L. R., Garley, R., Hartman, S. E., Hartman, M. C., Sagoo, N., Daniels, C. J., Achterberg, E. P. y Hydes, D. J. (2012). Predominance of heavily calcified coccolithophores at low $CaCO_3$ saturation during winter in the Bay of Biscay. P. Natl. Acad. Sci. USA. 109, 8845–8849.

Smith, H., Poulton, A., Garley, R., Hopkins, J., Lubelczyk, L., Drapeau, D., Rauschenberg, S., Twining, B., Bates, N. y Balch, W. (2017). The influence of environmental variability on the biogeography of coccolithophores and diatoms in the Great Calcite Belt. Biogeosciences. 14, 4905–4925.

Smith, S. V. (2013). Parsing the oceanic calcium carbonate cycle: a net atmospheric carbon dioxide source, or a sink?, L&O e-Books. Association for the Sciences of Limnology and Oceanography, pp. 42.

Takahashi, T., Sutherland, S., Chipman, D., Goddard, J., Ho, Ch., Newberger, T., Sweeney, C. y Munro, D. (2014). Climatological distributions of pH, pCO_2, total CO_2, alkalinity, and $CaCO_3$ saturation in the global surface ocean, and temporal changes at selected locations. Marine Chemistry. 164, 95–125.

Taylor, A., Brownlee, C. y Wheeler, G. (2017). Coccolithophore cell biology: Chalking up progress. Annu. Rev. Mar. Sci. 9, 283–310.

Thiel, M., Macaya, E. C., Acuña, E., Arntz, W. E., Bastias, H., Brokordt, K., Camus, P. A., Castilla, J. C., Castro, L. R., Cortés, M., Dumont, C. P., Escribano, R., Fernández, M., Gajardo, J. A., Gaymer, C. F., Gomez, I., González, A. E., González, H. E., Haye, P. A., Illanes, J. E., Iriarte, J. L., Lancelloti, D. A., Luna-Jorquera, G., Luxoro, C., Manriquez, P. H., Marín, V., Muñoz, P., Navarretes, S. A., Perez, E., Poulin, E., Sellanes, J., Sepúlveda, H. H., Stotz, W., Tala, F., Thomas, A., Vargas, C. A., Vasquez, J. A. y Vega, J. M. A. (2007). The Humboldt current system of northern and central Chile Oceanographic processes, ecological interactions and socioeconomic feedback. Oceanogr. Mar. Biol. 45, 195–344.

Torres, R., Turner, D. R., Silva, N. y Rutllant, J. (1999). High short-term variability of CO_2 fluxes during an upwelling event off the Chilean coast at 30º S. Deep Sea Res. Pt. I. 46, 1161–1179.

Torres, R., Pantoja, S., Harada, N., González, H., Daneri, G., Frangopulos, M., Rutllant, J., Duarte, C., Rúiz-Halpern, S., Mayol, E. y Fukasawa, M. (2011). Air-sea CO_2 fluxes along the coast of Chile: From CO_2 outgassing in central northern upwelling waters to CO_2 uptake in southern Patagonian fjords. J. Geophys. Res. 116, C09006.

Torres, R., Manriquez, P. H., Duarte, C., Navarro, J. M., Lagos, N. A., Vargas, C. A. y Lardies, M. A. (2013). Evaluation of a semi-automatic system for long-term seawater carbonate chemistry manipulation. Rev. Chil. Hist. Nat. 86, 443–451.

Torres, R., Silva, N., Reid, B. y Frangopulos, M. (2014). Silicic acid enrichment of subantarctic surface water from continental inputs along the Patagonian archipelago interior sea (41–56°S). Progress in Oceanography. 129, 50–61.

Torres, R., Reid, B., Frangopulos, M., Alarcón E., Márquez M., Haussermann, V., Försterra, G., Pizarro, G., Iriarte, J. y Gonzalez, H. (2020). Freshwater runoff effects on the production of biogenic silicate and chlorophyll-a in western Patagonia archipelago (50-51°S). Estuarine, Coastal and Shelf Science. 241, 106597.

Trimborn, S., Langer, G. y Rost, B. (2007). Effect of varying calcium concentrations and light intensities on calcification and photosynthesis in *Emiliania huxleyi*. Limnol. Oceanogr. 52, 2285–2293.

Tynan, E., Tyrrell, T. y Achterberg, E. (2014). Controls on the seasonal variability of calcium carbonate saturation states in the Atlantic gateway to the Arctic Ocean. Marine Chemistry. 158, 1–9.

Tyrrell, T. y Merico, A. (2004). *Emiliania huxleyi*: bloom observation and the conditions that induce them, en "Coccolithophores", editado por H. Thierstein y J. Young, Springer.

Tyrrell, T. y Young, J. (2009). Coccolithophores, en "Encyclopedia of ocean sciences", editado por J. Steele, S. Thorpe, y K. Turekian, vol. 1, pp. 606–614, Elsevier.

Utermöhl, H. (1958). Vervollkommnung der quantitativen phytoplankton-methodik, Mitteilungen. Internationale Vereinigung für theoretische und angewandte Limnologie. 9, 1–38.

van Bleijswijk, J., van der Wal, P., Kempers, R., Veldhuis, M., Young, J., Muyzer, G., Vrind-de Jong, E. y Westbroek, P. (1991). Distribution of two types of *Emiliania huxleyi* (Prymnesiophyceae) in the northeast Atlantic region as determined by immunofluorescence and coccolith morphology. J. Phycol. 27, 566–570.

Vardi, A., Haramaty, L., Van Mooy, B., Fredricks, H., Kimmance, S., Larsen, A. y Bible, K. (2012). Host-virus dynamics and subcellular controls of cell fate in a natural coccolithophore population. P. Natl. Acad. Sci. USA. 109, 19327–19332.

Vargas, C. A., Lagos, N. A., Lardies, M. A., Duarte, C., Manríquez, P. H., Aguilera, V. M., Broitman, B., Widdicombe, S. y Dupont, S. (2017). Species-specific responses to ocean acidification should account for local adaptation and adaptive plasticity. Nat. Ecol. Evol. 1, 84.

Venn, A., Tambutté, E., Holcomb, M., Laurent, J., Allemand, D. y Tambutté, S. (2013). Impact of seawater acidification on pH at the tissue-skeleton interface and calcification in reef corals. Proc. Natl. Acad. Sci. 110, 1634–1639.

Vivanco, X. y Seguel, M. (2009). Manual Técnico – Curso teórico-práctico para el muestreo, identificación y enumeración de *Alexandrium catenella* y otros taxa nocivos, Instituto de Fomento Pesquero, Puerto Montt, Chile, https://www.ifop.cl/marearoja/wp-content/uploads/sites/2/2016/07/Manual_Tecnico_curso_Marzo_2009-mod.pdf.

von Dassow, P., Van Den Engh, G., Iglesias-Rodriguez, D. y Gittins, J. R. (2012). Calcification state of coccolithophores can be assessed by light scatter depolarization measurements with flow cytometry. J. Plankton Res. 34, 1011–1027.

von Dassow, P., John, U., Ogata, H., Probert, I., Bendif, E., Kegel, J., Audic, S., Wincker, P., Da Silva, C., Claverie, J., Doney, S., Glover, D., Mella, D., Herrera, Y., Lescot, M., Garet-Delmas, M. y de Vargas, C. (2015). Life-cycle modification in open oceans accounts for genome variability in a cosmopolitan phytoplankton. The ISME Journal. 9, 1365–1377.

von Dassow, P., Díaz-Rosas, F., Bendif, E., Gaitán-Espitia, J.-D., Mella-Flores, D., Rokitta, S., John, U. y Torres, R. (2018). Over-calcified forms of the coccolithophore *Emiliania huxleyi* in high-CO_2 waters are not preadapted to ocean acidification. Biogeosciences. 15, 1515–1534.

Walker, Ch., Taylor, A., Langer, G., Durak, G., Heath, S., Probert, I., Tyrrell, T., Brownlee, C., y Wheeler, G. (2018). The requirement for calcification differs between ecologically important coccolithophores species. New Phytologist. 220, 147–162.

Young, J. R. y Westbroek, P. (1991). Genotypic variation in the coccolithophorid species *Emiliania huxleyi*. Mar. Micropaleontol. 18, 5–23.

Young, J. R. (1994). Variation in *Emiliania huxleyi* coccolith morphology in samples from the Norwegian EHUX experiment, 1992. Sarsia. 79, 417–425.

Young, J. R., Geisen, M., Cros, L., Kleijne, A., Sprengel, C., Probert, I. y Østergaard, J. B. (2003). A guide to extant coccolithophore taxonomy. J. Nannoplankt. Res. 1, 1–125.

Young, J. R., Poulton, A. J. y Tyrrell, T. (2014). Morphology of *Emiliania huxleyi* coccoliths on the northwestern European shelf – is there an influence of carbonate chemistry? Biogeosciences. 11, 4771–4782.

Zeebe, R. y Wolf-Gladrow, D. (2003). CO_2 in seawater: Equilibrium, Kinetics, Isotopes. 2nd Edition. Elsevier Science, pp. 360.

Zingone, A., Sarno, D., Siano, R. y Marino, D. (2011). The importance and distinctiveness of small-sized phytoplankton in the Magellan Straits. Polar Biol. 34, 1269–1284.

Ziveri, P., Bernardi, B., Baumann, K.H., Stoll, H. y Mortyn, G. (2007). Sinking of coccolith carbonate and potential contribution to organic carbon ballasting in the deep ocean. Deep-Sea Research. 54, 659–675.

Zondervan, I., Zeebe, R., Rost, B. y Riebesell, U. (2001). Decreasing marine biogenic calcification: A negative feedback on rising atmospheric pCO_2. Global Biogeochem. Cycles. 15, 507–516.

Zondervan, I., Rost, B. y Riebesell, U. (2002). Effect of CO_2 concentration on the PIC/POC ratio in the coccolithophore *Emiliania huxleyi* grown under light-limiting conditions and different daylengths. J. Exp. Mar. Biol. Ecol. 272, 55–70.

Zondervan, I. (2007). The effects of light, macronutrients, trace metals and CO_2 on the production of calcium carbonate and organic carbon in coccolithophores–A review. Deep-Sea Research II. 54, 521–537.